MICROSTRUCTURAL ANALYSIS OF SURFACE AND INTERFACE ZONES IN CONCRETE

GAMAL ELSAYED ABDELAZIZ

Doctor of Philosophy

ASTON UNIVERSITY

December 1997

ASTON UNIVERSITY

MICROSTRUCTURAL ANALYSIS OF SURFACE AND INTERFACE ZONES IN CONCRETE

Gamal Elsayed ABDELAZIZ **Doctor of Philosophy 1997**

ABSTRACT

The characterisation of microstructure variations across the cover zone of concrete and the effect of these variations on the rate of chloride ingress and carbonation were investigated. The effectiveness of using controlled permeability formwork (CPF) and electro-chemical realkalisation (ECR) as techniques for remedying the problems associated with such variations on the microstructure of the surface and interface zones was then studied.

The hydration, pore structure and microhardness gradients of OPC and blended cement pastes cured under various regimes were analysed by thermo-gravimetry, desorption and indentation microhardness techniques. An alternative method, scratch hardness determination, was developed to provide information regarding hardness and microstructure of hardened cement paste (HCP), mortar and concrete. HCP specimens of different microstructure gradient thicknesses were then exposed to both 100% CO_2 in 65% RH environment and 1M NaCl solution to establish a relationship between microstructure gradient and mass transport properties.

Several of OPC paste and concrete specimens, with different mix proportions, were cast against CPF and impermeable formwork (IF) and the profiles of pore structure, microhardness and scratch hardness of the cover zone were established. The chloride ingress and the depth of carbonation of the surface zone of concrete cast against CPF and IF were investigated.

The main mechanisms controlling the ECR processes and the factors affecting such treatment were critically reviewed. Subsequently, as a means of restoring passivation of steel embedded in carbonated concrete, such HCP specimens were subjected to ECR. The influence of ECR on the chemistry of the pore solution and the microstructure of the surface and the steel/cement paste interface zones was also studied.

The main findings of this investigation were as follows:

(a) The thickness of the microstructure gradient of cover concrete is significantly decreased with increasing period of water curing but is relatively unaffected by curing temperature, w/c ratio and the use of cement replacement materials.

(b) The scratch hardness technique was shown to be potential useful for characterising the microstructructure and microhardness gradients of the surface zone.

(c) A relationship between the microstructure gradient and mass transport properties of the surface zone was established.

(d) The use of CPF resulted in a significant reduction in porosity of both the cement paste matrix and the aggregate/cement paste transition zone, and a marked improvement in the resistance of the surface zone to carbonation and the ingress of chloride ions.

(e) The ECR treatment resulted in a marked densification of the pore structure and in changes to the pore solution chemistry and the cement phases of near-surface and steel/cement paste transition zones. This effect was more pronounced with current density, period of treatment and particularly with the use of sodium phosphate as an electrolyte.

KEY WORDS: **Microstructure, Cover concrete, Porosity, Durability, Curing, Chloride, Carbonation, Electro-chemical realkalisation, Formwork**

ACKNOWLEDGEMENTS

The author wishes to express his most sincere gratitude to Professor C L Page, under whose supervision this research was conducted and who gave so freely of his time and energy to advise, assist and encourage.

I am very grateful to the trustees of the Overseas Research Students (ORS) Award Scheme, the Department of Environment and Transport and Aston University for financing this research.

Sincere thanks are due to Drs G Seneviratne, G Sergi and V Ngala for their advice concerning the experimental work and for their constructive criticism of the manuscript. Research colleagues and friends, especially G Chadbourn, D Anstice and M Ismail, are also thanked for their help with day to day problems.

The entire technical staff of the Civil Engineering Department, in particular Mr C Thompson, are acknowledged for their assistance in the laboratory work. Mr R Poole's assistance in computing was immensely appreciated.

Finally, I am extremely grateful to my parents, wife, daughter, brother and sisters for their loving moral support and encouragement throughout. It is to them that this thesis is dedicated.

GLOSSARY OF ABBREVIATIONS

C_3A	-	Tricalcium Aluminate ($3CaO.Al_2O_3$)
$Ca(OH)_2$	-	Calcium Hydroxide
C_4AF	-	Tetracalcium Aluminoferrite ($4CaO.Al_2O_3.Fe_2O_3$)
Ca_2CO_3	-	Calcium Carbonate
Cap.	-	Capillary
CAZ	-	Curing Affected Zone or Microstructure Structure Gradient
C-H	-	Calcium Hydroxide
Cl^-	-	Chloride Ion
CO_2	-	Carbon Dioxide
CO_3^{2-}	-	Carbonate Ion
CPF	-	Controlled Permeability Formwork
CPFAZ	-	Controlled Permeability Formwork Affecting Zone
C_2S	-	Diacalcium Silicate ($2CaO.SiO_2$)
C_3S	-	Tricalcium Silicate ($3CaO.SiO_2$)
C-S-H	-	Calcium Silicate Hydrate
D_{cl}	-	Coefficient of Chloride Diffusion
DTA	-	Differential Thermal Analysis
E1 to E8	-	Curing Regime (Outlined in Table 2.3)
ECR	-	Electro-Chemical Realkalisation
HCP	-	Hardened Cement Paste
hV	-	Hardness Vicker
GGBS	-	Ground Granulated Blast Furnace Slag or Slag
I	-	current Density
IF	-	Impermeable Formwork
LiOH	-	Lithium Hydroxide
MIP	-	Mercury Intrusion Porosimetry
Na^+	-	Sodium Ion
NaCl	-	Sodium Chloride
Na_2CO_3	-	Sodium Carbonate
$NaNO_2$	-	Sodium Nitrite
NaOH	-	Sodium Hydroxide

Na_3PO_4	-	Sodium Phosphate
NEW	-	Non Evaporable Water
OH^-	-	Hydroxyl Ion
OPC	-	Ordinary Portland Cement
PFA	-	Pulverised Fuel Ash or Fly Ash
PSD	-	Pore Size Distribution
ϕ	-	Diameter of glass bead
RH	-	Relative Humidity
Scr.	-	Scratch
SSD	-	Saturated Surface Dry
SRPC	-	Sulphate Resistant Portland Cement
t	-	time
T	-	Period of Electro-chemical Realkalisation Treatment
TCP	-	Total Chloride Penetrated into Concrete Cover
TG	-	Thermo-Gravimetry
TZ	-	Transition Zone or Interface Zone
W/C	-	Water Cement Ratio
XRD	-	X-Ray Diffraction

TABLE OF CONTENTS

LIST OF TABLES

LIST OF FIGURES

CHAPTER 1

INTRODUCTION

1.1 FIELD OF STUDY

Reinforced concrete is a widely accepted and used construction material. A durable concrete will retain its original form, in terms of quality and serviceability when exposed to the environment. It must therefore provide adequate strength and withstand the effects of natural weathering and aggressive environments, affording sufficient protection to embedded reinforcement (ACI Committee 201, 1977 and Schiessl, 1989).

Over the last two decades, there has been a growing awareness that not all concretes are durable as previously believed. It has been found that reinforcement corrosion is one of the major problems affecting durability of reinforced concrete structures (Schiessl, 1989). Also, durability-related problems contribute over 95% of failures of concrete structures (Wood, 1994) and a large sum of money is spent to prevent structures undergoing this type of failure. In the UK alone about £150 million a year is spent on maintaining motorway and trunk road bridges, much of it on the repair of damage caused by steel corrosion. In Europe, the cost of bridge repair is estimated at £1000 million a year (Arya, 1994).

Carbonation and chloride contamination of concrete are known to be the major factors responsible for premature corrosion of steel reinforcement in concrete (Swamy and Tanikawa, 1993). These substances can penetrate concrete to the level of reinforcement and disrupt the passivity of the steel, initiating corrosion. The cover concrete is, therefore, considered to be the first line of defence against these harmful mechanisms and, consequently, the quality of the surface zone of any concrete structure is a critical factor in determining the long term durability. The microstructure of the cover concrete plays a major role in controlling the rate of ingress of deleterious elements. Therefore, it is important to have a good understanding of the microstructure of the concrete cover to enable an accurate assessment of the service life and durability of existing structures.

When exposed to a drying environment, the microstructure of the bulk concrete is different from concrete near the surface. This is due to the moisture gradient within the concrete , and consequently, the formation of a microstructure gradient in the cover zone (Patel et al, 1988). Cather (1994) defined the depth between the surface and the point within the concrete where the external environment has virtually no effect on the local humidity regime as the "*curing-affected zone* (CAZ)". The quantification of the CAZ will therefore lead to a better understanding of the covercrete microstructure system. Furthermore, the influence of the CAZ on mass transport properties of the concrete such as chloride ingress and carbonation can also be studied.

It is important to characterise the pore structure of hardened cement paste involved in the cover concrete and to quantify the CAZ in order to develop a durable concrete. There are many techniques available for characterising the microstructure of HCP, mortar and concrete (outlined in Section, 3.2.1). Most of these techniques are, however, time-consuming and cause irreversible changes to the microstructure of the material being tested. So, there is the need for the development of an alternative, simple and reliable method of measurement.

Many procedures are now available for improving the pore structure and for enhancing the mechanical and mass transport properties of the cement paste matrix and aggregate/cement paste transition zone. The most practical of these procedures involve treatment of the concrete surface with water curing, use of cement replacement materials and casting of fresh concrete on controlled permeability formwork fabrics (CPF). Water curing is the traditional method of curing concrete and prolonged water curing generally improves the properties of cover concrete through the modification of its microstructure. It is also believed that the use of PFA or GGBS as a cement replacement material tends to modify the microstructure of the concrete as a result of the pozzolanic reaction which occurs between these blending agents and the cement hydration products (Sergi, 1986; Ahmed, 1990 and Ngala, 1995).

In addition to curing and the use of cement replacement materials, CPF has been used in recent years to minimise drawbacks caused by conventional impermeable formwork (IF) and to improve the durability of concrete (Price and Widdows, 1991 and Basheer et al, 1993). The use of CPF appears to alter the microstructure of the near surface concrete

by allowing trapped air and water to escape from the near surface concrete (Price and Widdows, 1991). Thus, a good understanding of the effects these variables (curing, cement replacement materials and CPF) on the pore structure of the surface zone will be helpful in producing durable concrete.

Reinforcement corrosion remains the main cause of the premature deterioration of concrete structures world-wide. Many methods have been proposed to combat this problem including patch repairing, delaying the onset of corrosion by treating the surface of concrete with either waterproofing membranes or anti-carbonation coatings and applying electro-chemical techniques. Other measures will involve the use of less permeable concrete through the lowering of the w/c of the surface zone (using CPF) and the incorporation of cement replacement materials (RILEM Draft Recommendation, 1994 and Arya and Vassie, 1996). Recent evidence suggests, however, that such measures (patch repair and delaying the onset of corrosion) alone may not be sufficient in all circumstances (Wallbank, 1989; RILEM Draft Recommendation, 1994; Arya and Vassie, 1996 and Al-Kadhimi et al, 1996).

Various electro-chemical techniques for corrosion protection of reinforcing steel have been developed in the last few years. The advent of these techniques presents the possibility of lasting rehabilitation for concrete through tackling the causes instead of symptoms (RILEM Draft Recommendation, 1994). One of these methods is electro-chemical realkalisation (ECR) which provides a non destructive means for remedying the effects of carbonation.

The ECR technique is commercially available and aims to re-establish the corrosion protective qualities of concrete by increasing the alkalinity of carbonated concrete to a suitably high pH level (Odden and Miller, 1994 and Sergi et al, 1996). The mechanism of this technique is controlled by covercrete properties such as absorption, diffusion, migration and, according to some authors, electro-osmosis (Mietz and Isecke, 1994a and 1994b; Polder and Hondel, 1992 and Banfill, 1994). This technique, consequently, is affected by the pore structure of the concrete cover. Therefore, quantification of the covercrete microstructure, prior to and following the application of electro-chemical realkalisation may provide a better understanding of the mechanism of this technique and enable the detection of possible side effects on the concrete properties.

1.2 PURPOSE OF STUDY

It has been recognised that the durability of reinforced concrete is sensitive to the microstructure of cover concrete, especially that of the surface zone. Many direct and indirect techniques have therefore been introduced in the literature (see Section 3.2.1) for characterising the cover concrete microstructure. However, due to the limitations of these techniques (outlined in Section 3.2.1 and 4.1), there is the need for the development of an alternative method of measurement.

At the surface zone, the microstructure is not uniform as a result of the variation in the degree of hydration, thus leading to the formation of a microstructure gradient (curing affected zone, CAZ). However, there is lack of quantitative information regarding the CAZ and its effects on the mass transport properties of the cover concrete.

Controlled permeability formwork sheets (CPF) were adopted in the last few years to improve the mechanical and mass transport properties of reinforced concrete within the CAZ. However, the role of these sheets on the pore structure, microhardness and mass transport properties such as the rate of chloride ingress and carbonation within the surface zone are not fully understood.

Furthermore, electro-chemical realkalisation (ECR) is considered an infant technique with only a limited track record in treating problems associated with carbonation within the CAZ. The mechanism of this treatment and its effects on the composition of the cover concrete are in need of further investigation. In an effort to gain improved understanding of the above-mentioned phenomena, the present study was undertaken with the following main objectives:

(1) To characterise the microstructure of the cover concrete and to determine the thickness of the microstructure gradient (curing affected zone, CAZ) of the surface zone by a number of established methods.

(2) To establish a simple, reliable technique based on a scratch hardness measurement to quantify the covercrete microstructure and the thickness of CAZ.

(3) To determine the effect of CAZ on mass transport properties, e.g. chloride ingress and carbonation.

(4) To investigate the effectiveness of controlled permeability formwork (CPF) in modifying the microstructure and microhardness of cement paste and aggregate/cement paste transition zone (TZ) of covercrete.

(5) To examine the effect of CPF on the rate of carbonation and chloride ingress into the surface zone.

(6) To study the mechanism of electro-chemical realkalisation (ECR) and to determine the factors affecting the ECR treatment.

(7) To investigate the effect of ECR treatment on microstructure and the cement phases of the near-surface and steel/cement paste transition zones.

1.3 OUTLINE OF THESIS

This thesis is divided into eight chapters, Following this introduction (Chapter 1), chapter two details materials used, mix proportions, specimen preparation and testing techniques adopted throughout the present investigation. The experimental work is described in the next five chapters (3 to 7). Each experimental chapter contains a general introduction to the topic and, where applicable, a review of the relevant literature precedes the experimental procedure which in turn is followed by the results and discussion. At the end of each chapter, there is a summary of the conclusions. Finally chapter 8 contains the overall conclusions arrived at from the whole investigation followed by recommendations for further work.

More specifically, chapter 3 discusses the data obtained from the widely-used techniques such as thermo-gravimetry, water desorption and chloride ion diffusion measurement. These techniques have been adopted to characterise the microstructure and the mass transport properties of the surface zone of OPC, OPC/30%PFA and OPC/60%GGBS pastes cured with different regimes, and to determine the thickness of the curing affected zone or microstructure gradient (CAZ) of these pastes. This chapter relates the pore structure of the surface zone to its mass transport properties (in terms of the effective chloride diffusion).

Chapter 4 describes the development of scratch hardness equipment and the methods of analysing the scratch, followed by attempts to investigate the reliability of this

equipment by measuring the scratch hardness of OPC paste and concrete of different properties. This chapter also discusses the possibility of using the indentation microhardness and scratch hardness techniques in evaluating the CAZ of OPC paste. Finally, it also relates both indentation microhardness and scratch hardness results with each other and with the pore structure measurements.

Chapter 5 outlines the effect of the process of carbonation on the pore structure and chemical composition of OPC, OPC/30%PFA and OPC/60%GGBS pastes. It determines the influence of the CAZ on the rates of carbonation and chloride ingress into the surface zone of HCP.

Chapter 6 describes the pore structure of OPC paste cast against different formworks (CPF and IF) and the microhardness of aggregate/cement paste transition zones of OPC concrete cast on these formworks. It points out the influence of using CPF on microhardness and scratch hardness of OPC concrete with different w/c ratios, and on the rate of carbonation and chloride ingress into the surface zone of OPC, PFA and slag concretes.

Chapter 7 outlines the significance mechanisms controlling the process of ECR such as capillary absorption, diffusion and current-induced (possibly electro-osmosis). It determines the influence of varying internal relative humidity of the surface zone, intensity of polarisation, period of ECR treatment and type of electrolyte on the rate of realkalisation and the chemistry of the pore solution of the surface zone. Finally, it describes the effect of these variables on the pore structure and cement phases of the near-surface and steel/cement paste transition zones.

CHAPTER 2

MATERIALS, PREPARATION OF SPECIMENS AND EXPERIMENTAL TECHNIQUES

2.1 INTRODUCTION

This chapter outlines the materials, specimen preparation and some of the experimental procedures used in this research programme. Further experimental procedures are described in detail in the relevant chapters.

2.2 MATERIALS

2.2.1 Ordinary Portland Cement

Ordinary Portland Cement (OPC) complying with BS 12 (1978) was used throughout the study. The cement was received in a single batch and stored in air-tight plastic bins during the investigation. Details of the chemical and physical properties are summarised in Table 2.1.

2.2.2 Cement Replacement Materials

Two cement replacement materials, namely, Pulverised-Fuel Ash (PFA) and Ground Granulated Blast Furnace Slag (GGBS) were used in this investigation. The chemical compositions of the cement replacement materials are given in Table 2.1.

2.2.3 Aggregate

2.2.3.1 Natural aggregates

Natural siliceous sand and gravel of maximum nominal size of 15 mm complying with BS 882 (1983) were used to produce concrete specimens, and all aggregates were kept in saturated surface dry (SSD) condition.

2.2.3.2 Glass beads

Non-porous glass beads supplied by English Glass Ltd. were used to simulate aggregate to study the effect of underlying aggregate on microhardness and scratch hardness of concrete. The diameter (Ø) of the glass beads was 12 mm with a specific gravity of 2.95.

2.2.4 Water

De-ionised water was used throughout the study for mixing cement pastes, curing and preparation of aqueous solutions for chloride diffusion cell and chloride exposure tests. Distilled water was used for mixing concrete specimens.

2.2.5 Sodium Chloride

Analytical reagent grade sodium chloride (99.9% NaCl) was used for the preparation of aqueous test solutions required to investigate the chloride ion diffusion in cement paste.

2.2.6 Sodium Hydroxide

Analytical reagent grade sodium hydroxide was used for curing solution, chloride solutions for immersion tanks and diffusion cells to prevent leaching of hydroxides from the specimens.

2.3 MIX PROPORTIONS

Details of the mix proportions used for producing concrete and cement paste are given in Table 2.2-a and 2.2-b, respectively.

2.4 PREPARATION OF TEST SPECIMENS

2.4.1 Cement Paste

The cements were sieved through a 150 μm mesh to ensure homogeneity by avoiding the presence of the coarse unhydrated cement particles in the mix. In blended mixes, the OPC was added to PFA and GGBS in accordance with Table 2.2 and mixed manually to achieve a properly blended cementitious material. The cement blends and mix water were weighed according to the water/solid ratio and mixed together manually for a period of 5 minutes. The mix was then transferred to PVC cylindrical moulds of 49 mm diameter and 75 mm height and vibrated until air bubbles stopped appearing on the surface of the paste. Care was taken during the vibration to avoid excessive bleeding. The foamy layer that accumulated on the surface was removed and replaced with fresh paste and this process was repeated twice. A polythene sheet was then placed on the surface of the paste to prevent air being entrapped, and sealed with an air tight lid. The cylinders were then rotated end over end at 8 rpm for 24 hours to prevent bleeding and to minimise segregation. After 24 hours, the lids of the PVC containers and the

polythene sheets were removed. The region between the PVC mould and cast surface was sealed using paraffin wax leaving only the cast surface exposed to the curing environment (see Figure 2.1). The PVC containers were then transferred to various curing environments listed in Table 2.3.

2.4.2 Concrete

The concrete mixing procedure was essentially that specified in BS 1881: Part 125 (1970). The aggregates were mixed dry for one minute, then half of the mix water was added and mixing was continued for a further minute. The mix was then allowed to stand for 8 minutes. The cement was then added and mixed for another minute and the remaining water was added to the mix and mixing continued for a further two and a half minutes. The concrete was then hand mixed to ensure its complete homogeneity. Then, the concrete was poured into concrete moulds in three layers, compacting each layer on a vibrating table. The concrete was then levelled and wrapped in a polythene sheet. The concrete specimens were demolded after 24 hours and transferred to the specified curing environments.

2.4.3 Glass Bead/ Cement Paste Model

A PVC mould (60x60x30 mm) was designed to produce cement paste specimens to study the effect of underlying aggregates on microhardness and scratch hardness. The base of the mould had hemi-spherical pits of 12 mm diameter (Ø). These groves were spaced at ½Ø, Ø and 2Ø to contain non porous glass beads of 12 mm in diameter. The glass beads were fitted to the PVC mould before casting. OPC paste with water/cement ratio of 0.5 was used to produce specimens containing embedded glass beads. The cement paste was mixed as described in section 2.4.1 and the fresh cement paste was poured into the mould and vibrated on a small vibrating table to remove any trapped air. The specimen was then wrapped in a polythene sheet to prevent moisture loss. The specimens were demolded after 24 hours and cured for 2 months under water at 22°C prior to testing. The geometrical detail of a glass bead/ cement paste model is shown in Figure 2.2.

2.5 CURING

A wide range of curing regimes used in this investigation are summarised in Table 2.3. Specimens were subjected to curing 24 hours after casting in order to have the same

pre-curing condition. The three curing regimes used in this investigation were as follows:

Regime 1: Water curing at moderate temperature

Water curing was carried out in plastic curing tanks. De-ionised water used for curing contained 35 mM NaOH to prevent leaching of alkalis from the specimens. The tanks were stored in a curing room maintained at 21°±2°C and 65% RH. The specimens were immersed in the curing tanks for 3, 7 and 28 days. In addition, some specimens were subjected to air curing in the curing room for 28 days. Other specimens were cured for 3 and 7 days in de-ionised water followed by air curing in the curing room.

Regime 2 Water curing at elevated temperature

The specimens cured in this regime were immersed in tanks filled with de-ionised water containing 35 mM NaOH. These tanks were stored in a curing room at 38°±2°C and 65% RH for 3 and 28 days. Some specimens were air cured in the curing room for 28 days.

Regime 3 Interrupted curing

This curing regime was expected to simulate Middle Eastern site conditions by intermittent wetting of concrete. The specimens were wetted for 5 minutes twice a day; in the morning and evening, by immersing in a curing tank that contained water maintained at 38°±2°C. Wetted specimens were then exposed in air at 38°±2°C and 65% RH. The cyclic wetting and drying was continued for three days and then the specimens were left in air at 38°±2°C and 65% RH for 25 days.

2.6 TEST TECHNIQUES AND PROCEDURES

The method of sampling to obtain the specimens required for various investigations are described in detail in the relevant chapters. This section summarises the test techniques and procedures used throughout this investigation.

2.6.1 Determination of Non Evaporable Water (NEW)

The method adopted in this study to determine % NEW, assumes that all bound water in the cement paste can be removed by oven drying at 950°C.

After curing, the cylindrical cement paste specimen was sliced to obtain circular disc specimens at different distances from the casting surface as described in Chapter 3 (Section 3.3). Each specimen was then broken into small fragments and transferred into a platinum crucible. The crucible was then heated in an oven at 105°C until constant weight achieved and the weight was recorded (W_{105}). The cement paste sample was then heated at 950°C for 25±5 minutes and the weight was recorded (W_{950}).

At 950°C the cement itself looses some mass termed the ignition loss, which has to be determined for all types of cements used. Approximately 1 gram of unhydrated cement was used to determine the loss on ignition following the same procedures as for the cement paste specimens. The percentage "loss-on-ignition" was also determined for the pozzolanic cements (PFA and GGBS) blended with OPC.

The amount of non evaporable water was then calculated as a percentage of the weight of unhydrated cement using the following equation (Lambert, 1983 and Sergi, 1986) :

$$\%NEW = \frac{W_{105}(100 - i + a) - W_{950}(100 + a)}{W_{950}} \quad \ldots\ldots \quad (2.1)$$

Where,

NEW = non evaporable water (% gms/ gm of cement)

W_{105} = weight of cement paste at 105°C (gms)

W_{950} = weight of cement paste at 950°C (gms)

i = loss-on-ignition (% weight of cement)

a = total admixtures (% weight of cement)

The derivation of formula (2.1) and a worked example are given in Appendix 1. The average % NEW was calculated using triplicate specimens.

2.6.2 Determination of Capillary and Total Porosity

The sampling procedures are described in detail in Chapter 3 (Section 3.3) and Chapter 6 (Section 6.3). The specimens were vacuum saturated for 48 hours to ensure that all pores were filled with de-ionised water. Then, each specimen was weighed in water

(W1). The specimen was then removed from water and weighed in air in a surface dry condition (W2). The total volume of the specimen (W_2-W_1) was then calculated using Archimedes' law.

The specimen was then exposed to an environment of 90.7% relative humidity (RH) at 22°C until it attained constant weight (W3). The 90.7% RH environment was controlled using a saturated solution of barium chloride in an air tight desiccator. The capillary porosity was calculated using the following equation:

$$\text{Capillary porosity (\%)} = \frac{W2 - W3}{W2 - W1} \times 100 \qquad \ldots\ldots \quad (2.2)$$

The capillary porosity calculated in this study, represents the pores of size greater than approximately 30 nm (Parrott, 1992).

The specimen was finally oven dried at 105°±5°C for 24 hours and the weight (W_4) was recorded to determine the total porosity using the following equation:

$$\text{Total porosity (\%)} = \frac{W2 - W4}{W2 - W1} \times 100 \qquad \ldots\ldots \quad (2.3)$$

The average capillary and total porosity were calculated using triplicate specimens. A worked example is given in Appendix 2.

2.6.3 Mercury Intrusion Porosimetry (MIP)

The main principle of this technique is, to measure the volume of mercury penetrating a sample of paste, as a function of the increasing applied pressure, P. The total volume of mercury indicates the total porosity while the pressure at which the pores are penetrated is related to the pore diameter (d) by the Washburn equation;

$$P = \frac{4\gamma \cos \Theta}{d} \qquad \ldots\ldots \quad (2.4)$$

where γ is the surface tension and Θ is the contact angle.

The specimen was broken into small pieces and then approximately 3 gms of fragments were stored in a bottle containing iso-propan-2-ol for a week to remove the water from the material. The sample was then dried in cool air using a hair drier and placed in a desiccator. The desiccator was evacuated for a week to remove the alcohol from the sample. Approximately 2.5 gms of the sample was then weighed and transferred to the cell of the Pore Sizer Micrometer (Model 9310). PSD was calculated using the Washburn formula, assuming a constant contact angle of 117° and constant mercury surface tension of 485 dynes/cm. The assumed contact angle was based on earlier work by Winslow and Diamond (1970) who reported that the contact angle for cylindrical pores in hydrated cement paste (oven-dried at 105°C) was approximately 117°. This value of contact angle is considered to be accurate enough for this study since the PSD determinations are used only for comparison and not for providing exact values.

2.6.4 Identification of cement phases

2.6.4.1 Differential thermal analysis/ thermo-gravimetry

When a substance is gradually heated at a predetermined rate, at a particular temperature it may undergo a phase transformation that manifests itself as an endo-thermal or exo-thermal change. The intensity of these changes can therefore be identified as a function of temperature (Ramachandran, 1969). The temperature difference between the sample and a reference material is recorded by a differential thermal analyser (DTA), while the change in the mass of the sample due to increasing temperature is measured by a thermal gravimetry (TG) using a thermobalance.

The details of the sampling and specimen preparation are described in Chapter 5 (Section 5.3) and Chapter 7 (Section 7.3.4.6). Approximately 20 mg of the powder sample (≤ 150 μm) was packed into a platinum crucible and placed next to a similar crucible packed with alumina, a thermally inert substance, in the furnace of the Stanton Redcroft 1500 Thermoanalyser. The temperature of the furnace was then increased at a rate of 20°C/minute from ambient temperature to 950°C. Thermo-couples measured the difference in temperature between the two crucibles (reference and the sample) which was then plotted against furnace temperature. At the same time, the weight loss was also recorded as a function of temperature.

2.6.4.2 X-ray diffraction analysis

The details of sampling and specimen preparation are described in Chapter 7 (Section 7.3.4.6). Powdered specimens were passed through a 150 μm sieve and packed into sample holders before analysis in a Philips X-ray Diffractometer, which uses an electronic counter tube to measure the intensity of x-ray reflections. The specimen and counter are both rotated in the x-ray beam. The counter tube is rotated at twice the speed of the specimen so as to maintain the correct angle for each Bragg reflection. The output from the spectrometer is a trace of intensity (I) against Bragg angle (Θ) and the spacing of the reflecting planes (d) can therefore be obtained using Bragg's equation,

$$n\lambda = 2\,d \sin\Theta \qquad \ldots\ldots \quad (2.5)$$

where, n = order of the reflection

λ = wave length of radiation (λ= 1.542 $\mathring{A}$ with CuKα radiation)

With spacing (d) and Intensity (I), the identification of the crystalline compounds can be obtained by comparing with standard data.

2.6.5 Expression of Pore Solution

The high pressure pore solution expression device was first used by Longuet et al (1973) and modified by Diamond (1981) and Page and Vennesland (1983) to extract the capillary pore solution of the cement paste, mortar and concrete. The main parts of this device consist of a support cylinder, platten, die body and a piston, as shown in Figure 2.3. This device was used in this study to extract the pore solution from the specimens treated with electro-chemical realkalisation (ECR) to analyse for pH, Na^+ and CO_3^{2-} profiles. The full details of the sampling procedure and specimen preparation are described in Chapter 7 (Section 7.3.4.3).

The specimen was fragmented, placed in the support cylinder and covered with a PTFE disc to prevent the pore solution from escaping upwards. The piston was then placed on the PTFE disc and loaded from 0 to 600 kN at a rate of 0.3 kN./sec. The pore solution was consequently drawn through the outlet tube during the application of the force and

then collected in a sealed plastic vial to prevent exposure to air. At the beginning of the test, all the main parts of the pore expression device were thoroughly cleaned with de-ionised water and acetone and then sprayed with PTFE non-stick spray to minimise the friction between the contact surfaces.

2.6.6 Pore Solution Analysis

2.6.6.1 Hydroxyl ion and pH

The analysis of hydroxyl ion concentration was carried out immediately after expression of the pore solution to avoid any change in OH^- ion concentration. Two methods were used to determine pH, by titration and using a pH meter.

a- Titration

The titration method is mainly used for analysing pore solution where the pH is greater than 11. A 100 µl aliquot of the pore solution was made up to 1 ml by adding de-ionised water and then titrated using a standard 0.01 molar nitric acid solution with phenolphthalein indicator solution. The pH was then calculated from the hydroxyl ion concentration as follows:

$$pH = -\log_{10}(H)^+ \quad \text{.....} \quad (2.6a)$$

$$pOH = -\log_{10}(OH)^- \quad \text{.....} \quad (2.6b)$$

$$pH + pOH = 14 \quad \text{.....} \quad (2.6c)$$

$$pH = 14 + \log_{10}(OH)^- \quad \text{.....} \quad (2.6d)$$

b- pH meter

A pH electrode was used in this investigation for measuring the alkalinity of the expressed pore solutions where the pH is less than 11. A Pye Unicam pH electrode in conjunction with a Philips digital pH meter was used throughout this study. Prior to testing, the pH meter was calibrated using 3 standard buffer solutions of pH 4, 7 and 10. The pH measured using this method was accurate to ±0.01 pH.

2.6.6.2 Sodium ion

The concentration of sodium ions in the expressed pore solution was determined using a flame photometer. Prior to testing, 100 µl of the pore solution was diluted with de-

ionised water in a standard 250 ml flask. The diluted solution was then drawn through a thin tube into the flame photometer. The solution was then atomised and sprayed over the flame within the photometer. When a solution containing a metallic salt is sprayed onto the flame, it glows transmitting a light with a characteristic wave length. Therefore, the concentration of sodium ions could be determined by passing only the light through an appropriate filter.

2.6.6.3 Carbonate ion

The analysis was carried out by titration. A 100 µl aliquot of pore solution was diluted by adding 1 ml of de-ionised water. The diluted solution was then titrated with 0.01 nitric acid using two acid-base indicators. The acid-base indicators used were phenolphthalein and bromcresolgreen.

This method was used by Sergi (1986) and Walker (1994) and based on the following assumptions. When titrating carbonated solution with acid, two inflections are established at around pH 9 and 4, where the first coincides with the point of conversion from carbonate (CO_3^{2-}) to bicarbonate ion (HCO_3^-) and the second with complete neutralisation (i.e. from bicarbonate ion (HCO_3^-) to carbonic acid (H_2CO_3). In this study, phenolphthalein was used to determine the first conversion point while bromocresolgreen was used to determine the second conversion point. A full explanation of the method and a worked example is given in Appendix 3.

2.6.7 Indentation Microhardness Technique

The indentation hardness is defined as the ratio of the applied load, in kg, to the surface area of the indentation, in mm^2 (Sadegzadeh, 1985). In this method, when the diamond indentor (Vickers' Hardness Knoop) of diameter D is depressed onto the concrete surface using a static load (P), a permanent deformation (indentation) is produced. As a result, the microhardness (H) of the material being tested can be calculated as a function of the indentation diameter (d) which, in turn, depends on the indentor diameter (D) and test load (P), by using the following relationship (Kholmyansky et al, 1994):

$$d/D = A\,(P/HD^2)\,\beta \qquad \ldots\ldots (2.7)$$

where A and ß are dimensionless constants.

At ß=0.5 the above equation acquires a distinct physical meaning, reducing to:

$$H = \text{constant} \times \text{bearing stress (P/ area of the indentation)} \quad \ldots\ldots \quad (2.8)$$

The equation (2.8) shows that the microhardness is linearly proportional to the stress induced by the indentor.

Prior to testing, the specimen was ground and polished as described in Chapter 4 (Section 4.3.1). The polished specimen was then positioned with the test face on a horizontal plane under the microhardness tester (Micrometer 4). Then, the optical system provided within the microhardness instrument was focused until a clear image of the specimen was obtained. The load was then adjusted using the load dial and the indentor was forced onto the specimen. The length of the indentation was then marked and the microhardness reading was recorded in hardness Vickers (hV).

where, $hV = 1875 (P/ d^2)$ kg/mm^2 ..... (2.9)

2.6.8 Determination of Effective Chloride Diffusion Coefficient

2.6.8.1 Preparation of diffusion cell

Prior to setting up, the specimen was sliced into discs (≈ 3.5 mm thick) as described in Chapter 3 (Section 3.3). The discs were then vacuum saturated for 48 hours to ensure that all the pores were filled with water. The discs were then ground on both faces using emery paper and rinsed with de-ionised water. The cement paste disc was then mounted in a diffusion cell similar to that used by Page et al (1981), as shown in Fig 2.4. The diffusion cell is composed of two compartments. The first compartment was filled with 1M NaCl and 35 mM NaOH solution, while the second compartment was filled with a known volume of 35 mM NaOH solution. A water-tight seal between the cement paste disc and the cell was achieved using two rubber gaskets smeared with Apiezon grease to sandwich the sample in place. PTFE tape was used to hold the two halves of the cell together and form a water-tight seal. PVC tape was also used to strengthen the joints before the diffusion cells were installed in a water bath maintained at 25°C.

2.6.8.2 Analysis of chloride ion

From compartment 2 of the diffusion cell, 100 µl aliquots of the solution were withdrawn using a micropipette and diluted with 9.9 ml de-ionised water. Then, 2 ml of 0.25M ferric ammonium sulphate ($Fe(NH_4)(SO_4)_2.12H_2O$) in 9M nitric acid, and 2 ml of saturated mercuric thiocyanate in ethanol were added. The coloured solution formed was then lightly shaken and left undisturbed for at least 10 minutes before transferring into a test cell and analysing for chloride concentration using a spectrophotometer (JENWAY 6105 U.V./ VIS). The spectrophotometer measures the absorption of light (ABS) as a function of the chloride ion concentration at a specific wavelength of 460 nm.

Chloride ion concentrations were then estimated from a calibration curve constructed by plotting the concentration of standard chloride solutions against corrected absorption values (ABS) obtained from the spectrophotometer (Appendix 4).

2.6.8.3 Effective chloride diffusion coefficient

Variations of the chloride ion concentration in compartment 2 of the cell were monitored at regular intervals. The observed relationship took the form of a straight line and the slope of the straight line was determined (S). The effective chloride diffusion coefficient (D_d) was calculated using the following equation (2.10), derived from Fick's first law of diffusion.

$$D_d = \frac{Vl}{AC_1} S \qquad \text{.....} \quad (2.10)$$

Where,

D_d = effective chloride diffusion coefficient, (cm^2/s)

V = volume of the solution in compartment 2, (cm^3)

l = thickness of the specimen, (cm)

A = cross-sectional area of diffusion, (cm^2)

C_1 = concentration of chloride in compartment 1, (m mole/l)

S = gradient of the straight line relationship (Cl^- concentration Vs time), (m mole/l/s)

Average chloride diffusion coefficients were calculated using four test specimens. The derivation of formula 2.10 and a worked example are given in Appendix 4.

2.6.9 Determination of Total Chloride Content

The specimen preparation and exposure procedures for chloride ingress tests are presented in detail in Chapter 5 (Section 5.3). Immediately after removing the specimens from the chloride solution for testing, the specimens were sampled by profile grinding using a lathe. The grinding was carried out at progressive depths up to 50 mm into the specimen from the surface which was exposed to chloride ions. The dust produced from grinding was sieved though a 150 μm mesh to obtain a homogeneous sample. The samples were then kept in air tight plastic bags until required for chloride analysis.

The prepared dust from different depths was analysed for total chloride content according to BS 1881: part 124, 1989. The essential procedures for pre-analytical preparation (acid dissolution) according to BS 1881 were as follows:

(i) Oven dry the specimen for 24 hours at 105" C.

(ii) Disperse 5 gm concrete dust sample, or 0.5 to 0.8 gm cement paste dust sample in 25 ml de-ionised water.

(iii) Add 10 ml of concentrated nitric acid (HNO_3).

(v) Heat the solution to near boiling and keep warm for 10-15 min, using a hot plate, and leave to cool to room temperature.

(vi) Filter the solution and then dilute with de-ionised water in a standard flask to a volume of 500 ml.

(vii) Take 10 ml of solution and analyse for chloride ion concentration using a spectrophotometer, as described in section 2.6.8.2.

Total chloride content as percentage of concrete or cement paste weight was then calculated from the following equation:

$$Cl^-_t = \frac{Cl^-}{W_{105}} \times 100 \qquad \text{.....} \quad (2.11)$$

Where:

Cl_t^- = Total chloride content, % weight of concrete or cement paste, (m mole/l/gm)

Cl^- = Chloride concentration in tested solution, (m mole/l)

W_{105} = Weight of dust at 105° C (gm)

2.6.10 Determination of the Carbonation and Realkalisation Depth

Phenolphthalein indicator was used to determine the carbonation depth of specimens as described in Chapter 5 (Section 5.3) and 6 (Section 6.3.2.5). Two pH indicator solutions (phenolphthalein and thymolphthalein) were used in the investigation for monitoring the realkalisation depth (see Section 7.3.4.2). These two indicators were used because they change colour at specific pH levels, allowing the estimation of the pH level at the test location, and also for their convenience and reproducibility (Verbeck, 1958, Forrester, 1976, RILEM CPC-18, 1984 and Sergi et al, 1996).

When a freshly broken face of a concrete/cement paste specimen is sprayed with phenolphthalein solution, the colour of the test face would stay colourless for fully carbonated concrete/cement paste or change from colourless to pink for uncarbonated concrete/cement paste, where the pH is more than 9.5. Similarly, when a concrete/cement paste specimen is sprayed with thymolphthalein, the test face would stay colourless for carbonated regions and change to blue for the specimens where the pH is greater than 11 (Sergi et al, 1996).

Table 2.1 Properties of OPC and cement replacement materials.

PROPERTY		OPC	PFA	GGBS
a-Chemical Composition, %				
SiO_2		20.3	48.2	35.51
Al_2O_3		5.44	32.2	12.59
Fe_2O_3		2.80	8.02	0.580
CaO		63.7	1.45	40.09
MgO		1.44	0.66	9.110
SO_3		2.90	0.52	0.150
Na_2O		0.77	2.58	0.540
K_2O		0.09	0.98	0.240
Loss on ignition (L.O..I)		0.94	3.84	1.170
F/L		1.60	—	0.950
b- Bogue Compound Composition, %				
C_3S		61.14	—	—
C_2S		13.02	—	—
C_3A		9.740	—	—
C_4AF		7.840	—	—
c- Physical Properties				
Fineness, %		—	12.5	—
Setting time (min)	Initial	100	—	—
	Final	165	—	—
Moisture content, %		—	0.1	—
Water requirement, cm^3		106	—	—
Compressive strength,3 days		216	—	125
(kg/cm^2) 7 days		281	—	250
28 days		370	—	315

Table 2.2.a Mix materials, proportion and curing regime of concrete.

Mix No	OPC, kg/m³	Cement replacement Material.		Aggregate, kg/m³		w/c ratio	Curing conditions (see Table 2.3)
		Type	Content, kg/m³	Gravel	Sand		
1	300	—	—	1120	745	0.4	E4
2	300	—	—	1120	745	0.5	E4
3	300	—	—	1120	745	0.55	E4
4	300	—	—	1120	745	0.6	E1, E3& E4
5	300	—	—	1120	745	0.7	E4
6	210	PFA	90	1120	745	0.6	E4
7	120	GGBS	180	1120	745	0.6	E4

Table 2.2.b Mix materials, proportion and curing regime of paste.

Mix No	OPC, %	Cement Replacement Material, %		w/c ratio	Curing conditions
		PFA	GGBS		
1	100	—	—	0.4	E4
2	100	—	—	0.5	E4
3	100	—	—	0.6	E4
4	100	—	—	0.55	E1 to E8
5	100	—	—	0.7	E4
7	70	30	—	0.55	E4
8	40	—	60	0.55	E4

Table 2.3 Curing conditions for cement paste and concrete.

CODE	CURING CONDITION*
E1	Air at 22° C/65% RH for 28 days.
E2	Water at 22° C for 3 days and then in air at 22° C/65% RH to 28 days.
E3	Water at 22° C for 7 days and then in air at 22° C/65% RH to 28 days.
E4	Water at 22° C for 28 days.
E5	Air at 38° C/65% RH for 28 days.
E6	Water at 38° C for 3 days and then in air at 22° C/65% RH to 28 days.
E7	Water at 38° C for 28 days.
E8	65 % RH at 38° C water for 3 days (for only 5 minutes in morning and 5 minutes in evening), other times in air curing to 28 days.

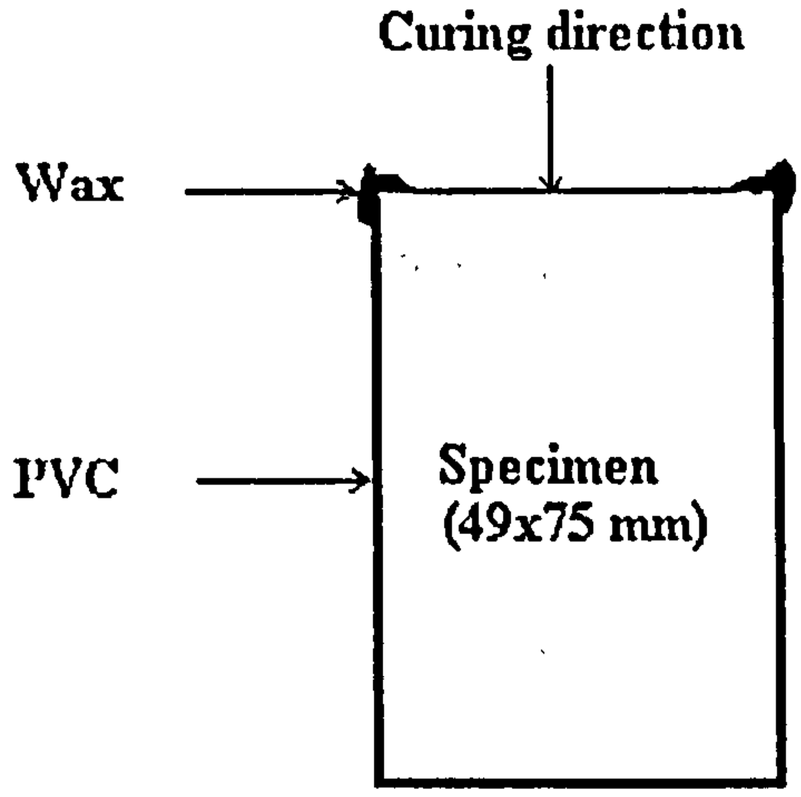

Figure 2.1 Scaling of the HCP specimens.

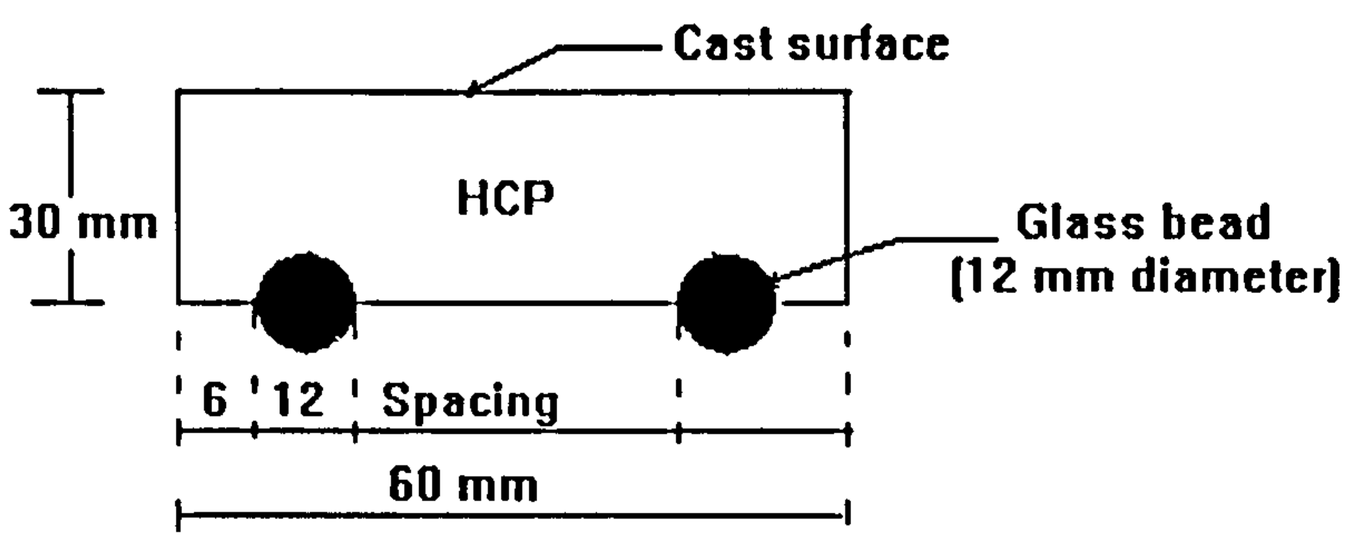

Figure 2.2 General view of glass bead/cement paste model.

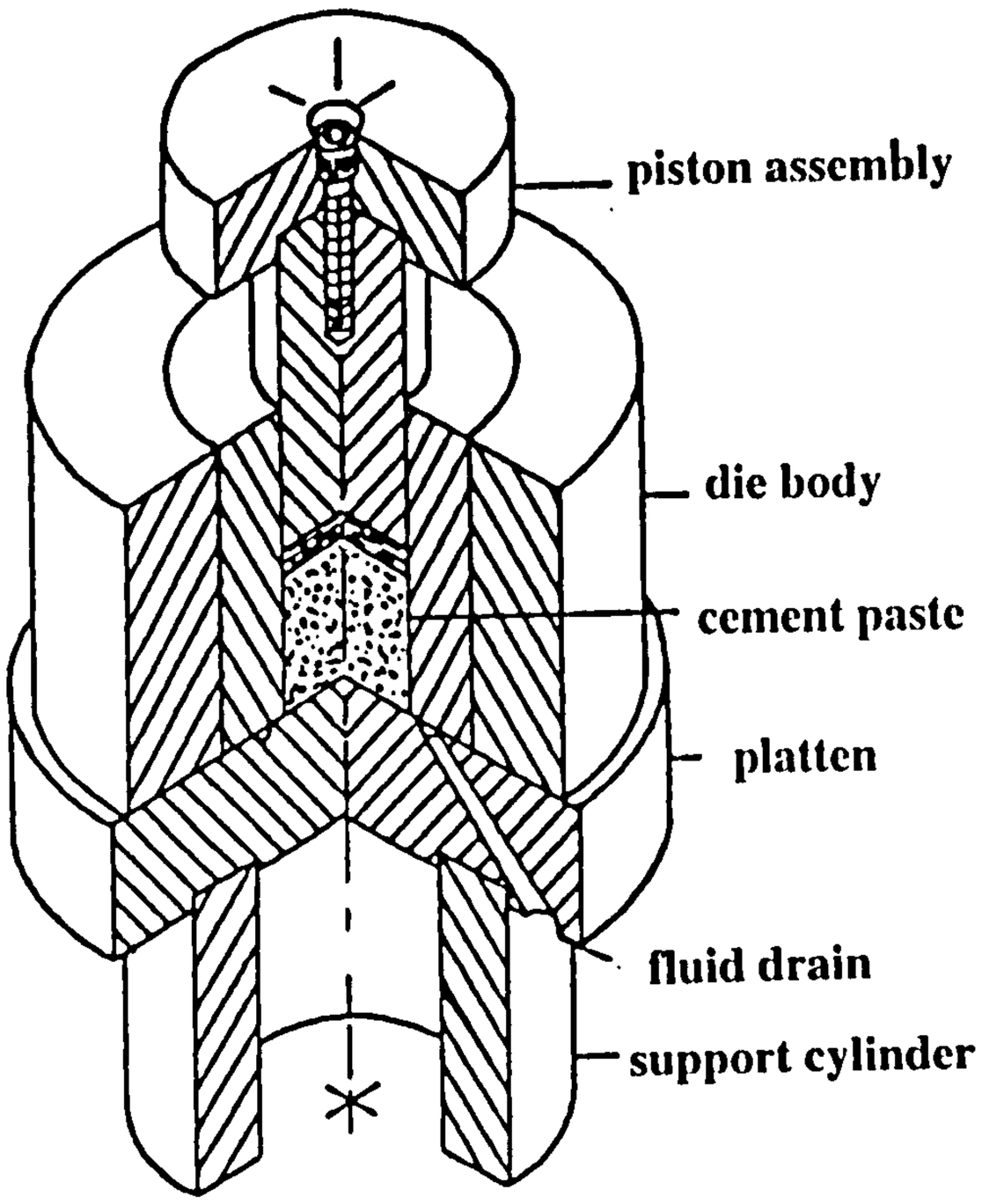

Figure 2.3 Main components of pore expression device.

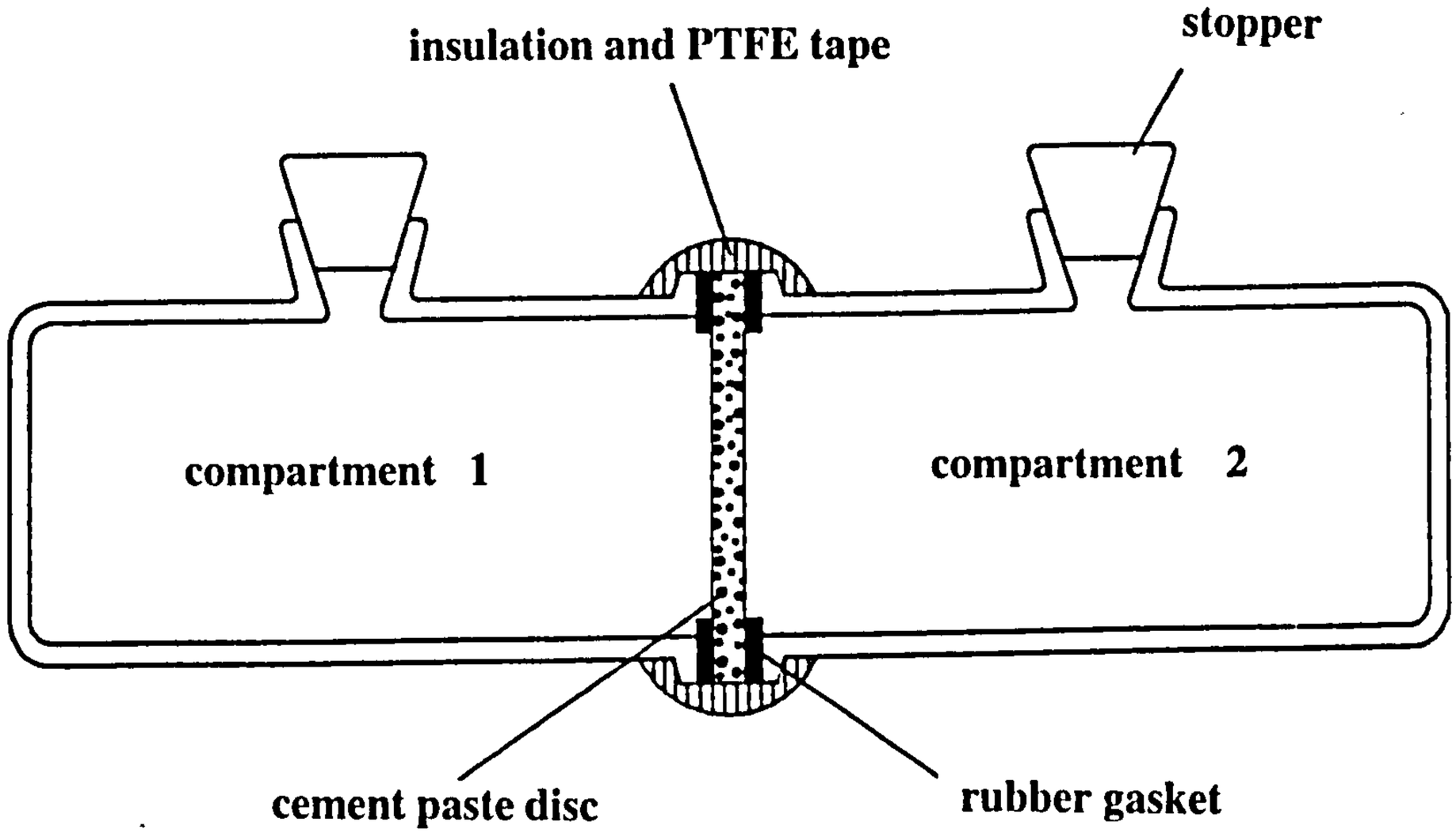

Figure 2.4 General view of the chloride diffusion cell.

CHAPTER 3

MICROSTRUCTURAL ANALYSIS OF THE SURFACE ZONE

3.1 INTRODUCTION

The process of damage due to reinforcement corrosion is often divided into two periods, as shown in Figure 3.1. T_1 is the time to initiate corrosion and depends mainly on the durability of concrete and exposure conditions while T_2 is the period between initiation and the point in time when the corrosion has reached unacceptable levels resulting in spalling or significant loss of bar cross-sectional area (Browne, 1980 and Tuutti, 1983). The period T_2 is less predictable than T_1 and its value in practice appears to range from 6 months to 5 years (Browne, 1980). The period T_2 is sometimes very small in terms of the service life of a structure and, in such cases, it seems reasonable to assume the service life of the structure to be T_1. The initiation period (T_1) can only be extended by improving the durability of cover concrete protecting the embedded reinforcement. The protection provided by the cover concrete is in the form of resistance to the ingress of deleterious chemicals from the environment. The degree of protection depends on many factors such as absorptivity, permeability, water diffusivity, and cement characteristics of the concrete cover (Wallbank, 1989).

The permeation properties and other concrete properties such as strength, creep and shrinkage are determined and controlled by the concrete microstructure (Feldman and Beaudoin, 1991; Raivio and Sarvaranta, 1994, and Lange et al, 1994). Therefore, it is vital to understand the factors influencing the pore structure of the concrete in order to develop a highly durable concrete.

Curing is one of the main methods used for improving the properties of the cover concrete through modification of its microstructure by enhanced hydration of cement. However, the degree of improvement is not uniform throughout the concrete cover. It varies from the surface to a certain point within the concrete where the external environment has virtually no effect on the local humidity regime. The distance between the surface to this point is known as the depth of the "curing affected zone (CAZ)" , which represents the thickness of the microstructure gradient.

The aim of this chapter and chapter 4 is to characterize the microstructure of the cover concrete and to determine the CAZ depth in terms of the variations in the pore structure and microhardness of the cement paste, respectively. This chapter also provides an insight into some of the factors influencing the microstructure and CAZ depth such as type of curing, w/c ratio and cement replacement materials.

3.2 LITERATURE REVIEW

3.2.1 Quantification of Concrete Microstructure

Various techniques have been used to investigate concrete microstructure and Pratt (1988) has divided these techniques into two categories, direct and indirect methods. The direct methods give the image of the microstructure in terms of the size and shape of the phases relative to each other in space. The common techniques in this category are optical microscopy, electron microscopy, image analysis and back scattered electron microscopy (BSE). On the other hand, indirect methods provide information about the average size and distribution of sizes of some or all the phases. Some common techniques in this category are the mercury intrusion porosimetry (MIP), ethanol adsorption and water absorption.

3.2.1.1 Direct methods

Optical microscopy is used for examining a thin section (0.03 mm) of concrete to study the cement and aggregate type, the presence of mineral admixtures, the water/cement ratio, the quality of the compaction and the presence of alkali silica reaction (Pratt, 1988). Winslow and Liu (1990) used an optical microscope to determine the amount of entrapped air in polished sections of mortar and concrete. He found that the majority of entrapped air voids were between 10 μm and 100 μm in diameter. However, the use of standard microscopy for characterization of entrained air in concrete is a time consuming processes (Chatterji and Gudumundsson, 1977).

Verbeck and Helmuth (1968) studied the microstructure of hardened cement paste by direct optical microscopy and electron microscopy to observe both the fragmental dispersed hydrated particles and sawn or fracture surfaces. The technique could not resolve the finely divided hydration products other than calcium hydroxide (C-H) and he concluded that the optical examination revealed very little about the microstructure of

cement paste. On the other hand, electron microscopy is capable of high magnification and resolution power but the main drawback of using electron microscopy is the difficulty in obtaining representative quantitative information.

Polished specimens impregnated with epoxy and deeply etched to remove cementitious material can be examined with a scanning electron microscope to provide information about the pore structure of hydrated cement paste (Jennings and Parrot, 1986 and Bentz, 1994). Micro graphs were used to analyze quantitatively the volume of porosity that was impregnated with epoxy and these results were compared with independent measurements of porosity using volumetric methods. The results suggested that pores less than 50 nm in diameter were not impregnated by epoxy and that they may be incorporated as part of the pore structure of the calcium silicate hydrate (C-S-H). The calcium silicate hydrate formed in the late stages of hydration may not incorporate as many fine pores as that found during the early stages of hydration. The structure of the large capillary pores (i.e., pores greater than 50 nm in diameter) changes with time from an open network to an array of disconnected pores.

Chatterji and Gudmundsson (1977) used the automatic image analysis technique to determine the amount of air bubbles in both fresh and hardened concretes. The results suggested that the amount of air bubbles measured in fresh concrete was similar to that in hardened concrete. This technique has also been used for measuring the percentage area of anhydrous cement, calcium hydroxide (C-H), other hydration products (mainly C-S-H) and volume of pores larger than 0.5 μm (Scrivener and Pratt, 1987 and Lange et al, 1994).

Using back scattered electron (BSE) images of polished cement paste sections, anhydrous material, C-H, other hydration products and porosity can be distinguished on the basis of the grey level in the image. A good correlation has been found between BSE image data and volume fractions derived from bound water measurements and methanol measurements (Scrivener and Pratt, 1987).

3.2.1.2 Indirect methods

Indirect techniques allow the calculation of pore size distribution (PSD) from principally two different types of experimental techniques; (a) porosimetry in which the

volume of mercury that is forced into the porous system is measured as a function of the applied pressure, and (b) capillary condensation of vapour from either an adsorption or desorption isotherm of the porous system (Pratt, 1988). Most commonly the pore sizes are calculated assuming that they are either a system of cylindrical capillaries or a system of parallel plates (Verbeck and Helmuth, 1968).

Mercury intrusion porosimetry (MIP) is a widely used technique for determining the total porosity and characteristic pore size distribution of HCP. Changes of the pore structure and pore volume of OPC mortar caused by extremely high or low temperature can also be identified using MIP. However, MIP can not provide adequate information regarding the manner in which the pores were altered or whether a micro fissuration has occurred (Rostasy et al, 1980). Marsh et al (1985) used MIP to develop an explanation for the dramatic reduction in permeability due to the use of fly ash in the OPC cement paste and to show the effect of curing temperature on the pore structure characteristics. Similarly, Li and Roy (1986) used MIP to investigate the relationship between porosity, pore structure and rapid chloride ion diffusion of fly ash and other blended cements. Winslow et al (1994) used MIP to differentiate between the pore size distribution (PSD) of cement paste, mortar and concrete, and also to study the phenomena of interfacial zone percolation in mortars.

Pre-drying of test samples prior to MIP measurement is considered to be one of the main drawbacks of MIP, due to the resulting alteration in the PSD of the specimen (Moukwa and Aitcin, 1988). There are other factors which require careful consideration when using this technique. Firstly, any pores or group of pores that are accessible only through narrow entrances or bottle necks (ink-bottle pores) are intruded at a pressure corresponding to the entrance diameter. These ink-bottle pores lead to an overestimation of the volume of small pores. Secondly, distortion of fine pores, particularity in blended pastes, is caused due to high applied pressure (Feldman, 1984). Thirdly, assumptions made for the contact angle between the mercury and cement paste hydrates can sometimes lead to inaccurate pore size distribution data (Shi and Winslow, 1985). Finally, the simplified geometrical assumptions that the pores are cylindrical, non-interacting and connected to the surface, required for the analysis of results are not necessarily representative of the HCP pore structure.

X-ray diffraction and thermo-gravimetric techniques were used to determine the degree of hydration of cement by measuring hydration of the individual compounds (Parrott, 1986, Beaudoin, 1987 and Larbi, 1991). However, neither technique gave information about the PSD or porosity. Patel et al (1985) used a methanol adsorption technique to determine the gel, capillary and total porosity of OPC and OPC/PFA paste and found a correlation between methanol adsorption results and the degree of hydration and diffusion resistance of OPC and OPC/PFA pastes. Beaudoin (1987) has shown that a new product, $Ca(OCH_3)_2$, is formed due to the reaction between C-H and the methanol and its effect on the HCP microstructure is considered to be the main drawback of the methanol adsorption technique.

Water absorption and desorption of cement paste and concrete were used as techniques to understand the covercrete permeation properties and to determine the gel, capillary, and total porosity (Parrott, 1992, McCarter, 1993; Ngala, 1995 and Ngala et al, 1995). Ngala (1995) and Ngala et al (1995) correlated desorption results with chloride and oxygen diffusion rates of well-cured OPC and OPC/PFA pastes and found that the measured capillary porosity was directly proportional to the coefficient of chloride and oxygen diffusion.

Sadegzadeh et al (1987 and 1989) used the abrasion resistance technique to characterize the concrete microstructure and correlated abrasion resistance results with MIP data. The results indicated that the abrasion resistance of concrete was controlled by the pore structure of the surface matrix. Initial surface absorption, intrinsic permeability and vapour diffusivity were also found to be related to the abrasion resistance (Dhir et al, 1991). Sadegzadeh and Kettle (1986) used ultrasonic pulse velocity and initial surface absorption to monitor the concrete surface structure. They found that the initial surface absorption method was more sensitive than ultrasonic pulse velocity to the variations of concrete ingredients and the resulting hydration products and porosity.

3.2.2 Cement Paste Structure

The main compounds of Ordinary Portland cement (OPC) are tricalcium silicate (C_3S), dicalcium silicate (C_2S), tricalcium aluminate (C_3A) and tetra calcium aluminoferrite (C_4AF). The addition of water to these compounds leads to several complicated

chemical reactions which finally lead to the formation of the hardened cement paste. The calcium silicates are the most important constituents, forming the strength bearing calcium silicate hydrate gel (C-S-H) and calcium hydroxide (C-H) in fully hydrated cement. C-S-H gel and C-H represent approximately 70% and 20%, by weight of the fully hydrated cement paste respectively. Other phases produced by the remaining compounds are calcium aluminate trisulphate hydrate (ettringite) and calcium monosulphate aluminate hydrate (about 7% in total); tricalcium aluminate hydrates, anhydrite clinker residue and other minor constituents making up the remainder (Diamond, 1976).

The hydration products are considered to contain a fixed amount of non-evaporable water and intrinsic gel porosity of 28% independent of the water/cement ratio and degree of hydration (Powers and Brownyard, 1948). These authors also deduced that a minimum water/cement ratio of 0.38 was required for complete hydration. However, this amount of water is considered to be small compared to the amount used in practice to ensure adequate workability of the concrete. Excess water gives rise to a continuous, open pore structure. The pores vary in size from ultra-fine gel pores (<10 nm) through coarser capillary pores to discrete microscopic air voids (>10 μm) (Powers and Brownyard, 1948). The capillary pores are the most important in terms of durability as they provide the majority of the interconnecting pathways which allow aggressive chloride ions and carbon dioxide gas to enter the concrete and cause reinforcement corrosion.

Many models have been suggested by different authors to represent the cement paste structure, as follows:

Powers' model

This model, based on extensive water vapour sorption studies, describes the cement paste as a body composed of gel particles (approximately 1000 nm in diameter) separated by a water film up to 60 nm thick. The solid to solid distance between particles is about 180 nm. Gel pores have entrances less than 4 nm in diameter. The cement paste system is considered as an ideal absorbent. It comprises interacted cement, hydration product and capillary pores (Powers and Brownyard, 1948 and Powers,1958). However, Powers' model is now thought to be oversimplified since pastes contain a

continuous distribution of pores classified by their behaviour in water (Young, 1988), as shown in Figure 3.2. Micro pores and smaller meso pores are considered to form the intrinsic porosity of the gel. Water in these pores is adsorbed and becomes involved in structural bonding, whereas in the larger meso pores and macro pores, the water present acts as bulk water.

Feldman-Sereda (F-S) model

The F-S model describes C-S-H as a layered, poorly crystalline, malformed tobermorite like material $[Ca_4(Si_3O_9H)_2(OH)_8]Ca.6H_2O$, as shown in Figure 3.3. These layers come together randomly to create interlayer spaces and to be bonded together by solid-solid contacts, whose strength lie between the weak Van der Waal's bonds and the strong covalent bonds. Water that enters the interlayer spaces becomes part of the structure and contributes to the rigidity of the system. Most of this water can not be removed from the system on drying until a relative humidity of less than 10% is achieved (Feldman and Sereda, 1970). This can be used to explain the humidity dependence of the mechanical properties of hardened cement paste, e.g. strength and modulus of elasticity (Beaudoin and Brown, 1992).

Diamond model

Diamond et al (1977) modified the F-S model based on adsorption studies on hydrated C_3S paste after the removal of calcium hydroxide. Adsorption measurements indicated the existence of two kinds of pores; a wider inter-gel particle pore which can be seen even in the inner C-S-H by scanning electron microscopy (SEM), and a smaller intra-gel pore existing within the gel particles which can not be observed by SEM. The intra-gel pores are further classified into intra-crystalline pores corresponding to the interlayer spaces in the F-S model, and inter-crystalline pores. They also suggested that some relatively large pores in dense paste are accessible to water only through interlayer spaces.

3.2.3 Cement Paste/Aggregate Interface Structure

During mixing, compaction and placement of concrete, the aggregate particles interact with the surrounding cement paste. As a result, the microstructure of the cement paste in the immediate vicinity of aggregate particles will differ in several respects from the microstructure of the remaining cement paste.

Barnes et al (1979) suggested a model for the microstructure of cement paste/aggregate interfaces, as follows:

(i) At the immediate vicinity of the aggregate surface is a duplex film of $Ca(OH)_2$ topped by or occasionally intermixed with C-S-H. Sometimes this duplex film occurs with close intimacy to the aggregate. At early ages of hydration, this duplex film is relatively porous. With increase in age, the film modifies into a dense layer , sometimes bonding with the surrounding cement paste. The side of the film in contact with the aggregate is a layer of crystalline $Ca(OH)_2$ of 0.5 μm thick. Following this layer is a thin deposit of C-S-H gel in the form of short fibers extending into the cement paste. The total thickness of the duplex film is about 10 μm.

(ii) Next to the duplex film is the "transition zone". This region is relatively large, 50 μm wide approximately, including the duplex film. Generally, this zone contains a large number of hollow-shell hydration grains, enriched in larger $Ca(OH)_2$ crystals and ettringite.

The occurrence of a large number of hollow-shell hydration grains suggests that cement hydration is accelerated at the interfacial zone. This acceleration is presumably due to the availability of excessive water in the vicinity of the aggregate particles. Since the growth of large crystals of calcium hydroxide and ettringite is enhanced in a more open system, the occurrence of such large crystals at the interfacial zone is an indication of the existence of a higher porosity (Larbi, 1991 and Scrivener and Pratt, 1996).

On the basis of a combination of tensile bond strength tests and SEM studies on debonded paste rock composites, at various ages, Zimbelmann (1978) presented a model to explain the microstructure of the interfacial zone, as follows:

(i) Directly at the surface of the aggregate is a dense layer of 3-5 μm thick, composed essentially of $Ca(OH)_2$ covering a network of ettringite crystals. This layer may be equivalent to the duplex film found by Barnes et al (1979). According to Zimbelmann, this layer is formed during the early stages of hydration, up to about 10 hours after mixing. After 12 hours, $Ca(OH)_2$ forms a continuous closed layer which he referred to as the contact layer.

(ii) Directly next to the contact layer is a zone of 5-10 μm thick, intermediate layer. This layer consists of needle shaped ettringite crystals, leaf or flake like $Ca(OH)_2$,

sporadic needle shaped calcium silicate hydrates (C-S-H) and big hexagonal C-H crystals aligned steeply with respect to the aggregate surface.

(iii) The transition zone (≈ 10 μm thick) is characterized by a dense paste merged into the bulk cement paste.

Zimbelmann (1978) attributed the origin of the interfacial zone to the formation of thin films of water (≈ 10 μm thick) on the cement grains and around large aggregate particles in fresh concrete. However, the formation of such films on the cement grains appears to be doubtful since they are likely to be destroyed during mixing, placement and subsequent compaction of the concrete (Larbi, 1991).

Two opinions have been put forward to explain the open and dense microstructure of the interfacial zone. Mehta (1986) and Scrivener and Pratt (1996) suggested that the porosity of the interface was higher than that of the bulk cement paste. It has been attributed to the wall-effect and micro-bleeding under coarse aggregate particles. The other opinion, which suggested that the microstructure of the interfacial zone was denser than that of the bulk cement paste, has been attributed to the little or total absence of anhydrous cement grains within a 15-25 μm thick zone around coarse aggregate particles (Zimbelmann, 1985).

The thickness of the interfacial zone reported in most studies varied between 50-100 μm (Bentur, 1991; Bentur and Odler, 1996 and Larbi, 1991) and depends upon the type of aggregate, cement, water-binder ratio, age of the composite, nature of bonding between the paste and aggregate particles, and the technique used to estimate the thickness.

3.2.4 Effect of Concrete Microstructure on Transport Properties

Many attempts have been made to correlate concrete permeability, which is an important property with respect to the durability of concrete, to its pore structure. Mehta and Manmohn (1980) have suggested an empirical formula to express the relationship between permeability and pore structure, as follows:

$$K = \exp.(3.84V_1 + 0.20V_2 + 0.56(10E\text{-}6)TD + 8.09MTP - 2.53) \quad \text{.....(3.1)}$$

Where; K is the coefficient of permeability, V_1 and V_2 denote the pore volume in the 1320 $\mathring{A}$ and 290-1320 $\mathring{A}$ range, respectively: TD is the threshold diameter and MTP is the modified total pore volume which is equal to the total pore volume divided by the degree of hydration.

Li and Roy (1986) established a linear relationship between total porosity and chloride diffusion. However, it was reported that only the large capillary pores (macro-pores), of diameter larger than 50 nm have an effect on concrete transport properties (Patel et al, 1985 and Young, 1988). This was supported by Ngala (1995) and Ngala et al (1995), whose work showed that oxygen and chloride diffusion rates have a significant relationship to the coarse capillary porosity, i.e. the volume of pores with diameters greater than 30 nm.

The structure of the interfacial layer between aggregate and cement paste has an influence on the transport properties, which, in turn, affect the durability of concrete. The findings of previous studies on the effect of the transition zone on transport properties have been contradictory. Wakely and Roy (1982) and Malek and Roy (1988) reported that the paste-aggregate interfacial zone does not play any major role in determining the permeability of the concrete. However, Young (1988) reported that the coefficient of permeability of concrete was about 100 times higher than that of comparable pastes, and for mortars it was 3-10 times higher. This agrees with Bourdette et al's computer model (1995) which signified the role of the transition zone in the ionic diffusion processes. Larbi (1991) has also noted that the fluid transport through 'cement mortar' was comparatively faster than through plain cement pastes of the same properties. He also pointed out that the fluid transport in the interfacial zone was relatively small compared to that in the cement paste.

Ngala (1995) has modelled the cement paste-aggregate interface using glass beads as model aggregate in order to determine the effective chloride diffusion coefficient of the mortar of paste/glass bead composite. He has found that both the capillary porosity and the effective chloride diffusion coefficient of the paste formed in model mortars with glass bead aggregates is higher than that of the corresponding plain cement pastes. He also found that the effective chloride diffusion coefficient tends to increase with

increasing volume fraction of glass beads in mortars. On the other hand, the overall chloride transport was found to be relatively slower in mortars than in plain cement pastes and seemed to remain fairly constant with increasing volume fraction of beads, as shown in Figure 3.4. Therefore, it was suggested that the cement paste matrix is the continuous phase in mortar and concrete which is mainly responsible for the fluid transport properties (Larbi, 1991 and Ngala, 1995).

3.2.5 Conspectus of Influence of Curing on Microstructure and Properties of Concrete

3.2.5.1 General

Curing can be defined as a procedure for promoting the hydration of the Portland cement in newly placed concrete. It generally implies the control of the moisture loss and sometimes temperature. The cement gel produced from the cement hydration can be laid only in water-filled spaces (Spears, 1983). A loss of this water medium will therefore cause the hydration reactions to cease quickly. Cather (1994) has defined 'curing' according to the subject of study as:

(a) Material Science, "curing is the creation of an environment in which the hydration reaction can proceed to help fulfill the aim of producing concrete of adequately low porosity".

(b) Engineering, "curing is adequate when the resulting concrete achieves the expected service performance".

Continuous water curing prevents damage to the capillary chains, which carry the water to the location of unhydrated cement particles (Carrier, 1983). However, it is practically difficult to keep the surface of the concrete continuously wet throughout the designed curing period under site conditions. Interrupted water curing is widely used, especially in Middle Eastern countries. This type of curing involves spraying water twice a day, once in the morning and once in the evening, for a few minutes at a time and leaving the concrete surface dry at all other times. Bentur and Jaegermann (1988) studied the effect of this type of curing on the development of the properties of the outer skin of OPC and OPC/PFA concrete using compressive strength and surface water absorption techniques. There has been, however, very little research carried out on the effect of interrupted curing on covercrete microstructure and transport properties.

Concrete curing practices have changed over the years and in many cases the shift has been from 'water adding' by ponding or covering with wet burlap, earth or straw to 'water retaining' techniques such as the use of membrane forming compounds. The main reason for this change is the increase in the rate of concrete production. Spray-on curing compounds are seen as the pragmatic solution to the difficulties of site curing although these are theoretically not as efficient as traditional water curing (Fattuhi, 1986; Cabrera et al, 1989; Dhir et al, 1989 and Wang et al, 1994).

The relative humidity of the curing environment has a major influence on the rate of hydration which, in turn, is related to the resulting cement paste microstructure. Parrott (1986) and Patel et al (1988) have noted that the relative humidity (RH) within the pores of the cement paste controls the rate of hydration. It is reported that at 90% RH the hydration proceeds at only 50% of the rate for saturated curing, and at 80% RH, hydration rate drops to 32%. The hydration virtually ceases when the internal RH is below 70% and 80% for OPC and OPC cement with pozzolanic additives, respectively. Parrott (1991a) studied the factors influencing the relative humidity within concrete and concluded that the water/cement ratio of the concrete and the period of initial moist curing had little effect on the measured RH. The measured RH dropped more rapidly in concrete made with pulverized fuel ash or ground granulated blast furnace slag than in concrete made with Ordinary Portland cement.

3.2.5.2 Effect of curing on concrete microstructure

Curing is one of the main factors that govern the development of the concrete microstructure (Neville, 1981). The distribution of the pore sizes varies considerably and becomes finer with an increase in the curing period (Diamond, 1971 and Carbrera, 1985). Prolonged curing increases the volume of pores smaller than 35 nm and decreases the volume of pores larger than 35 nm (Patel et al, 1985). Killoh et al (1989) studied the effect of water curing on hydration and porosity of a Portland/fly ash cement paste using thermo-gravimetry and methanol adsorption. Their findings, which were in agreement with those of Patel et al (1985), can be summarized as follows:

(1) Total porosity is not significantly affected by the relative humidity of the curing environment following the initial 7 days moist curing period.

(2) Both the gel porosity (< 4 nm) and the volume of small diameter capillary pores (< 37 nm) increase with increasing hydration.

(3) The large diameter capillary porosity (> 37 nm) decreases with increasing hydration.

(4) For both OPC and OPC+30%PFA pastes, the large diameter porosity obtained by conditioning at less than 70% RH is about 3 times greater than that obtained under saturated conditions.

Curing at elevated temperatures reduces the surface area of the hydrates formed and produces a less uniform distribution of the reaction products and coarser pore structure than those cured at moderate temperatures (Cao and Detwiler, 1995). The effect of heat curing and post-heat curing regimes of high performance and ordinary concrete on the microstructure and C-S-H composition were recently investigated by Kjellsen (1996) using scanning electron microscopy (SEM) and energy dispersive X-ray analysis (SEM-EDX). The study showed that heat cured-high performance concrete had a higher hollow shell porosity at later ages than a normally cured companion. The distribution of C-S-H for high performance concrete was not influenced by heat curing while the composition of C-S-H phases was influenced by curing regimes. The author, however, concluded that the effect of heat curing on the microstructure appeared to differ between high performance and ordinary concrete.

It is therefore clear from these findings that curing plays an important role in determining the concrete microstructure and yet , there is lack of information in the literature regarding the effect of different curing regimes (i.e. water curing at different temperatures, interrupted water curing, etc.) on the concrete microstructure.

3.2.5.3 Curing affected zone (CAZ)

In recent years, it has become increasingly clear that there can be significant differences between the cover concrete and the underlying material (bulk concrete) and that these differences are relevant when considering the durability of concrete. Kreijger (1984) suggested that the cover concrete is composed of three skins: the cement skin (about 0.1 mm thick) mortar skin (about 5 mm) and the concrete skin (about 30 mm). These are formed due to the wall effect, sedimentation, segregation, compacting methods, permeation and evaporation of water from the concrete.

Moisture gradients created by exposing concrete to a drying atmosphere can cause variations in the degree of hydration and porosity (Carrier, 1983; Patel et al , 1988 and Cather, 1994). The moisture gradient in the concrete cover occurs due to differences in the RH of the environment close to the concrete surface and the bulk RH within the concrete, where the external environment has no effect on the local humidity. The thickness of concrete measured from the concrete surface to a distance inside the cover concrete where it has the same property of the bulk concrete has been named the '*curing affected zone*' (CAZ).

Carrier (1983) has noted that there is a RH gradient between the concrete surface and the bulk concrete at the depth at which the RH remains constant, as shown in Figure 3.5. It can be estimated from Figure 3.5 that the maximum depth between the concrete surface and the point in the concrete where the RH is approximately 80%, is about 40 mm for air cured concrete. Therefore, maximum CAZ, for non-cured concrete, is approximately 40 mm. The thickness of CAZ, estimated by Cather (1994), ranged between 20 mm to 50 mm. However, this estimation was not based on experimental work.

The extent and severity of the gradient depends on a number of factors such as ambient temperature, relative humidity, wind speed, period of exposure to a drying atmosphere, etc. (Patel et al, 1988). Parrott (1992) has reported that the average absorption rate and capillary porosity in the 20 mm surface zone were generally greater than those of the underlying material. He has also related the amount of evaporable water to capillary porosity and found that fast drying of concrete increases the amount of evaporable water in covercrete, thus confirming that there is a capillary porosity gradient created between the surface and bulk concrete. The thickness of the capillary porosity and total porosity gradients are also affected by ambient conditions such as temperature, wind and RH (Patel et al, 1985 and Parrott, 1992).

To the author's knowledge there is no published literature regarding the determination and characterization of the CAZ.

3.2.5.4 Methods of testing the effect of curing

The common tests used for determining concrete performance are compressive strength, ultrasonic pulse velocity, rebound hammer, air and water permeability, abrasion, initial surface absorption test (ISAT), etc. Bentur and Foy (1989) and Day and Shi (1994) have reported that the compressive strength is not a good indicator of the effect of initial water curing. Rebound hammer testing was also found to lack the sensitivity to detect the variations in concrete surface properties (Sadegzadeh and Kettle, 1986). It has been mentioned that care is needed with water permeability testing to ensure that the test itself does not influence the result by increasing the hydration of cement while measurements are being taken. It has also been mentioned that the air permeability is very sensitive to the moisture content of the concrete (Cather, 1994).

However, the tests considered above for the determination of curing performance are unlikely to be suitable for the determination of the CAZ, due to the fact that the thickness of the CAZ can be anything up to 50 mm, as reported in the literature.

3.2.5.5 Effect of curing on concrete properties

Aitcin et al (1994) reported that both water and sealed curing improved the mechanical properties of both OPC and blended cement concrete. Improvements in compressive strength for specimens cured using water varied between 16% to 20% for different periods and maturity at testing. The amount of increase in compressive strength was also affected by the type of curing compound (Fattuhi, 1986). The efficiency of curing compounds measured in terms of compressive strength varied from 80% to 100%.

ACI 308-81 (1986) specifies prolonged curing periods for blended cement concrete in order to yield the equivalent strength of the corresponding OPC concrete. The minimum length of curing required for OPC and OPC+15%PFA to achieve identical strengths are 3.75 and 6.5 days respectively (Khan and Ayers, 1995). However, these findings depend on the temperature and mix proportions that were used in the production of the concretes.

Nisher (1986) and Tan and Gjorv (1996) studied the effect of water curing and sealed curing (using curing compounds) on properties of cover and the bulk concrete. It was shown that inadequate water curing has minor detrimental effects on the strength but it

can lead to a marked increase in the permeability and chloride penetration. Bentur and Jaegermann (1988 and 1991) studied the strength and permeability of concrete subjected to different curing regimes (i.e. hot, interrupted spraying of water and dry environment) and the findings were in agreement with those of Nisher (1986). The measured air permeability in OPC and blended concretes with 30%PFA and 50%GGBS decreased with prolonged moist curing (Hong and Pratt, 1989). Similar findings have been observed by Parrott (1992) by means of water absorption measurements.

The effect of curing on permeation properties, absorption, permeability and diffusivities has been widely investigated. Hansson et al (1985) and Kumar et al (1987) reported that chloride ingress in OPC and OPC/PFA pastes is affected by the period of water curing. They noted a significant reduction in the coefficient of chloride diffusion with increasing water curing period from 0 to 7 days. Ahmed (1990) studied the effect of OPC and OPC/PFA concretes exposed to a range of curing environments on chloride ingress. His findings confirmed the beneficial effects of prolonged water curing.

3.2.6 Concluding Remarks

The purpose of this literature review was to highlight the microstructure of concrete and its relationship with the properties of concrete. It has been shown that the microstructure of the surface zone is not yet fully understood, especially when concrete is subjected to different curing environments. It has also been revealed that, although a great deal of effort has been made to study how concrete performance is affected by different curing regimes, relatively few attempts have been made to characterize and determine the microstructure gradient of the cover concrete, CAZ. In this chapter, the above considerations are discussed in the light of the experimental results obtained.

3.3 EXPERIMENTAL PROCEDURES

Cylindrical cement paste specimens (75x49 mm) with different mix proportions (see Table 2.2b in Chapter 2) were cast and cured as described in Sections 2.4.1 and 2.5, respectively. After a specified curing period, the cement paste specimens were removed from their PVC moulds and the first 2 mm from the cast surface of the specimens was discarded by cutting with a diamond circular saw. Then up to eight 3.25-3.5 mm thick specimen discs were obtained from each specimen by cutting at progressive depths of 2-6, 6-10, 10-14, 14-18, 18-22, 22-26, 26-30 and 30-34 mm from the casting surface, as

shown in Figure 3.6. Disc specimens obtained at the same depth but from different cylinders were grouped together and used for the determination of %NEW, total and capillary porosity and effective chloride diffusion coefficient. The details of test techniques and experimental procedures are described in Section 2.6. The average %NEW and porosity were then calculated from triplicate specimens. The mean effective coefficient of chloride diffusion was determined using four disc specimens.

The work done in this chapter was carried out with cement pastes rather than mortars or concretes, so as to obtain accurate information regarding the CAZ, while avoiding possible interference from aggregates.

3.4 RESULTS AND DISCUSSION

3.4.1 Hydration

The degree of hydration of the cement paste plays a major role in controlling the microstructure of the system and it can be expressed by the amount of bound water (non evaporable water) present in the cement hydration products. Parrott (1986) found that there is a difference between the relative humidity (RH) within the concrete and the external environment. This means that when the concrete is subjected to a drying atmosphere the resulting moisture gradient can cause variations in the degree of hydration, i.e. variations in the non evaporable water present throughout the covercrete zone. This consequently leads to the formation of a hydration gradient (or CAZ) between the surface and a certain point within the concrete. The degree of hydration in the surface zone was determined in this study by thermo-gravimetric techniques to obtain the bound water, in terms of % non evaporable water which exists in the cement hydration products.

Figures 3.7 shows the percentage of bound water measured at different depths below the surface of OPC paste cured in water at temperatures of 22° C and 38° C. The curing conditions are listed in Table 2.3. It is shown that the degree of hydration, in terms of the percentage of bound water, increased with increasing water curing periods at both moderate and elevated temperatures. The degree of hydration also increased with depth below the surface of OPC specimens, except for specimens cured under E6 and E7. These variations diminish at a certain distance below the surface of OPC paste and can be regarded as the CAZ thickness.

It was estimated from Figure 3.7 that, at moderate temperature (22°C), the CAZ depths for 0, 3, 7, 28 day water cured OPC paste specimens are approximately 24, 20, 12 and 8 mm, respectively. The CAZ thickness appears to decrease with increasing water curing period. The thicknesses of the CAZ for specimens cured at elevated temperatures under curing regimes E5, E6, E7 and E8 were estimated to be 24, 24, 12 and 16 mm, respectively. These results suggest that the CAZ depth decreases with increasing water curing period at both moderate and elevated temperatures. It also appears that water curing at 38° C enhances the degree of hydration in the first 24 mm from the surface if specimens are compared with those specimens cured with water at 22° C.

It is apparent from Figure 3.7-b that the degree of hydration of the specimens cured with an interrupted regime (E8) was slightly higher than those cured in air for the same period of exposure (E5). On the other hand, the degree of hydration of specimens cured with an interrupted regime is less than that of specimens cured with continuous immersion in water (E6 and E7). This may be attributed to the insufficient period of exposure of the interrupted regime specimens to water and to the penetration depth of water into the surface zone.

The increase in the percentage of hydration with increasing water curing period at both moderate and elevated temperatures can be attributed to the prolonged period available for the hydration processes to occur before drying the specimens in air at 65% RH, when hydration is believed to cease (Parrott, 1986, and Patel et al, 1988). As a result of drying after different water curing periods, different RH gradients may be created between the surface and bulk cement paste. This leads to the formation of hydration gradients which in turn determine the thickness of the CAZ.

The increase in %NEW in the first 24 mm of OPC paste specimen when cured at 38° may be due to the increase in the rate of hydration at elevated temperatures. This increase diminishes at a certain depth from the specimen surface. Although, there is no supporting evidence in the literature, a possible explanation may be related to the temperature gradient created between the surface and bulk zones of the cement paste.

Figure 3.8 shows the effect of water/cement ratio on the degree of hydration (in terms of % NEW) for OPC cement pastes, cured in water at 22° C for 28 days. The results illustrate that a little change in %NEW with increasing w/c ratio from 0.40 to 0.7. It can also be seen that the CAZ depths appear to be the same for all three w/c ratios (about 4 to 8 mm).

The effect of cement type on the %NEW gradients of HCP cured in water (E4) for 28 days at 22° C is illustrated in Figure 3.9. It is shown that the degree of hydration of OPC and OPC/GGBS specimens are greater than those of OPC/PFA specimens. This is likely to be caused by differing hydration rates of the cement pastes. Furthermore, the difference between %NEW of OPC/PFA and OPC/GGBS may be caused by variations in the pozzolanic reactivity (Fraay et al, 1989). The CAZ for OPC, OPC/PFA and OPC/GGBS specimens cured in condition E4 are estimated from Figure 3.9 to be 8, 4 and 4 mm, respectively. It is clear from these estimates that the cement type has an insignificant effect on the CAZ thickness.

3.4.2 Pore Structure

The pore structure of the surface zone of HCP was investigated using a desorption technique. The desorption technique was considered to be a simple and successful technique as described in the literature for characterizing the total and capillary porosity of different mix proportions (Parrott, 1992; Ngala (1995); Ngala et al (1995) and Page and Ngala (1995). It was adopted in this study to obtain comparative results for the pore structure within the surface zone in order to estimate the CAZ thickness.

3.4.2.1 Total porosity

Total porosity gradients of OPC pastes, derived from desorption results, for different curing regimes are shown in Figure 3.10. It can be seen that the total porosity profiles of OPC specimens generally decrease with increasing water curing period. It appears that the effects of both 7 days water curing and 28 days water curing on total porosity are comparable. Total porosity tends to become constant at a certain distance below the surface of OPC paste specimens (beyond the CAZ). Thus, CAZ thicknesses were estimated as 20, 16, 16 and 8 mm for specimens cured in water for 0, 3, 7 and 28 days at 22°C, respectively. These CAZ values show similar trends to those found using thermo-

gravimetric techniques which showed that the thickness of the CAZ decreased with increasing water curing period.

Similar trends were observed for specimens cured at 38° C as shown in Figure 3.10-b, although the first few millimeters into the specimen showed a decrease in total porosity. No significant difference in terms of total porosity was noted between the specimens cured in air (E5) and those subjected to an interrupted curing regime (E8) and also between specimens cured in water at both moderate and elevated temperature. These results are, however, contrary to those reported by Cao and Detwiler (1995), where it was shown that water curing at an elevated temperature causes an adverse effect on the pore structure of OPC concrete specimens. From Figure 3.10-b, CAZ thickness can be estimated as; ≥ 32, 24, 20 and ≥ 32 mm, for specimens cured under regimes E5, E6, E7 and E8, respectively.

The overall reduction along the total porosity profiles (Figure 3.10) can be attributed to the occurrence of hydration gradients between the surface and bulk zones of the cement pastes as discussed in Section 3.4.1. Similarly, the reduction of total porosity in the first few mm of the specimens cured at 38° C may be caused by enhanced hydration near the surface.

The effect of water/cement ratio on the total porosity gradient of OPC cement pastes cured in E4 environment is demonstrated in Figure 3.11. It can be seen that the CAZ thickness is similar for all w/c ratios (about 4-8 mm), thus confirming the results obtained by thermo-gravemtric techniques (Figure 3.8). The results also showed that total porosity increased substantially (25%) when the w/c ratio increased from 0.4 to 0.7, whilist there was insignificant increase in total porosity when w/c ratio increased from 0.4 to 0.55.

The total porosity results of HCP shown in Figure 3.11 are in agreement with the work carried out by Ngala (1995) who investigated the total porosity of different well-cured pastes (OPC/PFA and OPC/GGBS) of different w/c ratios. He found that the amount of total porosity increase due to the increase in w/c ratio from 0.4 to 0.7, to be 33%. The increase in total porosity for the high w/c ratios specimens may be due to the evaporation of excess water producing a continuous open pore structure.

Figure 3.12 illustrates the effect of cement replacement materials on total porosity gradients of cement pastes cured in water for 28 days (E4). It can be seen that the CAZ depths for OPC, OPC/PFA and OPC/GGBS specimens are fairly similar (4-8 mm). These results are in agreement with the results obtained by thermo-gravimetric techniques which showed that the blended cements had no significant effect on the depth of the CAZ.

The paste specimens made with cement replacement materials (PFA and GGBS) produced coarser pore structures than the corresponding OPC pastes. These observations confirm the results reported by Ngala (1995) and Ngala et al (1995) which showed a slight increase in the total porosity of well-cured OPC/PFA and OPC/GGBS pastes compared to that of OPC paste. The differences in Portland and blended paste specimens in terms of total porosity may be attributed to the degree of OPC hydration and pozzolanic reactions.

3.4.2.2 Capillary porosity

Figure 3.13 shows the effect of different curing regimes at 22°C (E1 to E4) on the capillary porosity gradient of OPC pastes. It is shown that the capillary porosity of OPC paste specimens decreases with increasing water curing period and with increasing depth below the surface. The thickness of the CAZ can be estimated from Figure 3.13 as; 20, 20, 16, $\leq$ 4 mm for E1 to E4 curing regimes, respectively, which are in reasonable agreement with the corresponding trends estimated from NEW and total porosity results (Figures 3.7 and 3.10). These results signify that the development of the pore structure due to hydration, increases with increasing water curing period and the distance below the surface of the specimen.

The effect of cement type on the capillary porosity gradients of paste specimens exposed to 28 days water curing (E4) is demonstrated in Figure 3.14. There is a significant reduction in the capillary porosity gradients for OPC/GGBS paste specimens compared to those for Portland paste specimens, a finding which is in agreement with the results obtained by Ngala (1995) and Ngala et al (1995). The CAZ thicknesses, estimated from Figure 3.14, are approximately 4 mm for all OPC and blended paste specimens. These values indicate that the thickness of CAZ is unaffected by the use of

different cement replacement materials, which is in agreement with NEW and total porosity results shown in Figures 3.9 and 3.12, respectively.

The substantial decrease in capillary porosity for GGBS specimens compared to those of Portland specimens can be due to the pozzolanic reactions (Mehta and Gjorv, 1982 and Fraay et al, 1989). It is believed that the pozzolanic reaction products modify the microstructure by filling the unoccupied spaces within the paste matrix decreasing the amount of continuous pores (capillary porosity). The further reduction of capillary porosity in GGBS pastes compared to PFA paste may have resulted due to the fact that GGBS undergoes both hydration and pozzolanic reactions thereby producing a denser microstructure than other blended paste specimens.

3.4.3 Transport Properties of the Surface Zone

The effective chloride diffusion coefficient of HCP was determined in this investigation using a steady state technique. It was mainly adopted as a possible tool for characterizing the CAZ and also to study the relationship between the transport properties and pore structure of the surface zone.

The profiles of effective chloride diffusion coefficients (D_{cl}) of OPC paste specimens cured in different curing regimes (E4, E7 and E8) are illustrated in Figure 3.15. A worked example and summary of effective chloride diffusion coefficients data are given in Appendix 4. It can be seen that specimens cured in water at 22°C for 28 days (E4) exhibited a lower D_{cl} than the corresponding specimens cured in water at elevated temperature (E7), especially at the bulk. These results are however three times greater than the corresponding data reported by Ngala et al (1995). The difference between the results may be attributed to the different water curing periods used in the two studies. The D_{cl} of the specimens cured in continuous water curing (E4 and E7) was shown to be significantly lower than the corresponding specimens cured under the interrupted regime (E8). The difference in D_{cl} obtained for different curing regimes can be attributed to the effect of the curing on hydration and porosity of OPC paste.

It is also shown that the $D_{cl,}$ decreases with increasing depth below the surface of the specimen until a certain depth, upon which no further decrease in $D_{cl,}$ was observed. This depth can be considered to be the thickness CAZ and from Figure 3.15 it was

estimated as 16, 4 and 16 mm for specimens cured in E4, E7 and E8, respectively. However, these results are different to those estimated from %NEW and total and capillary porosity profiles. This may be due to further hydration during the diffusion process.

Figure 3.16 shows the relationships between effective chloride diffusion coefficients (D_{cl}) and the total and capillary porosity. It can be seen that the D_{cl} increase with increasing total and capillary porosity. Also, the correlation of D_{cl} with coarse capillary porosity suggests that all pores of diameters larger than 30 nm contribute to the mass transport properties. This relationship is close to that obtained previously (Ngala, 1995 and Ngala et al 1995), where it was suggested that as the capillary porosity approaches zero, the cement paste systems provide almost complete resistance to the diffusion of chloride ions.

3.5 CONCLUSIONS

1- The thickness of the microstructure gradient of cover concrete is significantly decreased with increasing period of water curing but is relatively unaffected by curing temperature, w/c ratio and the use of cement replacement materials.

2- The use of interrupted water curing at elevated temperatures did not cause any significant enhancement of the degree of hydration of OPC paste nor reduce the total porosity in the surface zone when compared with the effects of air curing. The use of interrupted water curing has also shown an adverse effect on the resistance of the surface zone against chloride ingress when compared with the effect of continuous water curing.

3- The results confirm that there is a significant correlation between the covercrete microstructure (total and capillary porosity) and mass transport (effective chloride diffusion coefficient) properties. The effective chloride diffusion coefficient was decreased owing to densification of the covercrete microstructure.

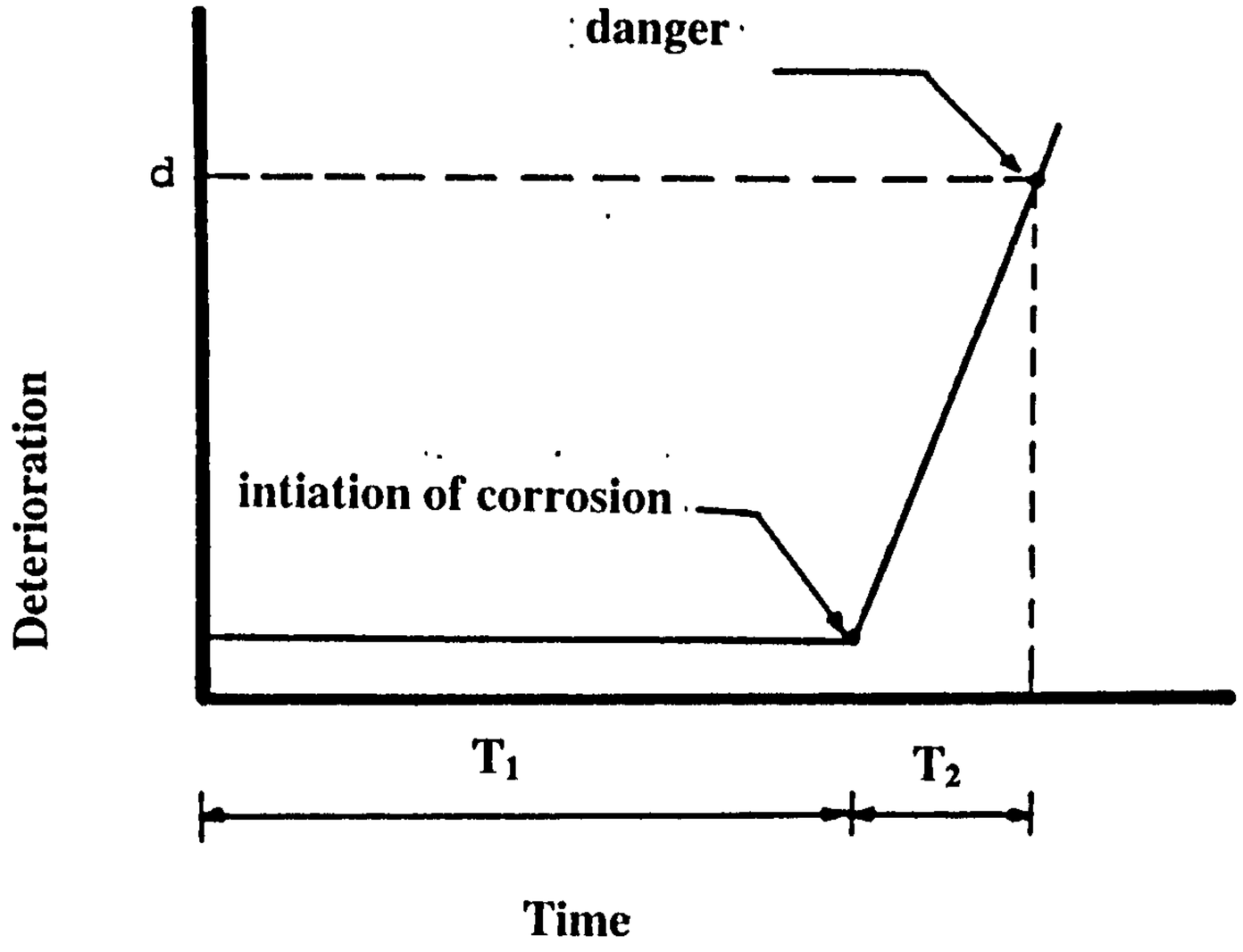

Figure 3.1 Time from exposure to significant deterioration due to steel corrosion (Tuutti, 1982).

Powers model

Gel	Capillary	Air voids
2.5	10 50	10 000 Pore diameter (nm)
Micro	Meso	Macro Air voids

Figure 3.2 Classification of the pore sizes for hardened cement pastes (Young, 1988).

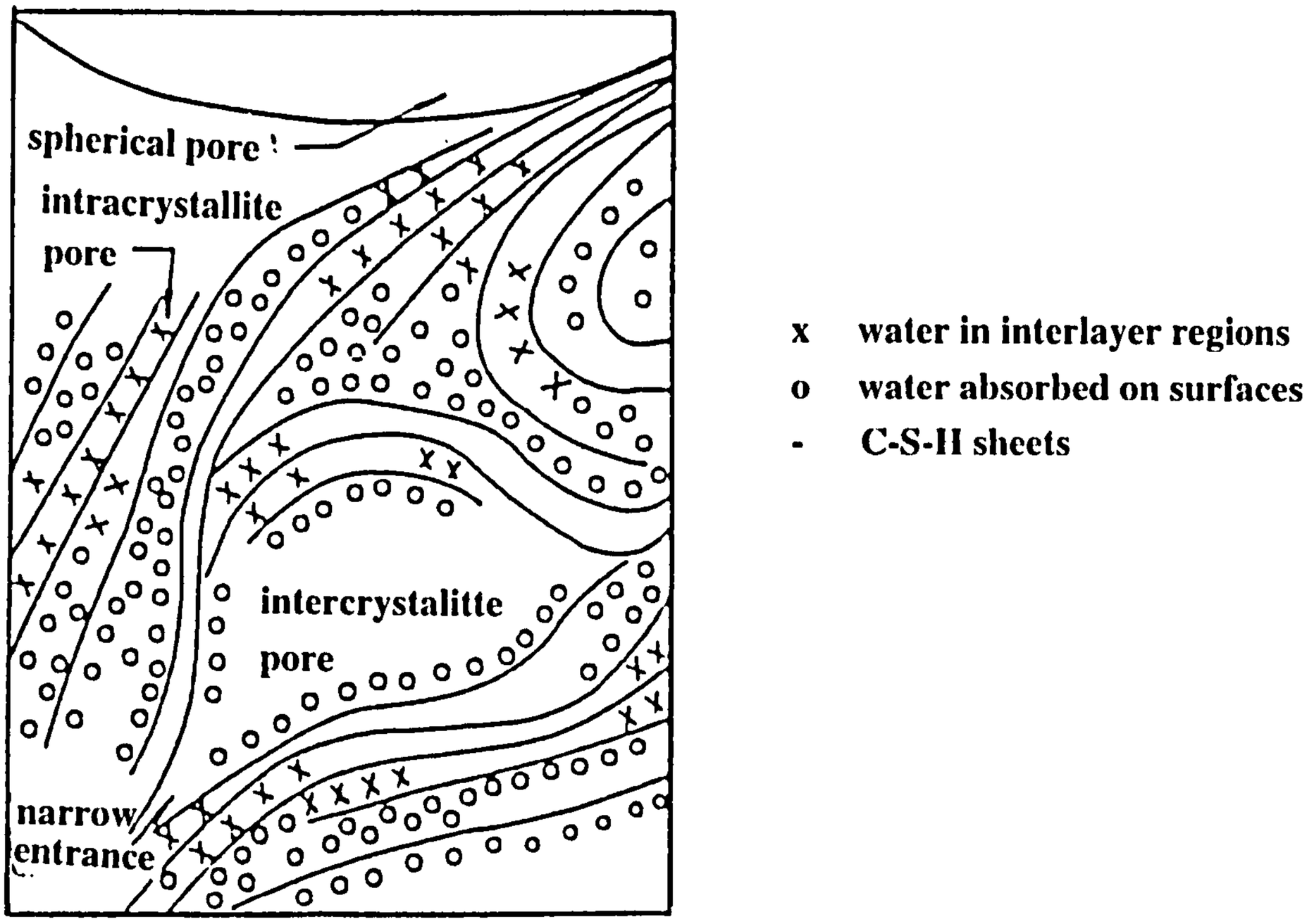

Figure 3.3 Feldman-Sereda model for the pore structure of the cement paste (Feldman and Sereda, 1970).

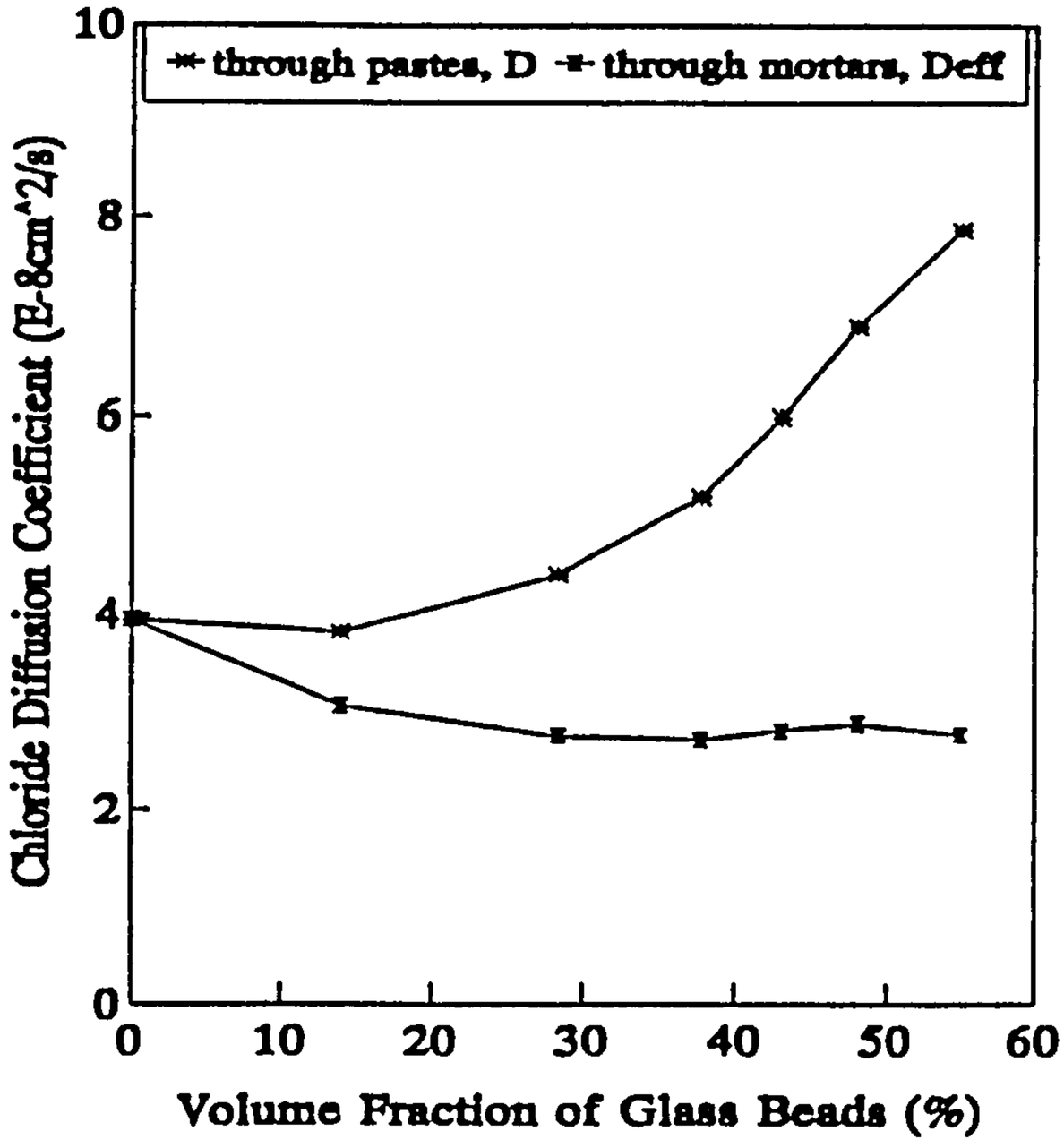

Figure 3.4 Chloride diffusion coefficient for pastes and mortars with varying volume fraction of glass beads (Ngala, 1995).

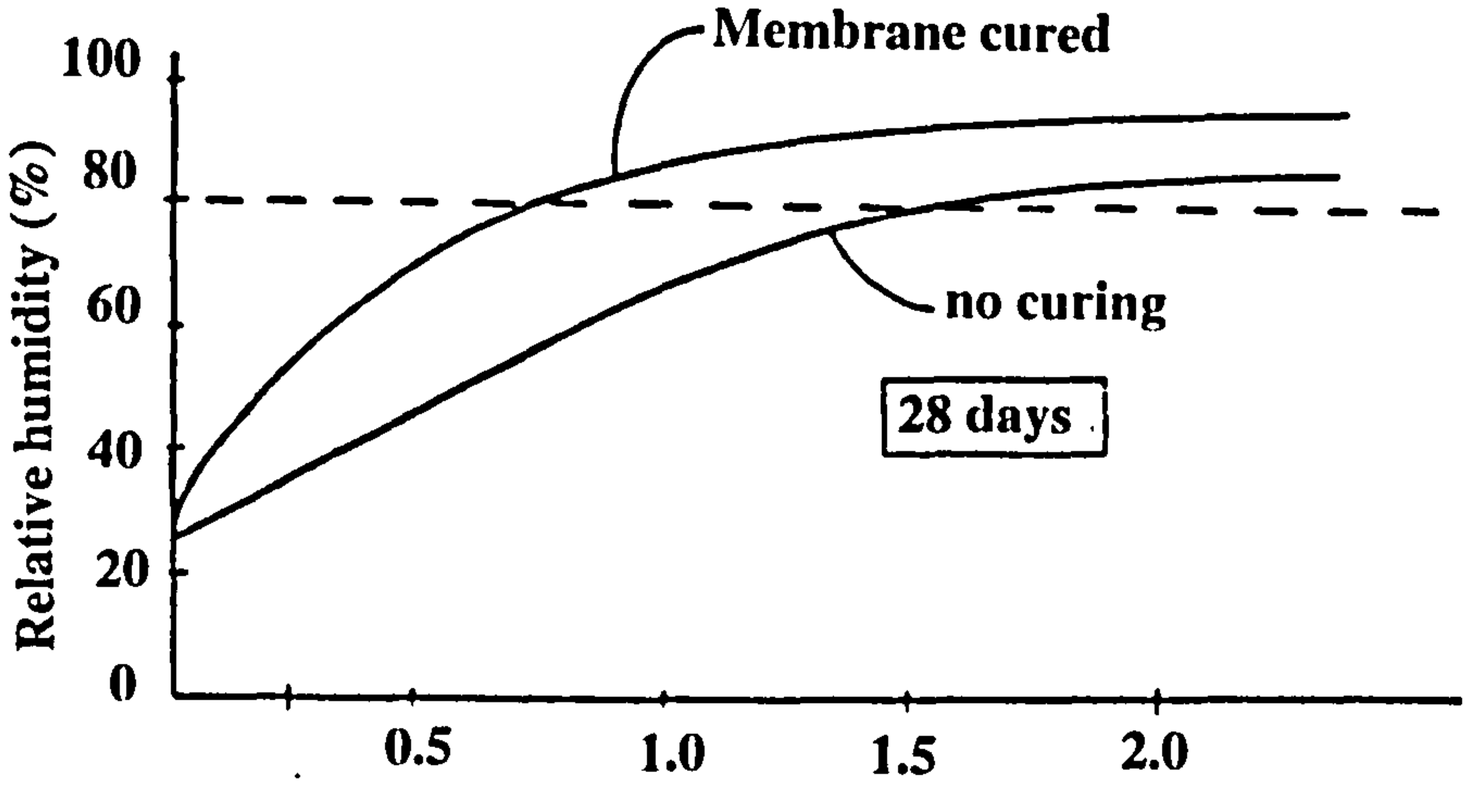

Figure 3.5 Relative humidity gradients of the concrete cured in air and membrane compound (Carrier, 1983).

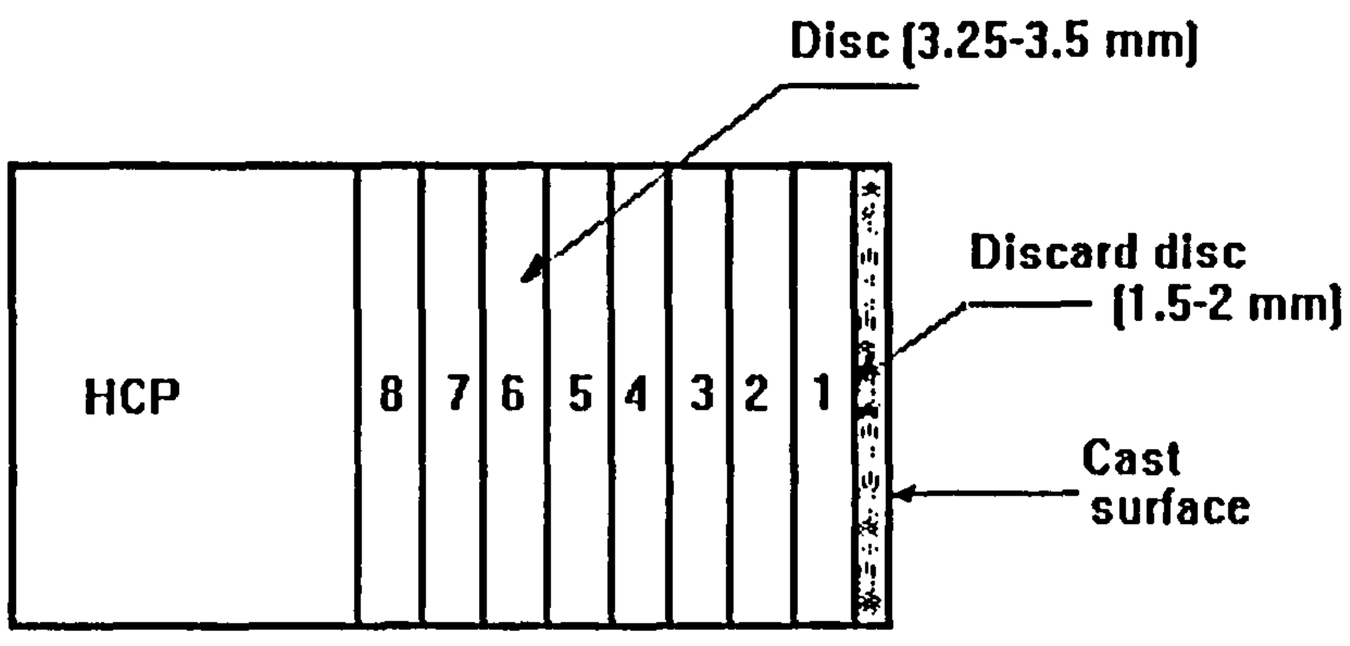

Figure 3.6 Cutting up arrangement for HCP specimen.

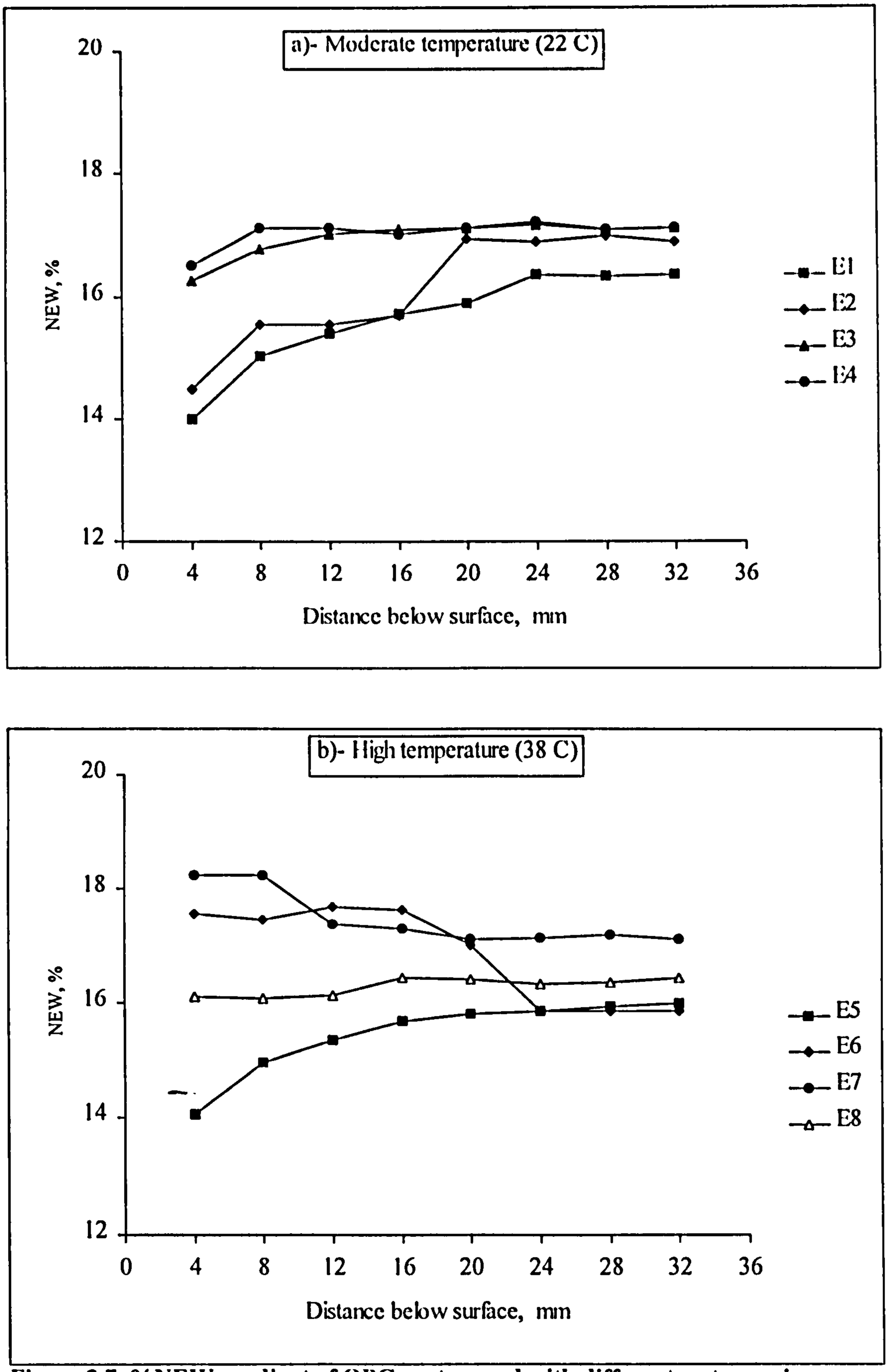

Figure 3.7 %NEW gradient of OPC paste cured with different water curing periods at a) moderate temperature (22°C) and b) high temperature (38°C), w/c = 0.55.

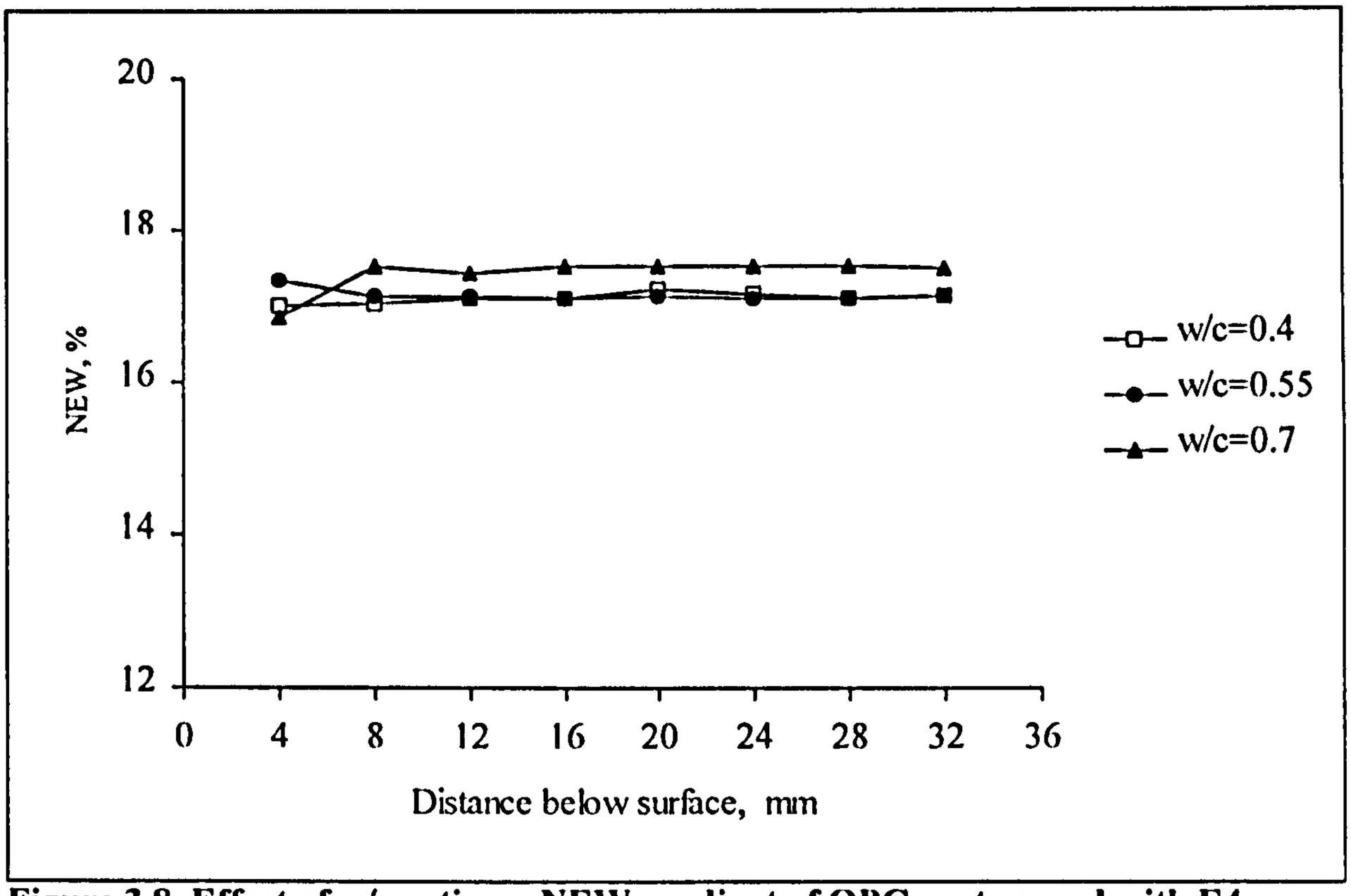

Figure 3.8 Effect of w/c ratio on NEW gradient of OPC paste cured with E4.

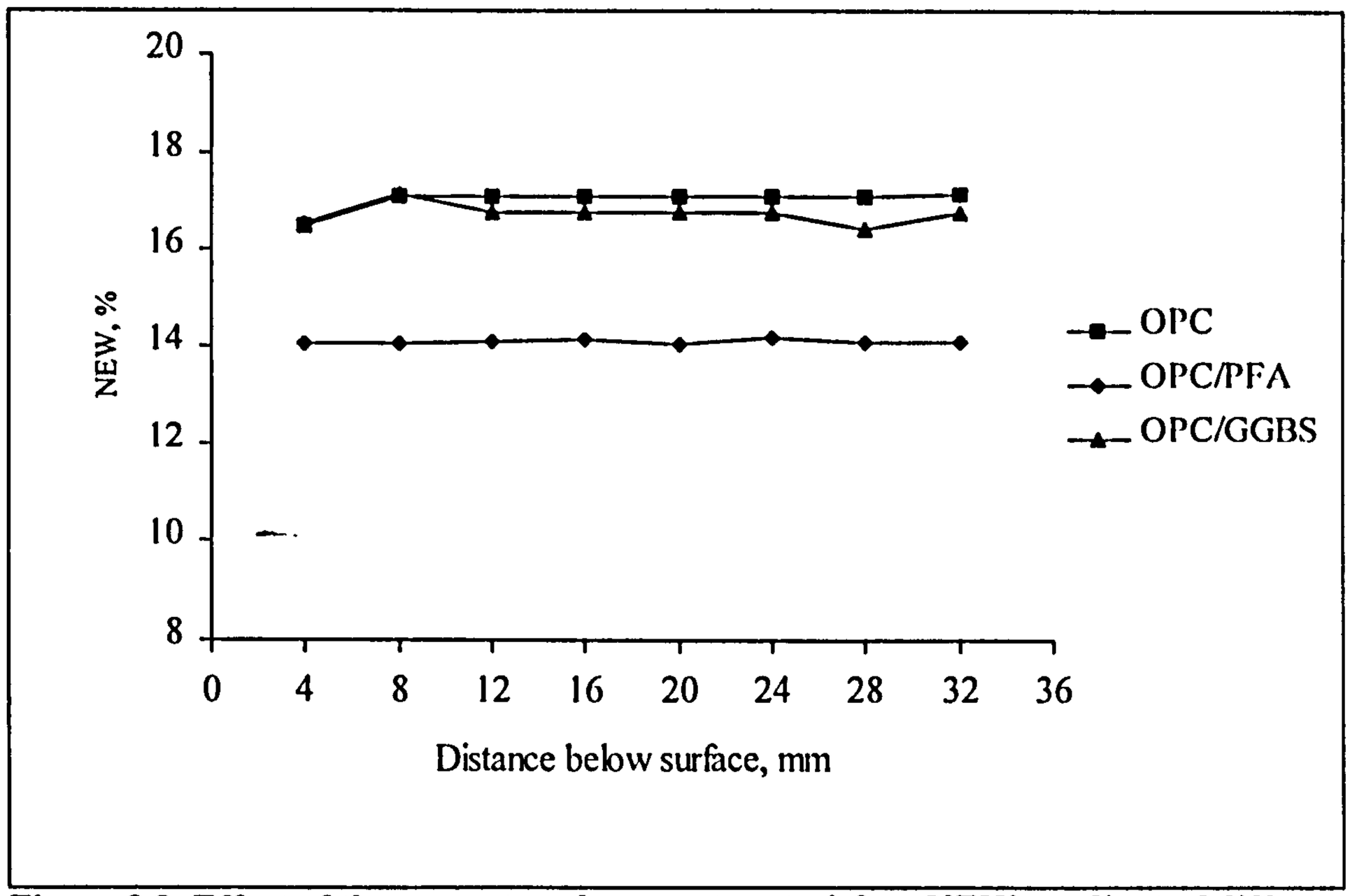

Figure 3.9 Effect of the cement replacement material on NEW gradient of different cement pastes cured with 28 days water curing (E4), w/c = 0.55.

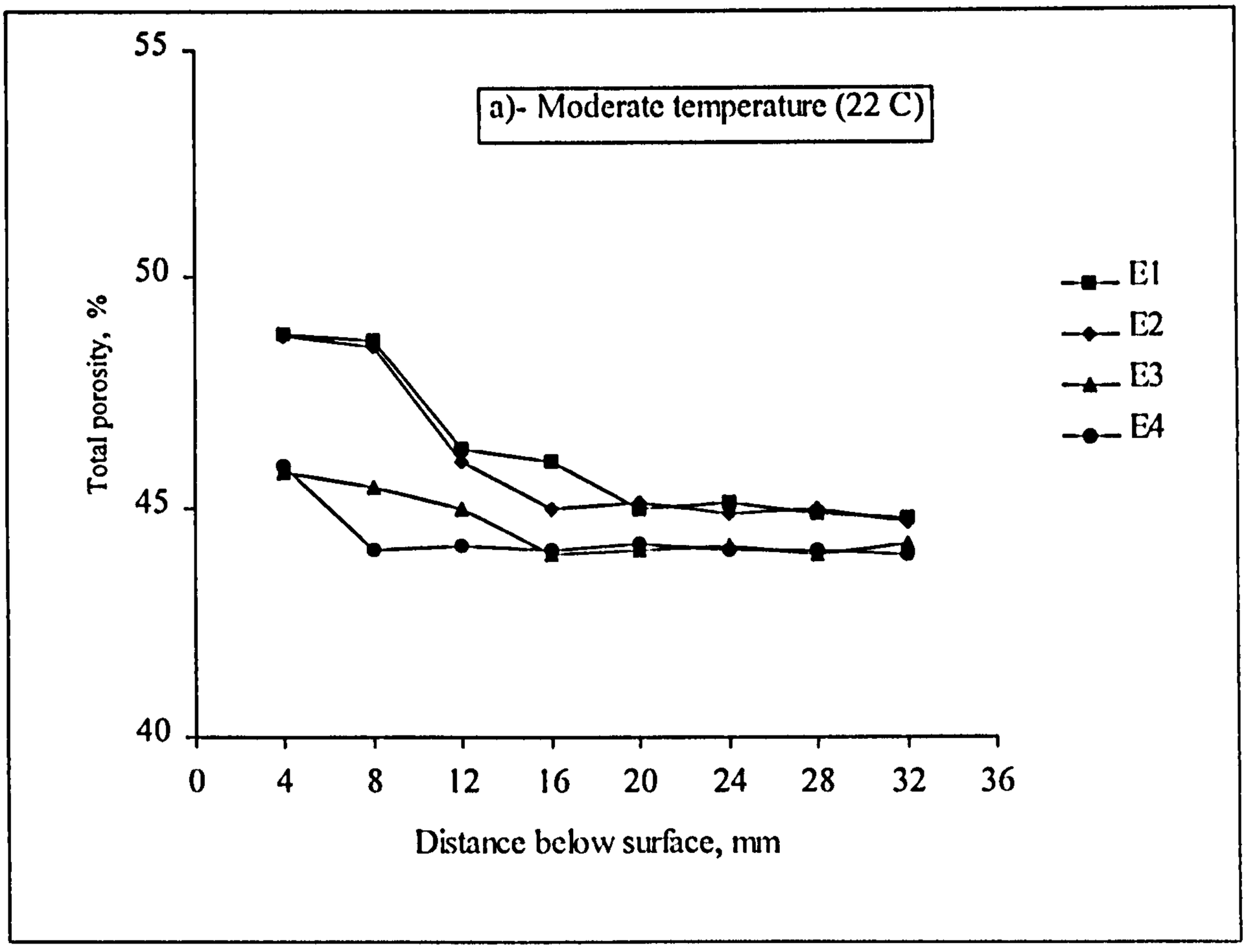

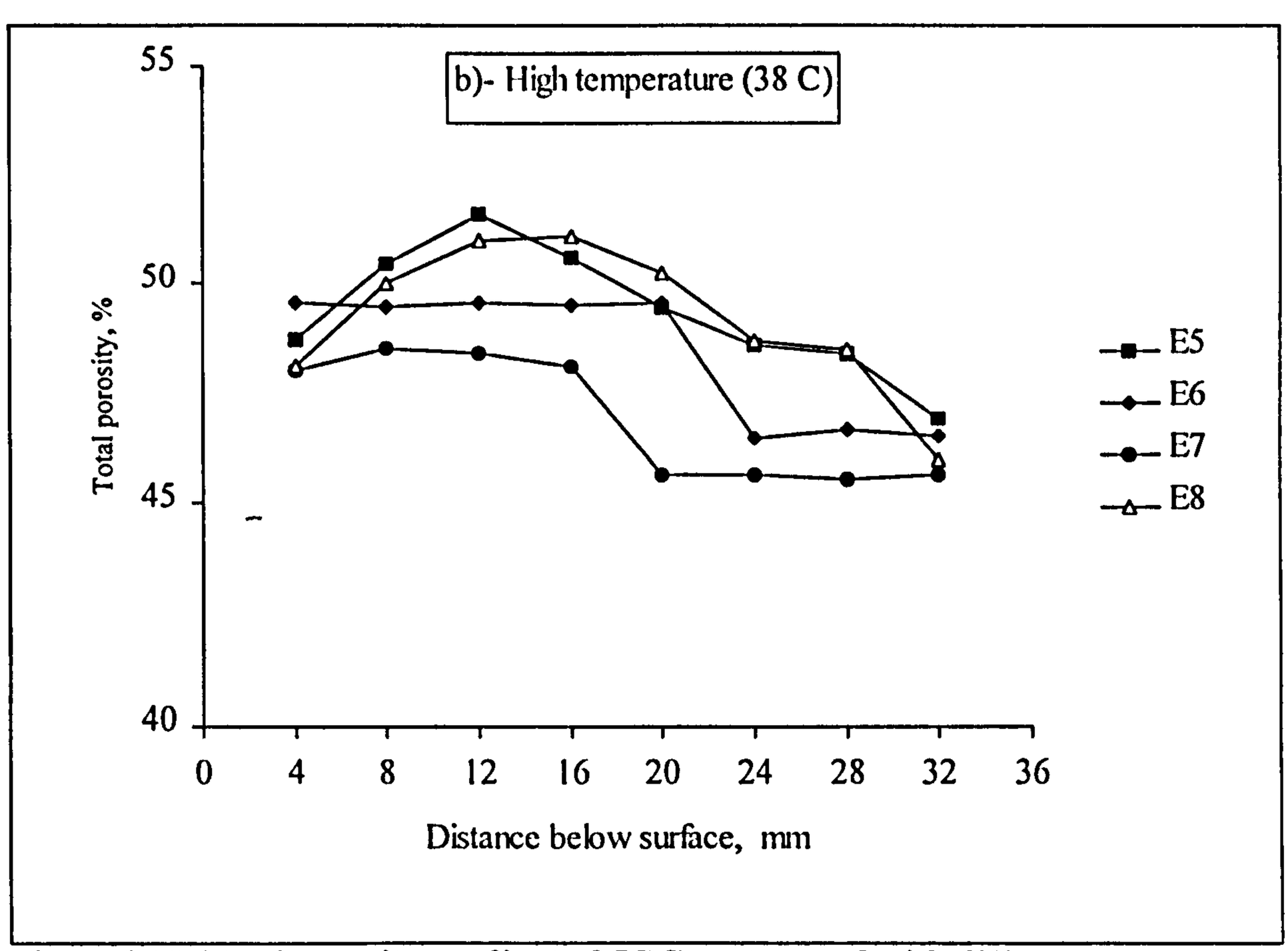

Figure 3.10 Total porosity gradient of OPC paste cured with different water curing periods at a) moderate temperature (22°C) and b) high temperature (38°C), w/c = 0.55.

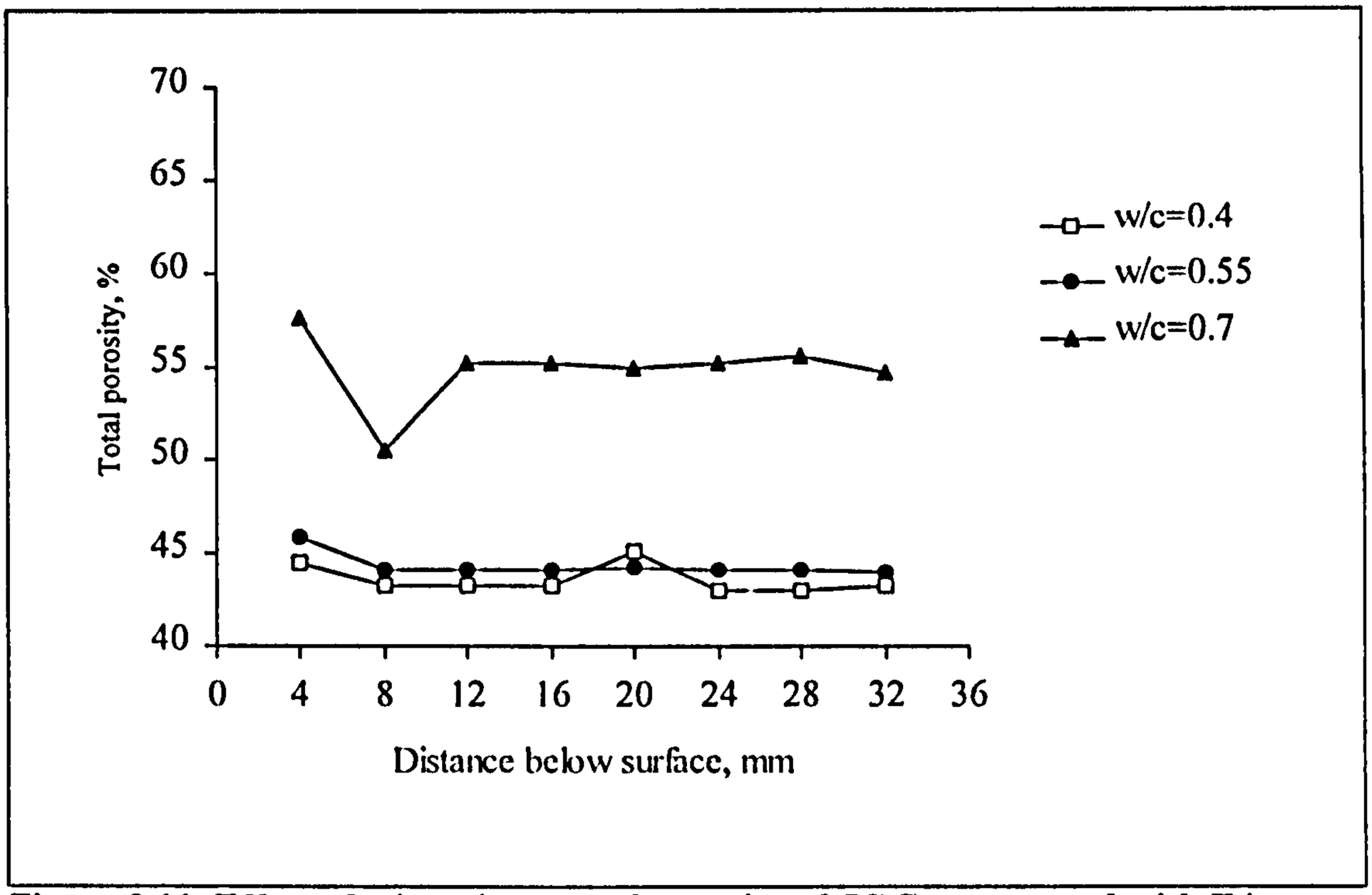

Figure 3.11 Effect of w/c ratio on total porosity of OPC paste cured with E4.

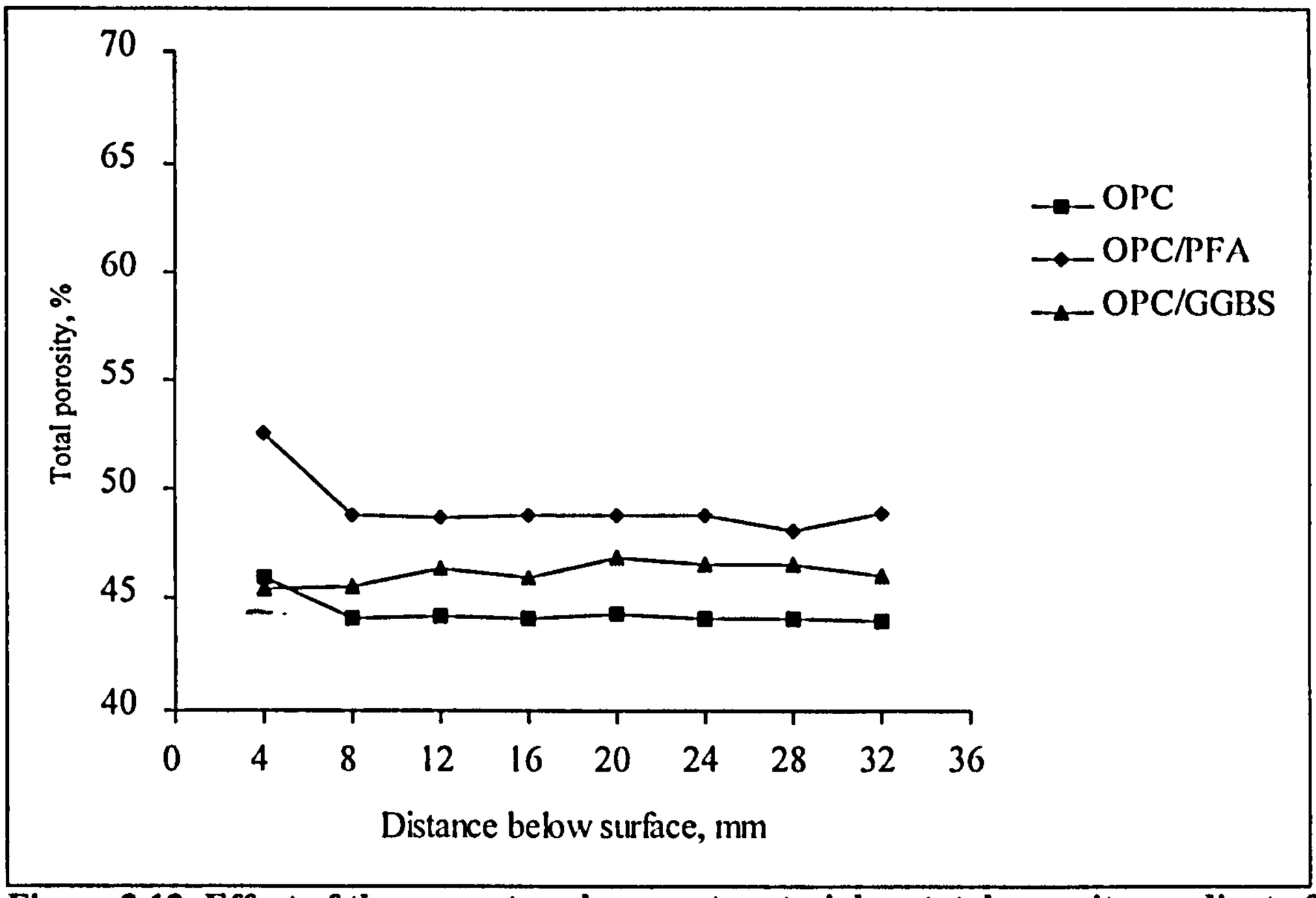

Figure 3.12 Effect of the cement replacement material on total porosity gradient of different cement pastes cured with 28 days water curing (E4), w/c = 0.55.

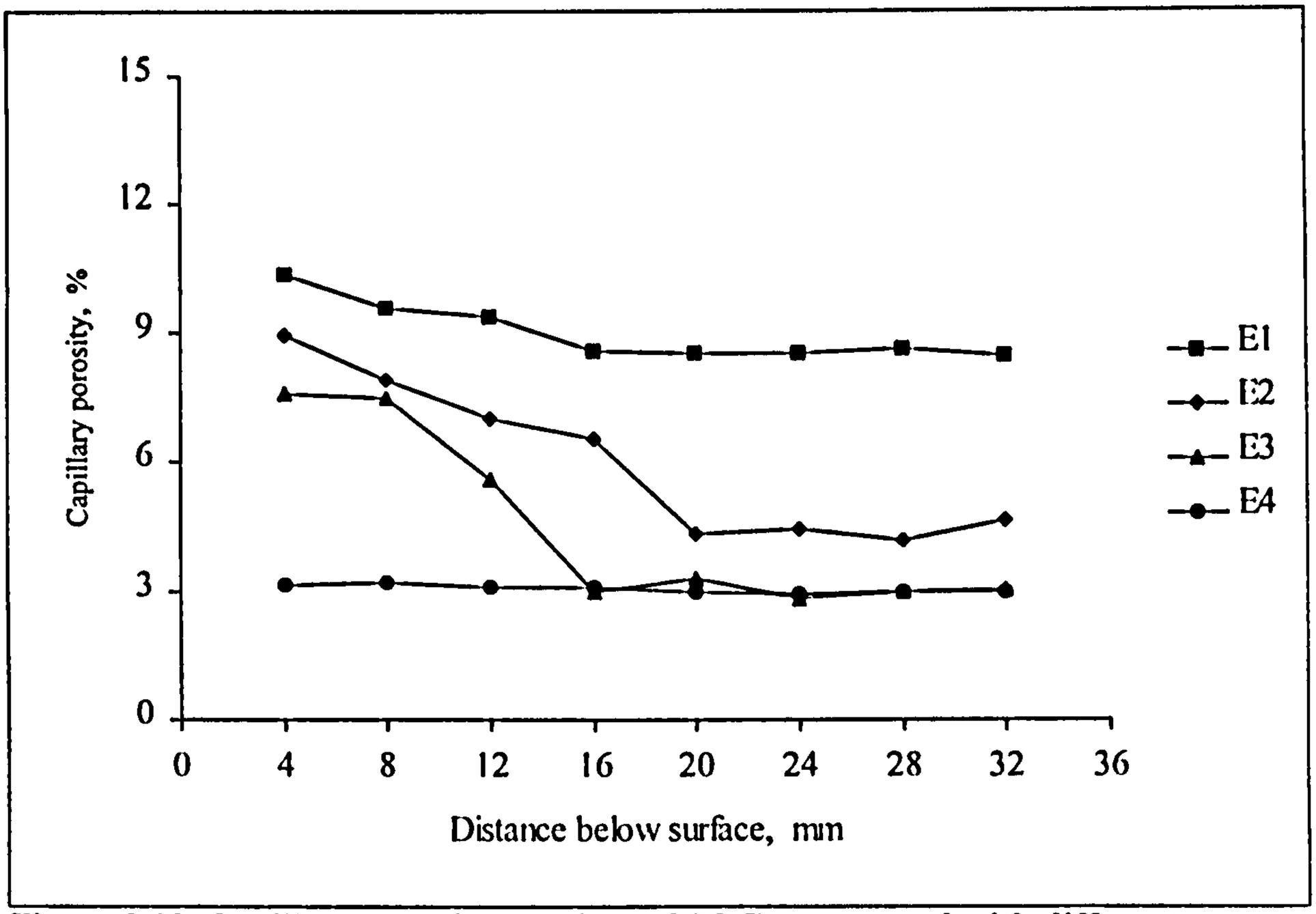

Figure 3.13 Capillary porosity gradient of OPC paste cured with different water curing periods at 22°C, w/c = 0.55.

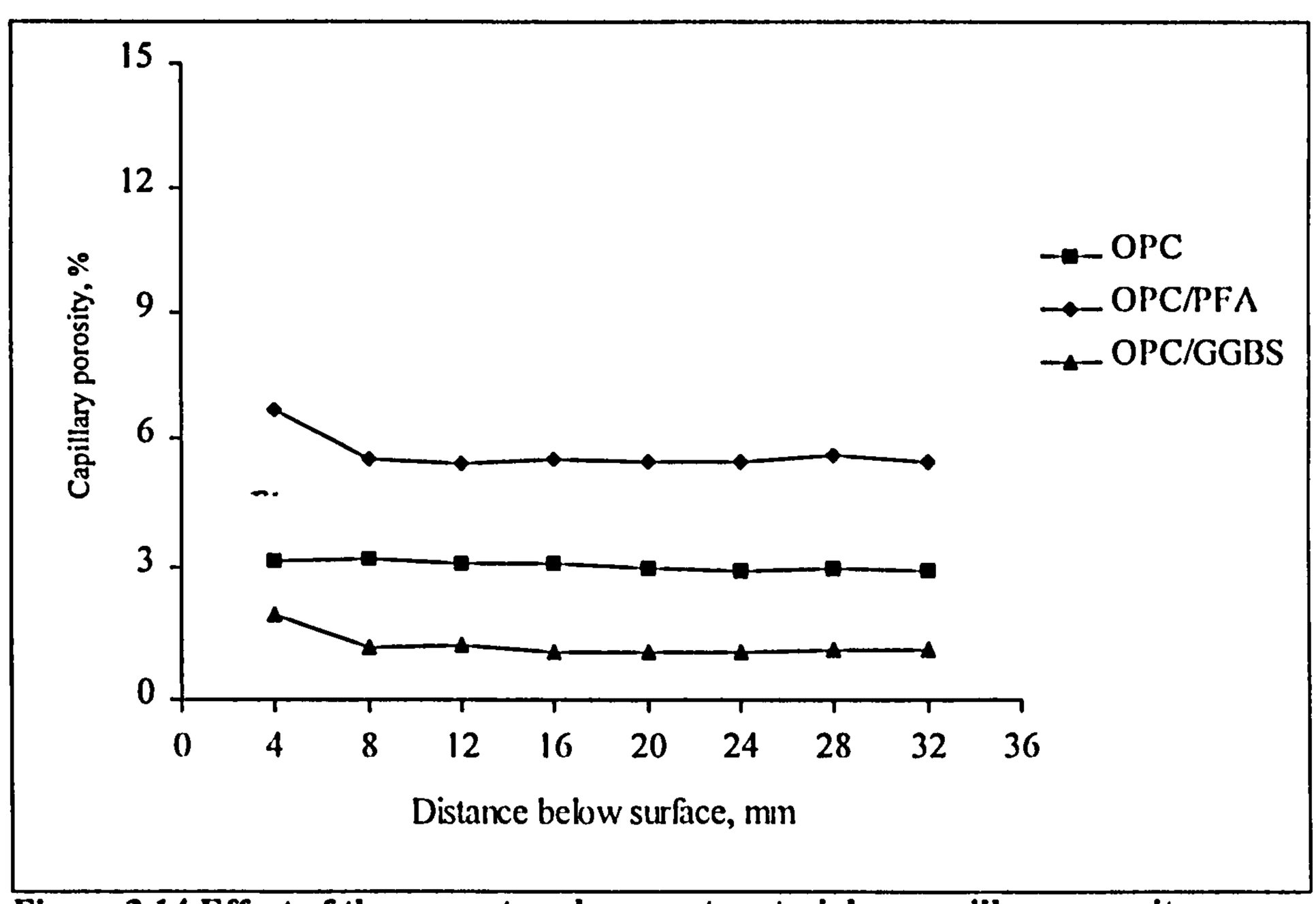

Figure 3.14 Effect of the cement replacement material on capillary porosity gradient of different cement pastes cured with 28 days water curing (E4), w/c = 0.55.

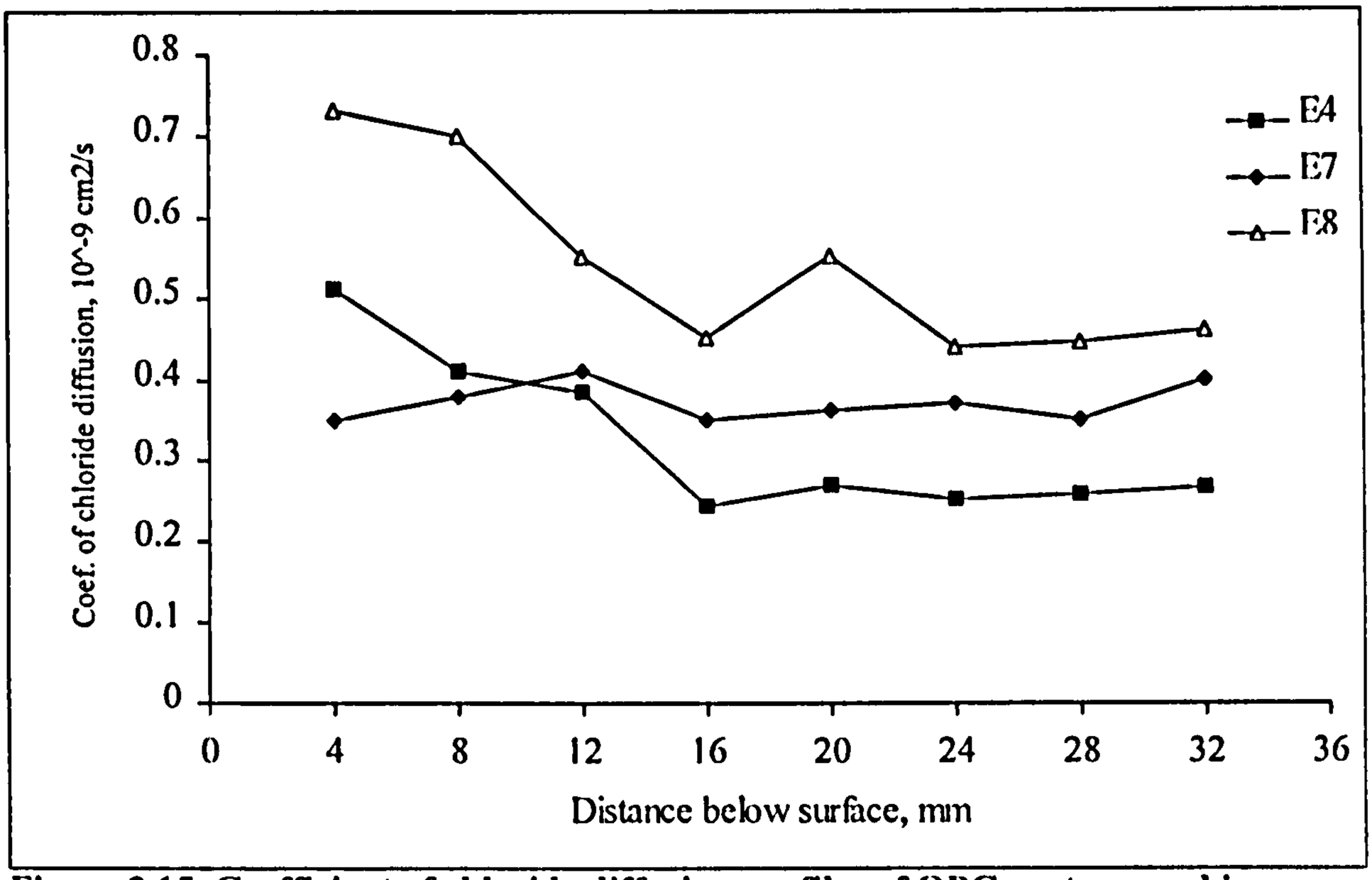

Figure 3.15 Coefficient of chloride diffusion profiles of OPC pastes cured in different curing regimes, w/c = 0.55.

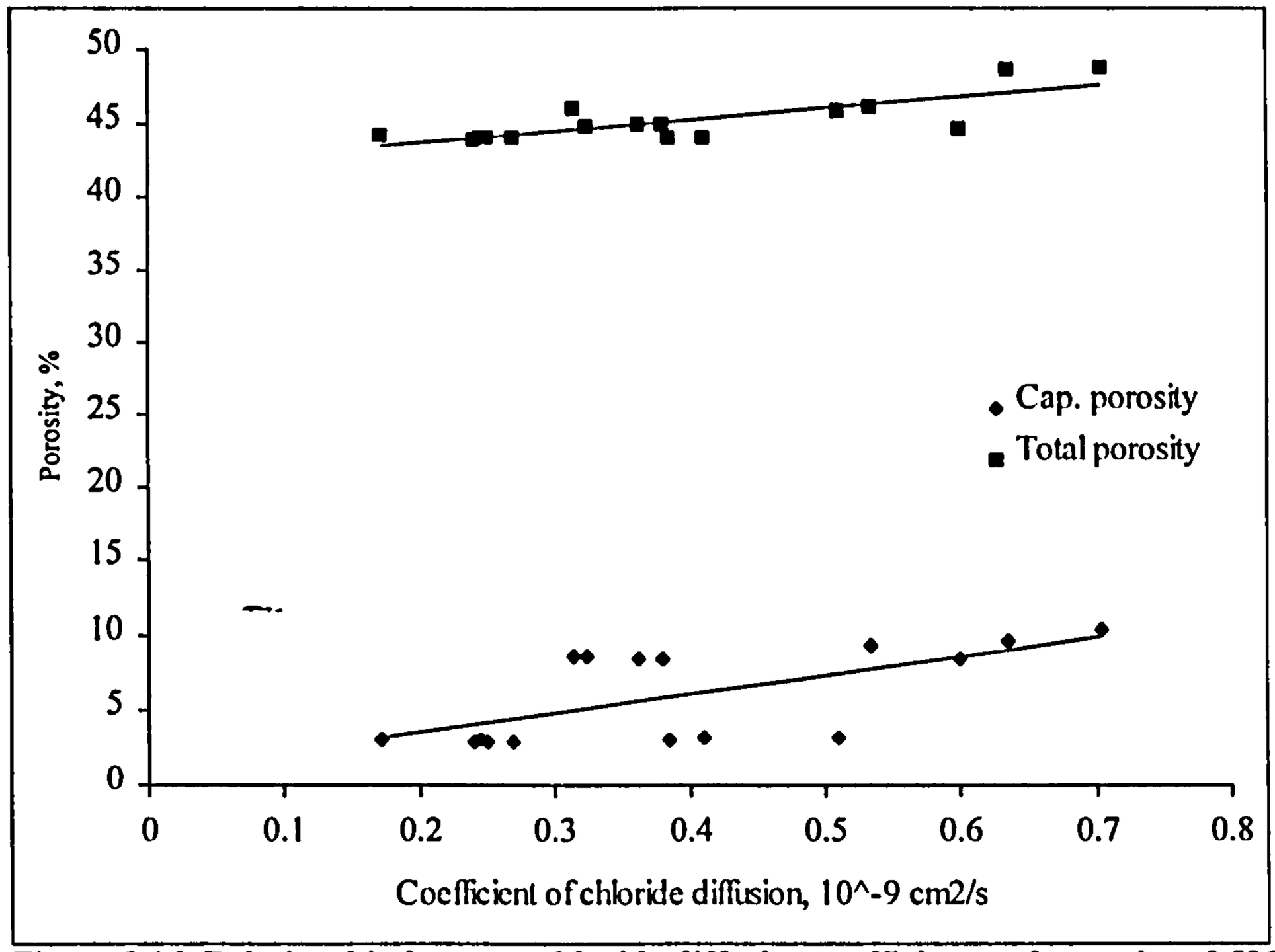

Figure 3.16 Relationship between chloride diffusion coefficient and porosity of HCP.

CHAPTER 4

MICROHARDNESS ANALYSIS OF THE SURFACE ZONE

4.1 INTRODUCTION AND LITERATURE REVIEW

Concrete technologists are interested in understanding the microstructure of cover concrete for two main reasons. First, to produce durable reinforced concrete by understanding the role of the microstructure in the development and modification of the mechanical and mass transport properties of concrete. Secondly, to assess residual durability of existing structures and to determine the service life of new structures. This requires a simple and effective technique which can define and quantify the concrete microstructure within the cover concrete.

There are many techniques available for characterising the microstructure of HCP, mortar and concrete. Some of the most widely-used techniques are MIP and sorption isotherm measurements (Section 3.2.1). However the main drawback of MIP and capillary condensation methods is the alteration of the original pore structure of the test specimen as a consequence of the process of removing pore water from the pores, i.e. the drying effect, (Feldman, 1972; Parrott, 1983 and Marsh and Day, 1985). In other techniques such as water permeability and absorption, the test specimen is exposed to water during the test and this can cause changes in the original pore structure of the cementitious material. These changes are mainly attributed to further hydration. Furthermore, most of the tests considered for the determination of concrete microstructure are time consuming.

To avoid the above-mentioned drawbacks, indentation microhardness and scratch hardness techniques were suggested to be used in this study as alternative methods for characterising the microstructure of the surface zone.

The microhardness of a material is obtained by calculating the ratio between the load applied to an indentor of prescribed shape and the impression area, in units of stress (Igarashi et al, 1996). This technique can be used successfully to estimate the denseness

of a cement paste system. Low microhardness values imply that the cement paste contains a high volume of pores.

Measurement of local variations in the pore structure of hardened concrete is possible by indentation microhardness and the approach has been used to characterise surface modified zones with distinct properties from those of the bulk material (Sadegzadeh, 1985; Sadegzadeh et al, 1987; Larbi, 1991 and Igarashi et al, 1996). Sadegzadeh (1985) and Sadegzadeh et al (1987) has used this technique to study the effect of surface finishing procedures on concrete microstructure. The results showed a direct relationship between the microhardness measurements and the porosity of the surface matrix. The microhardness technique has also been used to study the effect of w/c ratio on the microstructure of cement pastes made from OPC and OPC/10% silica fume (SF) (Igarashi et al, 1996). It was found that the microhardness increased with decreasing w/c ratio and when silica fume was used in the mix. The enhancement of the microhardness of specimens containing silica fume was attributed to the homogenisation of the microstructure, as the C-H is converted to C-S-H by the pozzolanic reaction.

Indentation microhardness testing is a widely used technique for characterising the aggregate/ cement paste transition zone of concrete (Bentur, 1991 and Larbi, 1991). It was shown that the technique can measure the variations at the transition zone (TZ) between the aggregate and cement paste matrix. Larbi (1991) has used microhardness measurements to study the effect of cement replacement materials such as PFA, GGBS and SF on the microstructure of the aggregate/cement paste transition zone (TZ). The results showed a significant improvement in the microhardness of the TZ due to the use of cement replacement materials. This improvement was attributed to the reduction of the bleeding and to pozzolanic reactivity at the interfacial region. Indentation microhardness was also used to investigate certain effects of electro-chemical chloride removal close to an embedded steel cathode, due to the pore solution changes in the surrounding concrete (Page et al, 1994). However, the technique is very time consuming because of the need to take large numbers of individual readings in order to obtain representative average values at various depths.

To provide a more convenient method of analysis, a scratch hardness test was devised at Aston University permitting rapid assessment of the variations in pore structure of cement paste and concrete. The main idea behind the use of this technique is to produce a permanent deformation (scratch) on the surface of the test material by means of a scratch bit with a constant applied load. The geometry of the scratch is then analysed using surface roughness and image analysis techniques. The geometry of the scratch is expected to be a function of the pore structure of the material (e.g. wider and deeper in porous material than in dense material). The development and the details of scratch hardness test procedure are described in Sections 4.2 and 4.3.2.2. The scratch hardness instrument was used in this study for characterising the microstructure of cement paste and concrete.

Scratch hardness is a technique widely used by mineralogists to classify the hardness of various rocks and minerals (West, 1989; Bhansali and Kattamis, 1990 and Berns et al, 1991). West (1989) used this technique for assessing the abrasiveness of the rocks for machine tunnelling applications. He found a good correlation between the scratch hardness measurements and grades of Moh's hardness scale.

The possibility of using this approach for friction measurements of adhesion sliding contacts was investigated by Nieminen et al (1989). He found that a scratch test was a useful technique for friction measurements of minerals of different compositions. This test was also used to study the effect of temperature on the hardness of alloys and the results showed that the technique was sensitive to such variations (Berns et al, 1991). Scratch hardness testing was also used for evaluating the soundness and integrity of material coatings (Kattmis et al, 1990; Hedenqvist et al, 1990; Bhansali et al, 1990 and Chalker et al, 1991). It was shown that the scratch data of the coatings were correlated well with the microstructural data obtained by optical and scanning electron microscopy (SEM). However, to the author's knowledge, there is no published literature regarding the application of this technique to concrete.

The main aim of this chapter is to assess the reliability of the scratch hardness technique as an indirect method for qualitative and quantitative assessment of the microhardness and microstructural properties of cement paste and concrete. It also investigates the potential of using microhardness and scratch hardness techniques in evaluating the

microstructure gradient (CAZ) of the surface zone, and the effect of embedded aggregates on microhardness and scratch hardness measurements using a glass bead/cement paste model.

4.2 SCRATCH HARDNESS TOOL

The main components of the scratch hardness instrument are as follows; 1) a sharp triangular tungsteon carbide scratch bit fixed at the bottom end of a steel rod weighing 125 g, 2) a vice to hold the sample on a platform which can be moved longitudinally and laterally on a horizontal plane, 3) a gear system to control the rate of longitudinal movement of the platform and 4) a micrometer to enable precise distance measurements between successive scratches. The steel rod holding the scratch bit is held in a frame fixed to the base of the apparatus such that it is free to move vertically. The weight imposed on the scratch bit can be increased by adding extra weights at the top end of the steel rod. The shape of the scratch bit was as shown in Figure 4.1. General views of the steel rod with the scratch bit and scratch hardness apparatus are shown in Figure 4.2 and 4.3, respectively.

The test involves positioning and clamping the specimen on to the platform which can be moved longitudinally at a given speed by means of a motorised system of gears. Then the scratch bit is lowered on to the test surface of the specimen and a scratch is induced by activating the movement of the specimen platform. The direction of the movement of the scratch needle is from B to b (Figure 4.1). Methods of analysis of the scratch are described in detail in Section 4.3.2.2.

4.3 EXPERIMENTAL PROCEDURES

4.3.1 Specimen Preparation

The HCP, glass bead model and concrete specimens were cast as described in Section 2.4 and subjected to different curing regimes as listed in Section 2.5. At the end of curing, cement paste specimens specified for the microhardness study were sliced longitudinally to obtain a sample of 75x49x12 mm using a circular saw lubricated with water. The test face of each specimen was then ground using 15 μm alumina powder and ethanediol lubricant for 10 minutes followed by 9 μm powder for another 5 minutes. The test face was then polished to 6 μm for 15 minutes and 1 μm for another 15 minutes using a Metaserv Universal Polisher and diamond paste.

In the same manner, a 100x60x12 mm slab specimen was taken for microhardness and scratch hardness tests from the centre of each 100 mm concrete cube. The test surface of the concrete was ground using 15 μm alumina powder for 3 hours followed by 9 μm powder for another 1½ hours. The concrete specimens were then polished, to 6 μm for half an hour and 1 μm for another half hour.

For glass bead model specimens, the test surface was prepared following the same procedures of grinding and polishing described above. The distance from test surface to the glass bead surface (Y) (see Figure 2.2) was varied for successive testing at different depths by subjecting the test surface to successive grinding and polishing procedures until reaching the required level above the glass bead.

4.3.2 Techniques

4.3.2.1 Indentation microhardness

The polished specimen was positioned under the microhardness tester (Micrometer 4) and the optical system provided within the microhardness instrument was focused to obtain a clear image of the specimen surface. The indentor was then positioned at the test point by moving the specimen platform using control knobs. A constant load of 100 gm was applied for 30 seconds to make an indentation on the polished surface of the specimen and the microhardness reading was recorded. All readings were taken at the central region and around the longitudinal centre line of the specimen, to avoid any variations near the edges. The space between any two adjacent indentations was always more than the last indentation diameter (> approximately 300 μm) to avoid overlapping. The test technique was described in detail in Section 2.6.7.

Twelve microhardness measurements were made at ≈ 0, 4, 8, 12, 16, 20, 24, 28 and 32 mm from the cast face of HCP paste. For glass bead model specimens, measurements were made at different distances above the glass bead (Y), 2, 1, 0.5, 0.25, 0.1, 0.05, 0.025 and ≈0 mm. Microhardness measurements were also made on the cement paste matrixes between the glass beads positioned 6, 12 and 24 mm apart. On concrete specimens, twelve microhardness measurements were made at 32 mm from the cast surface. The highest and the lowest microhardness readings were discarded and the

average of the ten remaining readings was calculated. The overall average microhardness was calculated from data obtained on duplicate specimens.

4.3.2.2 Scratch hardness

Scratch hardness tests were carried out on the specimens used for microhardness tests. The polished specimen surface was coated with black ink prior to the scratch test to enhance the contrast between the scratch and the background. The test specimen was positioned and clamped on to the platform, the scratch bit was lowered on to the test surface of the specimen and a scratch was induced by activating the platform to move at a constant speed of 1 mm/s. Extra dead loads of 100 gm and 550 gm were imposed on the scratch bit for cement paste and glass bead model specimens and for concrete specimens, respectively.

The scratches were drawn at ≈0, 4, 8, 12, 16, 20, 24, 28 and 32 mm from the cast surface of HCP and at 2.5, 1, 0.5, 0.25, 0.1, 0.05, 0.025 and ≈0 mm above the glass bead (Y) of the glass bead model specimens. For concrete specimens, scratches were drawn at 32 mm from the cast surface. The scratch bit was regularly replaced with a new one to avoid the possible effects of wear of the scratch bit. Duplicate specimens were tested for each case of study and the scratch geometry was then analysed by the following two methods.

a- Talysurf technique

The scratch depth was measured by analysing the scratched surface profile perpendicular to the scratch using a Talysurf 4. A detecting soft needle under a constant load was traced across the scratches, and the profile of the surface was analysed using a computer connected to the Talysurf equipment. A computer print out of the magnified surface profile allowed the determination of the scratch depth. Ten discrete readings of the scratch depth were obtained at 2 mm intervals along the scratch around the longitudinal centre line of the specimen. The average scratch depth for duplicate specimens was then calculated.

b- Image analysis

An optical microscope (Olympus) connected via a computer to an image analyser (Sight Systems Freelance), was used to measure the scratch width. The image analysis system

magnified the image of the scratch by 50 times, see Figure 4.4. Five discrete images along each scratch (1.875x1.875 mm) were obtained around the longitudinal centre line of the specimen. The scratch width was then measured on the duplicate specimens using the following methods.

Optical processing of the image

In this method, the edges of the scratch were defined visually on the computer screen and a perpendicular line was drawn manually between the two edges of the scratch image. On each image, five discrete measurements of scratch width, the perpendicular distance between the two edges, were taken and the average width for each image was determined. The overall average of the scratch width for the 10 images taken on the duplicate specimens was then calculated.

Computer processing of the image

This method is commonly used for analyses of maps and technical drawings in order to quantify patterns like lines, circles, ellipses, etc. The analyses of these patterns are carried out by automating the extraction of data by means of digital image processing to cover all the segments within the image (Taxt et al, 1985). This technique was used in this study as an alternative method for the determination of the scratch width.

The image produced by the microscope attached to the image analyser was formatted as a suitable greyscale image of 512x512 pixels and the redundant information was then removed before determining the width and area of the scratch. The edges of the scratch were first identified by analysing the brightness values inside and on the edge of the scratch using GRASS 4.1 program (Shapiro et al, 1993). Then the unwanted region outside the scratch was removed by taking further density slices leaving only the scratched area. The computer program then counted the number of pixels on both sides of the scratch and hence the number of the pixels contained within the scratch, to determine the scratch geometry in terms of scratch width and area. This produced 512 scratch width measurements for each image. This technique was applied to all images taken on duplicate specimens and a statistical analysis of the scratch width measurements of all images taken was then carried out. This allowed the relationship between the scratch width and the cumulative area of the scratch and then the distribution of the scratch width along the scratch length to be determined.

4.4 RESULTS AND DISCUSSION

4.4.1 Microhardness of the Surface Zone

The microhardness gradients of the surface zone of OPC pastes (w/c=0.55) cured with different regimes (see Table 2.3) are shown in Figure 4.5. The results emphasise the role of curing on the microhardness gradient of the surface zone. The microhardness of OPC specimens increased with increasing water curing period and increasing depth below the surface of the specimen up to a certain distance (CAZ). The estimated thicknesses of the CAZ were 20, 16, 12 and 4 mm, for specimens cured in E1, E2, E3 and E4, respectively. These values are in reasonable agreement with the results represented in Chapter 3 using thermo-gravimetry and desorption methods, which showed that the CAZ depths decreased with increasing water curing period.

The effect of water/cement ratio on the microhardness of OPC cement paste cured in water (E4) is presented in Figure 4.6. The results show that the microhardness of specimens decreased with increasing water/cement ratio. The amount of microhardness reduction reaches 40 % and 50% when the w/c ratio increased from 0.4 to 0.55 and from 0.55 to 0.7, respectively. On the other hand, the w/c ratio did not show a significant effect on the estimated thicknesses of the CAZ which were 8, 4 and 4 mm for specimens with 0.4, 0.55 and 0.7 water/cement ratio, respectively.

The relationships between microhardness and degree of hydration and porosity of OPC paste are presented in Figures 4.7 and 4.8, respectively. The results show that the microhardness of OPC paste specimens increased with increasing %NEW (a measure of the hydration products) and decreasing total and capillary porosity. This relationship elucidates the enhancement observed in the microhardness of OPC specimen at low w/c ratio and prolonged water curing. These results confirm that the pore structure has a major influence on the microhardness of the surface zone, as seen by other investigators (Sadegzadeh et al, 1987; Bentur, 1991, Larbi, 1991, Kholmyansk et al, 1994; Igarashi et al, 1996).

It can be seen from the results reported in Figures 4.5 to 4.8 that indentation microhardness is a useful tool for identifying the microstructural variations within the surface zone. However, it was noted that the technique is time consuming due to the

lengthy specimen preparation procedures, in terms of grinding and polishing. The reliability of this technique is also dependent on the number of individual measurements taken at each depth to give a representative average of the microhardness.

4.4.2 Scratch Hardness of the Surface Zone

4.4.2.1 Reliability of the scratch hardness tool

The scratch hardness test was used to evaluate the scratch dimensions (width and depth) for cement paste specimens with different water/cement ratios subjected to different curing regimes. The validity of this technique for hardened cement paste (HCP) was first studied and then the test was applied to concrete. All scratch width results shown in Figures 4.9 to 4.13 were determined by optical processing of the image as described in Section 4.3.2.2.

The effect of applied load on the scratch geometry for OPC paste is illustrated in Figure 4.9. It can be seen that both scratch width and depth increase with increasing applied load and the relationships appear to be linear. The relationship between the water curing period (22°) and scratch geometry of OPC cement paste show that both the scratch width and depth decrease with increasing water curing period (Figure 4.10). The relationships shown in Figure 4.11 illustrate that the scratch width and depth decrease with decreasing w/c ratio. The decrease in scratch width and depth due to prolonged water curing and decreasing water/cement ratio can be attributed to the improvement of the cement paste pore structure.

From Figures 4.9 to 4.11, it can be seen that the scratch technique is sensitive to the applied load, variations in the mix proportions of OPC paste (water/cement ratio) and curing conditions. It therefore indicates that this technique has the potential to be considered as an indirect method for the qualitative determination of the variations in the cement paste microstructure.

The validity of the scratch hardness technique for concrete was studied using OPC concrete specimens with different w/c ratio. The scratch width and depth increased with increasing w/c ratio, as shown in Figure 4.12. The significance of the scratch hardness results for OPC concrete was studied statistically using the t-test (Table 4.1). The statistical analysis confirms that the scratch hardness results for OPC concrete with w/c

ratio 0.40 and 0.55, and 0.55 and 0.70 are significantly different (P <= 0.05). Therefore, it is apparent that the scratch hardness tool has the potential for measuring microstructural variations in concrete.

Although both scratch width and depth provided useful indices of microstructural variations in the HCP and concrete, the analysis of scratch geometry in terms of scratch width was considered to be preferable. This may be attributed to the fact that the analysis of the scratch width using image analysis provided more information about the test surface, namely the presence of voids, cracks, unhydrated particles, small aggregate particles and the background of the scratch. This allowed the selection of positions unaffected by the above factors when taking measurements of the scratch width when the image was processed optically. In addition, the scratch width results were less dependent upon the roughness of the specimen surface than were scratch depth measurements.

The relationship between scratch dimension (width and depth) and the microhardness is shown in Figure 4.13. It can be seen that both scratch depth and width increase with decreasing microhardness of the cement paste. There is a linear relationship between microhardness and scratch dimension. This indicates the possibility of using the scratch hardness testing as an alternative method for measuring the microhardness of HCP. The use of the scratch hardness technique has the following advantages: 1) it is simple to use and inexpensive; 2) time required for specimen preparation is reduced; 3) scratch geometry can provide a continuous trace of microstructural variations along distance.

The scratch width and depth are plotted against the capillary porosity for OPC paste as illustrated in Figure 4.14. It can be seen that there is a significant increase in scratch width with increasing capillary porosity. The significance of this relationship can be used to understand the effect of curing and water/cement ratio on scratch hardness of the cement paste. It also highlights the potential of the scratch hardness measurements for characterising the HCP microstructure.

Automated extraction of data from technical drawings and images using digital image processing has become a practical tool during the last decade and is popular in extracting global curve segments of the studied image (Taxt et al, 1985). It was used in

this study for the following reasons: 1) to take advantage of the fact that computer processing covers all the segments of the scratch while the manual processing can miss out some data between the consecutive measurements; 2) to overcome the human errors which may result when defining the scratch boundary visually on the computer screen and determining the scratch width; 3) to study the reliability of manual analysis (optical) of scratch dimensions.

The results shown in Figure 4.15 were deduced by computer processing the scratch images and they present the relationship between the scratch width and the cumulative area of the scratch of OPC paste and concrete mixed with different w/c ratios. It can be seen that the scratch widths for OPC paste were more uniform than those for the corresponding OPC concrete. For both paste and concrete specimens, the average scratch widths calculated at 50% of the cumulative area of the scratch were close to the point of inflection of the curve. The range of scratch width results was within ± 10% and ± 15% of the average scratch width for OPC paste and concrete, respectively.

The differences found in scratch width distributions for HCP and concrete shown in Figure 4.15 may be attributed to the presence of aggregate. The exposed aggregate resulted in a reduction in scratch width measurements, especially at the lower end of the scale of scratch width.

Table 4.2 compares the scratch width results obtained via the optical (manual) and the computer processing methods of the scratch image for OPC paste and concrete with different w/c ratios. The average scratch width obtained manually did not coincide precisely with the corresponding results obtained by the computer processing method but, the average values of the optical (manual) results lay well within the range of scratch widths obtained by the computer processing method. The difference in the results may be attributed to the inability of the manual method to cover the entire scratch. However, this particular study has shown that the use of the optical method for analysing the scratch width gave results that were still reasonably comparable with the results obtained by the computer processing method.

4.4.2.2 Characterisation of CAZ using scratch hardness equipment

The potential of the scratch hardness test for characterisation of the microstructure gradient of the surface zone (CAZ) was investigated. Figure 4.16 shows the scratch width gradients of the surface zone of OPC pastes after exposure to different water curing regimes at 22°C. The results indicate that the scratch width decreased with increasing water curing period and increasing depth below the surface up to the limit of the CAZ. The thicknesses of the CAZ estimated from Figures 4.16 are 20, 20, 8 and 4 mm for specimens cured in E1, E2, E3 and E4, respectively. These results indicate that the thickness of the CAZ decreases with increasing water curing period.

The CAZ thicknesses estimated from the porosity (thermo-gravimetry and desorption), indentation microhardness and scratch hardness techniques are summarised in Table 4.3. It is apparent that the values estimated by the scratch hardness technique are in agreement with those estimated by the porosity and indentation techniques, except for the slight difference in the results noted for specimens cured with E3. An investigation undertaken using this approach for evaluation of the microstructural variations in cover concrete cast against different formwork types is described in Chapter 6.

4.4.3 Effect of Aggregate on Microhardness and Scratch Hardness Measurements

A cement paste specimen containing embedded glass beads was used in this investigation for modelling the effect of underlying aggregate on microhardness and scratch hardness measurements. Hardness measurements were made on the cement matrix at different distances above the glass bead (Y) and the results are presented in Figure 4.17. It can be seen that the microhardness is decreasing with increasing distance above the glass bead up to a certain distance (≈ 0.1 mm) and then it stabilises despite increasing distance above the glass bead. Similarly, both scratch depth and width increased with increasing distance above the glass bead (Y) up to about the same distance (≈0.1 mm) before becoming stable. This means, both microhardness and scratch hardness results are only influenced by the presence of the underlying aggregate if the aggregate particles are located close (0 to 100 μm) to the test surface.

The microhardness and scratch hardness measurements of the cement paste located between the glass beads embedded at different spacings were also studied as illustrated in Figure 4.18. It can be seen that the glass bead spacing had no significant effect on either microhardness or scratch hardness results. The other variables such as curing regime, w/c, aggregate texture and shape, should be considered in a further study to give a comprehensive clarification of the role of underlying aggregate particles on microhardness and scratch hardness measurements.

The use of the scratch hardness technique for characterisation of the TZ between aggregate particles and the cement paste matrix was investigated. It was noted that the measured scratch widths in the first 200 μm from the aggregate surface were scattered and not significantly different from those noted in the bulk. The inconsistency of the scratch hardness results in the first 200 μm may be attributed to the resistance imposed upon the movement of the scratch bit at the edge of aggregate particles.

The difficulty of using the scratch technique for characterisation of the TZ may also be attributed to the geometrical shape of the scratch bit used, which was not appropriate for measuring the TZ according to the work done previously by Bentur (1991) and Larbi (1991). They found that the thickness of the TZ varies from 20 to 100 μm. These values are small compared with the size of scratch bit. The geometrical shape of the scratch bit could however be subjected to a further modification for measuring such variations.

4.5 CONCLUSIONS

The main findings of this part of the investigation can be summarised as follows:

1- There is a good correlation between the surface zone microstructure (total and capillary porosity) and the degree of hydration and microhardness. The indentation microhardness appears to be a reliable technique for qualitative determination of the microstructure and microhardness gradients of the cover concrete.

2- The scratch hardness technique could be considered as a simple and an effective indirect method for the evaluation of cement paste and concrete hardness and a possible alternative technique to the indentation microhardness.

3- It has been shown that the scratch hardness technique is capable of producing valuable information with regard to the microstructure of cement paste and concrete. The determination of scratch geometry in terms of scratch width is more convenient and appears to be more reliable than the scratch depth approach.

4- Although there was some discrepancy between manual and computer processing methods of analysing of the scratch width, both analytical techniques were effective in identifying variations in the pore structure as indicated by the scratch width.

5- The use of the scratch hardness technique was also effective in the characterisation of the hardness and the porosity of the surface zone (CAZ). The equipment has the potential to be improved to increase its sensitivity to detect certain variations, such as properties of the aggregate/cement paste transition zone.

6- There is a significant effect of the underlying aggregate on the microhardness and scratch hardness measurements when the aggregate surface is less than 100 μm below the test surface. On the other hand, the aggregate spacing does not show any significant effect on these measurements.

Table 4.1 Summary of the statistical analysis of scratch hardness results of OPC concrete mixed with different w/c ratios, using t -test.

W/C ratio	Mean, μm	Variance	standard deviation	Variation, %	t	P(T<=t) two tail	Significance of the difference
0.40	412.0	2803.1	52.94	12.8	-2.3	0.0234	significant
0.55	576.6	2761.6	52.55	9.12			
0.55	576.6	2761.6	52.55	9.11	-1.9	0.0459	significant
0.70	642.0	7560.5	86.90	13.5			

Table 4.2 Scratch width results obtained by the manual and computer processing of the scratch image of OPC paste and concrete.

W/C ratio	Specimen type	Scratch width, μm		
		Range	Computer processing average	Manual average
0.4	paste	312-508	400	498
	concrete	310-612	450	412
0.7	paste	945-1335	1150	1135
	concrete	562-861	730	642

Table 4.3 Summary of CAZ of OPC pastes cured with different regimes, using different techniques.

Technique	CAZ, mm			
	E1	E2	E3	E4
1- Thermo-gravimetry	24	20	12	8
2- Desorption (capillary porosity)	20	20	16	4
3- Indentation microhardness	20	16	12	4
4- Scratch hardness	20	20	8	4

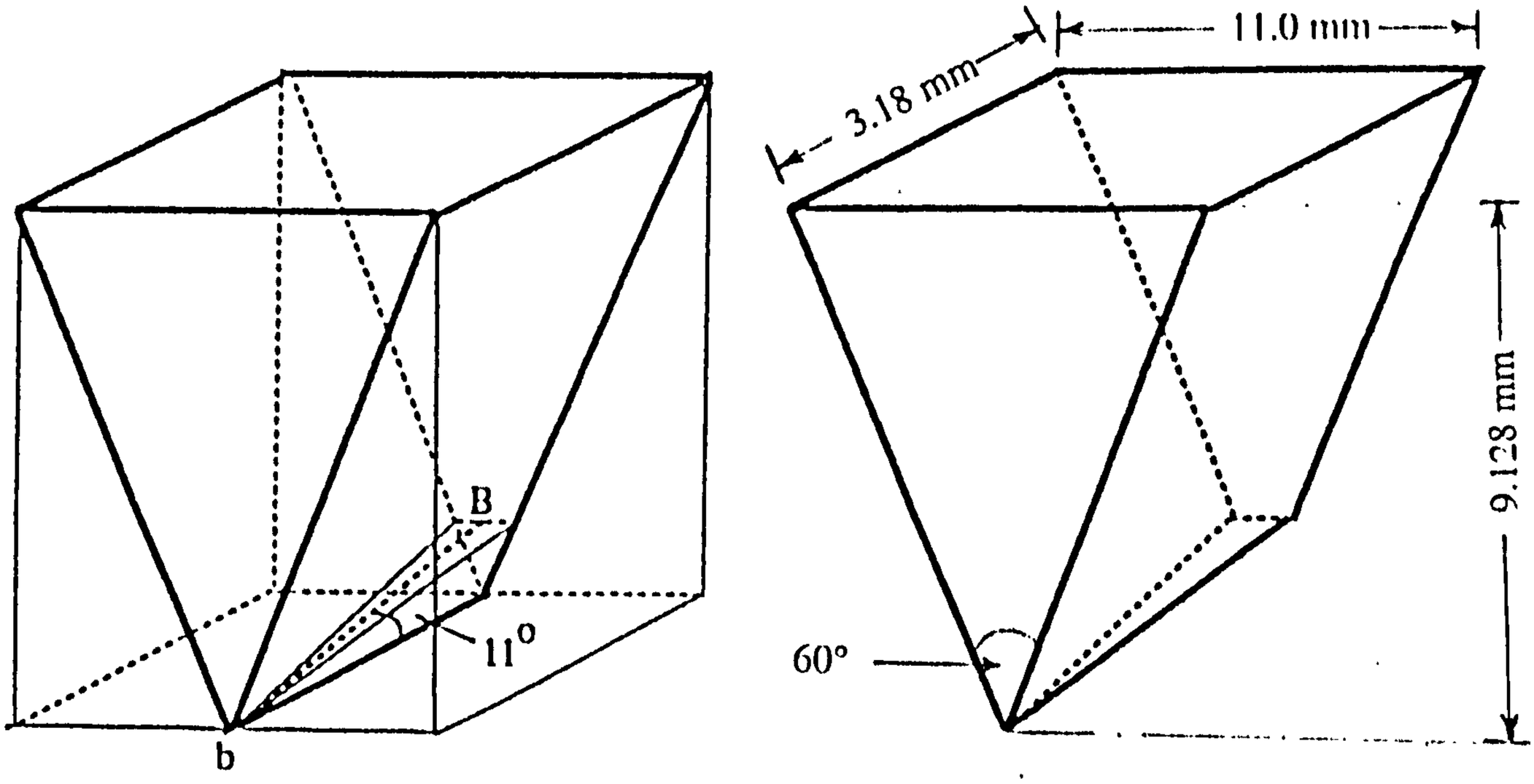

Figure 4.1 Geometrical details of the scratch bit.

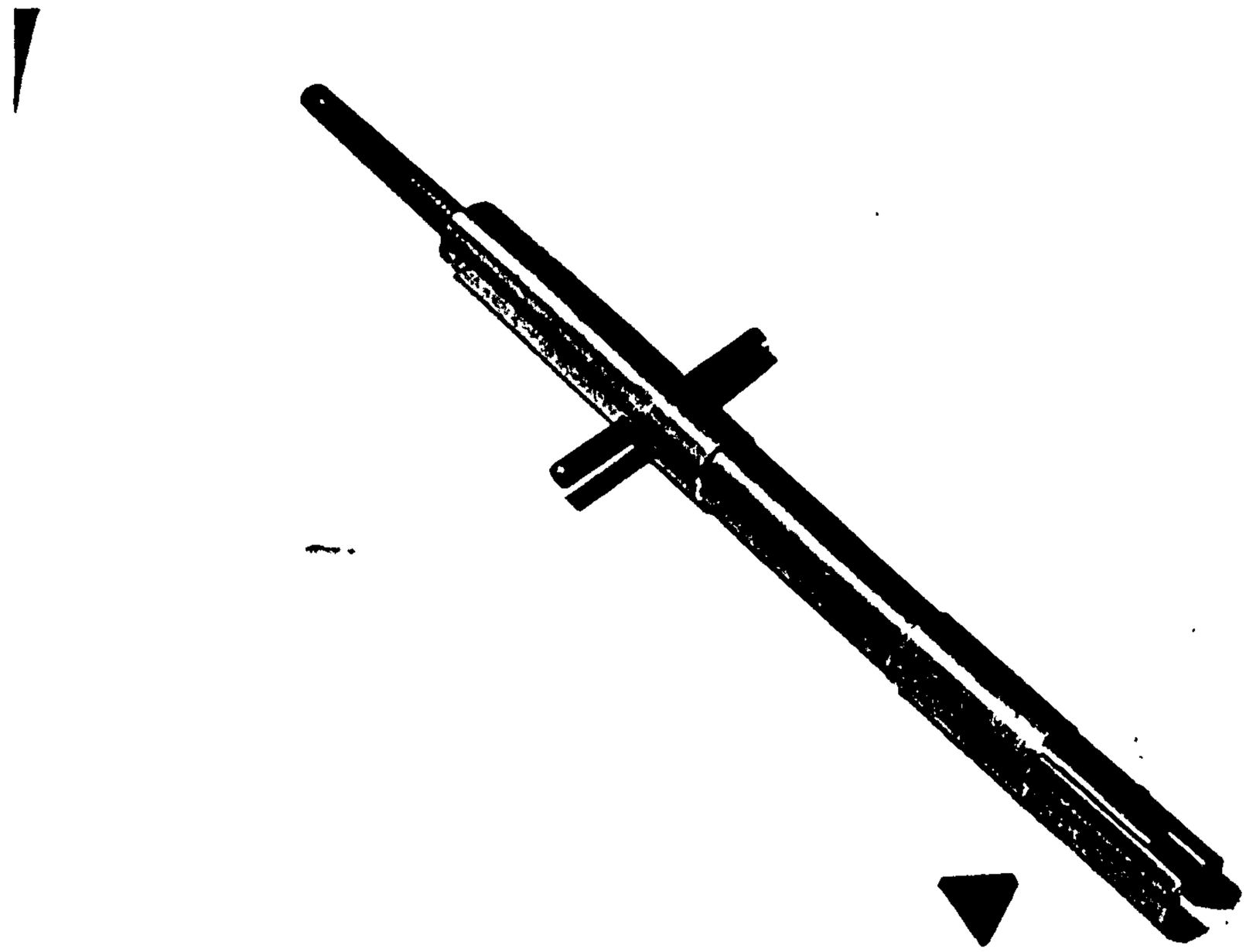

Figure 4.2 General view of the steel rod and the scratch bit used in the scratch hardness technique.

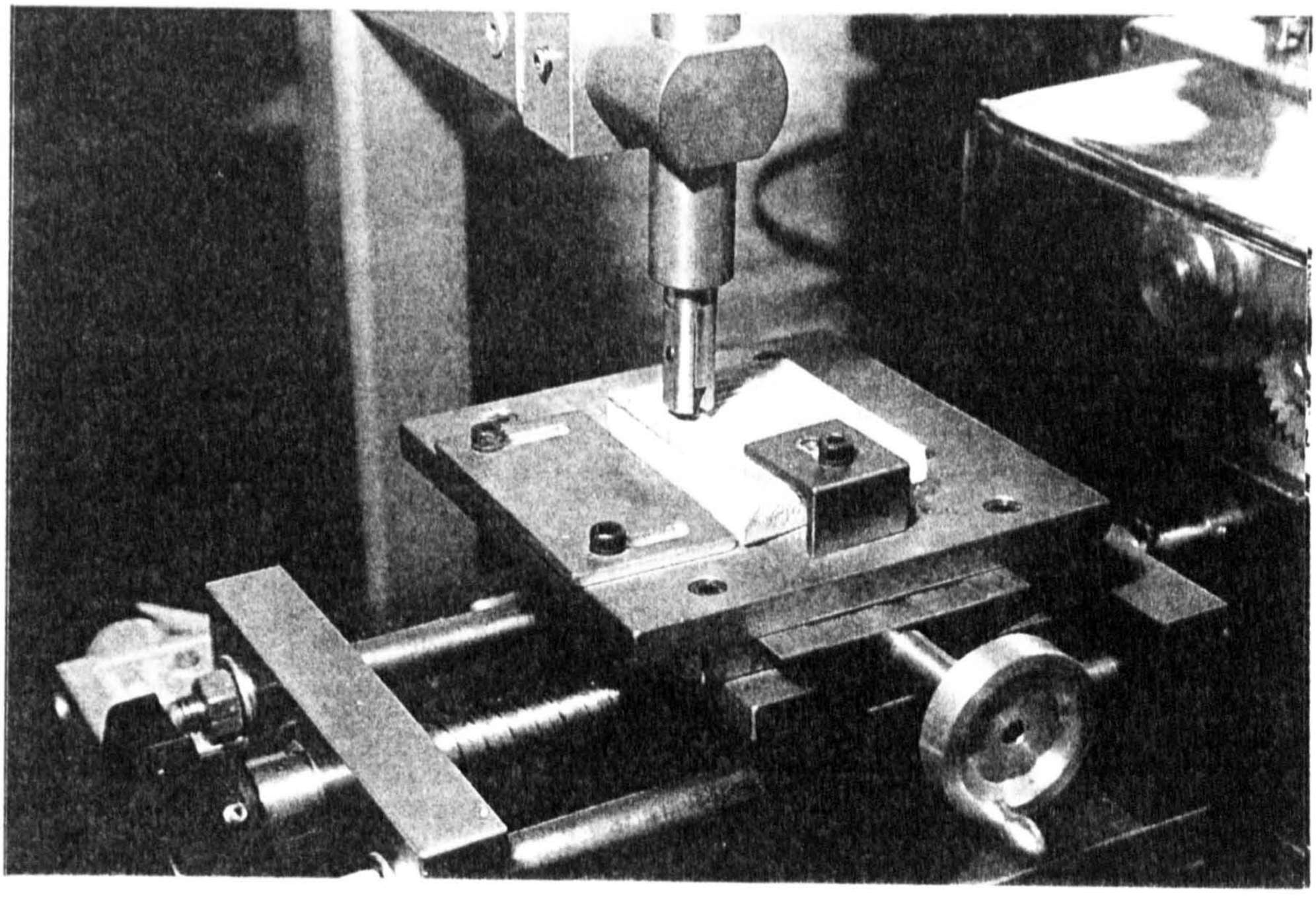

Figure 4.3 General view of the scratch hardness apparatus.

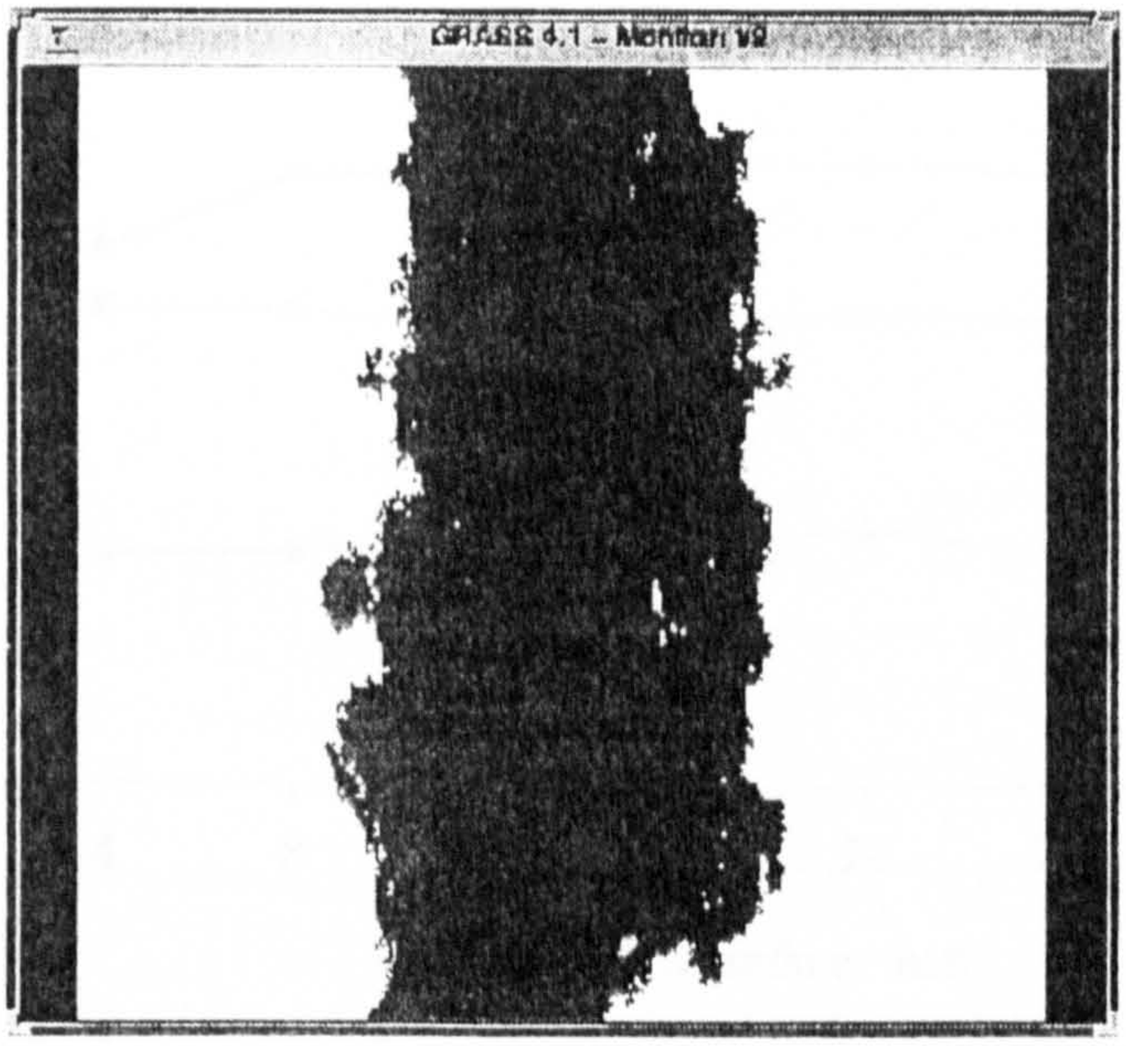

Figure 4.4 General view of the drawn scratch with magnification of 50 times after image processing.

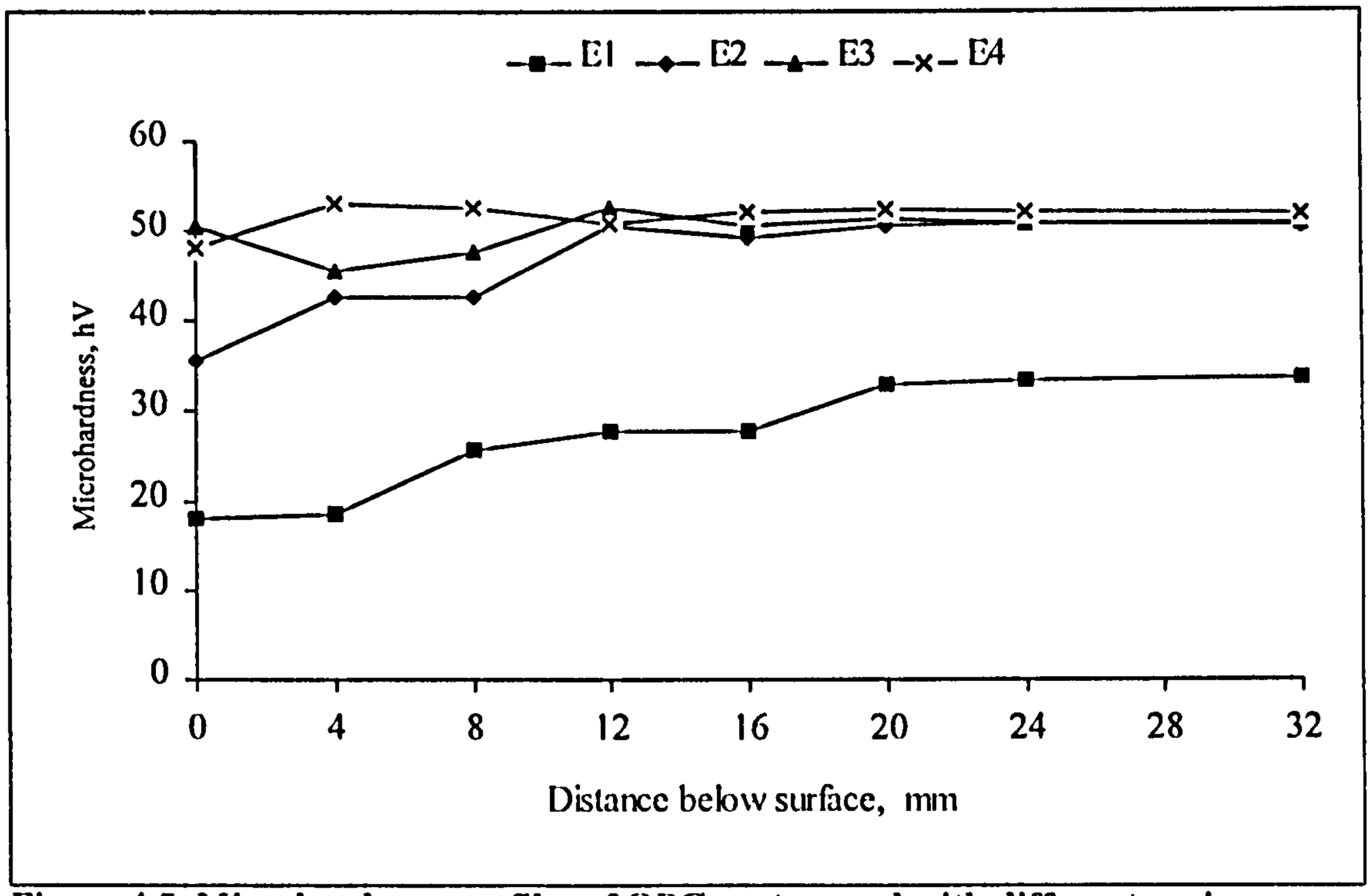

Figure 4.5 Microhardness profiles of OPC paste cured with different curing regimes, w/c = 0.55.

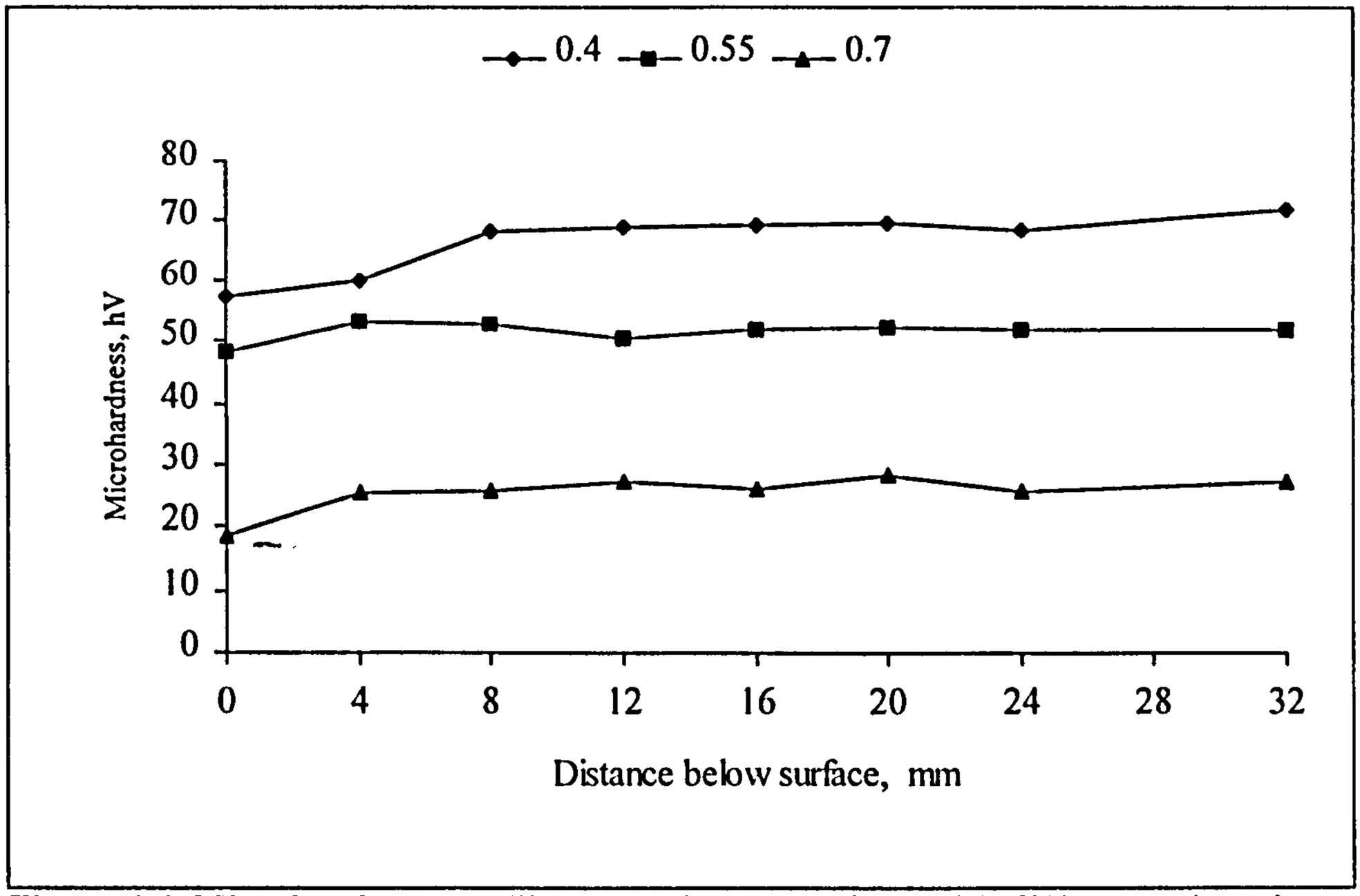

Figure 4.6 Microhardness profiles of OPC pastes mixed with different w/c ratios, E4 regime.

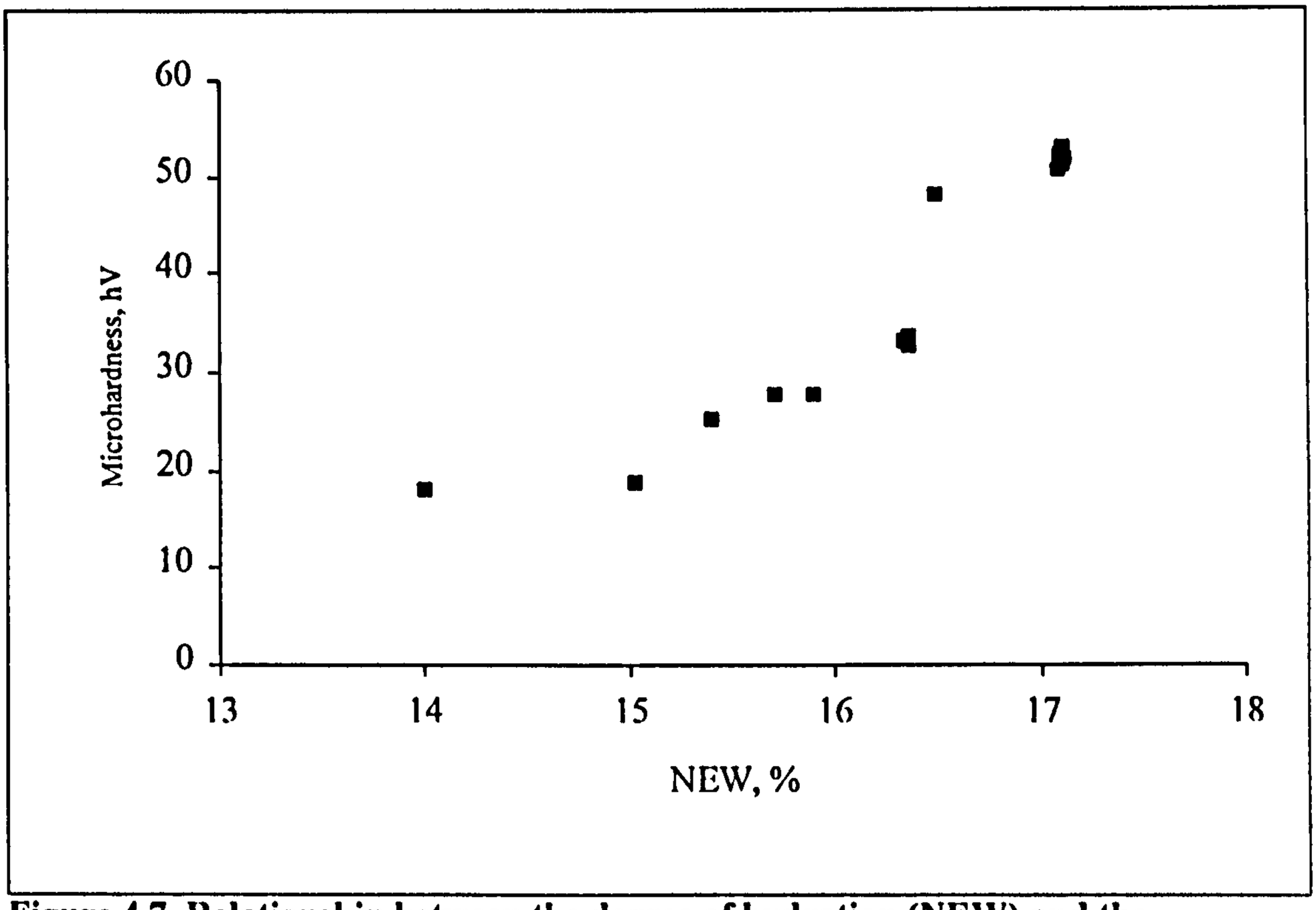

Figure 4.7 Relationship between the degree of hydration (NEW) and the microhardness properties of HCP, w/c = 0.55.

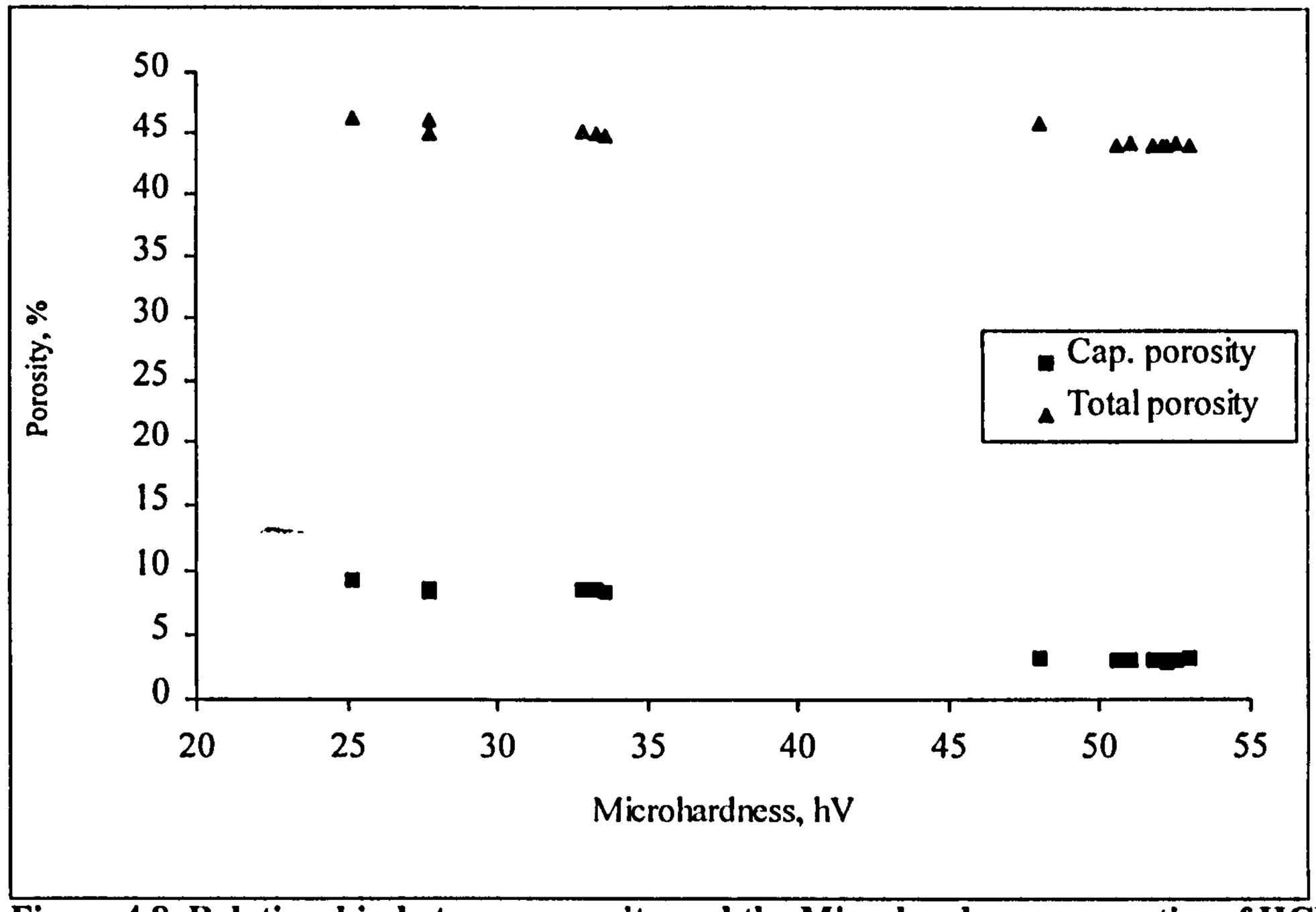

Figure 4.8 Relationship between porosity and the Microhardness properties of HCP.

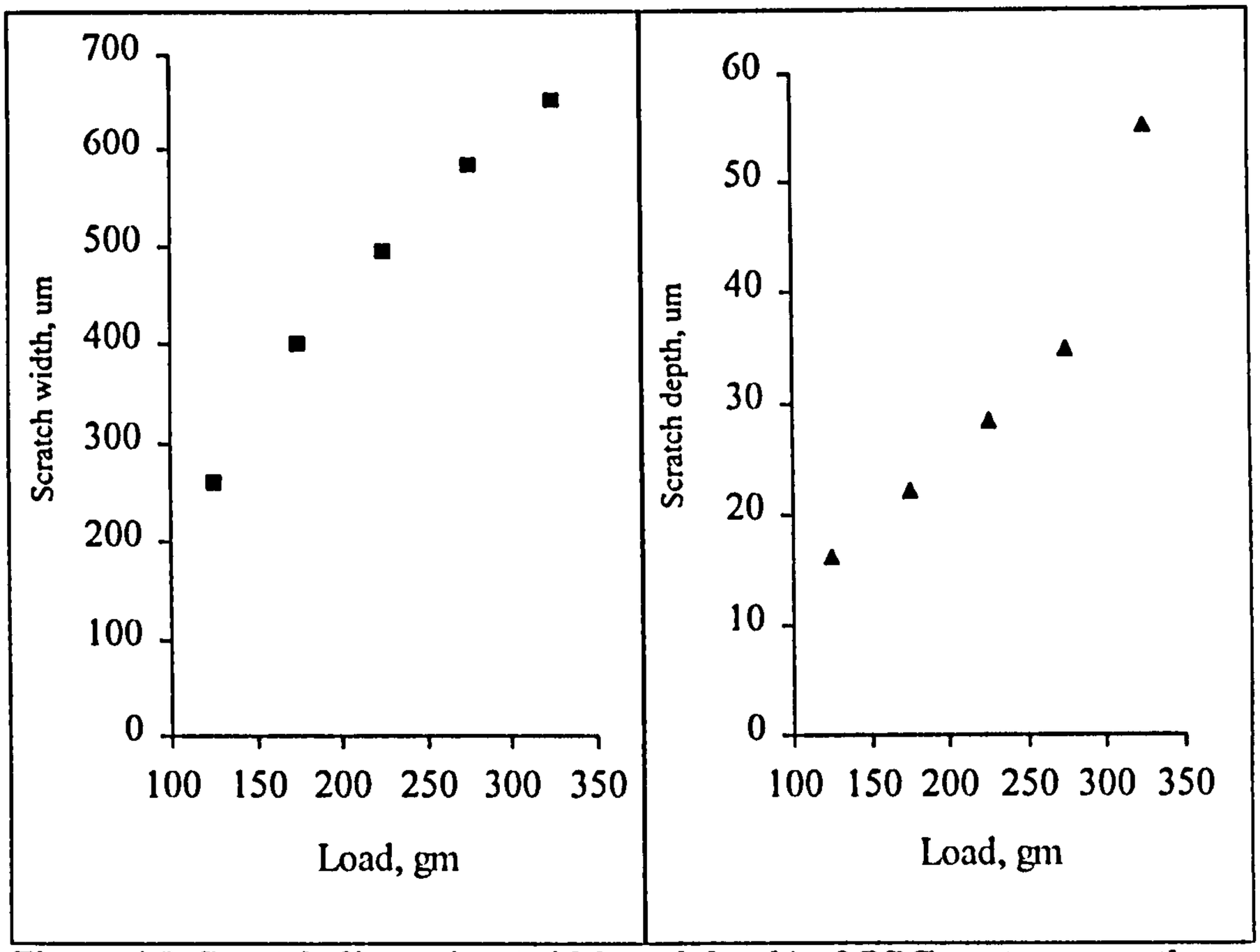

Figure 4.9 Scratch dimension (width and depth) of OPC paste versus the applied load, using w/c = 0.40 and E4 curing.

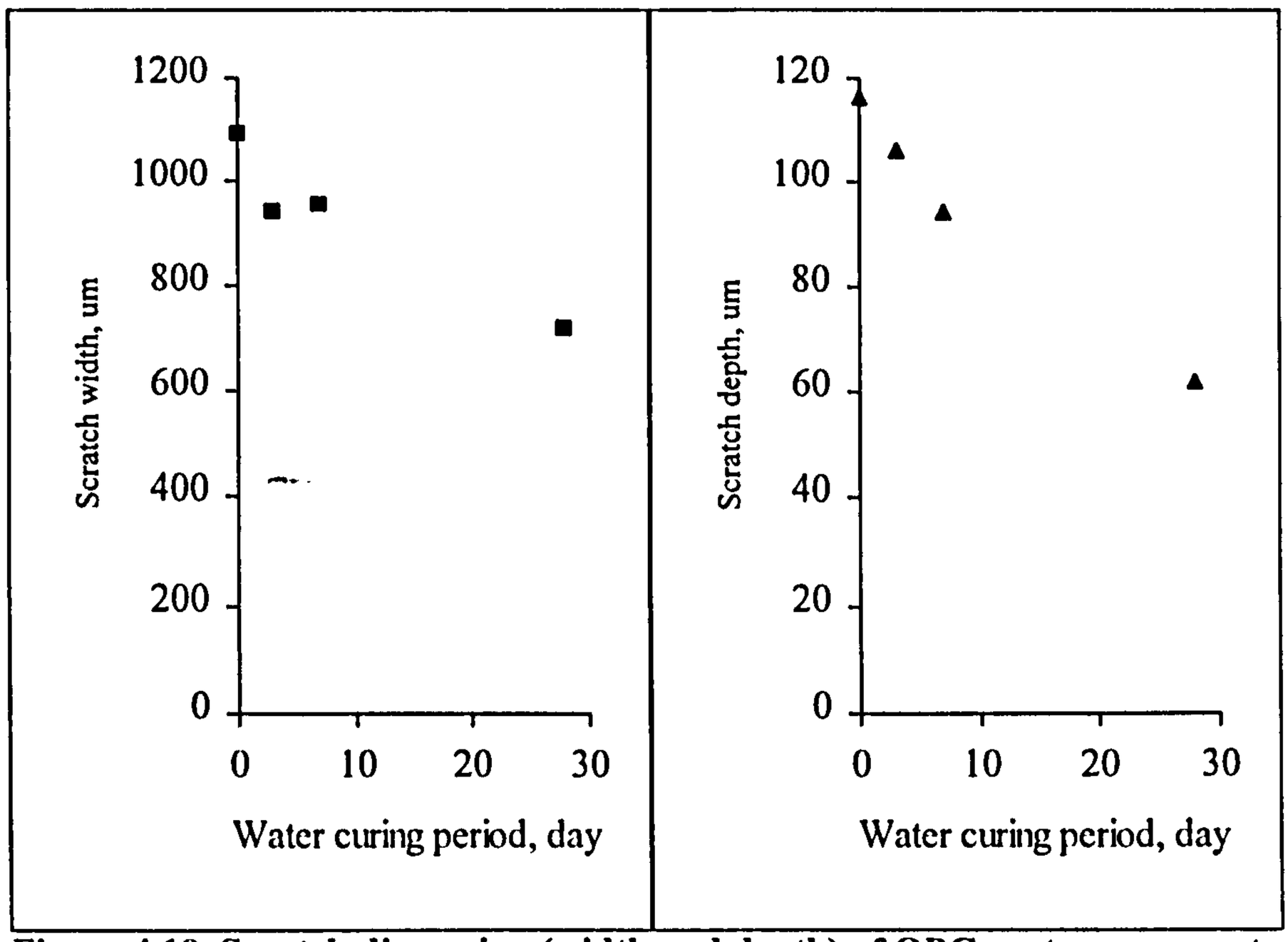

Figure 4.10 Scratch dimension (width and depth) of OPC paste versus water curing period, w/c = 0.55.

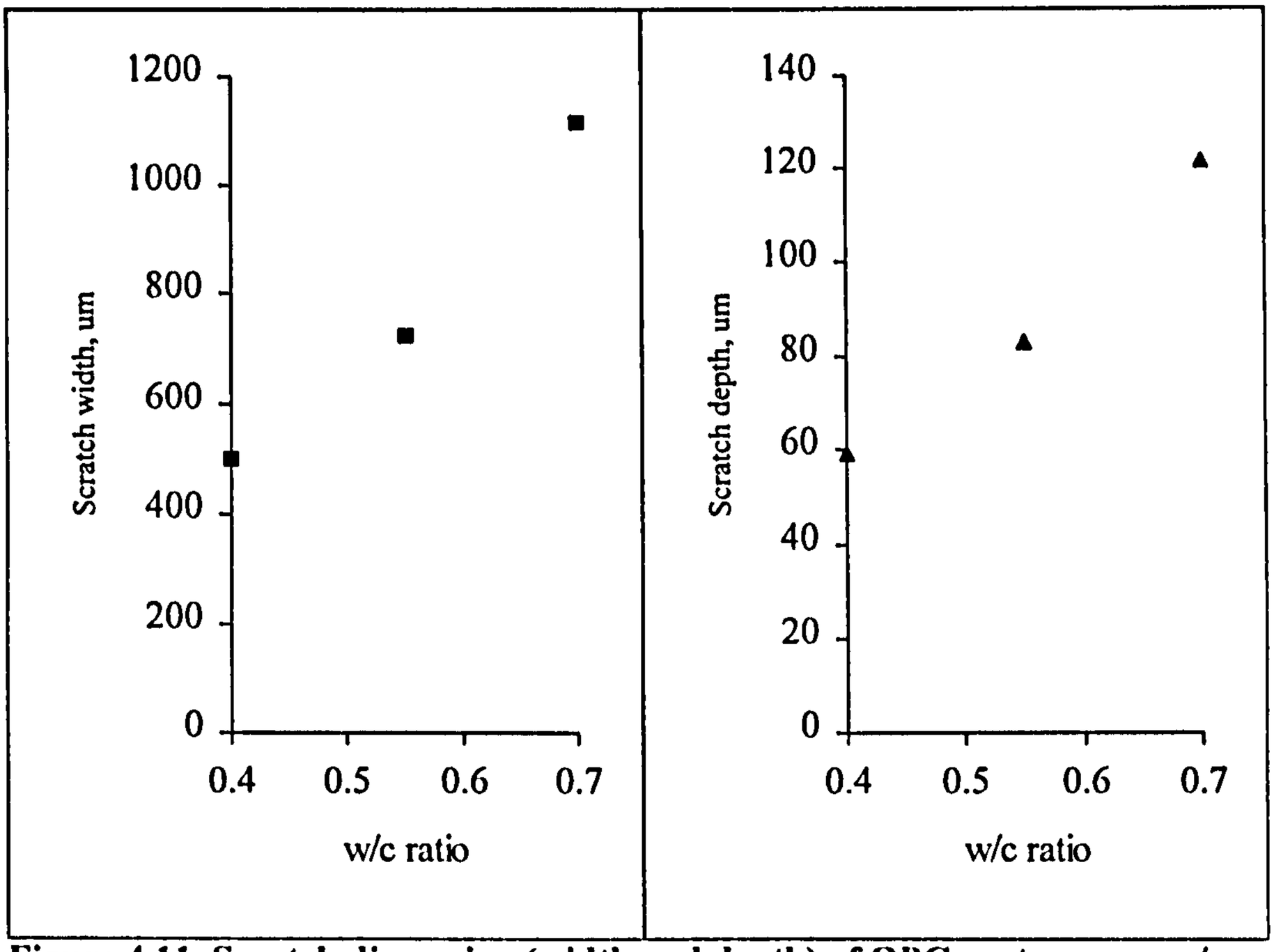

Figure 4.11 Scratch dimension (width and depth) of OPC paste versus w/c ratio, E4 curing.

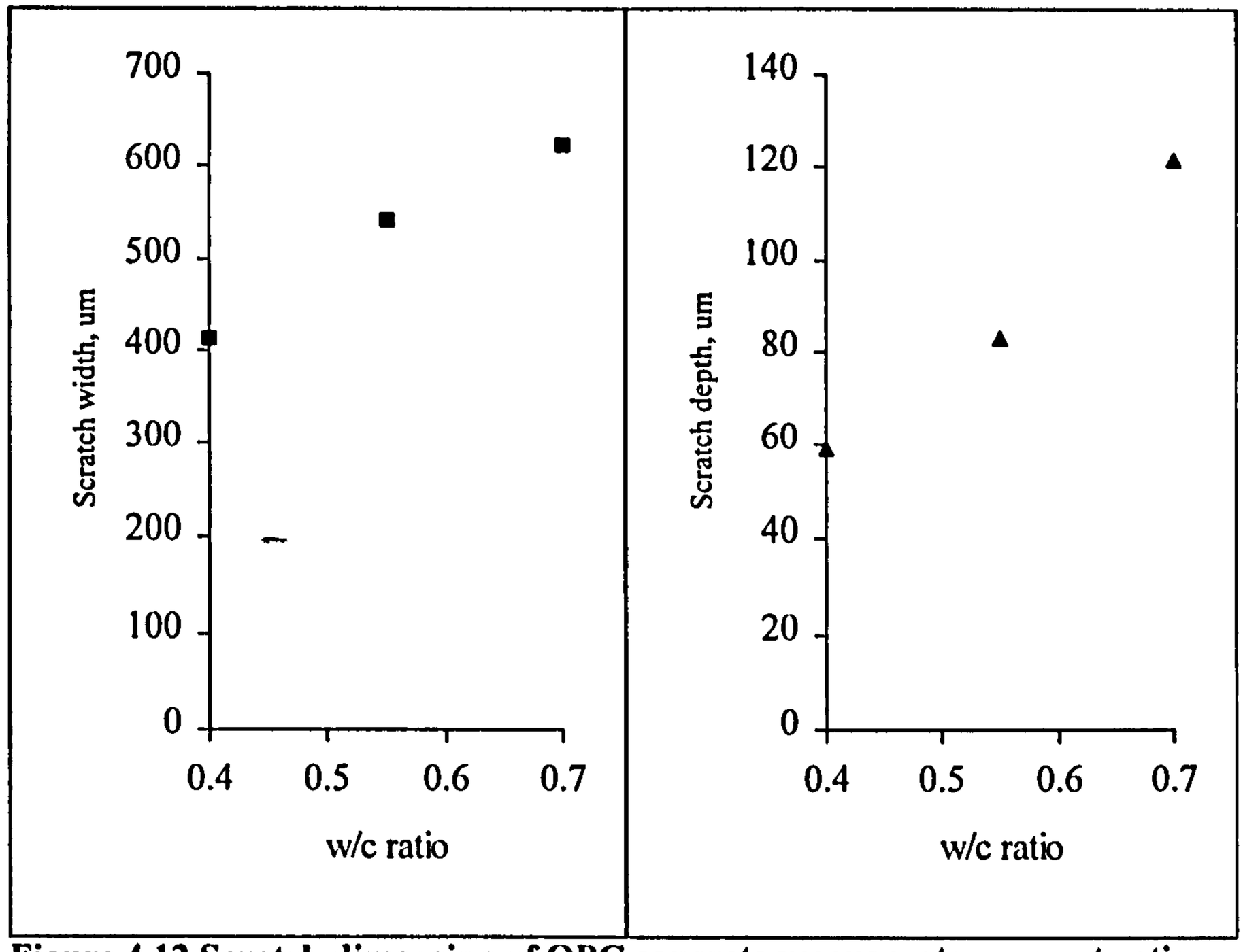

Figure 4.12 Scratch dimension of OPC concrete versus water cement ratio, E4 curing.

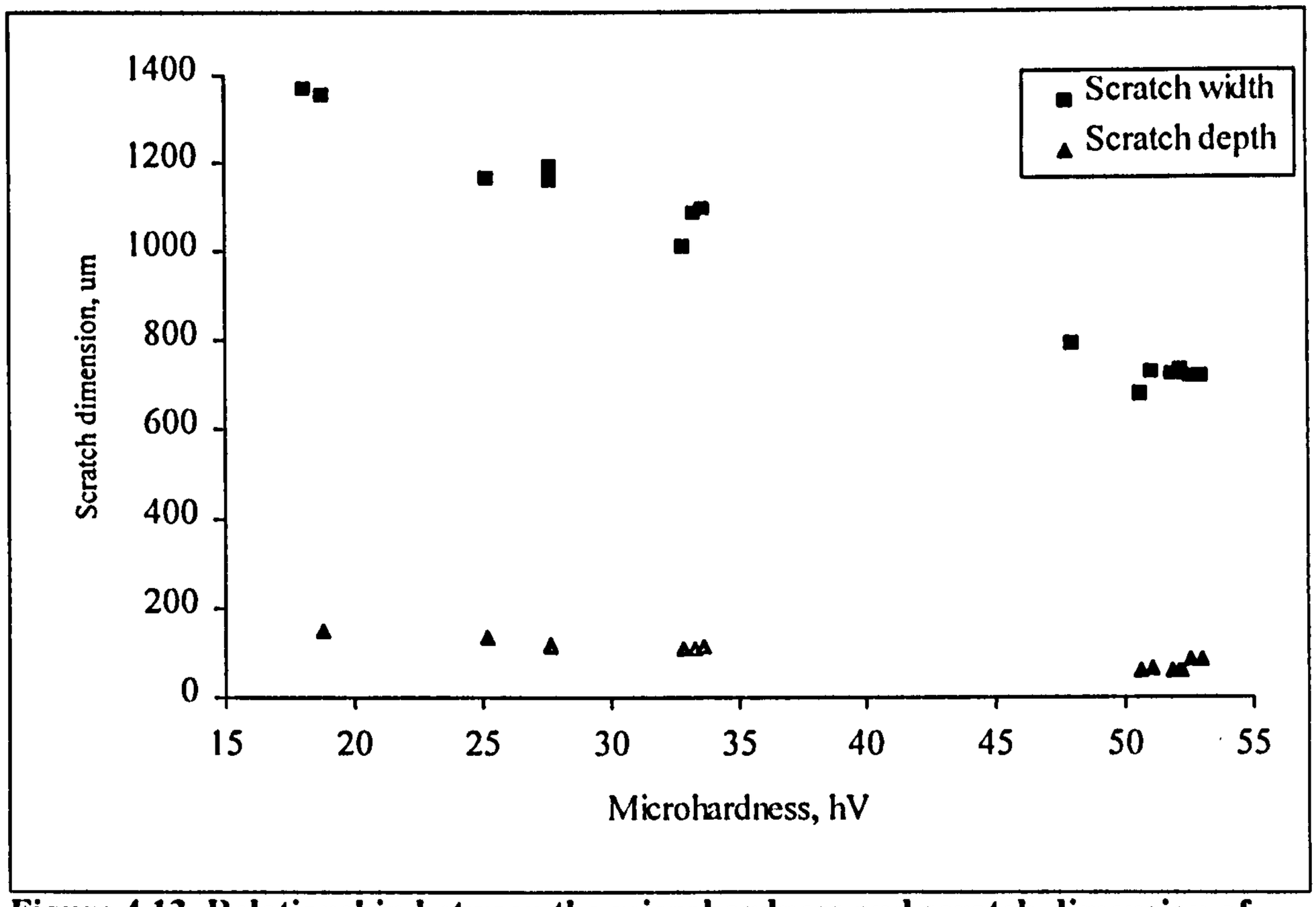

Figure 4.13 Relationship between the microhardness and scratch dimension of OPC paste.

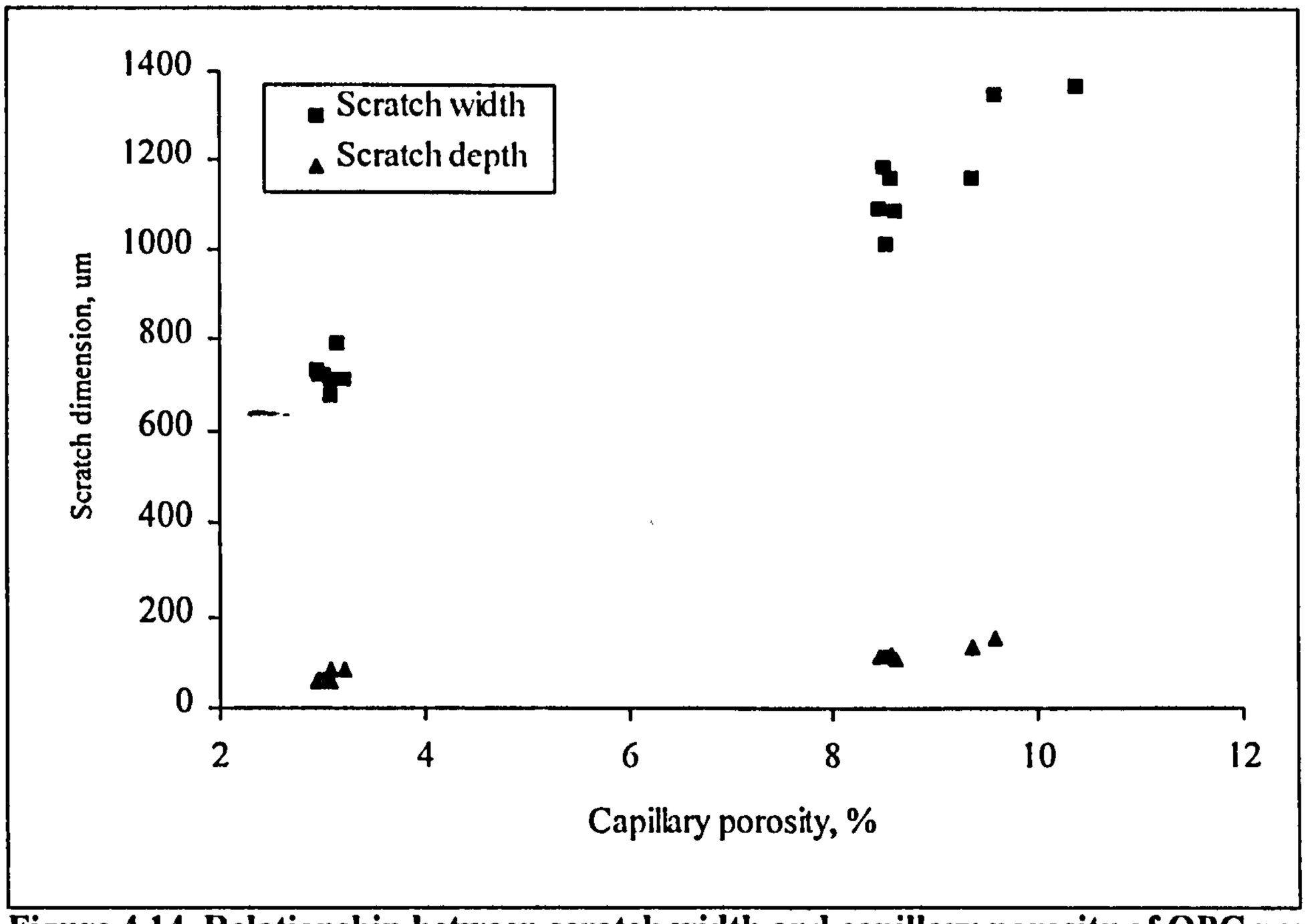

Figure 4.14 Relationship between scratch width and capillary porosity of OPC paste.

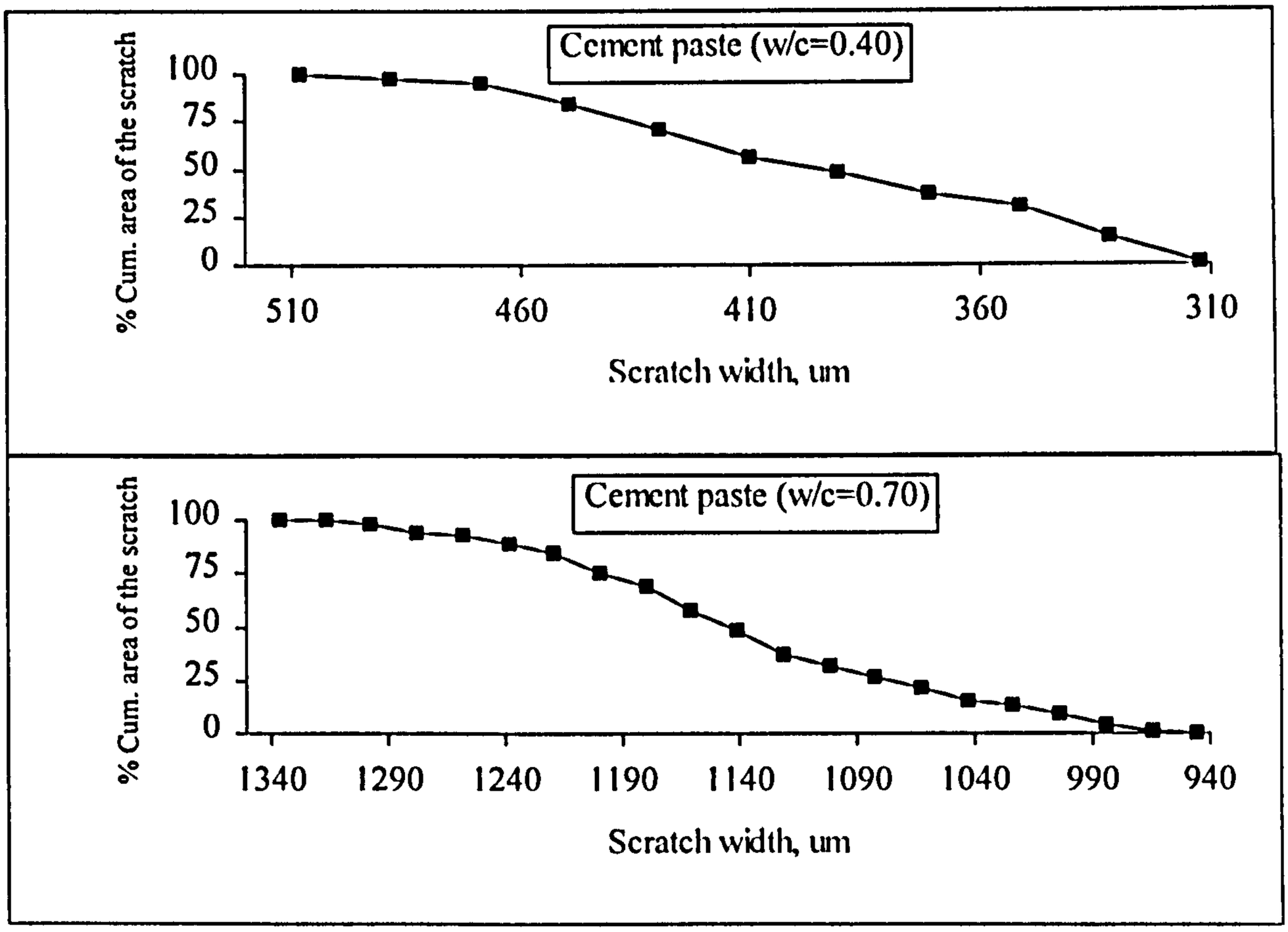

Figure 4.15 Relationship between the % cumulative area of the scratch and the scratch width for OPC paste and concrete with different w/c ratios.

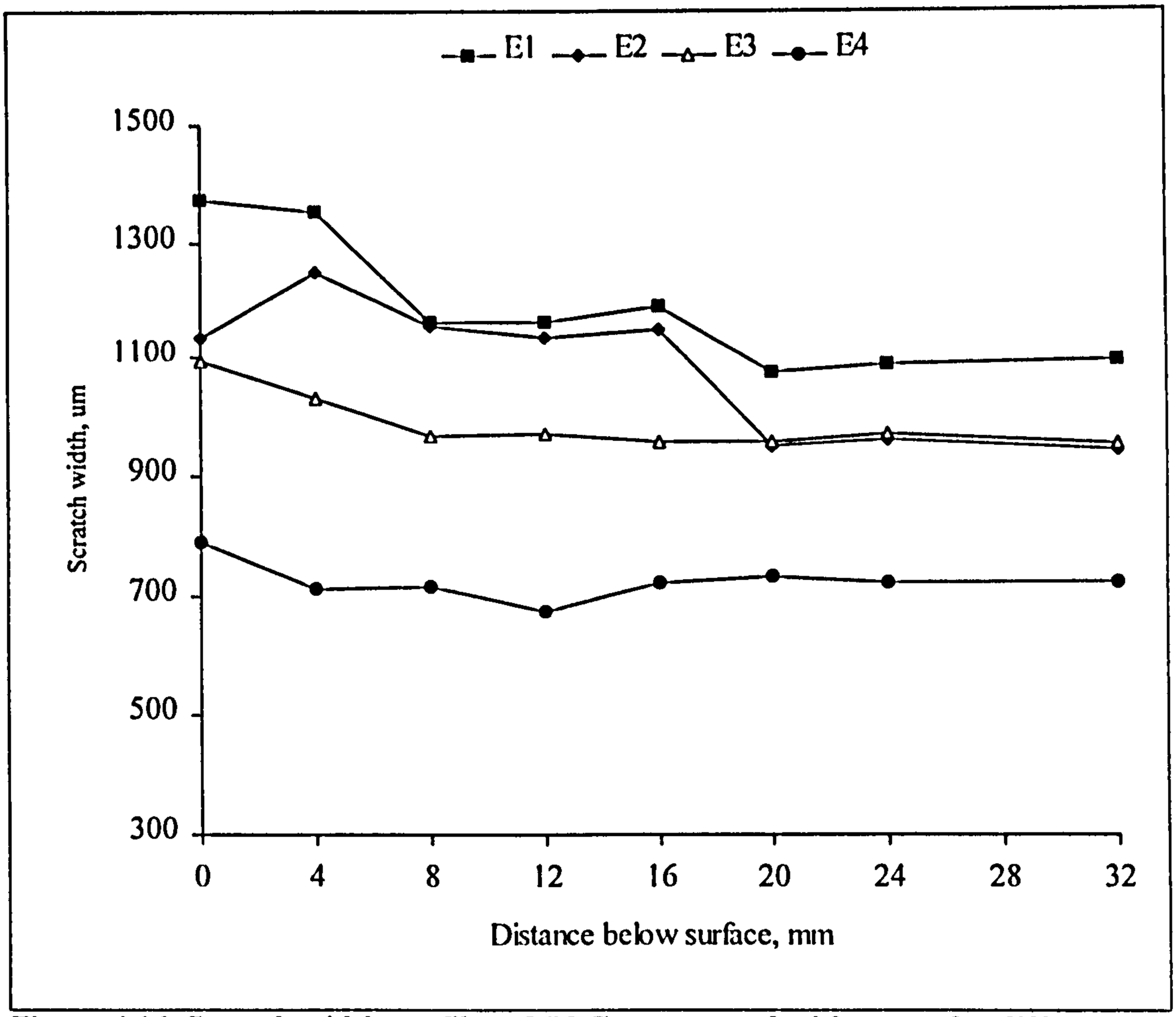

Figure 4.16 Scratch width profiles of OPC paste cured with water for different periods at 22°C, w/c = 0.55.

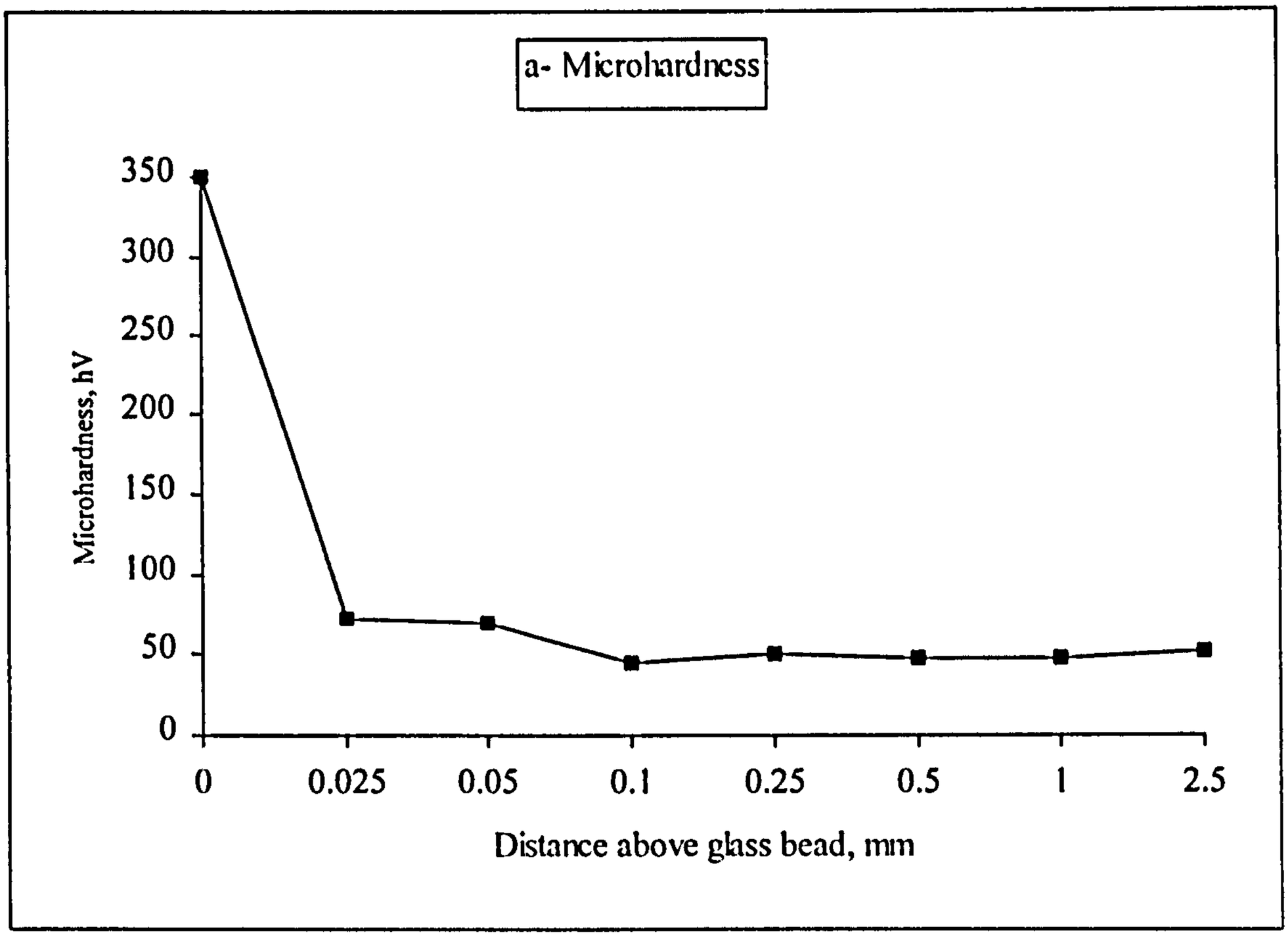

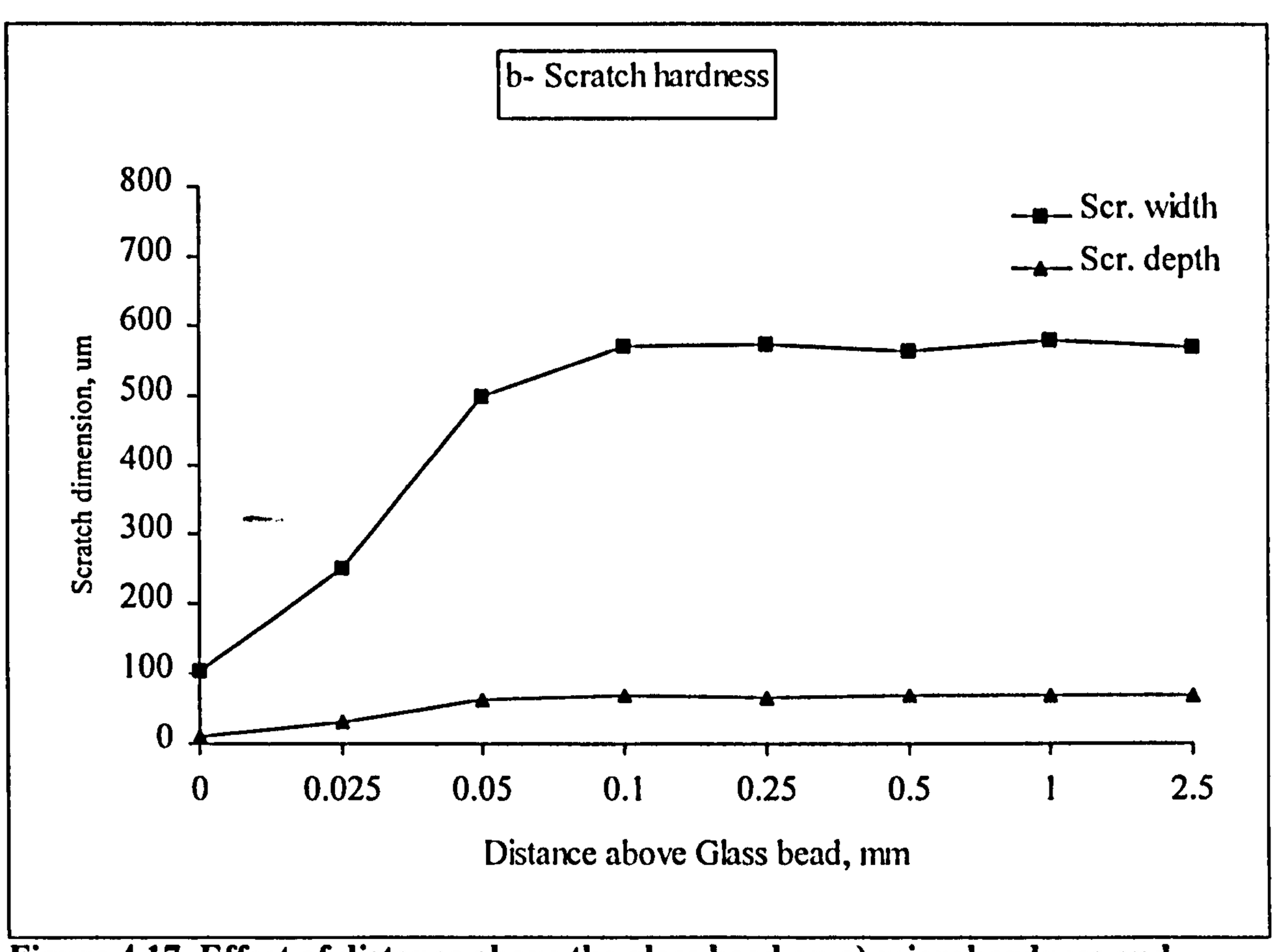

Figure 4.17 Effect of distance above the glass bead on a) microhardness and b) scratch hardness measurements.

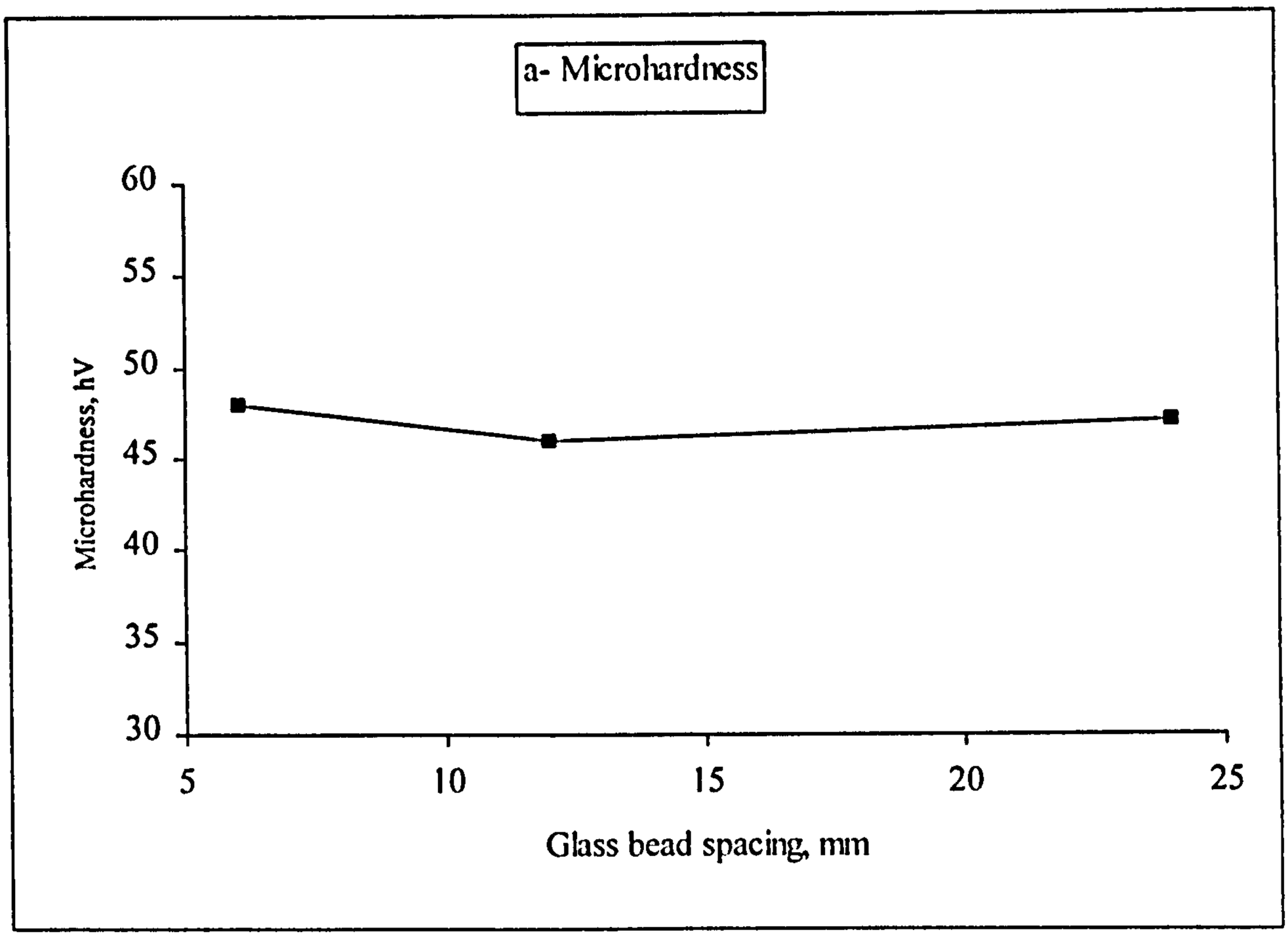

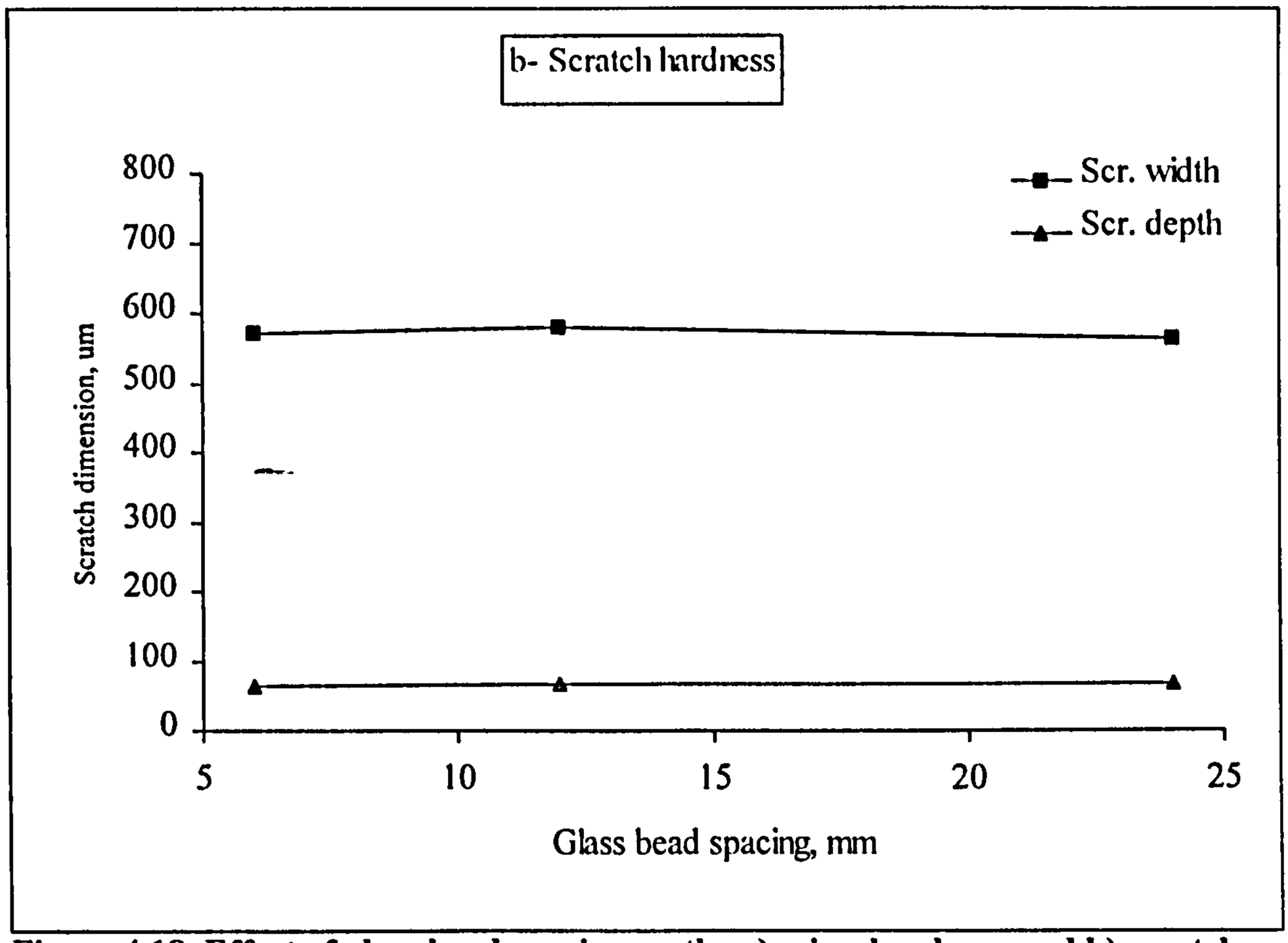

Figure 4.18 Effect of glass bead spacing on the a) microhardness and b) scratch hardness measurements.

CHAPTER 5

EFFECT OF THE MICROSTRUCTURE GRADIENT ON THE MASS TRANSPORT PROPERTIES OF THE SURFACE ZONE

5.1 INTRODUCTION

The aim of this chapter was to study the effect of the CAZ on the rate of carbonation and chloride ingress by using different cement pastes with previously determined CAZs as described in Chapter 3 and 4. This Chapter also provides an insight into the effect of carbonation on the pore structure and phase composition of different HCPs.

5.2 LITERATURE REVIEW

The first part of this review highlights the mechanism of carbonation and the factors affecting it. It also deals with the effect of carbonation on the pore structure and properties of concrete. The second part concentrates on the mechanism and factors affecting chloride ingress into concrete.

5.2.1 Part I: Carbonation of Concrete

5.2.1.1 Mechanism of carbonation

The pore solution in concrete is normally highly alkaline, with pH values above 12.5. The high pH is generally due to the presence of hydroxyl ion associated with Ca^{2+}, Na^{+} and K^{+}, derived from the cement. In this highly alkaline environment, the embedded steel is surrounded by a layer of protective oxide film and therefore remains in a passive condition. However, steel may become susceptible to corrosion in the presence of deleterious ions such as chloride or if the pH of concrete is reduced to a level at which passivity of embedded steel is no longer maintained (Page, 1992). The reduction in alkalinity of the concrete can occur due to leaching of OH^{-} ions to the surrounding environment, such as sea water, or by carbonation of concrete due to penetration of carbon dioxide from air. The most common process responsible for the reduction in alkalinity of concrete is carbonation.

Lawrence (1981) and Jungermann (1982) have subdivided the process of carbonation in concrete into three stages, as follows:

i) ingress of CO_2 by diffusion.

ii) reaction of CO_2 with pore fluids to form carbonic acid (H_2CO_3).

$$CO_2 + H_2O \Leftrightarrow HCO_3^- + H^+ \Leftrightarrow CO_3^{2-} + 2H^+ \quad \ldots\ldots \quad (5.1)$$

iii) ionic diffusion of carbonate ions (CO_3^{2-}) in the pore fluids.

The carbonate ions can then combine with other compounds present in the pore fluids, such as Ca^{2+}, Na^+ and K^+, with a consequent loss of OH^- ions and an accompanying reduction in alkalinity (Jungermann, 1982).

Verbeck (1958), Parrott (1987, 1990a and 1990b), Rahman and Glasser (1989) and Loo et al (1994) have reported that the diffused CO_2 may react with cement hydration products, such as calcium hydroxide (C-H), as follows:

$$Ca(OH)_2 + CO_2 \rightarrow CaCO_3 + H_2O \quad \ldots\ldots \quad (5.2)$$

In addition, CO_2 causes the sulphate originally present in the cement to revert to gypsum after complete carbonation as follows:

$$C_3A.31CaSO_4.3H_2O + 3CO_2 + 3H_2O \rightarrow 3CaCO_3 + 2Al(OH)_3 + 3CaSO_4.H_2O + 30H_2O \quad \ldots\ldots \quad (5.3)$$

However, the reaction in equation (5.3) is unlikely under normal atmospheric conditions due to the low reactivity of the cement hydration products.

5.2.1.2 Assessment of carbonation

The most common method for determining the carbonation depth is using a pH indicator. This method involves spraying the freshly broken concrete with phenolphthalein solution which differentiates between the natural colour of the concrete with a pH ≥ 10-10.3 which gives a magenta colour and the carbonated area of pH < 9-10 which remain colourless (Parrott, 1987 and Sims, 1994). Although this method is

convenient to use and can give reproducible results, it can only differentiate between fully carbonated concrete, where the pH is already at the critical value of about 9-10 or less, and other areas of concrete, which might vary between being completely unaltered and partially carbonated.

A number of alternative methods are available for monitoring carbonation. Parrott (1987, 1990a and 1990b), Bier et al, (1987 and 1989), Rahman and Glasser (1989), and Kobayashi et al (1994) have reported that X-ray diffraction, thermal analysis (DTA) and thermo-gravimetry (TG) can be used to assess the extent of carbonation in concrete by measuring the reduction of calcium hydroxide ($Ca(OH)_2$) and the increase of calcium carbonate ($CaCO_3$) contents. Also, optical microscopy under polarized light can be used to observe directly the presence of ($CaCO_3$) in concrete (Meyer, 1968). According to Parrott (1991a), the progress of carbonation in laboratory specimens can also be determined non-destructively from the difference in weight and dry bulk density of carbonated and uncarbonated concrete.

5.2.1.3 Factors influencing carbonation

The rate of CO_2 diffusion into concrete depends mainly on the amount and continuity of pores in the concrete, which provide the paths for CO_2 to diffuse into the material (Diamond et al, 1981 and Parrott, 1991b). In dry pores, CO_2 diffuses without causing significant carbonation to the concrete due to the absence of water which is necessary for carbonation reactions. On the other hand, when the pores are completely saturated with water, the rate of CO_2 diffusion is negligible. This implies that the rate of carbonation is negligible in dry and saturated pore conditions. There is in fact an intermediate moisture content at which maximum carbonation rate can be achieved. It has been reported by Tuutti (1982) that this intermediate moisture content is between 60% to 70% RH, as shown in Figure 5.1. Tuutti (1982) noticed that there, however, was some slow carbonation even at 99.9% RH.

Rahman and Glasser (1989) observed that carbonation of OPC concrete after 80 days of exposure in air at 60% RH was significantly enhanced at 40°C where the depth of carbonation was 6 mm compared to 2-3 mm at 20°C. This observation was contradicted by Thomas and Matthews (1992), who showed an insignificant increase in the rate of

carbonation when the temperature increased from 20 to 40°C. Diamond et al (1981) and Parrott (1987) have also mentioned that elevated ambient temperature could increase or decrease the rate of carbonation depending on the degree of drying.

Verbeck (1958) has found that the % weight gain due to carbonation reactions increased with increasing concentration of CO_2, as shown in Figure 5.2. However, it can clearly be seen from Figure 5.2 that the increase in CO_2 concentration from 0.03 % (atmosphere) to 1% has the most significant effect on % weight gain compared to subsequent increases in the concentration of CO_2 (1% to 100%). Loo et al (1994) found that the effect of CO_2 concentration on the carbonation depth is dependent on the concrete grade. He observed that the effect of CO_2 concentration (ranging from 7 to 18%) was greater on specimens with lower 28-day strengths than on specimens with higher 28-day strengths ($\geq$ 400Kg / cm^2).

Many researchers, who studied the factors influencing carbonation depth, have agreed that carbonation progress is governed by Fick's law and can be defined reasonably well by the following equation (Sergi, 1986; Parrott, 1987 and Vaysburd et al, 1993):

$$d = k_t \sqrt{t} \qquad \ldots\ldots \quad (5.4)$$

where, d (mm) is the depth of the carbonation reaction front after time t (years) and k_t is the carbonation coefficient. It was reported by Parrott (1987) that the depth of carbonation varies for different mix compositions and water/cement ratios, i.e., it is related to the compressive strength of concrete. They have also noted that the use of higher cement contents at constant water/cement ratio decreased the depth of carbonation. However, it was found by Loo et al (1994) that the effect of cement content on the rate of carbonation was marginal when compared with the effect of the w/c ratio. This was attributed to the role of the w/c ratio in determining the gel/space ratio. He has also represented the relationship between k_t and w/c ratio as follows:

$$k_t = \alpha[w / c - \beta] \qquad \ldots\ldots \quad (5.5)$$

where, α and β are constants. Recently, Houst and Wittmann (1994) studied the influence of w/c ratio on the effective diffusivity of CO_2 and O_2 at 55% RH, as shown in Figure 5.3. He observed that the effective diffusivity of CO_2 increased by a factor of 20 to 25 when the w/c increased from 0.4 to 0.8.

The replacement of Portland cement with PFA and GGBS generally leads to an increase in the rate of carbonation for concretes of constant w/c ratio (Parrott, 1987 and 1993). The author showed that the replacement of 70% and 50% of OPC by PFA and GGBS, respectively, increases the average carbonation depth by 46% and 69%, respectively. Thomas and Matthews (1992) also mentioned that the rate of carbonation was increased with increasing content of cement replacement materials. He has also reported that the concrete containing 15-30% PFA carbonated to a slightly greater extent than OPC concrete of the same strength grade but the rate of carbonation for concrete containing 50% PFA had a higher carbonation rate than OPC concrete of equal strength grade. This increase in the rate of carbonation is attributed to the reduction in the amount of $Ca(OH)_2$ which is consumed during the pozzolanic reaction. Smolczyk (1976) related the rate of carbonation to calcium oxide content (CaO) as follows:

$$carbonation \approx \frac{1}{\sqrt{CaO}} \qquad \ldots\ldots \quad (5.6)$$

It is clear from this equation (5.6) that an increase in CaO content reduces carbonation significantly. Therefore, depleting CaO from OPC concrete by additives such as pozzolans and slag, would offer less resistance to carbonation. This was confirmed by Bier et al (1987 and 1989) who studied the effect of slag content on the rate of carbonation in terms of calcium carbonate content at different CO_2 concentrations, as shown in Figure 5.4. His results showed that carbonation rate increases with increasing slag and CO_2 concentration. However, contrary to the abovementioned studies, Hobbs (1994) reported that, at an age of 8.3 years, the depth of carbonation in OPC and 65%OPC/35%PFA concretes of the same 28-day compressive strengths were similar.

Thomas and Matthews (1992) emphasized the importance of adequate curing for the resistance of concrete to carbonation. He reported that, in some cases, increasing the

initial water curing period from 1 to 7 days resulted in a 50 % reduction in the carbonation depth. A similar observation was made by Loo (1994), who reported that longer water-curing periods help to reduce the rate of carbonation, but beyond 14 days of water curing, the reduction becomes marginal. Dhir (1989) arrived at the same conclusion, and noted that extending the water curing period beyond 14 days had much less effect on the carbonation rate than the initial 14 days curing. Parrott (1993) has shown that the differences in carbonation depth due to variable cement types are somewhat greater than those due to variable curing. He reported that the carbonation depths at a given strength for 28 days water curing were somewhat higher than those with 1 and 3 days water curing, an observation which was in disagreement with previous findings (Dhir, 1989; Thomas and Matthews, 1992 and Loo et al , 1994).

To sum up, the main factors influencing carbonation are as follows:

(1) Weather conditions such as ambient temperature, relative humidity, and CO_2 concentration.

(2) Pore structure system and moisture conditions (RH).

(3) Cement content and water/cement ratio.

(4) Type and content of cement replacement material in the mix.

(5) Degree of hydration (initial curing).

Therefore, a good understanding and proper control of these factors can lead to a greater reduction in the rate of carbonation.

5.2.1.4 Effect of carbonation on microstructure and properties of concrete

The chemical reactions shown in equation 5.2 would be expected to modify the concrete composition, pore structure, physical and mechanical properties. Pihlajavaara (1968) and Bier et al (1987 and 1989) observed that carbonation generally causes a reduction in porosity of the affected zone because the volume of calcium carbonate ($CaCO_3$) formed during carbonation reactions exceeds that of the parent hydrates.

Pihlajavaara (1968) studied the effect of carbonation on the porosity and pore size distribution of OPC cement paste. He concluded that there was a reduction in the amount of pores of diameter between 1,000 and 125 Å compared to pores of diameter less than 125 Å owing to carbonation. He also showed that the total porosity under 125

Å was similar for both carbonated and uncarbonated cement paste. Similar results have been reported by Vaysburd et al (1993), who reviewed the consequence of carbonation to the void space of concrete. He reported that the void space of pores 0.01-0.1 and 0.1-1 μm across is almost doubled due to carbonation, while voids and capillaries, 12 nm across and greater remains unchanged and free from carbonation reaction products. Houst and Wattmann (1994) reported that all the pores of HCP of w/c=0.4 were affected by carbonation, in particular those below 0.1 μm, thus confirming the findings of Pihlajavaara (1968). He observed a reduction in the amount of pores with radii below 2 μm for very porous HCP, with w/c=0.80. It was also found that after carbonation, the amount of gel pores of 2 nm diameter decreased. This means that the xerogel was also modified, i.e. coarsened by carbonation.

Bier et al (1987 and 1989) studied the effect of carbonation on the pore structure of OPC and OPC/GGBS cement pastes when exposed to 0.03% (atmosphere) and 2% CO_2 by volume and concluded that:

(1) The pore volume of OPC paste was decreased compared to OPC/GGBS paste, which showed a slight or no reduction in the cumulative pore volume but a shift in PSD towards coarser pore radii.

(2) Accelerated carbonation (2% CO_2) caused a greater reduction in the pore volume of OPC paste and a distinct shift towards coarse pore radii of OPC/GGBS paste when compared to atmospheric carbonation. This was attributed to higher $CaCO_3$ content and to the distinct decomposition of C-S-H gel caused by accelerated carbonation.

(3) Carbonation increased the capillary porosity of OPC/GGBS paste.

Malami and Kaloidas (1994), Page and Ngala (1995) and Ngala and Page (1997) confirmed Bier et al's results when studying the effect of carbonation on specific pore volume of OPC, OPC/PFA and OPC/GGBS cement pastes. Malami and Kaloidas (1994) reported that, after 13 months of exposure to atmospheric CO_2, the total specific pore volume (SPV) of carbonated specimens was less than that of uncarbonated specimens. He derived this variation from the difference observed between meso pores ($125\ nm < R_b \leq 12.5\ nm$) and micro pores ($7500\ nm < R_b \leq 125\ nm$). Page and Ngala (1995), Ngala (1995) and Ngala and Page (1997) also reported that carbonation caused

an increase in the capillary porosity (pore diameter ≥ 30 nm) by about 5% in OPC cement paste. However this was negligible compared with the marked increase of approximately 145% and 230% for blended fly ash and slag pastes respectively.

Mechanical properties of carbonated concrete such as compressive and flexural strengths are enhanced due to the reduction in its total porosity (Meyer, 1968; Vaysburd et al, 1993 and Kobayashi, 1994). However, a reduction in compressive strength in carbonated GGBS concrete was observed by Meyer (1968). This was attributed to the formation of more porous silica gel in GGBS concrete due to the decomposition of the C-S-H gel (Bier et al, 1989).

The Carbonation reaction shown in equations (5.1 and 5.2) sometimes produces a weight change (gain or loss) for concrete due to the replacement of water by CO_2. When $Ca(OH)_2$ is carbonated there is a resultant increase in the weight of concrete due to the replacement of one mole of water by the heavier one mole of CO_2. Similar behaviour is also expected for the carbonation of C-S-H gel. At the other extreme, when ettringite is carbonated, 27 moles of water are replaced by 3 moles of CO_2, resulting in a considerable weight loss (Sergi, 1986 and Parrott, 1987 and 1991b). Weight gain densifies the concrete microstructure, which may tend to enhance the mechanical properties of carbonated concrete. On the other hand, weight loss produces less dense concrete which may lead to poor mechanical properties.

Carbonation has also been reported to increase the modulus of elasticity and surface hardness (Sereda, 1968), whilst reducing permeability (Hilsdorf et al, 1984). Moreover, it was mentioned by Pihlajavaara (1968), Parrott (1986) and Vaysburd et al (1993) that the chemical reaction of carbonation is accompanied by carbonation shrinkage which is greater when carbonation occurs after drying, rather than during drying, except at low humidities.

Chloride diffusion was found to be accelerated by carbonation (Sergi, 1986 and Ahmed, 1990). This was attributed partly to the releasing of Cl^- from complex calcium chloro-aluminate (Friedel's salt), established by the binding of Cl^- with cement constituents,

which provides more free chloride ions available for diffusion, as shown in equation 5.7 (Suryavanshi and Swamy, 1996);

$$3CaO.Al_2O_3CaCl_2.10H_2O + 3CO_2 + 3H_2O \rightarrow 3CaCO_3 + 2Al(OH)_3 + CaCl_2 + 10H_2O \quad \ldots\ldots (5.7)$$

The release of $CaCl_2$ shown in equation 5.7 leads to an increase in the $[Cl^-/OH^-]$ ratio, increasing the risk of chloride induced pitting corrosion. Dhir (1993) observed that the sequential carbonation and chloride attack was a worse degradation problem than either process acting separately. He also reported that carbonation processes accelerate the rate of sulphate attack.

As a result of the reduction in the pH of the pore solution due to carbonation, the passive film could be damaged and reinforcement corrosion initiated. This can occur at a pH of about 11 and does not coincide exactly with the pH value detected by phenolphthalein (Parrott, 1987). Therefore, the corrosion of reinforcement is mainly controlled by the unneutrralized remainder, i.e. the depth of reinforcement cover minus the depth of carbonation detected by phenolphthalein (Parrott, 1990b and 1994).

It is clear from the above literature that a good understanding of the role of carbonation on concrete microstructure and concrete properties may help to deal with the problem of reinforcement corrosion.

5.2.2 Part II: Chloride Ingress

5.2.2.1 General

Chloride is the main ion which may provoke corrosion problems and the effect of chloride on durability has been widely studied for many years. It may be introduced to concrete from several sources. Soluble chlorides may be included in fresh concrete by the use of contaminated constituents such as aggregate, water, cement and admixtures. Chloride ions may also enter hardened concrete from external sources such as sea-water and de-icing salts used in cold winter periods (Verbeck, 1975; Jones et al, 1993 and Bamforth and Price, 1994).

Chloride ions can be present in hardened concrete in three forms, i.e. free, physically adsorbed and chemically bound (Bamforth and Price, 1994). The three phases are summarized as follows:

1- Free chlorides

As the name implies free chlorides are those ions present in the pore fluid and moving within the concrete by ionic diffusion through the pore solution. Free chlorides increase the electrical conductivity of the pore water. As a result of their electro-chemical properties, they influence the rate of dissolution of metallic ions, hence affecting the initiation of reinforcement corrosion. As the amount of free chlorides increase, the risk of corrosion increases (Bamforth and Price, 1994).

2- Physically adsorbed chlorides

The physically adsorbed chloride ions are those ions adsorbed on to the pore walls of the cement hydrates (Ramachandran, 1971) and do not directly affect the risk of corrosion of reinforcement under normal conditions. The amount of physically adsorbed chloride ions is mainly dependent on the surface area of the cement hydrates (Byfors, 1986) and on the nature of the hydration products (Hansson and Sorensen, 1987).

3- Chemically bound chloride ions

Chemically bound chloride ions are those ions that have reacted with the cement compounds, forming solid compounds which are effectively immobile and have no direct influence on the corrosion activity. The chloride binding capacity depends mainly on cement composition, cement fineness, type of cement, replacement materials, water cement ratio and percentage of chloride present and associated cation (Tritthart, 1989 and Arya et al, 1990).

The tricalcium aluminate (C_3A) is the main controlling factor in the chloride binding process. C_3A reacts with chloride ions to form insoluble complexes. The reaction product is as shown in equation 5.8 (Verbeck, 1975).

$$CaCl_2 + 3CaO.Al_2O_3 \leftrightarrow 3CaO.Al_2O_3.CaCl_2.10H_2O \quad \ldots\ldots \quad (5.8)$$

The product in equation (5.8) is calcium chloro-aluminate which is commonly known as Friedel's salt. C_4AF also reacts with chlorides to form two insoluble complexes which are calcium chloro-aluminate and calcium choloro-ferrite ($3CaO.Fe_2O_3.CaCl.10H_2O$) (Suryavanshi and Swamy, 1996). C_3S and C_2S can also bind with chloride ions to form interlayer of chemisorbed complexes within C-S-H gel (Ramachandran, 1971). On the other hand, Diamond et al (1981) and Lambert et al (1985) concluded that silicate phases have no major effect on the chloride binding capacity.

5.2.2.2 Mechanism of chloride ingress

The mechanism of chloride ingress is mainly controlled by diffusion occurring on fully saturated concrete, and absorption occurring by wetting and drying processes which occur on most structures exposed to chloride environments. The mechanism of chloride attack could be summarized as follows:

a- Diffusion

It is a process by which chlorides from external sources penetrate the cover concrete under the action of a concentration gradient (Page et al, 1981 and Kumar et al, 1987). Only free chlorides are available for transport into deeper layers. As more chloride ions penetrate with time, some of them will bind with the cement hydrates, whilst the remainder will further saturate the pore solution. Some of these free ions diffuse further creating a concentration gradient from the surface of the concrete to the inner layers, as illustrated in Figure 5.5 (Schiessl, 1983).

b- Absorption

Owing to the wetting and drying of concrete surfaces with chloride containing water, an enrichment of chlorides in the surface layer is possible. At the beginning of the wetting period a relatively large amount of chloride containing water will penetrate into the concrete by capillary suction. During the drying period, the water dries out and the chloride remains in the concrete. On subsequent wetting, more chloride ions are conveyed into the concrete and deposited ions from the previous cycles are sucked in deeper. On repeated drying, the water or much of it departs leaving behind an increased amount of chloride. This process may cause a high enrichment of chlorides in the drying and wetting zone of the concrete, as shown in Figure 5.6 (Schiessl, 1983).

5.2.2.3 Factors affecting the rate of chloride ingress

The type of cement plays an important role in the rate of chloride ingress. Investigations with various types of cement have confirmed that chloride diffusion is strongly influenced by cement composition (Page et al, 1981 and Bamforth and Price, 1994). Tricalcium aluminate (C_3A) is considered to be the most important phase affecting the rate of chloride ingress due to its ability to bind chloride ions (Rasheeduzzafar et al, 1992). It is therefore a cement of high C_3A content such as OPC which would induce better resistance to chloride attack rather than those of low C_3A contents such as SRPC.

The use of blended cements could also reduce the rate of chloride ingress. Page et al (1981), Ahmed (1990), Dhir (1993) and Thomas (1995) found that the inclusion of PFA in concrete has a beneficial effect on reducing both the proportions of water soluble chlorides in concrete and the coefficient of chloride diffusion. It was reported by Dhir et al (1991) that it is PFA quantity and not the quality that affects chloride diffusion and in some extreme cases the value of the diffusion coefficient was reduced by up to 70%.

In the same manner, slag cements showed the same beneficial effect on the rate of chloride ingress (Page et al, 1981 and Tumidajski and Chan, 1996). Ngala et al (1995) and Ngala and Page (1997) studied the chloride diffusion of different carbonated and non-carbonated HCP (OPC, OPC/30%PFA and OPC/70%GGBS) with different w/c ratios and concluded that:

(1) Non-carbonated slag pastes were slightly less permeable to the diffusion of the chloride ions than fly ash and the reverse being true for carbonated pastes.

(2) The diffusion rate of chloride ions through carbonated OPC, OPC/30%PFA and OPC/70%GGBS pastes diminished markedly with decreasing w/c ratio, the effect being more marked in the blended fly ash and slag pastes.

(3) For a given w/c ratio, the chloride diffusion rates for carbonated blended pastes are two orders of magnitude greater than those of the corresponding non-carbonated pastes. On the other hand, chloride diffusion rates for carbonated OPC are about 2 to 5 times higher than those of the corresponding non-carbonated pastes.

The beneficial effect of PFA and slag in reducing the rate of chloride ingress has been attributed to the influence on the pore structure of the cement paste matrix of concrete (Kumar et al 1987 and Ahmed, 1990), to the pore surface interaction (Sergi, 1986) and to the chloride binding capacity of these blending materials (Mangat and Mallovy, 1995).

Many researchers have studied the effect of water/cement ratio on the rate of chloride ingress (Page et al, 1981; Hansson and Sorensen, 1985 and Ahmed, 1990). Page et al (1981) used the ionic diffusion cell to study such effect and found that increasing the water cement ratio from 0.4 to 0.5 of HCP caused an increase in the chloride diffusion coefficient (D_{cl}) by a factor of approximately two and this factor increased to five when the w/c was increased to 0.6. This finding was recently supported by Sugiyama et al (1996) who used an accelerated electrical method for estimating D_{cl} of OPC concrete. This rapid increase of the coefficient of chloride diffusion is believed to be due to the increase in the amount of void space and its continuity at higher water cement ratios (Ngala et al, 1995 and 1997).

Ahmed (1990) found that the period of moist curing greatly influences the resistance of OPC and OPC/PFA concretes to chloride ingress. Kumar et al (1987) reported that the critical period of water curing, beyond which an insignificant effect on chloride ingress was noted, was 7 days. On the other hand, Babu and Rao (1993) and Higgins (1995) concluded that the initial curing has little effect on the chloride diffusion in concrete of the same grade. However, there is insufficient data in the literature to assess the effect of curing on the rate of chloride diffusion.

Some other factors such as carbonation, exposure condition, temperature and salt type can also influence the rate of chloride ingress. The role of carbonation was described in Section 5.2.1.4. Schiessl (1983) stated that concrete exposed to wetting and drying cycles is likely to convey greater amounts of chloride ions than the concrete which is exposed to a well-saturated environment. It was also found that the chloride diffusion coefficient was increased with increasing temperature (Page et al, 1981 and Higgins, 1995). A higher temperature leads to a decrease in the chloride binding capacity and this may affect the equilibrium between free and bound chlorides, with more chlorides

penetrating the concrete. However, an appreciable effect was only noticed for exposure temperatures of 55° C and above (Maslehuddin et al, 1996).

To sum up the main factors influencing chloride ingress are as follows:

(1) Internal factors including, cement type, curing and w/c ratio.

(2) External factors such as temperature, type of exposure and carbonation.

It is therefore clear that a good understanding and control of these factors may lead to reduced risks of reinforcement corrosion.

5.3 EXPERIMENTAL PROCEDURES

Cylindrical paste specimens (75x49 mm) were cast as described in Section 2.4.1 and cured under conditions E1, E3 and E4 (Table 2.3) to produce specimens of CAZ thicknesses 4-8, 12-16 and 20-24 mm, respectively. These CAZ values were previously determined from the work carried out in Chapter 3 and 4. After curing, the specimens of known CAZ were then exposed to CO_2 gas and Cl^- ions, as shown in Figure 5.7, and according to the following procedures.

1- Carbonation test

The specimens chosen for carbonation tests were pre-conditioned in a constant 65% RH environment over saturated sodium nitrite ($NaNO_2$) for at least three months until a steady weight was achieved signifying a constant internal RH of the specimen. After pre-conditioning, the specimens were sealed with four layers of wax around all faces apart from the cast surface and then transferred to a carbonation chamber maintained at 21 ±2° C and 65% RH. 100% CO_2 gas was passed through the chamber for half an hour a day to accelerate carbonation. The experimental set-up used for the carbonation of cement pastes is shown in Figure 5.8. The specimens were then split open at different exposure periods and sprayed with a phenolphthalein indicator along the whole length of the specimen. The depth of carbonation from the cast surface was measured using a traveling microscope (Nikon Measurescope), as described in Section 2.6.10.

Fragments of carbonated and uncarbonated samples were taken from their respective zones to study the effect of carbonation on the pore structure of HCP using MIP. Details of the experimental procedure are described in Section 2.6.3. Similarly,

differential thermal analysis/ thermo-gravimetry (DTA/TG) were also carried out on fragmented samples specified for this study. Prior to testing, the fragmented samples were ground to powder, sieved through a 150 μm mesh to obtain a homogeneous sample, and kept in desiccators containing silica gel until analysis. DTA/TG tests were then carried out as described in Sections 2.6.4.1. A worked example of calculations of the identified peaks in DTA thermo-graphs using TG results is given in Appendix 5

2- Chloride penetration test

After curing, another set of specimens chosen for chloride penetration testing was sealed with four layers of wax around all faces apart from the cast surface. The specimens were then vacuum saturated with de-ionized water for 48 hours followed by immersion in a solution of 1 M NaCl containing 35 mM of NaOH. The specimens were exposed to the chloride solution for different immersion periods (2, 4 and 8 months). Care was taken to maintain a constant chloride concentration in the solution throughout the period of study by changing the solution every 15 days.

After the specified exposure period, the specimens were removed from the solution and immediately profile-ground from the cast surface, using a precision lathe to collect dust specimens at progressive depths from the exposed face. The dust from grinding was then collected and tested for total chloride content as described in Section 2.6.9.

5.4 RESULTS AND DISCUSSION

5.4.1 Carbonation of the Surface Zone

Prior to studying the effect of CAZ on the rate of carbonation of the surface zone, the pore and phase structure of the cement paste matrix were initially studied to identify the role of carbonation on the parameters which control the rate of CO_2 ingress. The pore size distribution (PSD) for uncarbonated and carbonated OPC, OPC/PFA and OPC/GGBS pastes were obtained using MIP, as shown in Figure 5.9. It can be seen that the PSD of OPC paste is not greatly influenced by the processes of carbonation, which is in disagreement with results reported by Ngala (1995). The reverse is true for the blended pastes, where the carbonation coarsened the pore structure. Similarly, carbonation also affected the threshold diameter D_{th} of the blended pastes to a greater extent than that of OPC paste. The D_{th} reduced from 500 to 30 nm after carbonation of

the blended pastes. These results are in agreement with the findings reported by Ngala (1995).

The total and capillary porosity of the pastes were deduced from MIP results, as presented in Table 5.1. The results show that the total porosity of OPC was reduced by about 15% as a result of carbonation. This is in agreement with the results reported previously by Bier et al (1987 and 1989), Vaysburd et al (1993) and Ngala and Page (1997). On the other hand, for blended matrices, the total porosity of carbonated pastes was 45% higher than that of uncarbonated pastes, a finding in disagreement with the results of Ngala and Page (1997). This disagreement may be arised as a result of the using OPC with different chemical compositions and exposing the specimens to different curing regimes in the both investigations, where, in Ngala's study, the specimens being tested were cured in water for 90 days, whilst in this study the specimens were cured in water for 28 days.

The results reported in Table 5.1 also show that the capillary porosity (of pore diameter more than 30 nm) increased after exposing the cement paste matrix to carbon dioxide. The amount of increase was 30, 45, and 90% for OPC, OPC/PFA and OPC/GGBS pastes, respectively. This indicates that carbonation increases the amount of inter-connected pores of blended pastes, especially for OPC/GGBS, an opinion which is supported by Bier et al (1987 and 1989), Parrott (1987 and 1993), Thomas and Matthews (1992) and Ngala and Page (1997).

The reduction in the total porosity of OPC paste due to carbonation may be attributed to the deposition of calcium carbonate ($CaCO_3$) in the pores. The increase in the total porosity of the blended pastes and capillary porosity of all carbonated pastes may be due to the decomposition of C-S-H gel in the matrix forming silica gel which has a high porosity (Bier et al, 1989). The formation of silica gel may also result in the rearrangement of the PSD. The difference in the pore structure (PSD and porosity) of OPC/PFA and OPC/GGBS following carbonation is likely to be associated with the natural variabilities in the original composition of the blended cements which would have resulted in the production of different hydration products.

The DTA thermographs for uncarbonated and carbonated OPC, OPC/PFA and OPC/GGBS pastes cured under condition E4 (w/c=0.55) are presented in Figure 5.10. It can be seen that the endo-thermal peaks associated with calcium hydroxide (C-H) at 450-600°C for all the uncarbonated pastes are no longer evident after carbonation. They were replaced by a large endo-thermal peak of calcium carbonate ($CaCO_3$) at about 700-900°C. Another peak of calcium silicate hydrate (C-S-H) for uncarbonated pastes is also observed at just after 110-250°C but it is reduced substantially after carbonation.

In order to quantify the amounts of the various phases that existed in the cement paste matrix shown in Figure 5.10, the weight loss due to increasing temperature was determined by thermo-gravimetry (TG) and the results are presented in Table 5.2 (see Appendix 5). It can be seen that the amount of C-S-H and C-H was reduced as a result of carbonation for all pastes, whilst, there was a significant increase in the calcium carbonate phase due to carbonation. It is also clear from the results reported in Table 5.2 that the bound water, which represents the amount of hydration products, increased when the HCP pastes were exposed to CO_2. The level of increase in bound water due to carbonation was calculated to be about 60% for all pastes. These findings are in agreement with the results reported by Sergi (1986), Rahman and Glasser (1989) and Thomas and Matthews (1992).

The role of carbonation on OPC pastes with different microstructure gradients (CAZ) is illustrated in Figure 5.11. The results show that the carbonation rate of the surface zone increases with increasing CAZ thickness. It can be seen that the relationship between the CAZ depth and carbonation rate is non-linear and that the effect of CAZ on carbonation rate is more pronounced when the CAZ increases from 12-16 mm to 20-24 mm than when it increases from 4-8 mm to 12-16 mm. The amount of increase in the rate of carbonation reached 150% and 350% when the CAZ was increased from 4-8 mm to 12-16 mm and 12-16 mm to 20-24 mm, respectively. These results signify the important role of the CAZ in controlling the rate of CO_2 ingress into the cover concrete.

The increase in carbonation rate with CAZ thickness could be attributed to the amount of hydration products (C-H and C-S-H) present in the surface zone available for reaction with CO_2. The hydration products act as a defensive line against the ingress of CO_2 gas by consuming it in the carbonation reactions (see equations 5.1 and 5.2). Therefore, the

specimens of low CAZ thickness show more resistance to CO_2 ingress than those of high CAZ thickness.

Figure 5.12 illustrates the role of the cement replacement materials on the rate of carbonation for pastes with similar CAZ depth (4-8 mm). It can be seen that the use of blending material has a marked effect on the carbonation rate. The OPC/PFA and OPC/GGBS pastes of 4-8 mm CAZ carbonated at a rate of about 100-150% higher than that of the corresponding OPC paste. However, there was no significant difference in the carbonation rates between the two blended cement pastes with CAZ of 4-8 mm.

The difference in the behavior of OPC and blended cement pastes with CAZ depths of 4-8 mm can be associated with the reduction in the amount of C-H and C-S-H hydrates due to pozzolanic reactivity of the blended pastes. These results are consistent with the levels of C-H and C-S-H shown in Table 5.2 and are in agreement with results reported by Smolczyk (1976) and Bier et al (1989). Consequently, the similarity in behaviour between the PFA and GGBS blended cements in terms of carbonation rate for pastes with 4-8 mm CAZ may be attributed to the similarity in values of C-H and C-S-H hydrates observed for both the OPC/PFA and OPC/GGBS pastes (see Table 5.2).

5.4.2 Effect of CAZ on Chloride Ingress

The effect of the microstructure gradient of the surface zone (CAZ) on the total chloride content profiles of OPC paste (0.55 w/c) immersed in 1M of NaCl for 8 months is illustrated in Figure 5.13. Specimens with higher CAZ appear to show a lower chloride binding capacity so that the total chloride near the surface of the specimens is at lowest when the CAZ is at its highest. Conversely, the highest total chloride concentration is highest for the specimens with lowest CAZ. Overall penetration of the chloride appears, on the face of it, to be higher for specimens with the lowest CAZ. The depth of chloride penetration is, however, lowest for the specimen with 4-8 mm CAZ and its concentration is close to zero at around 38 mm depth.

The explanation may lie in the degree of chloride binding and equilibrium ratio of the free to total chloride for the different specimens. A specimen with a high CAZ may possibly have its chloride capacity reduced either because of an originally low hydration level or because of leaching constituents into the NaCl solution.

It is evident from the deviation of the concentration profile from that expected from normal Fickian diffusion that the total chloride concentration is influenced by the CAZ. The free chloride concentration is more likely to resemble one controlled by Fickian diffusion and is probably similar in shape for all three specimens, even though they may have different depths of penetration, particularly as the surface concentration has to be equal to the external chloride concentration (Sergi, 1986).

The total chloride content profiles for OPC, OPC/PFA and OPC/GGBS pastes with 4-8 mm CAZ are shown in Figure 5.14. It can be seen that, at the first 8 mm (CAZ), the total chloride concentration seems to be similar for all pastes, whilst in the bulk, the total chloride concentration for the blended pastes is less than that of the corresponding OPC paste. It also appears that the total chloride penetration for the blended pastes is less than that of the corresponding OPC paste. The use of GGBS seems to offer the greatest resistance to chloride ingress.

The effect of the cement replacement materials on the chloride penetration may be attributed to the pozzolanic reactions which occur between these materials and the cement hydration products, which could lead to densifying the pore structure of blended pastes (Page et al; 1981, Ngala; 1995a and 1995b and Tumidajski and Chan, 1996). The use of GGBS showed more resistance to chloride ingress than PFA owing to the marked influence of GGBS on the capillary porosity and the pozzolanic reactivity.

To study the effect of exposure period on the rate of chloride ingress in HCP of known CAZ (4-8 mm), the total chloride profiles were established for OPC, OPC/PFA and OPC/GGBS pastes after exposure to 1M of NaCl for 2, 4 and 8 months, as shown in Figure 5.15. It can be seen that the effect of the exposure time on the total chloride content of the first few millimeters (≈CAZ) appears to be insignificant, as the total binding capacity of each material appears to remain constant, whilst, in the bulk, the total chloride content increases with increasing time of exposure.

The insignificant effect of the exposure period on the total chloride content of the CAZ may be due to the microstructural variations in the first few millimeters of the surface. The marked effect of the exposure period on the total chloride content in the bulk could

be attributed to the continuous process of chloride binding as more and more chlorides diffuse into the pores (Schiessl, 1983 and Ahmed, 1990). This effect may be also associated with the further hydration occurring during the exposure period, which could affect the amount of bound chloride and consequently the total chloride content.

5.5 CONCLUSIONS

1- Carbonation of cement pastes composed of OPC, OPC/PFA and OPC/GGBS was showed to modify the pore structure and the phase compositions in several ways as follows:

a) There was a marked increase in the capillary porosity for OPC, OPC/PFA and OPC/GGBS pastes as a result of carbonation.

b) Carbonation processes resulted in an increase in the total porosity of OPC/PFA and OPC/GGBS pastes and in a slight reduction in the total porosity for OPC.

c) As a result of carbonation of the OPC paste, there was a marked increase in calcium carbonate ($CaCO_3$) and bound water contents and a reduction in calcium hydroxide (C-H) and calcium silicate hydrate (C-S-H) contents. However, this effect was significantly affected by the use of PFA and GGBS.

2- A good correlation between CAZ thickness and the rate of carbonation of the surface zone was established, where the carbonation rate increased with increasing CAZ depth. For HCP of similar CAZ thickness, the use of the cement replacement material blended with OPC showed a marked increase in the rate of carbonation compared with those of OPC paste. However, this increase was not significantly influenced by the type of blending material used in this investigation (PFA and GGBS).

3- Similarly, a relationship between CAZ depth and total chloride profile of cover concrete was established . For a given water/binder ratio, as the depth of CAZ increased, the depth of chloride penetration of OPC paste increased. Surface chloride concentration was, however, decreased significantly with increasing depth of CAZ.

Table 5.1 Porosity of carbonated and uncarbonated specimens cured with E4 regime, w/c = 0.55.

Specimen type	Carbonation condition	Porosity, cc/g	
		Total	Capillary
OPC	uncarbonated	0.1613	0.0538
	carbonated	0.1365	0.0690
OPC/PFA	uncarbonated	0.1521	0.1080
	carbonated	0.2189	0.1567
OPC/GGBS	uncarbonated	0.1413	0.0670
	carbonated	0.2077	0.1262

Table 5.2 Effect of Carbonation on the chemical phases of different cement pastes, w/c = 0.55.

Specimen type	Carbonation condition	Bound water, %	Weight loss, %		
			C-S-H (110-250°C)	C-H (450-600°C)	$CaCO_3$ (700-900°)C
OPC	Uncarbonated	18.98	8.01	4.74	1.32
	Carbonated	30.18	5.23	3.24	14.51
OPC/PFA	Uncarbonated	15.42	6.91	2.14	3.50
	Carbonated	23.61	3.49	1.30	14.34
OPC/GGBS	Uncarbonated	15.5	6.34	2.33	2.77
	Carbonated	24.35	4.41	1.66	11.90

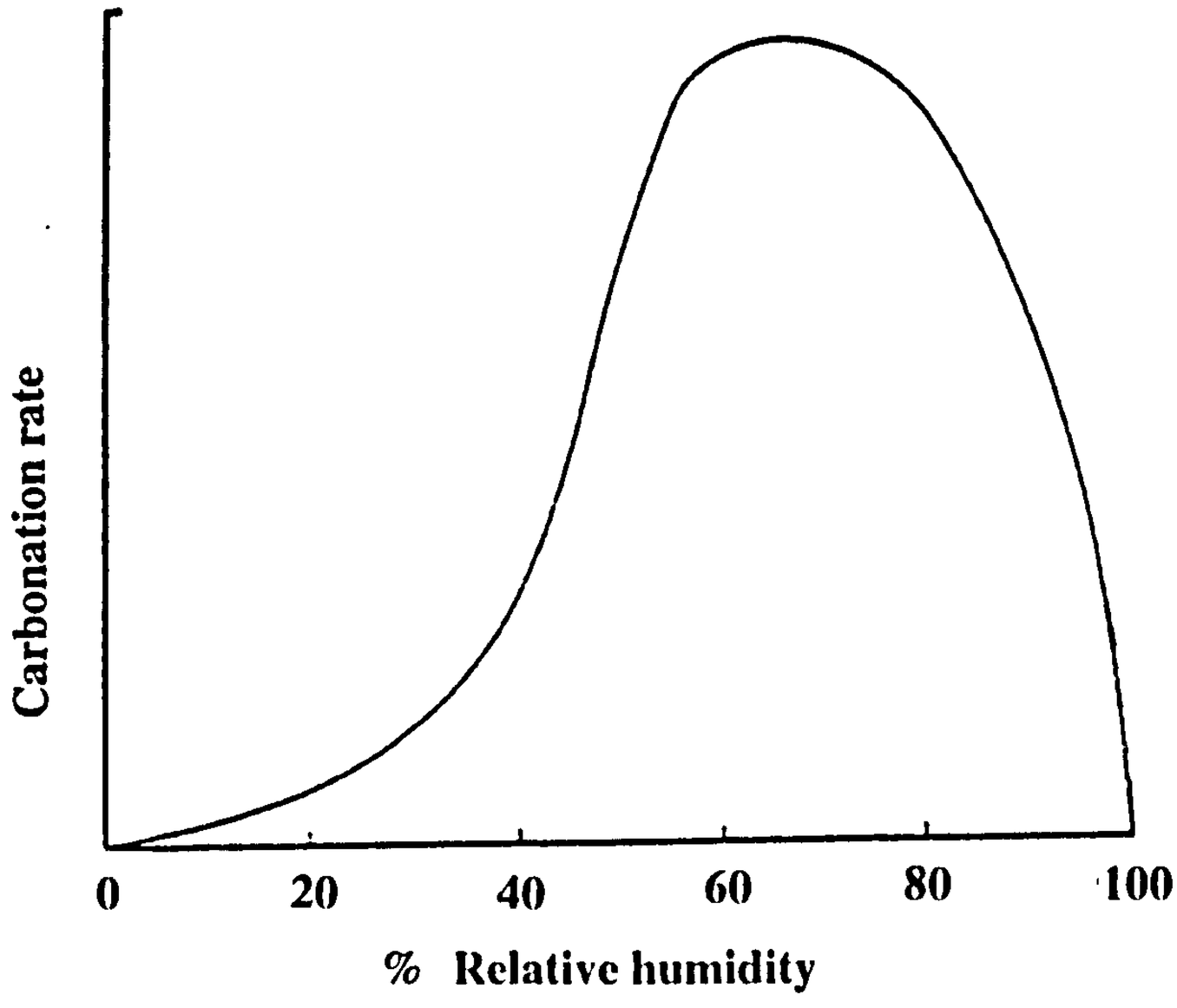

Figure 5.1 Rate of carbonation of hardened cement paste or concrete as a function of relative humidity (Tuutti, 1982).

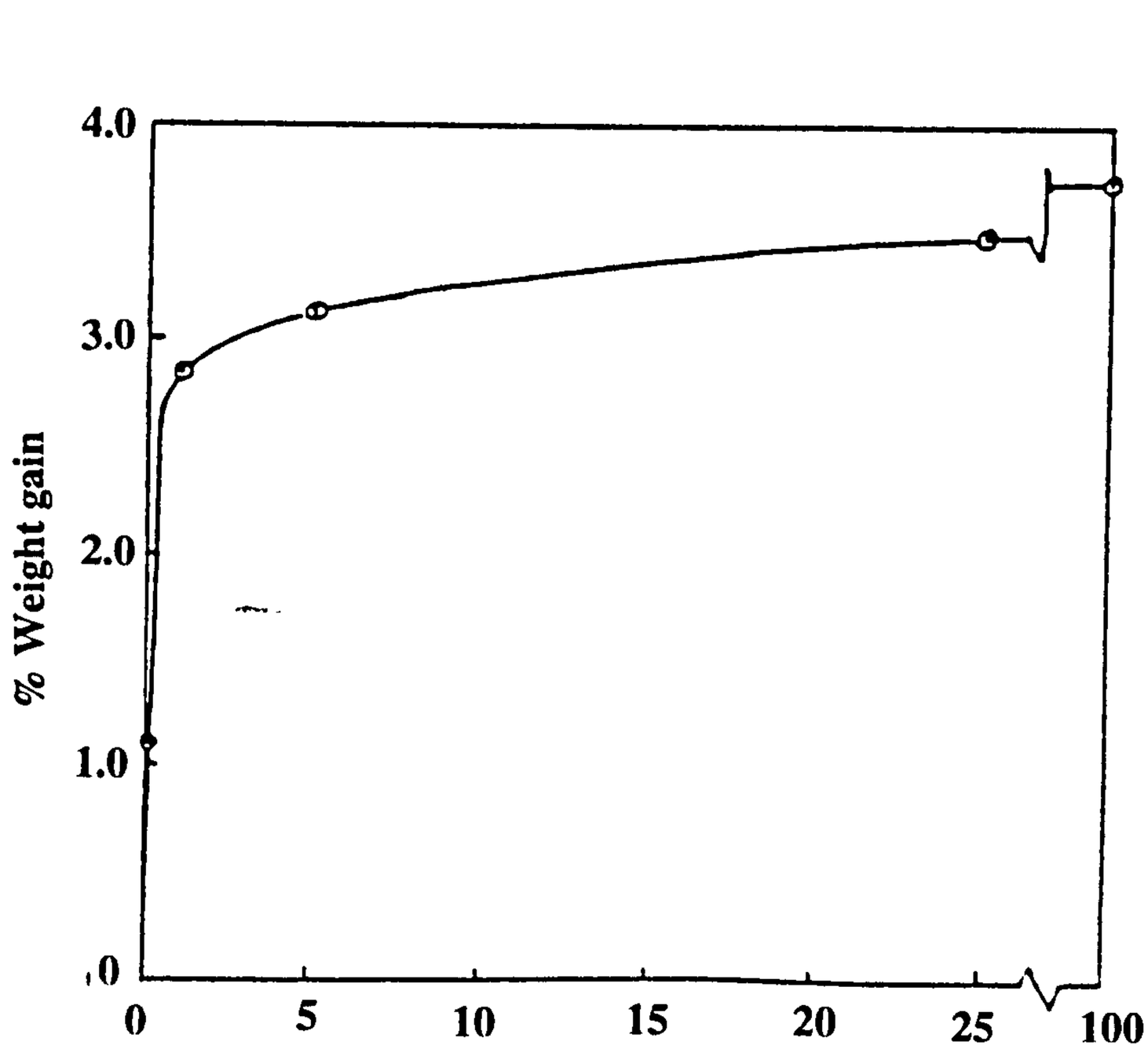

Figure 5.2 Weight gain due to carbonation at different carbon dioxide concentrations (Verbeck, 1958).

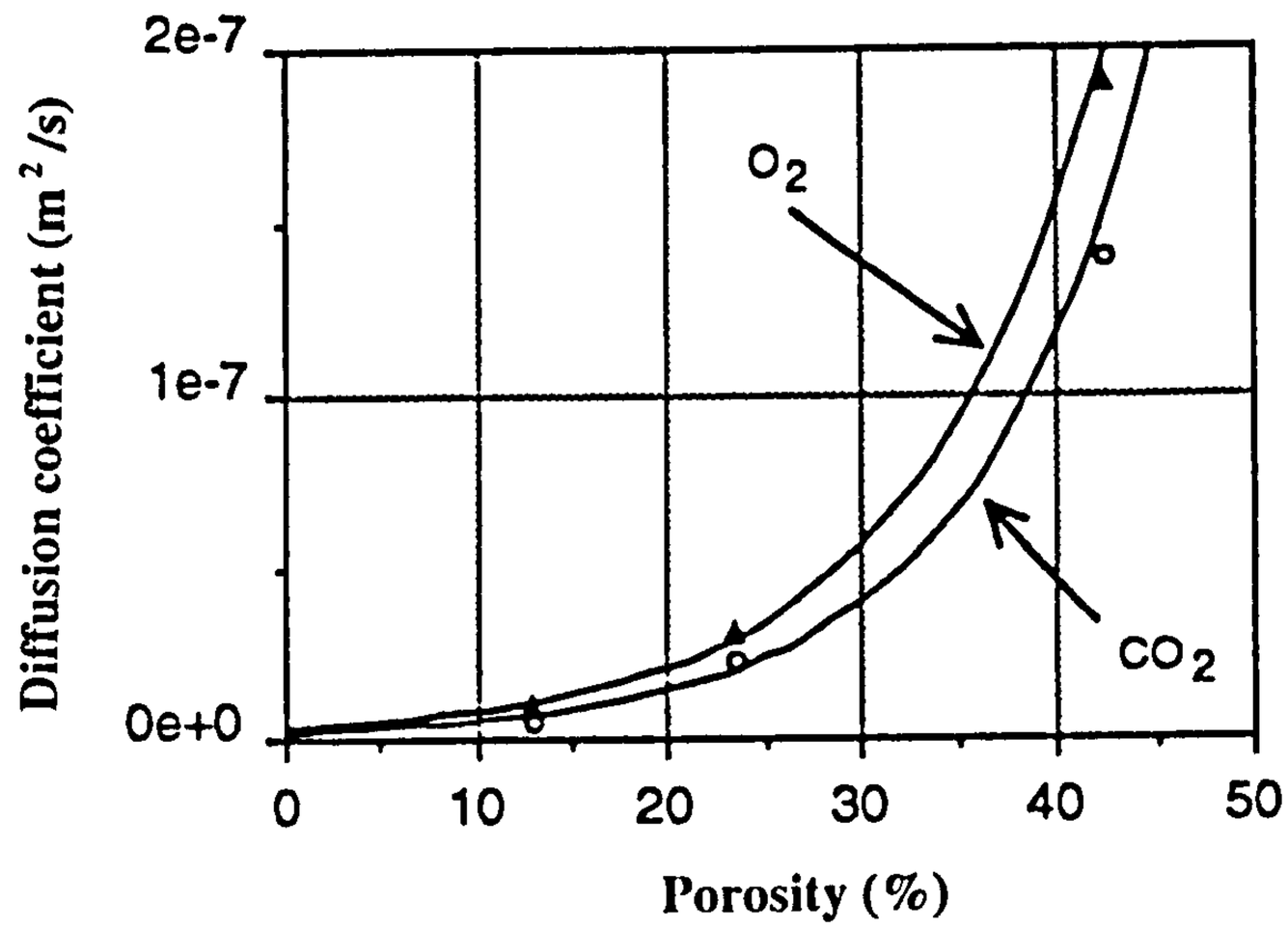

Figure 5.3 Influence of the porosity of HCP on effective diffusion of CO_2 at 55% RH (Houst and Whittmann, 1994).

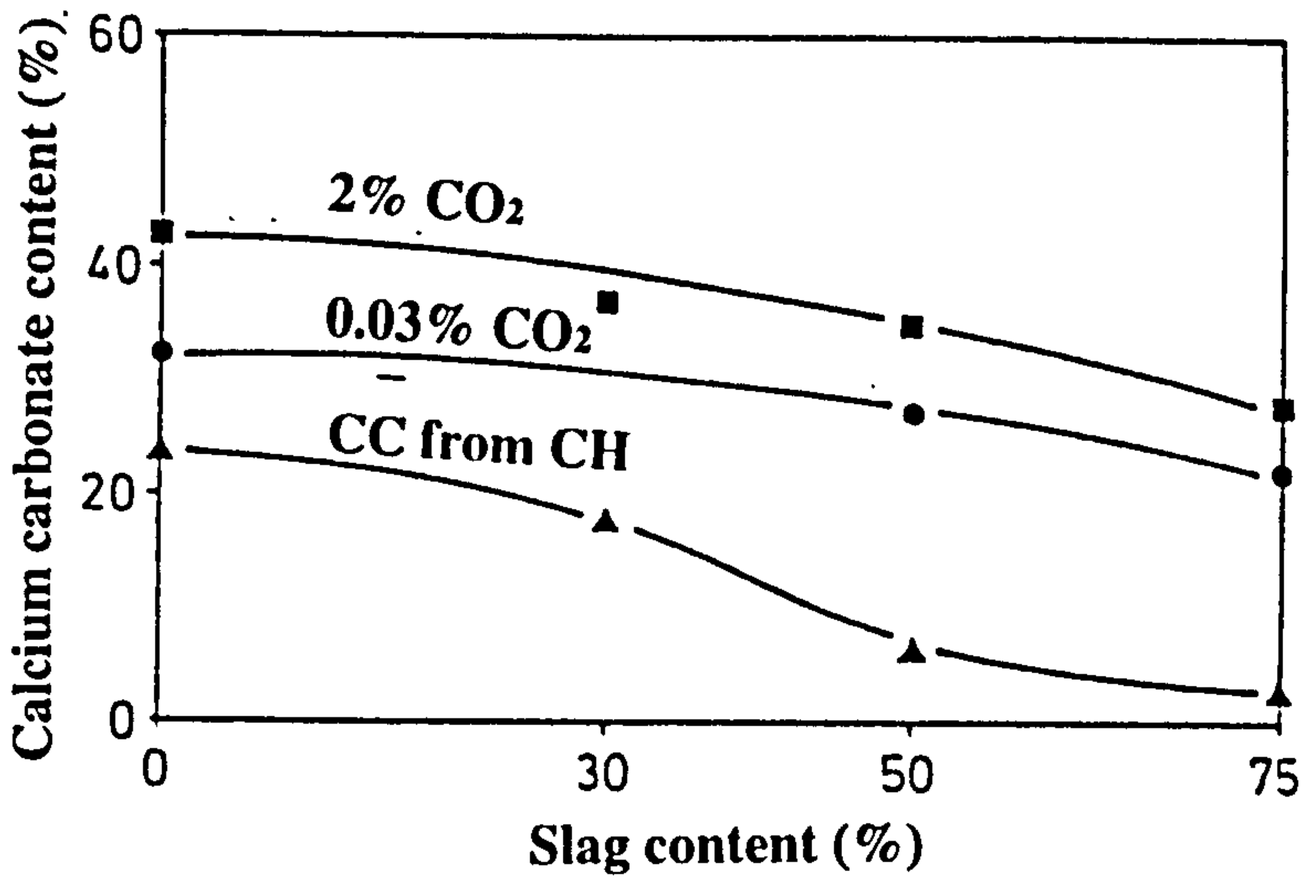

Figure 5.4 Effect of slag content on the rate of carbonation as a function of calcium carbonate content (Bier et al, 1987).

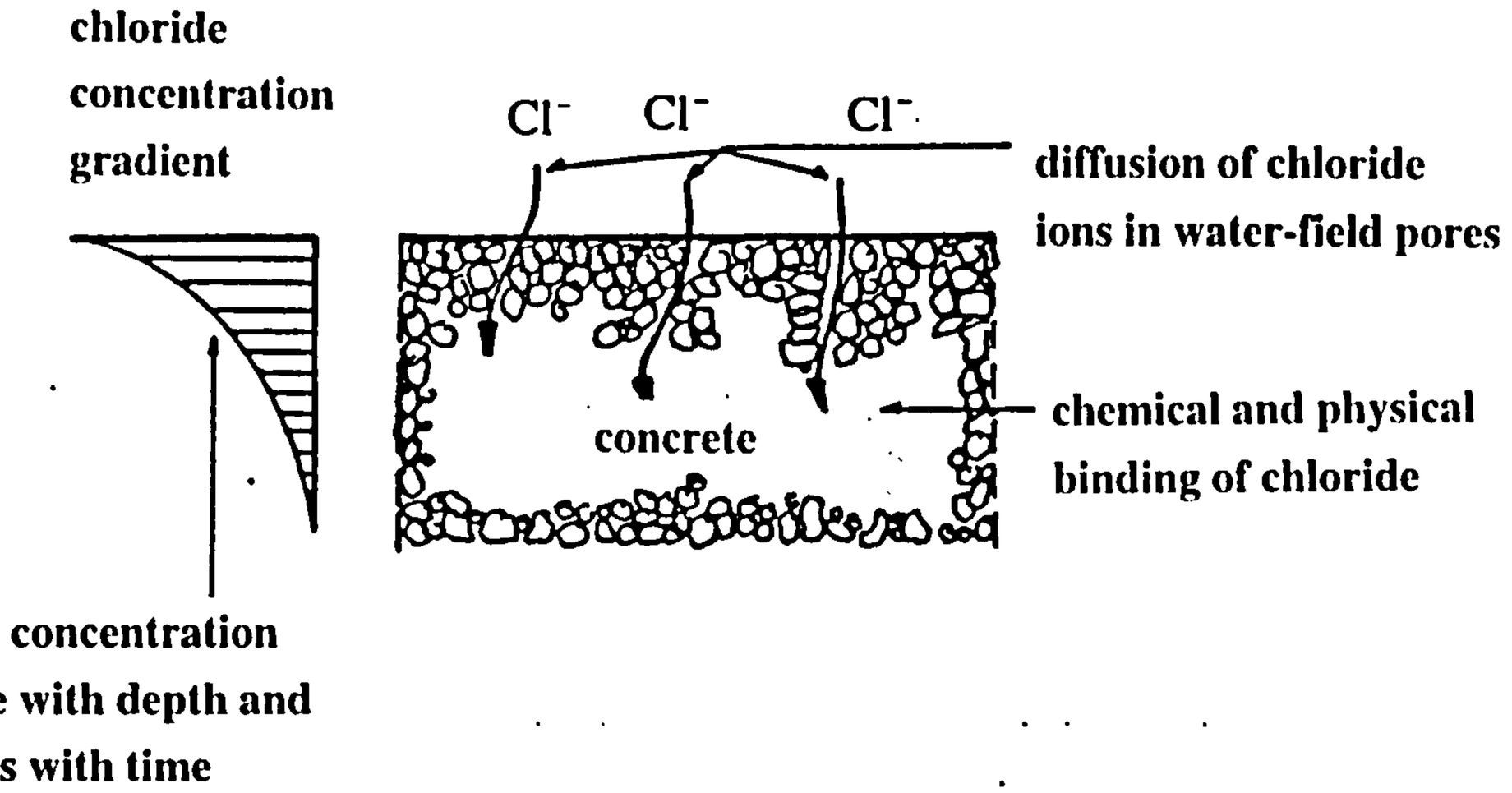

Figure 5.5 Diffusion of chloride into hardened concrete (Schiessl, 1983).

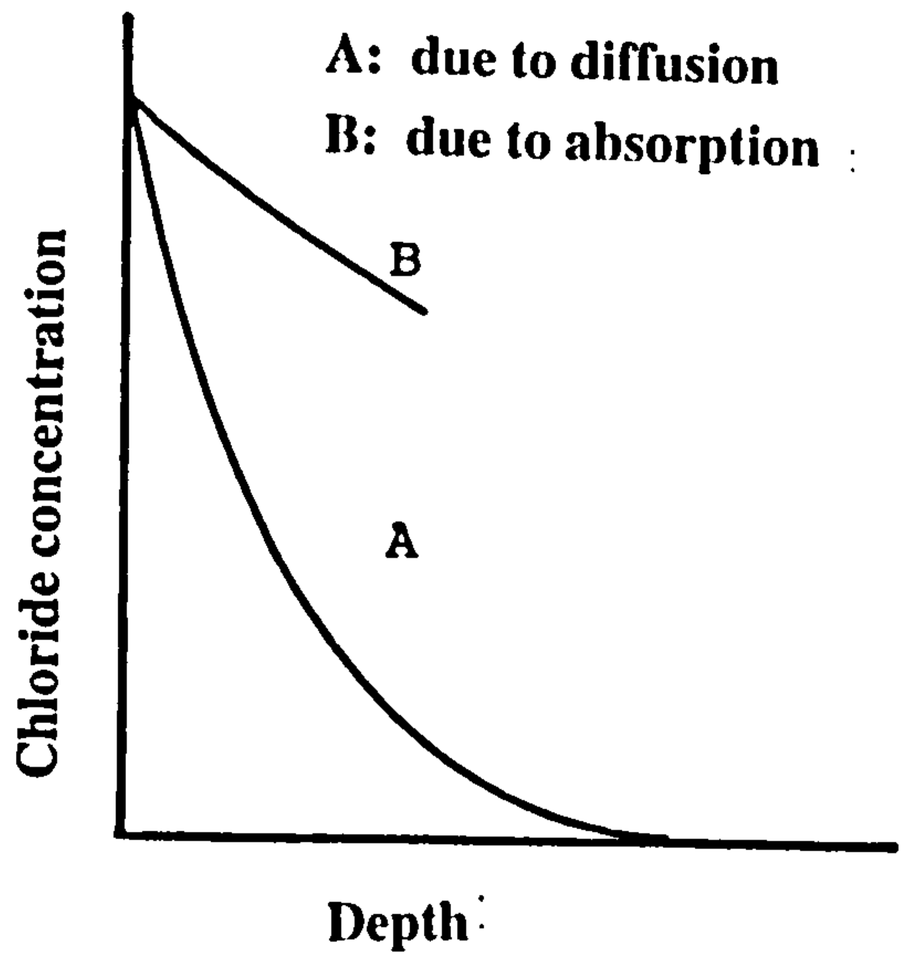

Figure 5.6 Comparison between chloride content profile due to diffusion and absorption (Schiessl, 1983).

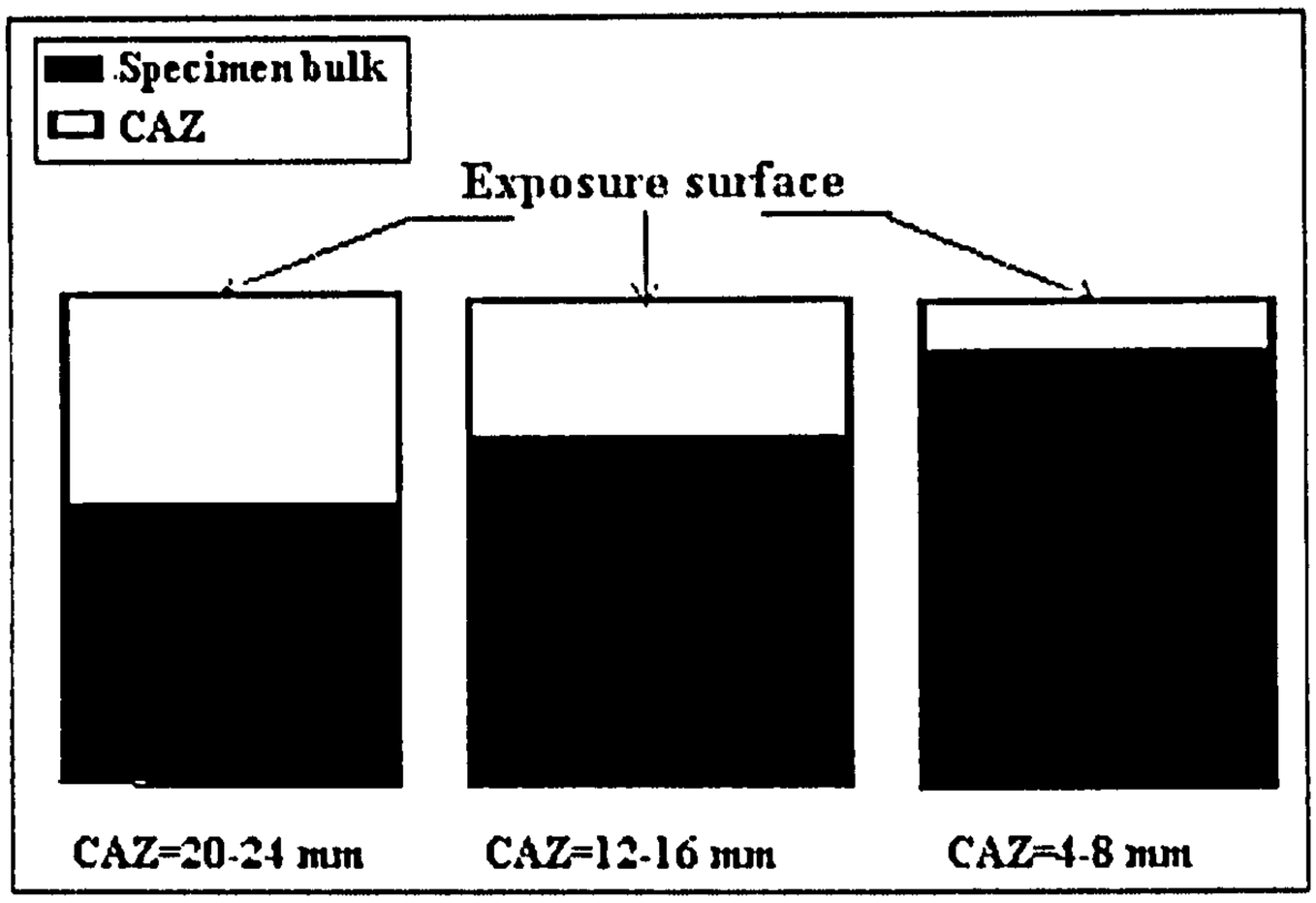

Figure 5.7 Exposure of specimen of different CAZ to carbon dioxide and chloride.

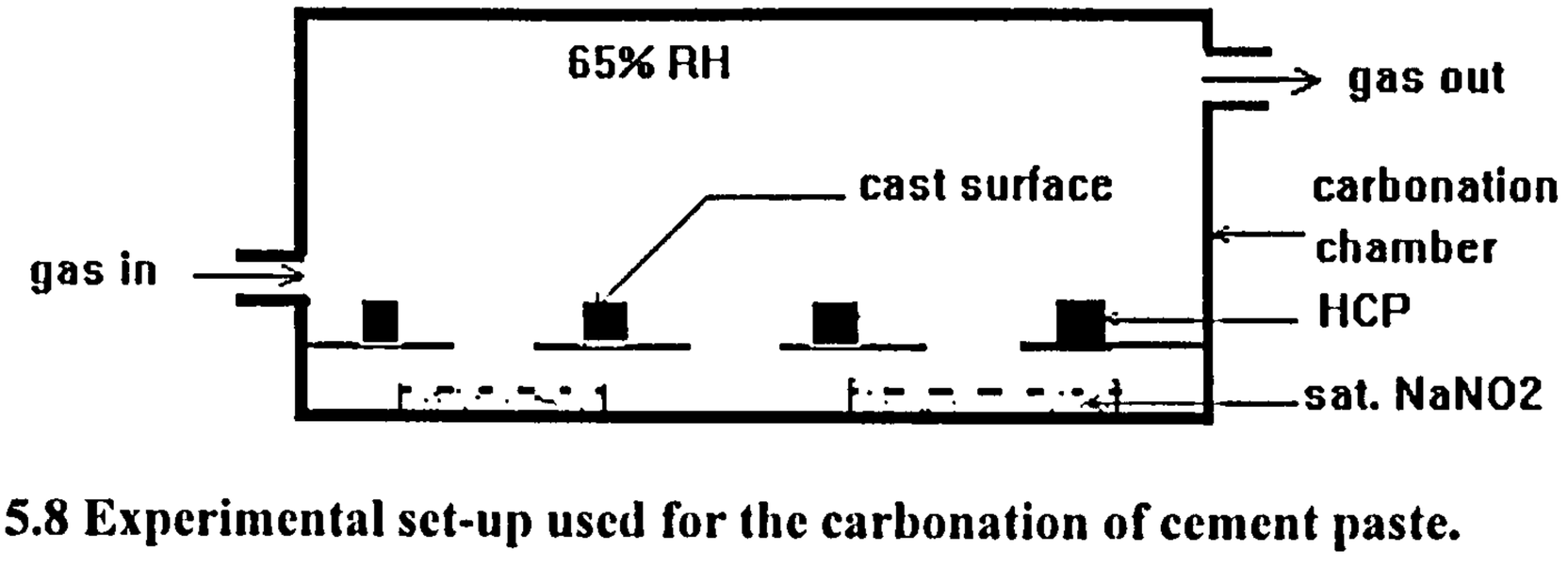

Figure 5.8 Experimental set-up used for the carbonation of cement paste.

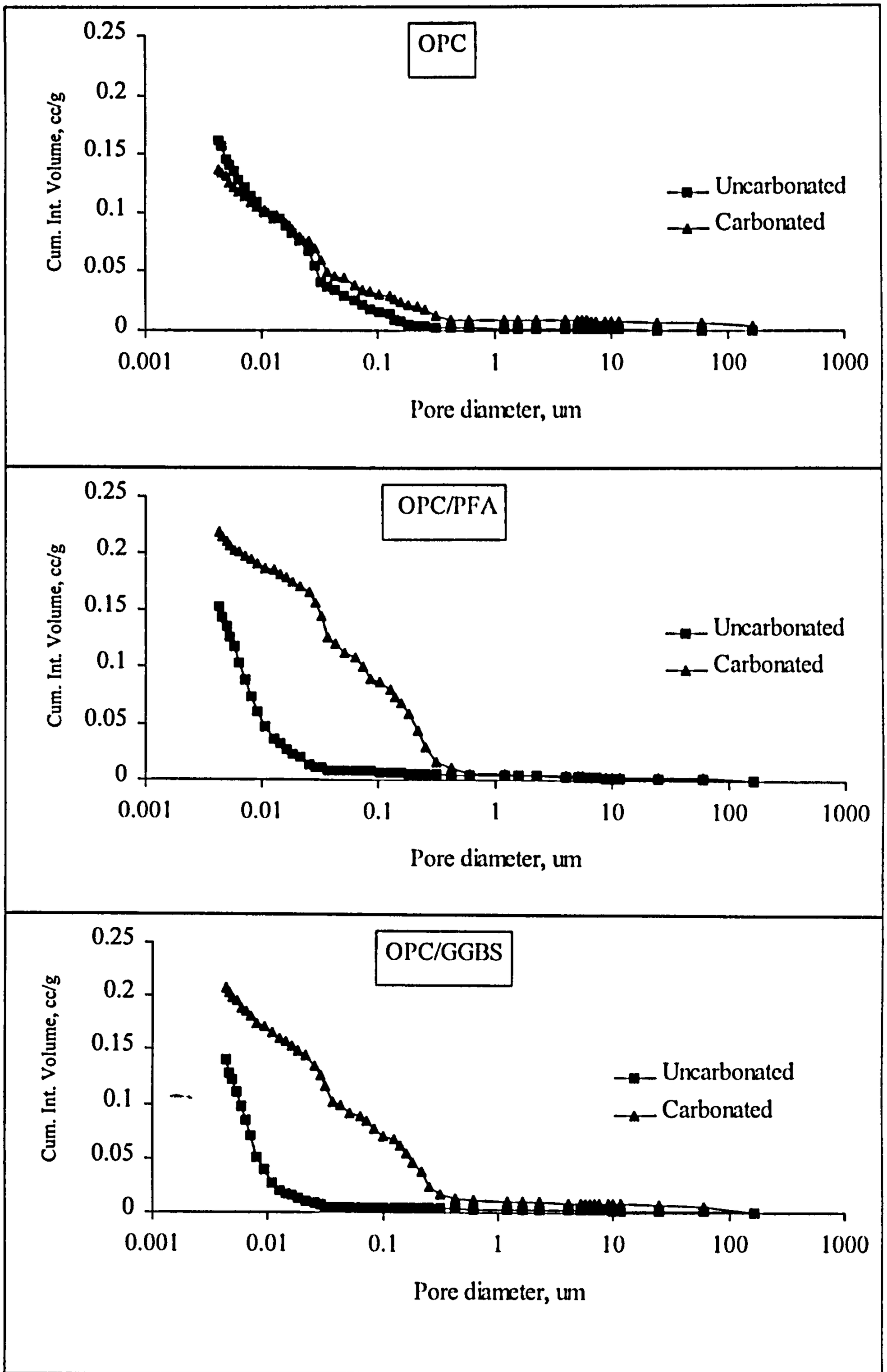

Figure 5.9 PSD of different carbonated and uncarbonated cement pastes, using w/c = 0.55 and E4 curing.

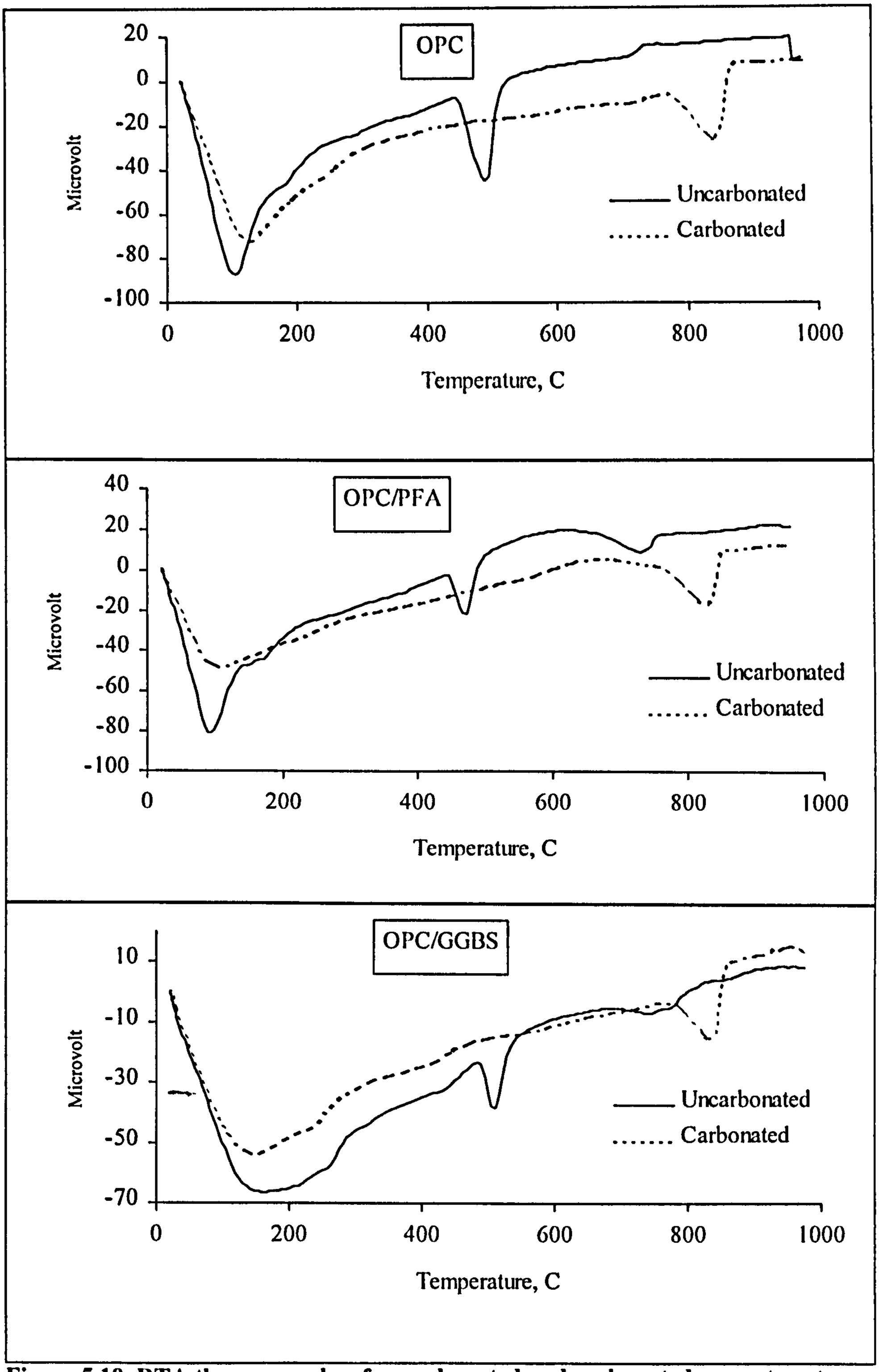

Figure 5.10 DTA thermographs of uncarbonated and carbonated cement pastes made from different materials, using w/c = 0.55 and E4 curing.

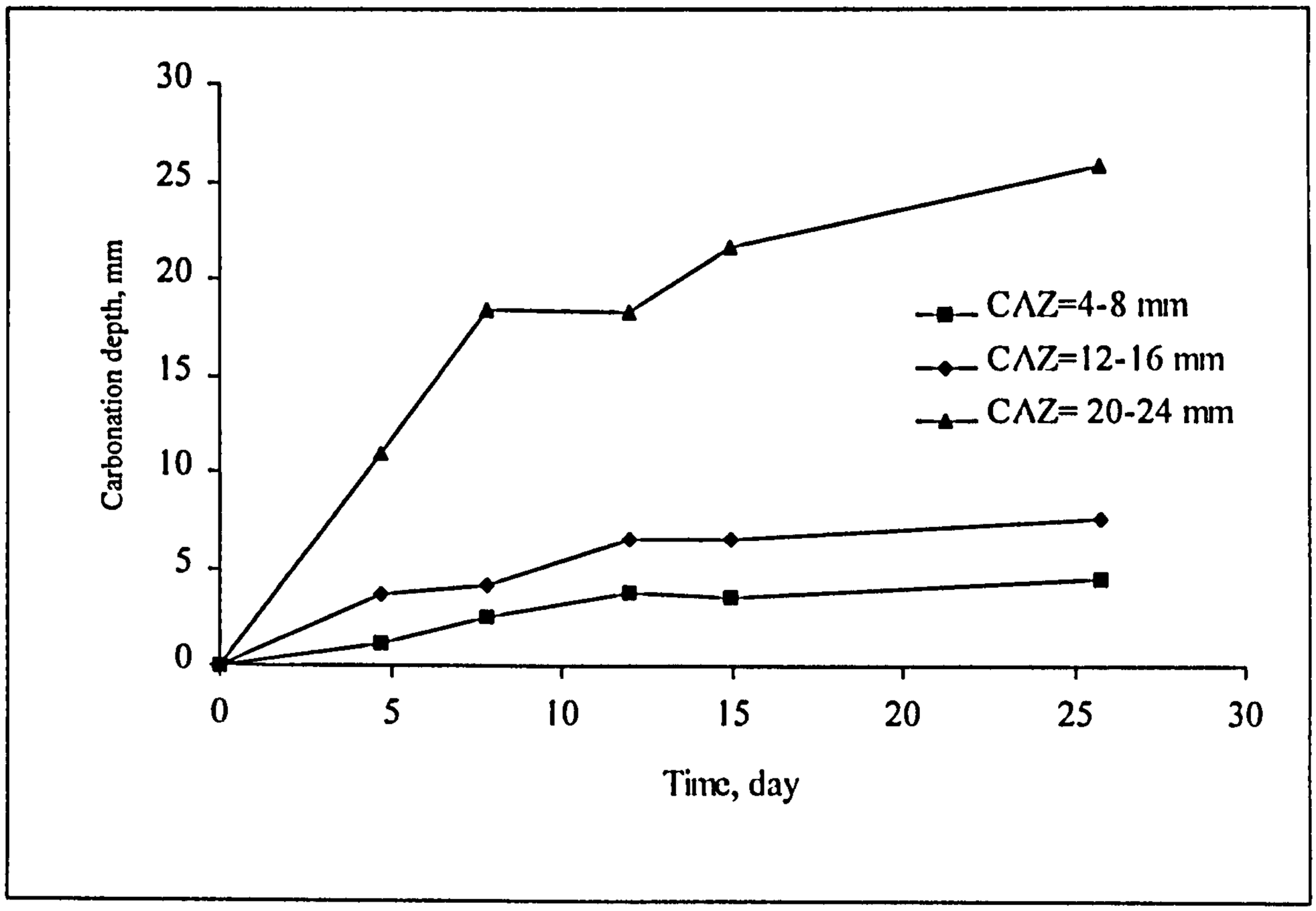

Figure 5.11 Effect of CAZ depth on the rate of carbonation of OPC concrete, w/c = 0.55.

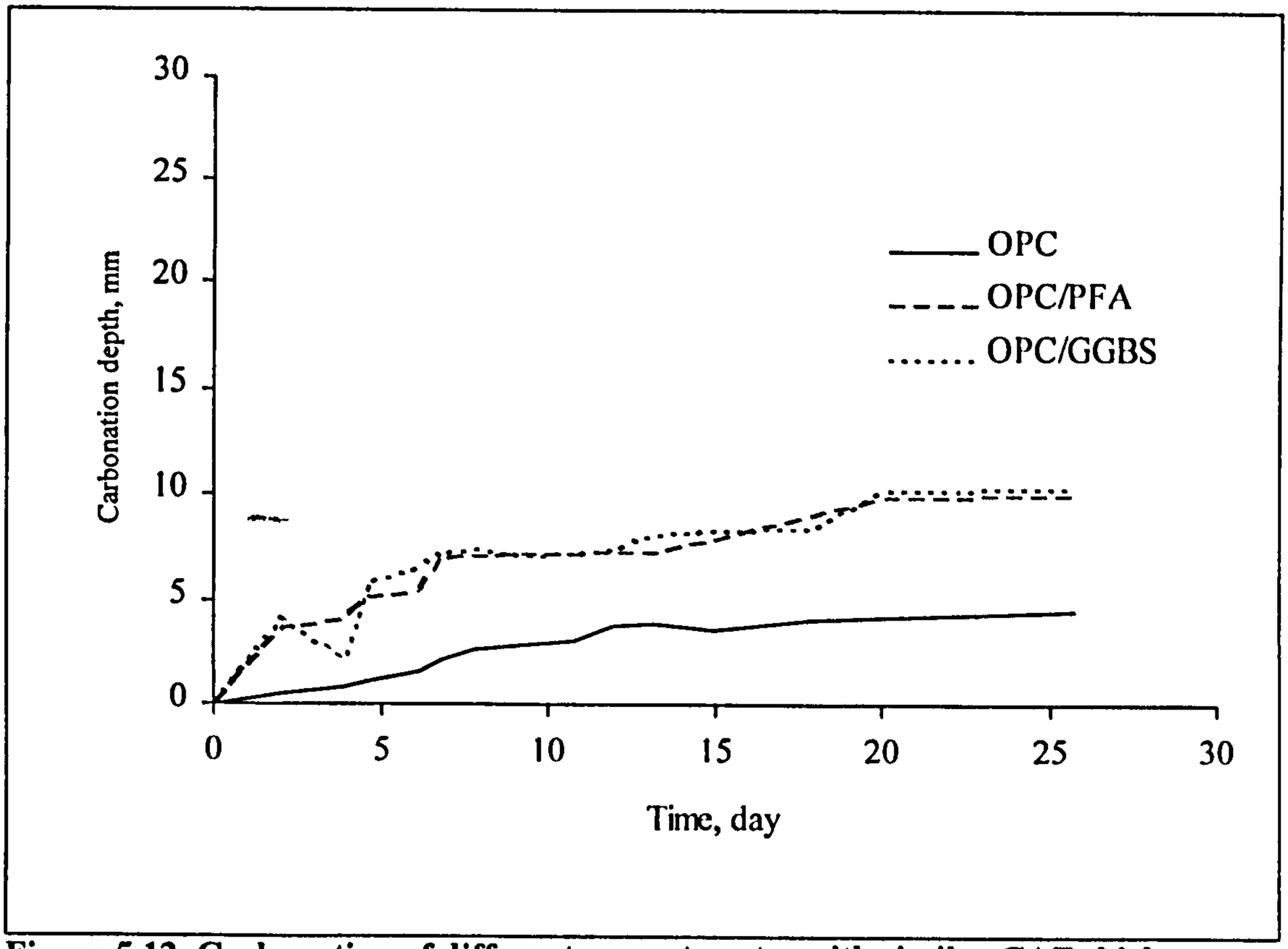

Figure 5.12 Carbonation of different cement pastes with similar CAZ thickness (4-8 mm), w/c = 0.55.

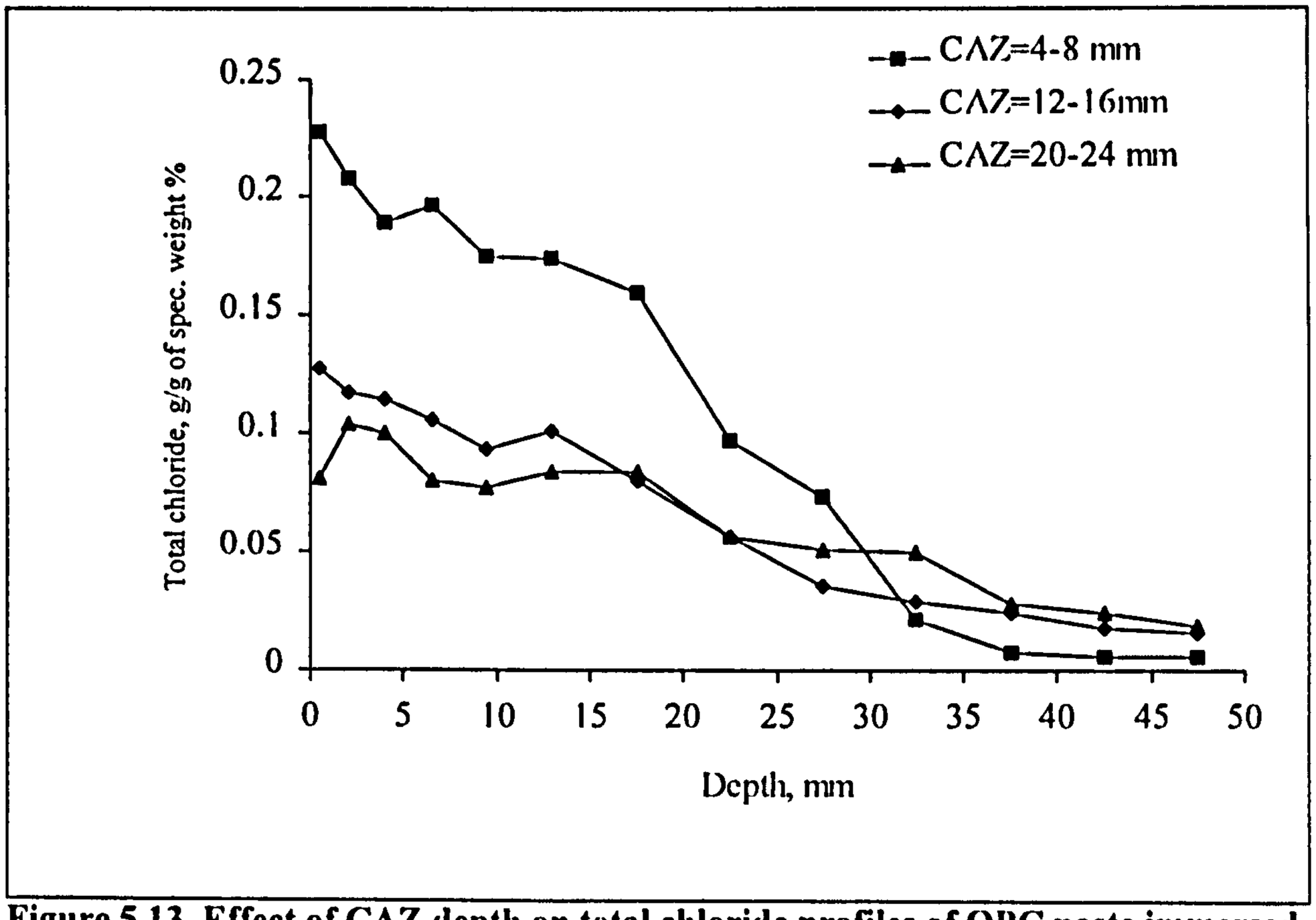

Figure 5.13 Effect of CAZ depth on total chloride profiles of OPC paste immersed in 1M of NaCl solution for 8 months, w/c = 0.55.

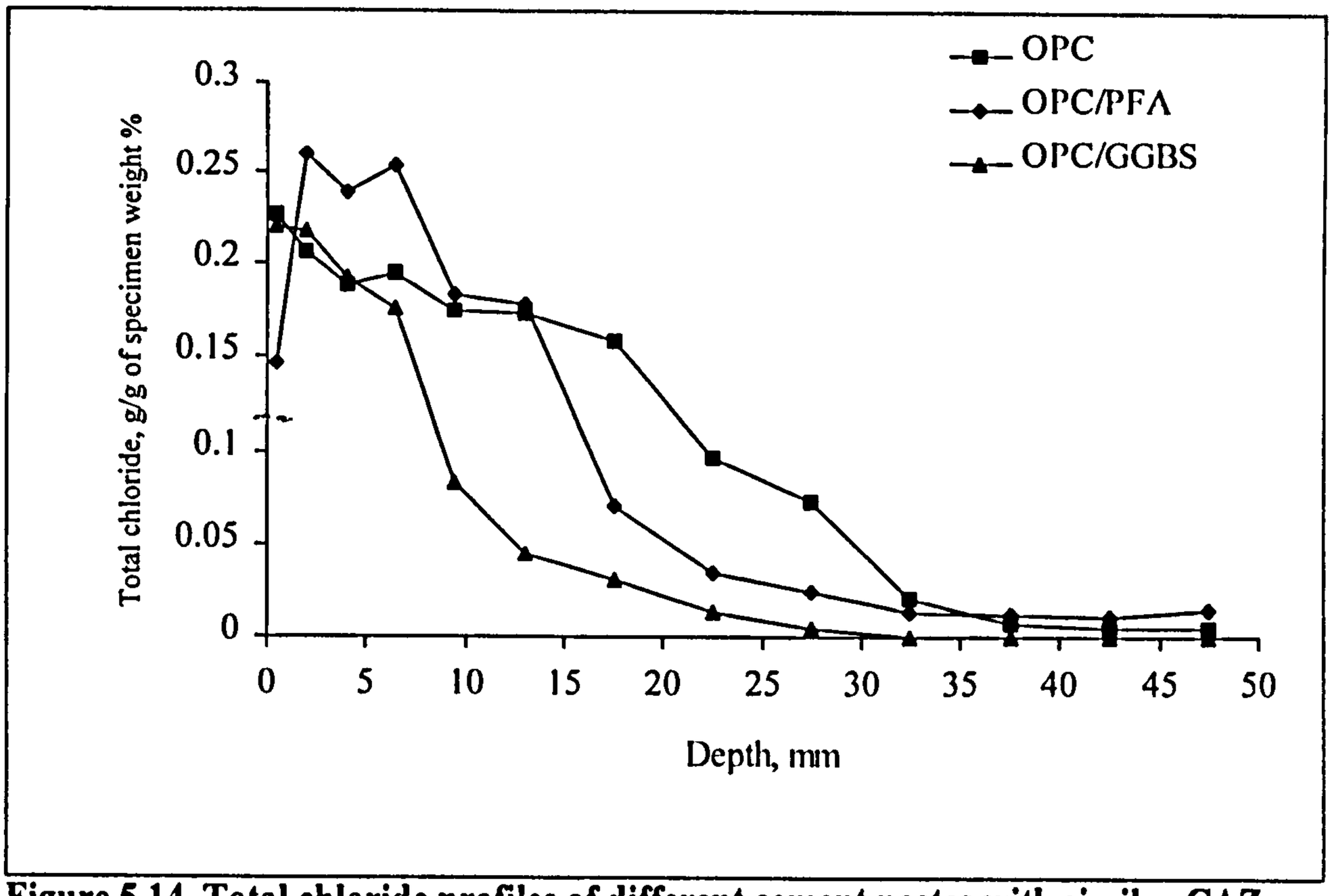

Figure 5.14 Total chloride profiles of different cement pastes with similar CAZ thickness (4-8 mm), w/c = 0.55.

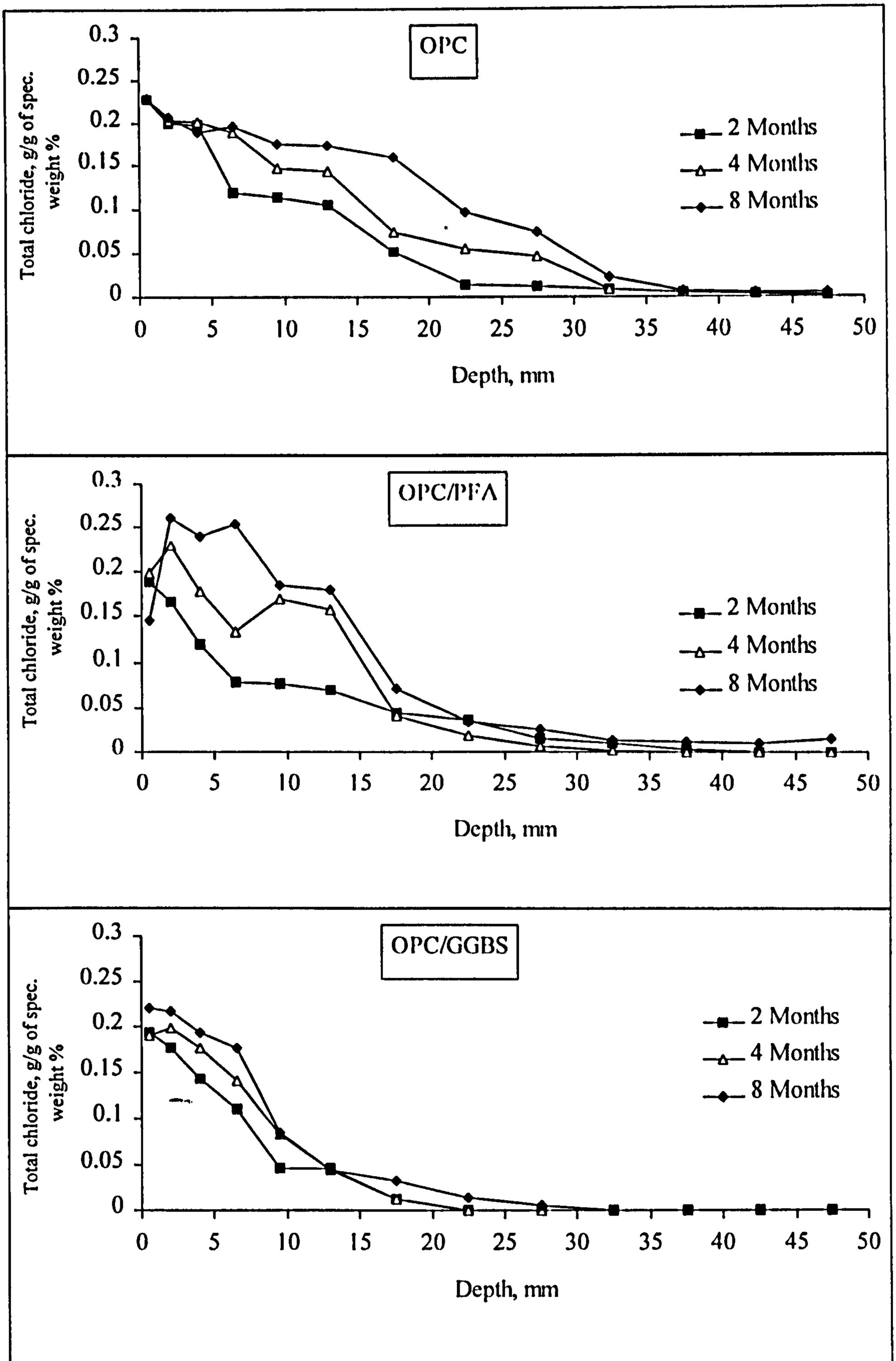

Figure 5.15 Effect of exposure period on total chloride profiles of different cement pastes of similar CAZ thickness (4-8 mm), w/c = 0.55.

CHAPTER 6

INFLUENCE OF CONTROLLED PERMEABILITY FORMWORK ON MICROSTRUCTURE AND TRANSPORT PROPERTIES OF THE SURFACE ZONE

6.1 INTRODUCTION

It is generally understood that good concreting practice including low w/c ratio, sufficient concrete cover to the reinforcement and adequate curing should, in most circumstances, produce concrete capable of resisting carbonation and moderate exposure to chloride (Swamy and Tanikawa, 1993). There are still cases, however, either because of inadequate control during construction or owing to adverse climatic conditions, where poor quality concrete is produced. This appears to be a major problem in hot Middle Eastern countries where w/c ratio can be much higher than levels recommended in the specifications and curing is inadequate as the excess mix water evaporates very quickly allowing the formation of large capillary pores.

Proper curing is the most common method for improving the durability of concrete (Section 3.2.5). However, curing can be expensive (if a curing membrane is used) or time consuming and laborious (if the surface is sprayed with water at regular intervals). In some cases, even prolonged curing may not be adequate to achieve high durability requirements. Therefore, alternative methods have been used in the recent past in order to improve the durability of near surface concrete. This includes the use of surface treatments such as silanes on hardened concrete and the removal of excess water from fresh concrete during the initial setting and hardening stage with a controlled permeability formwork system (Long et al, 1992 and Basheer et al, 1993).

The use of controlled permeability formwork (CPF) minimises the drawbacks of the conventional impermeable formwork (IF) which is either steel or hard faced plywood (impermeable to both air and water). Air and water migrate during the compaction towards impermeable formwork and get trapped near the concrete/formwork interface leading to higher water/cement ratio near the surface than in the bulk concrete (Price and Widdows, 1991). Therefore, the cover concrete is more porous than the bulk

concrete. This process leads to the formation of excessive amounts of blowholes on the cast concrete surface. Therefore, the use of permeable formwork would be expected to alleviate the problems caused by trapped air and water at the cover concrete zone. This means that the use of controlled permeability formwork (CPF) can be considered to be one of the possible practical ways of minimising the penetration of aggressive agents into concrete by improving the properties and performance of the near surface zone.

This chapter explores the microstructural and microhardness properties of concrete cast against both permeable and impermeable formwork and determines the depth of the CPF affected zone (CPFAZ) for concrete with various mix proportions. CPFAZ is the distance from the surface to a certain point within concrete where the use of CPF has no significant effect on the properties of concrete. The use of CPF on OPC concrete and OPC/30%PFA and OPC/60%GGBS concrete with a range of w/c ratios was investigated to study the influence of CPF on chloride ingress and the rate of carbonation.

6.2 LITERATURE REVIEW

6.2.1 Basic Concept of CPF

CPF systems consist of a specially engineered permeable membrane tensioned on to a structural support made from one of many traditional types of formwork material. The CPF liner is made up of a multitude of micro pores, so that it acts like a filter retaining the concrete fines but allowing the water and air normally trapped at the formwork/concrete interface to be evacuated (Wilson, 1994a), as shown in Figure 6.1. During placing and compaction, air and a proportion of the free water in the mix move towards the face and pass through the CPF liner to drain away at the interface between the liner and the backing material. This drainage period is believed to vary between 2 and 4 hours and the quantity of water drained is dependent upon the water/cement ratio and generally varies between 1 and 2.5 l / m^2. The use of CPF, therefore ensures that the water/cement ratio of the cover concrete is kept low producing a denser, less permeable surface (Barfoot, 1991 and Price and Widdows, 1993), as shown in Figure 6.2. It can also be seen in Figure 6.2 that the thickness of the cover concrete affected by the use of CPF is in some cases about 10-20 mm.

Kasai et al (1988) compared the cement content of near surface concrete cast against permeable and conventional formwork (plywood) and found that the cement content increased with depth, up to 5 mm from the concrete surface for concrete cast in permeable formwork. The cement content of concrete cast against permeable formwork was 23 kg/m^3 to 76 kg/m^3 higher than that of the corresponding conventional formwork. This was attributed to the cement displacement towards the formwork surface due to bleeding. Since there is only a limited knowledge about the use of CPF and its effectiveness in providing a sound durable surface concrete layer, further work is necessary to characterise its performance.

6.2.2 Effect of CPF on Cover Concrete Microstructure

The reduction of water/cement ratio and the percentage of air content due to the use of CPF influences the development of the pore size distribution (PSD) leading to modification of the pore structure of the cover concrete. Kasai et al (1988) studied the total pore volume (TPV) of concrete specimens cast against CPF and impermeable formwork, at different depths from the cast surface. He found that the TPV at 0 to 7.5 mm and 0 to 30 mm from the CPF surface was reduced by 50% and 70% respectively, compared to that of conventional specimens. There was no considerable difference between the use of CPF and impermeable formwork in terms of TPV for locations at depths further than 30 mm from the surface. However, the effect of CPF on the pore size distribution and total and capillary porosity of concrete has not been fully investigated.

6.2.3 Properties of Concrete Cast Against CPF

Long et al (1992) compared the mechanical properties of concrete surfaces cast against both CPF and impermeable formwork using pull-off tests and concrete surface abrasion resistance measurement, and found that there was a significant increase in surface strength and surface resistance due to the use of CPF. Tsukinaga and Shoya (1993) assessed different types of CPF using pull-off strength test and found that all CPF types increased the strength of the cover concrete zone, confirming Long et al's (1992) findings. However, the amount of increase in strength was found to be dependent upon the CPF type. Basheer et al (1993) treated concrete surface cast against both CPF and IF with silane and found that the surface tensile strength for both treated and untreated

CPF concrete was greater than the corresponding concrete cast against IF. They also reported that the surface treatment had no effect on the tensile strength of the cover concrete cast against either CPF or IF.

It was also found that the surface hardness of concrete increased when cast against CPF (Price and Widdows, 1991 and Long et al, 1992). Price and Widdows (1991) reported that the increase in surface hardness (using schmidt hammer) for grades C20 and C30 concrete produced material surface hardness equivalent to that conventionally produced of grade C50 concrete. This has been confirmed again by Price et al (1993) who assessed the concrete surface hardness in different environments and noted marked improvements due to the use of CPF in both hot/dry and hot/wet environments.

The main findings reported by Price and Widdows (1991) on the use of CPF are summarised as follows:

(i) A marked reduction in sorptivity for OPC concrete cast against CPF.

(ii) A considerable reduction in the initial surface absorption (ISA) for OPC concrete cast against CPF.

(iii) A reduction in the water permeability and an increase in the tensile strength for OPC concrete cast against CPF.

(iv) A reduction in the carbonation depth for all grades of OPC concrete examined.

In addition to the above-mentioned improvements in the concrete permeation properties, Long et al (1992) has found that the use of CPF results in a marked reduction in air permeability (ten fold) of OPC covercrete. Price et al (1992 and 1993) studied the effect of CPF on water absorption and chloride diffusion of OPC covercrete in different environments (hot/dry and hot/wet) and their findings are summarised below:

(i) There was a reduction in surface absorption for concrete cast against CPF in both hot/wet and hot/dry conditions.

(ii) The effective chloride diffusion coefficient of concrete cast against CPF was decreased by about 50% in hot/dry conditions and by as much as an order of magnitude in hot/wet conditions in comparison with the corresponding data for conventional formwork.

They also found that the effect of curing on cover concrete properties was less significant than the effect of CPF. However, curing after removal of CPF was recommended to produce highly durable concrete.

Many investigations reported that the use of CPF has improved the resistance of the cover concrete to freeze-thaw effects (Basheer et al, 1993 and Sugawara et al, 1993). The resistance increased when concrete cast against CPF was treated with hydrophopic surface penetrants (silane) after removing CPF. Similar results have been reported by Price et al (1993) who attributed those effects to the reduction of surface water/cement ratio and not to modifications in the air void system.

However, there is need for further information concerning the role of CPF on the microstructure, hardness and transport properties of the cover concrete. It is clear from the available literature, for example, that the effect of different curing regimes and cement replacement materials on the properties of the concrete cast against CPF has not yet been fully investigated.

6.2.4 Economic Aspects of Using CPF

Although, it is evident from the previous studies that a CPF system can significantly increase the durability of cover concrete, the feasibility of the extra cost incurred for CPF compared to other conventional formwork requires consideration. In an economic study carried out in Japan, it was reported that the use of CPF increased the cost of producing concrete by £3.5/ m^3 (Dept. of Trade and Industry, 1989). Wilson (1994b) has reported the main potential savings during construction and service life of the structure and compared these savings with the extra cost incurred due to the use of CPF.

As a result of the improvement in the properties of the cover concrete due to the use of CPF, the thicknesses of cover concretes cast against CPF might reasonably be reduced compared to those cast against impermeable formwork. However, the question arises as to how much extra covercrete can be saved due to the use of CPF.

6.3 EXPERIMENTAL PROCEDURES

6.3.1 Preparation of Specimens

Test specimens of 100x200x600 mm were constructed in a mould made of hard plywood (impermeable) to simulate an unreinforced wall. 5 mm diameter holes were drilled at 50 mm spacing on one of the vertical surfaces (200x600 mm) of the mould, to allow drainage of excess water from the vertical surfaces. CPF sheets (Zemdrain) were fixed to the drilled vertical face by fastening with adhesive tape around the perimeter allowing the fabric to be extended below the base to allow drainage of excess water.

The concrete and cement paste mix proportions used in this investigation are presented in Table 2.2. The specimens were cast in three equal layers and compacted on a vibrating table according to the procedures described in BS 1881: Part 125 (Section 2.4.1 and 2.4.2). Immediately after compaction, the upper surface of the specimen was covered with a hard plywood cover of 100x200 mm. It was noted that the drainage of the excess water observed in the cover concrete cast against CPF continued after casting for approximately three hours. The formwork was removed 24 hours after casting and the specimens were then cured with E1, E3 and E4 curing as described in Section 2.5.

After curing, 100 mm diameter cores were cut through the central region of the CPF surface of the cement paste and concrete specimens and this provided a core with two surfaces, one cast against CPF and the other against IF. These cores were used for PSD, total and capillary porosity, chloride and carbonation studies. 12x50x100 mm slices for microhardness and scratch hardness studies were also cut from the central region of the concrete specimens perpendicularly to the CPF surface with a circular saw, using water as the lubricant. The specimens were taken from the central region to avoid variations caused by bleeding and segregation in the top and the bottom layers of the specimens.

6.3.2 Tests

Immediately after coring and slicing, the following tests were carried out.

6.3.2.1 Pore size distribution (PSD)

The cement paste cores chosen for PSD study were dry cut into discs at 5, 10, 15, 20, 25 and 35 mm from the two end surfaces, as shown in Figure 6.3. The discs were broken into small fragments and approximately 3.0 g of the sample was weighed and then

subjected to mercury intrusion porosimetry (MIP) with a Micrometric Model 9310 Pore Sizer. The specimen preparation and test procedures for PSD are described in detail in Section 2.6.3.

6.3.2.2 Total and capillary porosity

The cement paste cores chosen for this study were sliced into discs similar to those for PSD study and the discs were immediately vacuum saturated for 48 hours to ensure that all pores were filled with de-ionised water. The disc specimens were then conditioned in a desiccator maintained at 90.7% RH for the determination of capillary porosity, and finally oven dried at 105° C to determine the total porosity. The detail of this test is described in Section 2.6.2. The capillary porosity measured in this investigation represents the pores of diameter greater than 30 nm (Parrott, 1992; Ngala, 1995; Ngala et al 1995 and Page and Ngala, 1995).

6.3.2.3 Indentation microhardness and scratch hardness

12x50x100 mm concrete slice specimens were prepared and tested for indentation microhardness and scratch hardness following the procedures described in Sections 4.3.2.1 and 4.3.2.2, respectively. The indentation microhardness and scratch hardness tests were carried out at 2, 6, 10, 14, 18, 22, 26 and 34 mm from both CPF and IF surfaces. The geometry of scratch drawn on the specimens was evaluated by means of optical processing of the image which is described in detail in Section 4.3.2.2. The means of thirty microhardness and seventy five scratch width results were obtained for each depth from triplicate specimens.

To study the effect of formwork type on the aggregate/cement paste transition zone (TZ) in concrete, indentation microhardness measurements were taken at $\cong$ 0, 10, 20, 40 and 80 μm from the aggregate surface and within the first 3 mm from CPF and IF surfaces (see Figure 6.4). The measurements were taken around at least 3 aggregate particles in each specimen such that all the indentations were on a plane parallel to the CPF and IF surfaces. An average of thirty results was obtained for each distance from the aggregate surface from triplicate specimens.

6.3.2.4 Chloride penetration test

The circumferential face of the cores chosen for this study were masked with four layers of wax leaving the CPF and IF surfaces exposed, as shown in Figure 6.5. Then, the cores were vacuum saturated in de-ionised water for 48 hours to ensure that all pores were filled with water. The cores were then immersed in a solution of 1M NaCl and 35 mM of NaOH, and maintained at 21 ±2° C for 110 days. The specimens were then removed from the solution and immediately profile ground from the CPF or IF surface inwards, using a precision lathe. Dust from grinding was then collected at successive depths and analysed for total chloride content as described in Section 2.6.9.

6.3.2.5 Carbonation test

The specimens for carbonation test were pre-conditioned in a chamber maintained at 65% RH using saturated sodium nitrite for at least three months until a steady weight was achieved signifying a constant internal RH of the specimens. After pre-conditioning, the specimens were sealed similarly to those used for chloride penetration study, as shown in Figure 6.5. The specimens were then transferred to a carbonation chamber maintained at 21 ±2° C and 65% RH filled with 100% CO_2 for 24 days. The experimental set-up used for carbonation is similar to that used for cement paste specimens as described in Section 5.3 (see Figure 5.8). At the end of exposure period the cores were split open and the broken surface was sprayed with a phenolphthalein indicator along the whole length of the specimen. The depth of carbonation from both the CPF and IF surfaces was measured using a travelling microscope, as described in Section 2.6.10.

6.4 RESULTS AND DISCUSSION

6.4.1 Effect of CPF on Pore Structure

Figure 6.6 shows the PSD at different depths for OPC paste of w/c 0.6 cast against CPF. It can seen that CPF produced a finer PSD near the surface than in the bulk of the specimen, and the effect diminished with depth below the surface. There was also a reduction in the pore threshold diameter in the surface layer and this reduction diminished with increasing depth below the CPF surface (from 30 nm at the CPF surface to 100 nm).

The total and capillary porosity determined from water desorption tests applied to triplicate specimens at different depths from the surface of OPC paste cast against both CPF and IF are presented in Figure 6.7. There is a significant reduction in the capillary and total porosity due to the use of CPF at all depths. However, the effect of CPF was more pronounced for the capillary porosity than for the total porosity and the maximum reduction of the capillary and total porosity was about 220% and 15%, respectively. These reductions diminished with increasing distance below the surface and are in agreement with the PSD results shown in Figure 6.6.

The modification of the PSD and reductions of the total and capillary porosity of cement paste cast against CPF can be attributed to the removal of excess water from the covercrete, resulting in a lower w/c ratio in the cover zone (Basheer et al, 1993 and Wilson, 1994a and 1994b). On the other hand, the diminishing effect of CPF with increasing depth below the CPF surface can be as a result of a w/c ratio gradient established due to drainage of excess water from the paste.

6.4.2 Effect of CPF on Microhardness of Cement Paste Matrix

The microhardness profiles of OPC concrete cast against CPF and IF with different water cement ratios are presented in Figure 6.8. At a low w/c ratio (0.5), there was no significant difference between the microhardness profiles of concrete cast against both CPF and IF. The statistical analysis (Table 6.1) of microhardness data taken at 2 mm depths from the formwork surface showed that there was no significance difference between the mean microhardness values near the surface of OPC concrete with 0.5 w/c cast against CPF and IF. On the other hand, at higher w/c ratios (0.6 and 0.7) the near surface microhardness of the cement paste matrix cast against CPF increased by about 210 and 200% compared with those of the corresponding specimens cast against IF for w/c 0.6 and 0.7, respectively. These results were confirmed statistically using a t-test as shown in Table 6.1, which shows that there is a significant difference between the microhardness of 0.6 and 0.7 w/c ratio concrete cast on CPF and IF. However, this enhancement diminished with increasing depth from the CPF surface and the CPFAZ increased with increasing w/c ratio. It can be estimated from Figure 6.8 that the CPFAZ was 0, 14 and 18 mm for concrete of w/c 0.5, 0.6 and 0.7, respectively. The increase in CPFAZ thickness with increasing w/c ratio was attributed to the profile of water content

in the concrete cover (Wilson, 1994b), which consequently affected the microstructure and hardness of the cover concrete.

Figure 6.9 shows the scratch width profiles of OPC concrete with different w/c ratios cast against CPF and IF. The results of the statistical analysis (t-test) for scratch width data are given in Table 6.2. It can be seen from Figure 6.9 that the use of CPF reduced the scratch width in the cover zone and the percentage reduction increased with increasing w/c ratio. The amount of this reduction at the near-surface zone reached 20, 90 and 125% for 0.5, 0.6 and 0.7 w/c concrete, respectively. However, these reductions diminished at a certain distance from the concrete surface (i.e. CPFAZ) and the thickness of the CPFAZ varied between 8 and 18 mm for concrete with w/c 0.5, 0.6 and 0.7. CPFAZ results shown in Figure 6.9 were, however, not entirely similar to those reported in Figure 6.8. The results of t-tests for scratch width data, taken at 2 mm from the formwork surface (Table 6.2) confirmed that there was no significant difference between the use of CPF and IF for concrete with w/c 0.5, whilst for concrete with w/c 0.6 and 0.7, there was a significant difference.

The effects of CPF on the microhardness of concrete cured in air (E1) and water (E4) for 28 days were also studied and compared with those of IF as shown in Figure 6.10, to signify the role of CPF on the properties of both poor and well cured concretes. It can be seen that the CPF enhances the microhardness of all concretes, and the amount of enhancement reached 100% and 210% for the concretes cured with E1 and E4, respectively. The CPFAZ determined from figure 6.10 is 12 and 18 mm for concrete cured with E1 and E4, respectively. These results confirm that CPF is not only a means of decreasing the thickness of the microstructure gradient (CAZ) but also a good method for enhancing the microstructure of the near surface zone.

The enhancement of the microhardness and the reduction of the scratch width of the concrete cast against CPF can be attributed to the improvement of the PSD and the significant reduction in porosity.

The results presented in Figures 6.8 and 6.9 have shown that both indentation microhardness and scratch hardness data provide fairly similar information about the extent of the curing affected zone for CPF and IF concrete. This is in agreement with the

findings reported in Chapter 4, which showed a good correlation between the microhardness and scratch hardness results. It was also concluded that the scratch hardness technique is a quick and convenient method of analysis of the microstructural variations of concrete and consequently could be applied to cores taken from existing structures.

6.4.3 Effect of CPF on Aggregate/Cement Paste Transition Zone (TZ)

The microhardness at successive distances from the aggregate surface (interface) in the near surface region of OPC concrete cast against both CPF and IF are shown in Figure 6.11. The statistical analyses of the microhardness data were carried out using a t-test and the results are summarised in Table 6.3.

It can be seen from Figure 6.11 that the microhardness of the cement paste matrix for specimens cast against IF is lower at all points away from the aggregate surface when compared to those results for specimens cast against CPF. The microhardness of IF specimens increased with increasing distance from the aggregate surface up to about 40 μm. This finding was supported by the t-test results given in Table 6.3 which shows a significant difference between the mean of the results reported at 0 μm and 40 μm from the aggregate/cement paste interface. On the other hand, the use of CPF appeared to have improved the microhardness of the aggregate/cement paste transition zone (Figure 6.11 and Table 6.3). Moreover, it can be seen from the consistent microhardness results at successive points away from the aggregate that the use of CPF resulted in decreasing the TZ width and this was confirmed by t-test results given in Table 6.3.

The enhancement in the microhardness of aggregate/cement paste TZ in the first 3 mm from the surface of concrete cast against CPF compared with those cast against IF was a result of the improvement to the near surface microstructure provided by the use of CPF. The presence of the TZ in concrete cast against IF was attributed to the formation of a thin film of water (10 μm thick) and also due to accumulation of bleeding water around the aggregate surface (Zimbelmann, 1978, Mehta, 1986 and Larbi, 1991). This led to an increase in the porosity of the cement paste matrix around the aggregate interface, hence affecting the microhardness properties of the TZ. On the other hand, the enhancement of the microhardness in the aggregate/cement paste TZ of OPC concrete

cast against CPF can be attributed to the decrease in bleeding water around the aggregate surface by the drainage provided by CPF.

6.4.4 Effect of CPF on Mass Transport Properties

6.4.4.1 Chloride ingress

The total chloride profiles for OPC concrete with different w/c ratios cast against CPF and IF are illustrated in Figure 6.12. It can be seen that at a low w/c ratio (0.50) the total chloride profiles for concretes cast against CPF and IF seem to be similar, while at high w/c ratios (0.60 and 0.70), the use of CPF shows a marked reducing effect on the chloride contents of the surface zone. As expected, for OPC concrete cast against IF, the degree of chloride ingress diminished when the w/c ratio was reduced from 0.70 to 0.50. When CPF was used, the effect of the w/c ratio practically disappeared and 0.70 and 0.60 w/c ratio concretes behaved in a similar way as the 0.50 w/c ratio concrete. For all three w/c ratios, the penetration of chloride in CPF concrete was lower than that found in the 0.5 w/c ratio concrete cast against IF.

The insignificant reduction in chloride concentrations within the near surface zone of 0.5 w/c OPC concrete cast against CPF compared to those of concrete cast against IF agrees with the work described in Sections 6.4.1 and 6.4.2, which showed that the surface zone had similar microstructural and hardness properties. The significant reduction in surface chloride concentration for high w/c ratio concretes (0.6 and 0.7) cast against CPF is likely to be as a result of the substantial effect of the CPF on capillary porosity (see Figure 6.7).

The total chloride content profiles for different concretes (OPC, OPC/PFA and OPC/GGBS) cast in CPF and IF are illustrated in Figure 6.13. The effect of CPF was not pronounced in both types of blended concretes mainly because blended concretes have a better resistance to chloride penetration (Bamforth et al, 1994 and Ngala et al, 1995).

The amount of total chloride penetrated (TCP) into the concrete cover was calculated by determining the area under the graphs shown in Figures 6.12 and 6.13. The TCP values for OPC concrete at different w/c ratios are illustrated in Figure 6.14. It shows that the

TCP for OPC concrete cast against IF increases with increasing w/c ratio and the TCP remains stable for the corresponding specimens cast against CPF.

Figure 6.15 shows the TCP values for the three types of concrete cast against either CPF or IF. It can be seen that, even though the reduction in the level of TCP achieved by the use of CPF for the blended concretes was lower than for OPC concrete cast against IF, all three types of concrete cast against CPF had similar levels of TCP. As movement of the chloride ions in CPF concrete is not expected to be restricted in the bulk of the concrete any more than for concrete cast IF, the reduction in the level of chloride penetrated into specimens cast against CPF must be related to the denser surface layer produced by the CPF.

6.4.4.2 Carbonation

The carbonation fronts and the depths of carbonation for OPC concrete with differing w/c ratios are illustrated in Figures 6.16 and 6.17, respectively. The level of carbonation in OPC concrete cast in IF was shown to increase with increasing w/c ratios from about 5 mm at 0.5 w/c ratio up to about 25 mm at 0.7 w/c ratio. These results are in agreement with other published literature which have shown that the rate of carbonation increased with increasing capillary porosity which, in turn, increases with increasing w/c ratio (Page and Ngala, 1995). When CPF was used, the depth of carbonation was less than 1 mm in all cases irrespective of the w/c ratio. This suggests that CPF reduces the capillary porosity of the surface layer of concrete and creates a dense surface to restrict the penetration of CO_2 .

The effect of water curing period (at 22°C) on the carbonation depth of OPC specimens cast against CPF and IF (w/c = 0.6) are illustrated in Figure 6.18. The carbonation profiles of these specimens are shown in Figure 6.16. It can be seen that, for concrete cast in IF, the carbonation depth decreased with increasing water curing period. These results can also be attributed to the reduction of capillary porosity due to increasing water curing period, as described in Section 3.4.2.2. On the other hand, the carbonation rate remains very low for concrete cast against CPF for all curing periods. This may be attributed to the densification of the surface layer as a result of the remarkable reduction in the capillary porosity.

Figure 6.19 shows the depth of carbonation for blended concretes (OPC/PFA and OPC/GGBS) of 0.6 w/c, cast against CPF and IF. The depth of carbonation recorded for blended concretes cast against IF was found to be higher than that of OPC concrete possibly because there was a lower level of carbonatable material to react with CO_2 (Parrott, 1993; Houst and Wittmann, 1994 and Page and Ngala, 1995). The use of CPF was once again effective in reducing the level of carbonation to almost zero, irrespective of the type of cement and the curing regime used (see Figure 6.16). The carbonation period used in this investigation was short (24 days) and carbonation was carried out under accelerated conditions so that the results need to be confirmed by long term studies under natural conditions.

6.5 CONCLUSIONS

1- The use of CPF refined the pore size distribution (PSD), and reduced the total and capillary porosity of OPC covercrete. The use of CPF also improved the properties of the aggregate/cement paste transition zone (TZ) in the near-surface zone affected by the CPF.

2- The hardness of the OPC cover concrete cast in CPF, measured in terms of microhardness and scratch width, was enhanced due to the use of CPF. The degree of enhancement was more pronounced in concrete with higher w/c ratios.

3- The use of CPF causes a reduction in the surface chloride concentration and the total chloride penetration into OPC concrete when compared with the use of IF. The reduction for OPC concretes is a function of the w/c ratio, where the greatest benefit is at the highest w/c ratio. For blended concretes (OPC/PFA and OPC/GGBS), the use of CPF did not show a significant effect on the rate of chloride ingress when compared with the use of IF.

4- A substantial reduction in the carbonation rate for OPC, OPC/PFA and OPC/GGBS concrete was found when CPF was used instead of IF. The effect of the w/c ratio on the reduction in the carbonation rate was investigated for OPC concrete and the reduction was found to be more significant at higher w/c ratios.

5- The use of CPF can offer a substantial improvement to the durability of reinforced concrete in terms of carbonation and chloride penetration in cases where inadequate control or hot climatic conditions hinder the production of good quality concrete.

Table 6.1 Summary of statistical analysis carried out on microhardness results of concrete cast with different w/c ratios and formwork types , using t-test.

W/C ratio	Form-work	Mean, hV	Variance	standard deviation	Variation, %	t	P(T<=t) two tail	Significance of the difference
0.5	CPF	55.00	182.30	7.420	13.10	-0.20	0.811806	insignificant
	IF	56.06	130.60	11.43	20.38			
0.6	CPF	96.62	798.90	28.27	29.20	8.21	1.13E-07	significant
	IF	34.12	127.85	11.30	33.10			
0.7	CPF	73.81	284.03	16.85	22.80	10.3	3.08E-08	significant
	IF	28.40	44.990	6.700	23.60			

Table 6.2 Summary of statistical analysis carried out on scratch width results of concrete cast with different w/c ratios and formwork types, using t-test.

W/C ratio	Form-work	Mean, µm	Variance	standard deviation	Variation, %	t	P(T<=t) two tail	Significance of the difference
0.5	CPF	516.0	27595.0	166.1	32.18	-1.87	0.07	insignificant
	IF	599.9	4245.00	65.15	10.80			
0.6	CPF	373.5	7049.00	83.950	22.50	-8.11	9.0E-08	significant
	IF	684.0	16497.2	128.40	18.77			
0.7	CPF	333.2	24711.0	157.19	47.10	-9.03	3.7E-09	significant
	IF	732.0	6475.00	80.460	10.99			

Table 6.3 Summary of statistical analysis carried out on microhardness results of concrete cast in CPF and IF at the TZ, using t-test.

Variables*	Mean, hV	Variance	standard deviation	Variation, %	t	P(T<=t) two tail	Significance of the difference
IF/0 μm	27.81	97.760	9.880	35.00	-3.5	1.50E-03	significant
IF/40 μm	40.68	117.69	10.85	26.67			
IF/0 μm	27.81	97.760	9.880	35.00	-8.3	4.94E-09	significant
CPF/0 μm	142.8	142.80	11.94	19.9			
CPF/0 μm	60.00	142.80	11.94	19.90	-0.1	9.19E-01	insignificant
CPF/ 40 μm	60.38	70.780	8.410	14.00			
IF/40 μm	40.68	117.69	10.85	26.67	-5.7	3.73E-06	significant
CPF/40 μm	60.38	70.780	8.410	14.00			

*where,

IF/0 μm = measurements taken at ≅ 0 μm from IF surface

IF/40 μm = measurements taken at ≅ 40 μm from IF surface

CPF/0 μm = measurements taken at ≅ 0 μm from CPF surface

CPF/0 μm = measurements taken at ≅ 40 μm from CPF surface

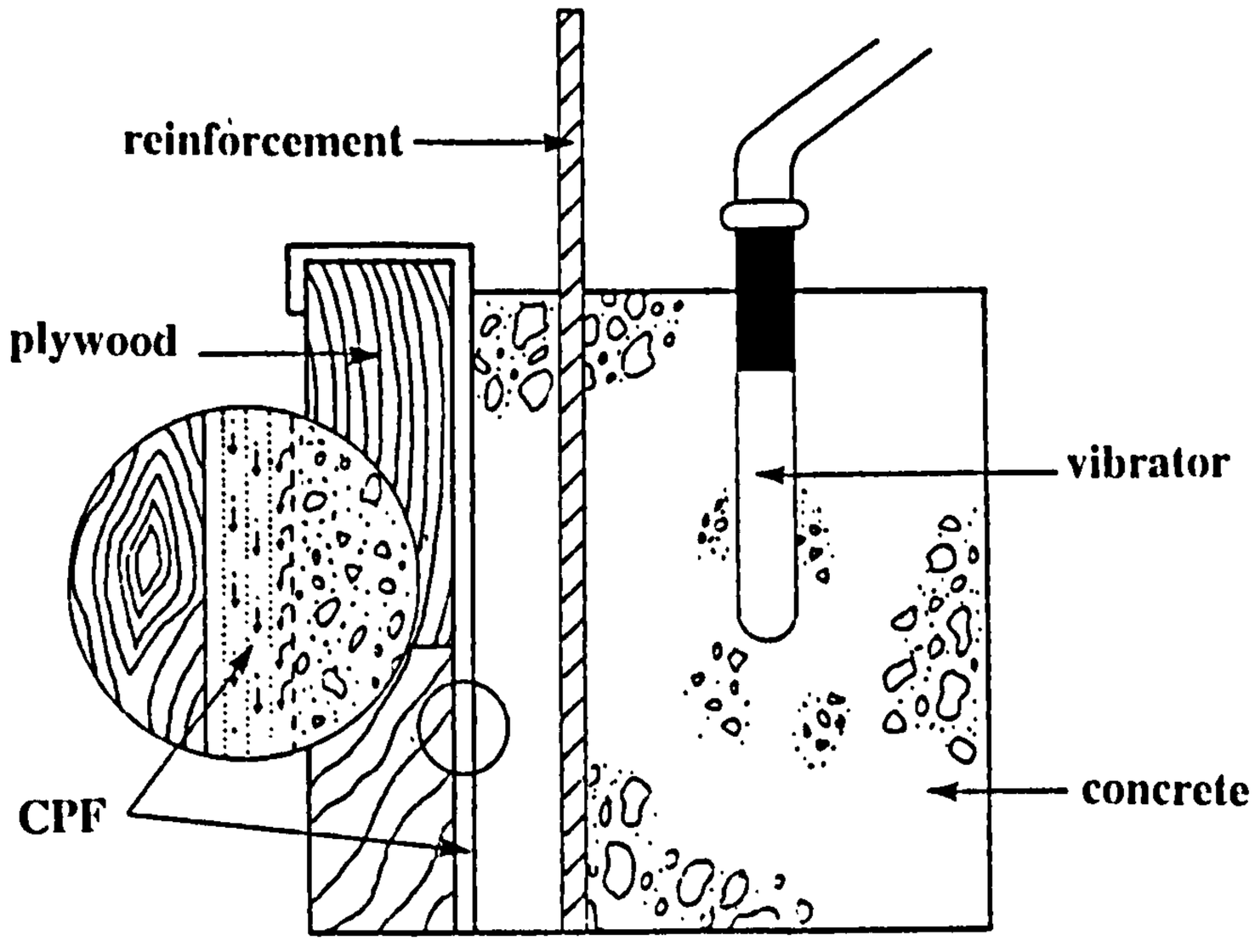

Figure 6.1 Basic concept of controlled permeability formwork (Wilson, 1994a).

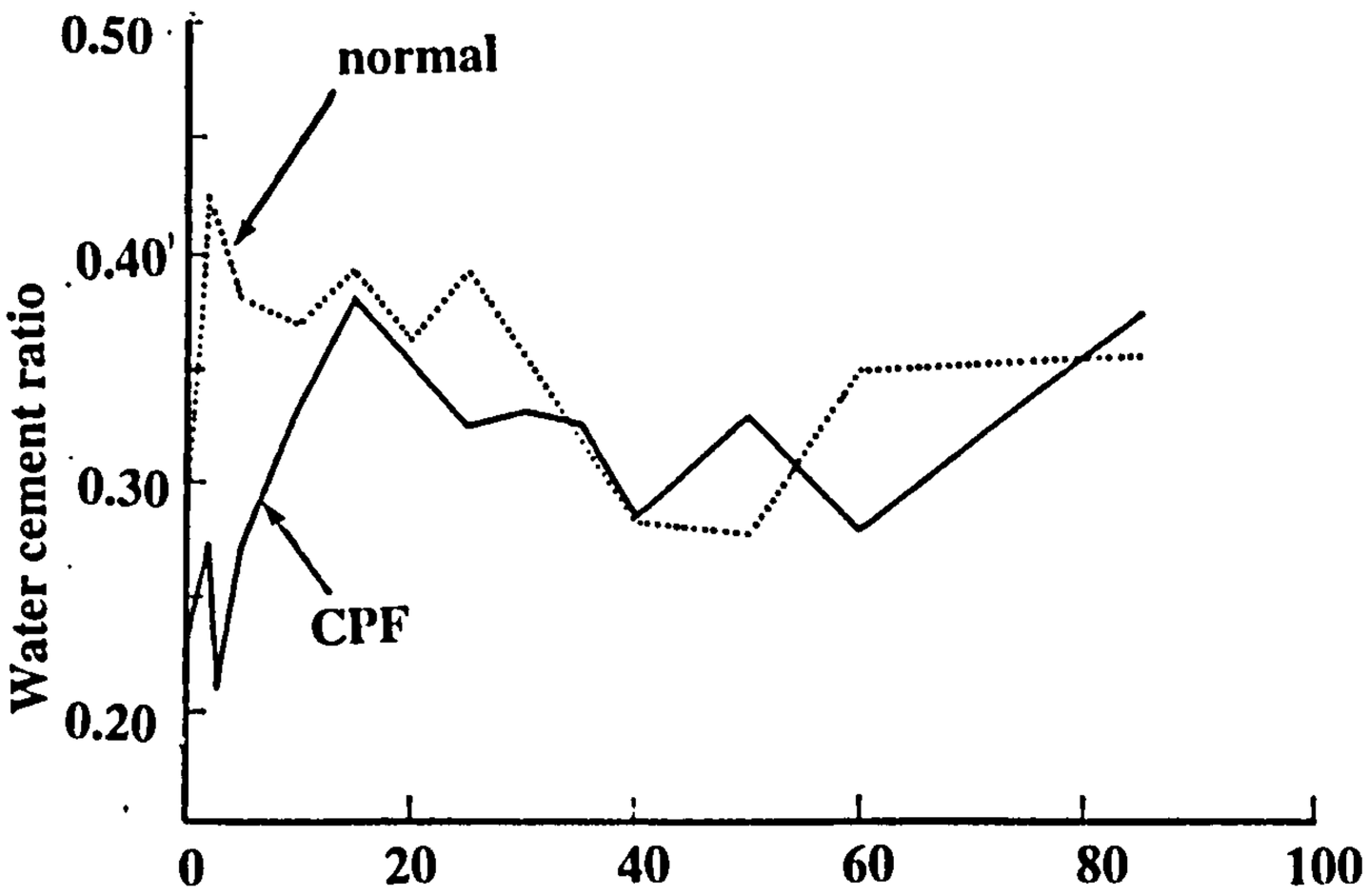

Figure 6.2 Effect of CPF on the water/cement ratio near the surface of the concrete (Price, 1993).

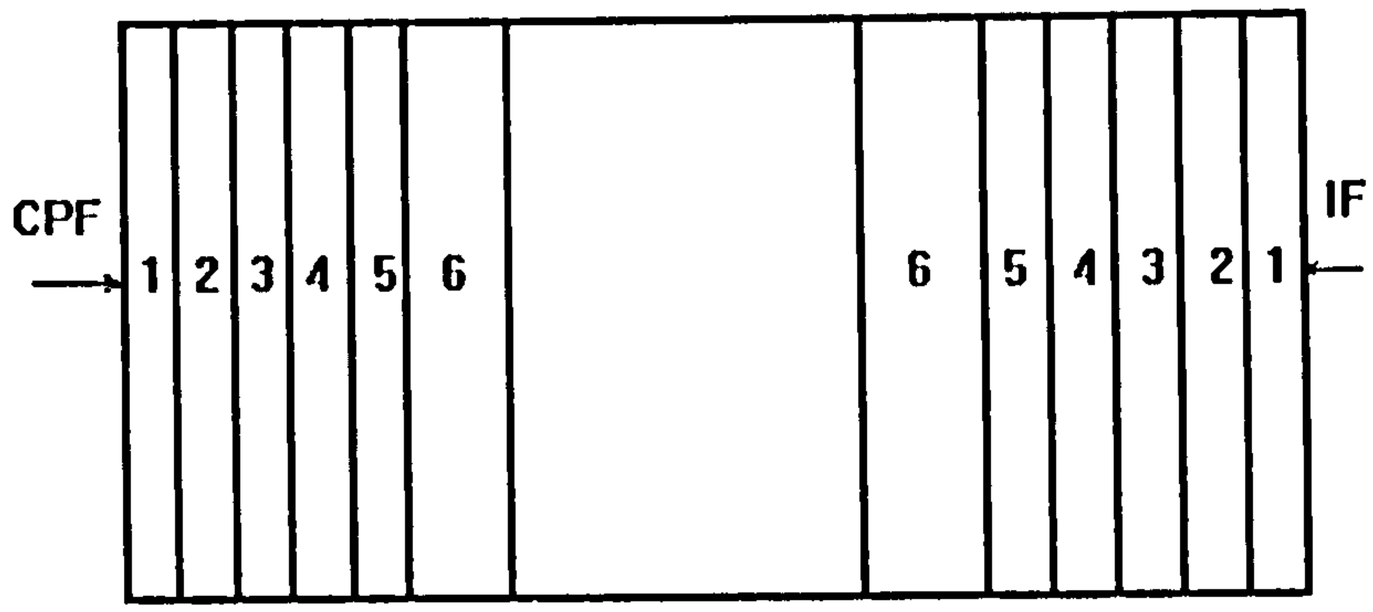

Figure 6.3 Sampling arrangement for HCP cores used for PSD and porosity measurements.

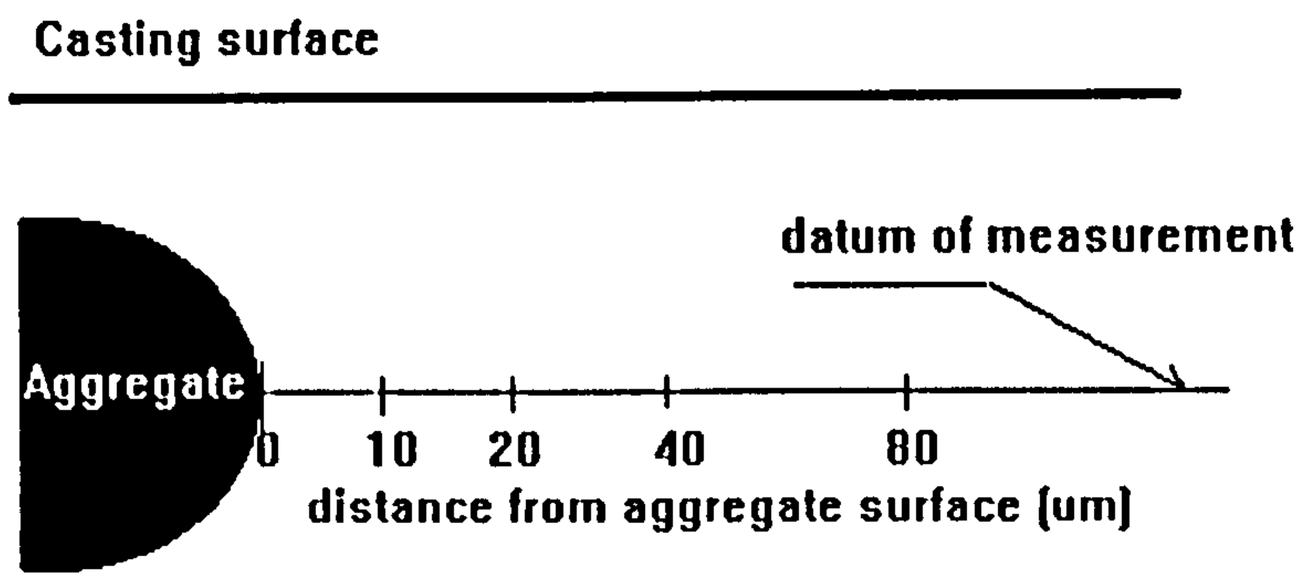

Figure 6.4 Diagram showing the datum of microhardness measurements taken at aggregate/cement paste transition zone (TZ).

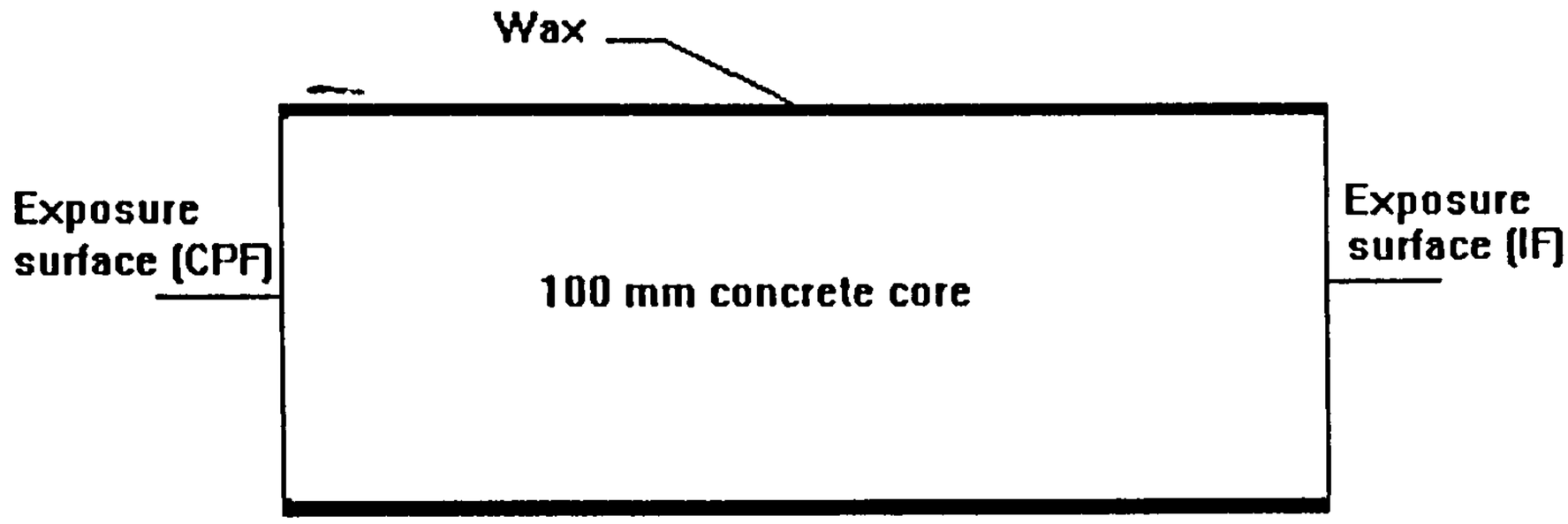

Figure 6.5 Diagram showing the details of concrete specimens used for chloride penetration and carbonation test .

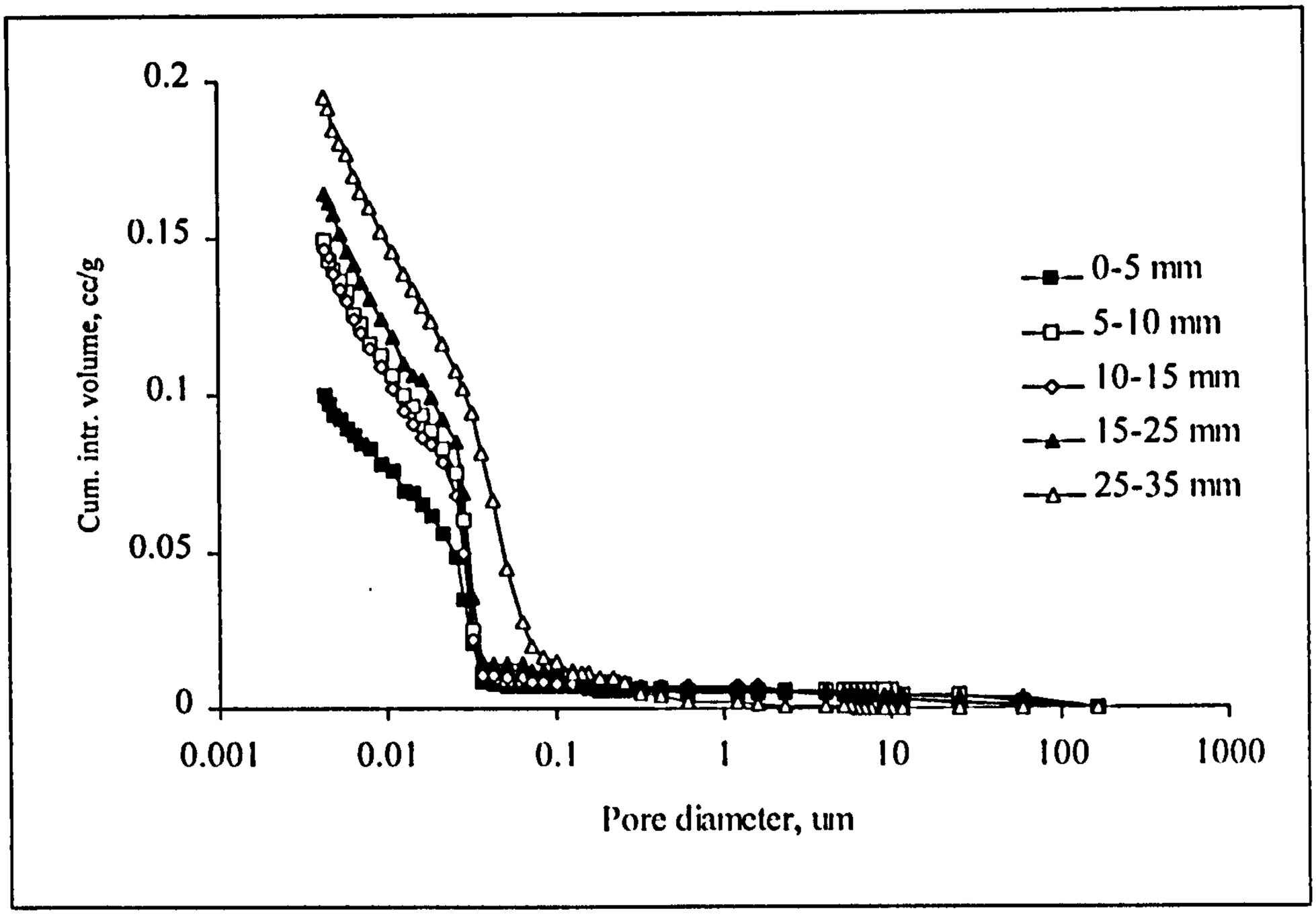

Figure 6.6 PSD at different distances below the CPF surface of OPC paste.

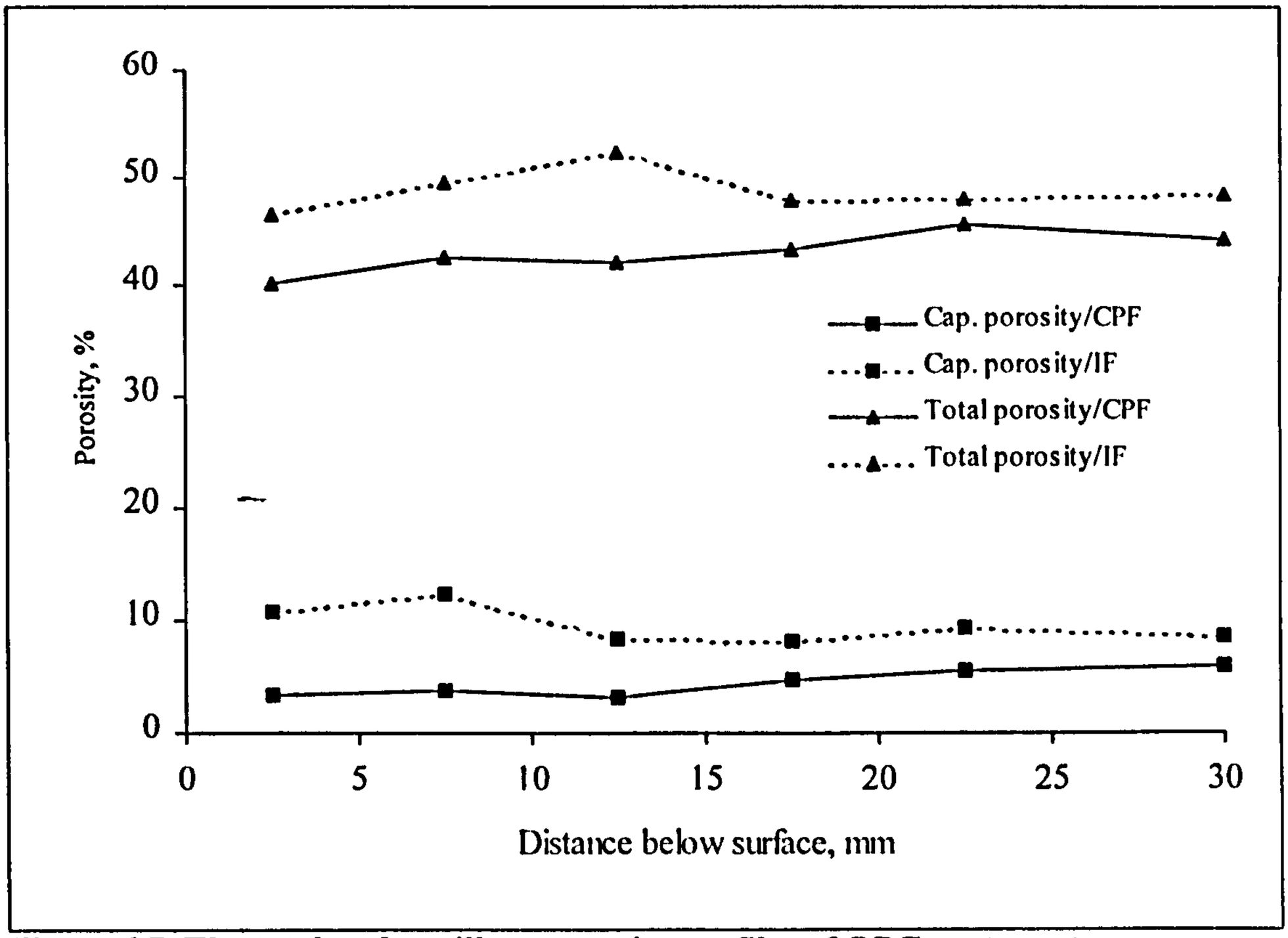

Figure 6.7 The total and capillary porosity profiles of OPC paste cast in CPF and IF.

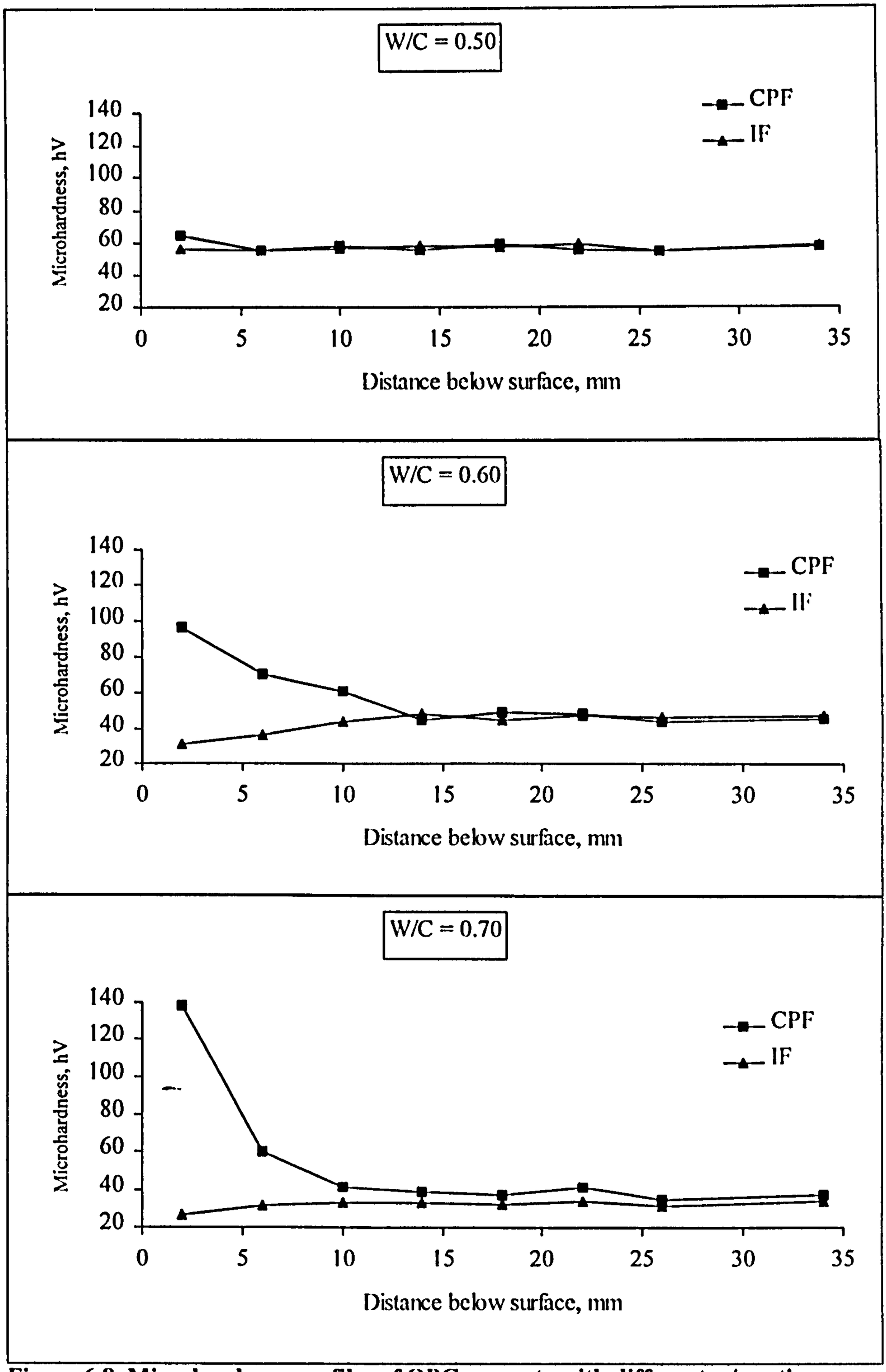

Figure 6.8 Microhardness profiles of OPC concrete with different w/c ratios cast in CPF and IF.

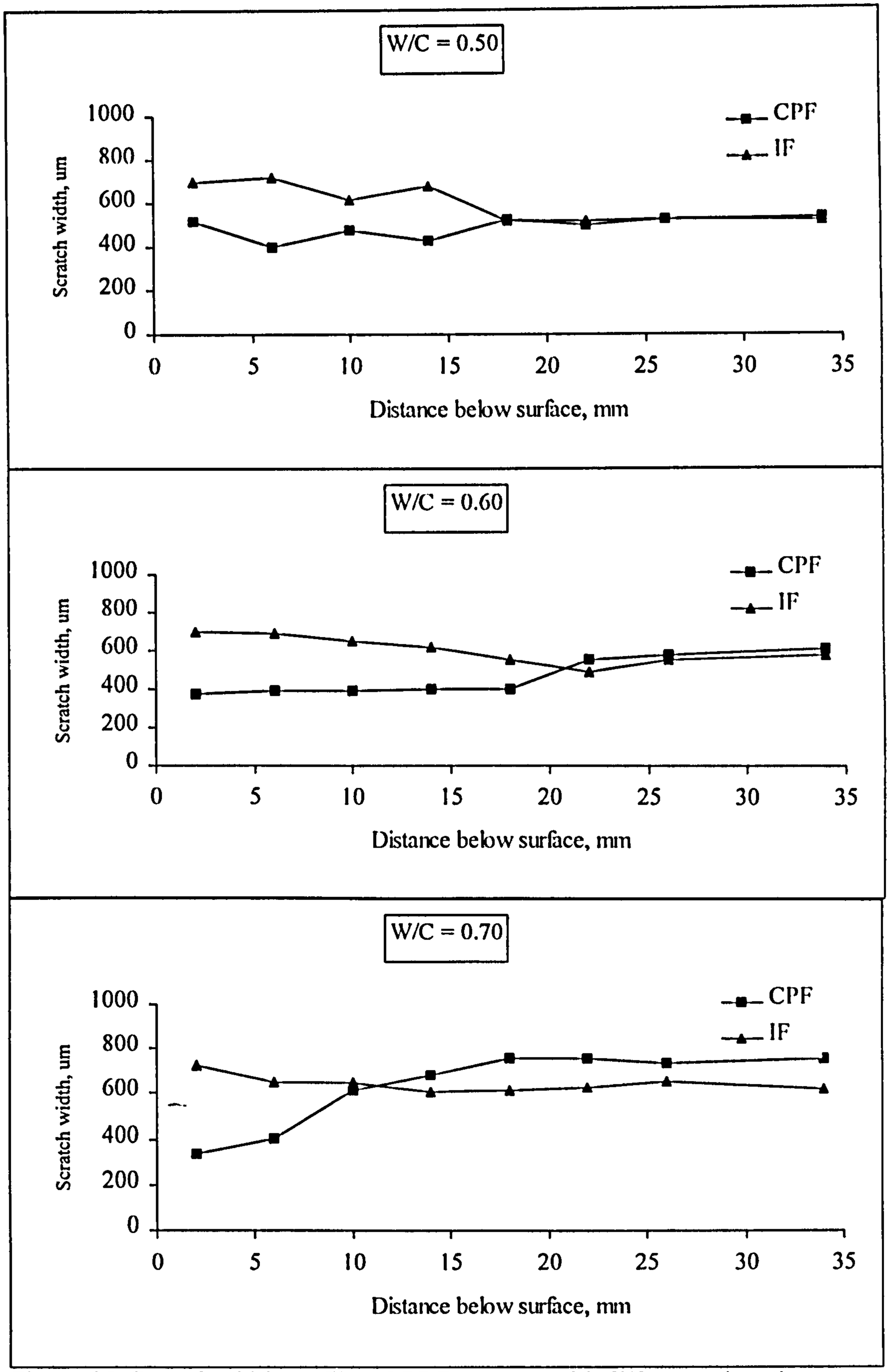

Figure 6.9 Scratch width profiles of OPC concrete with different w/c ratios cast in CPF and IF.

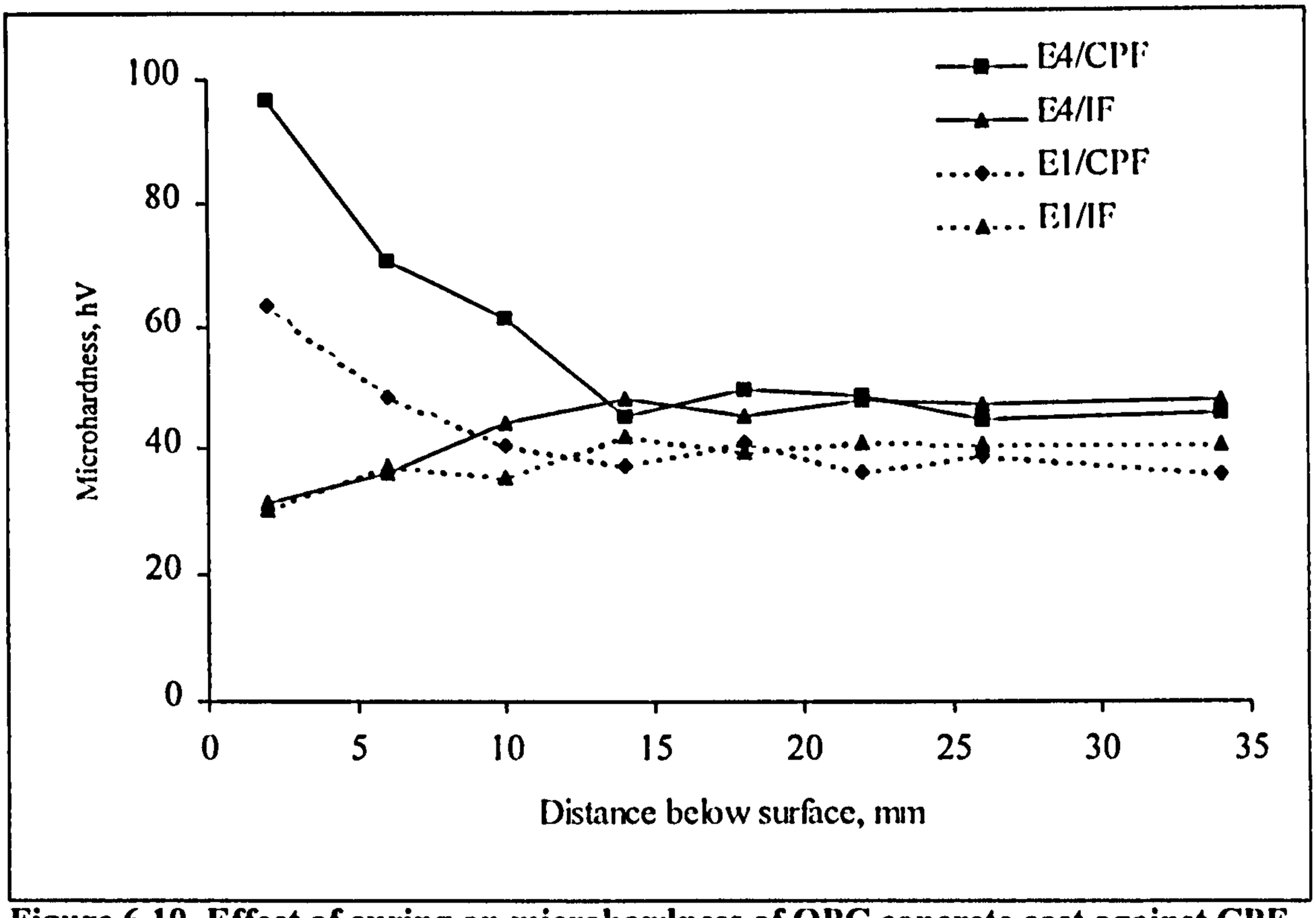

Figure 6.10 Effect of curing on microhardness of OPC concrete cast against CPF and IF, w/c = 0.60.

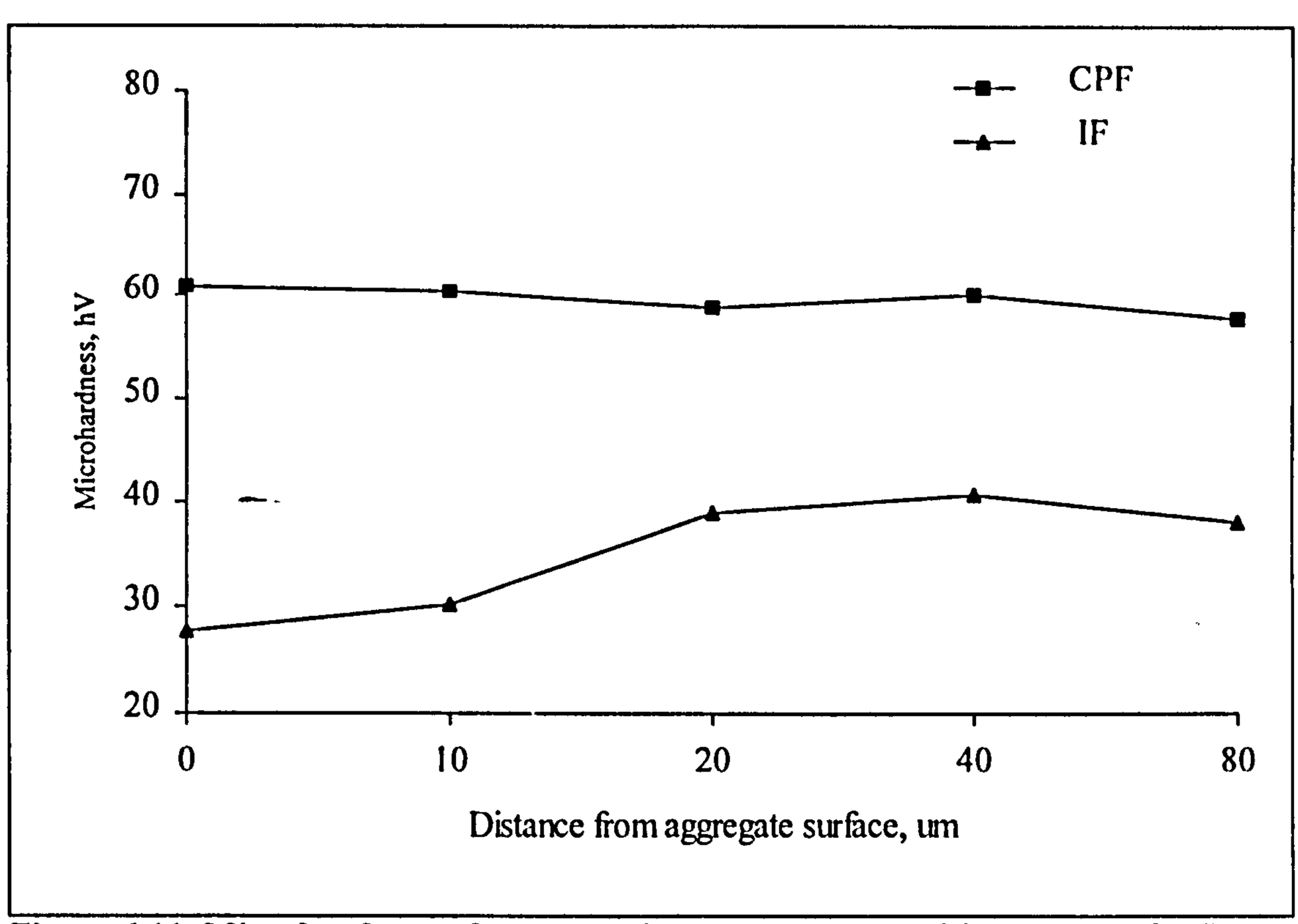

Figure 6.11 Microhardness of aggregate/cement paste transition zone at the first 3 mm from surface of OPC concrete cast in CPF and IF, w/c = 0.36.

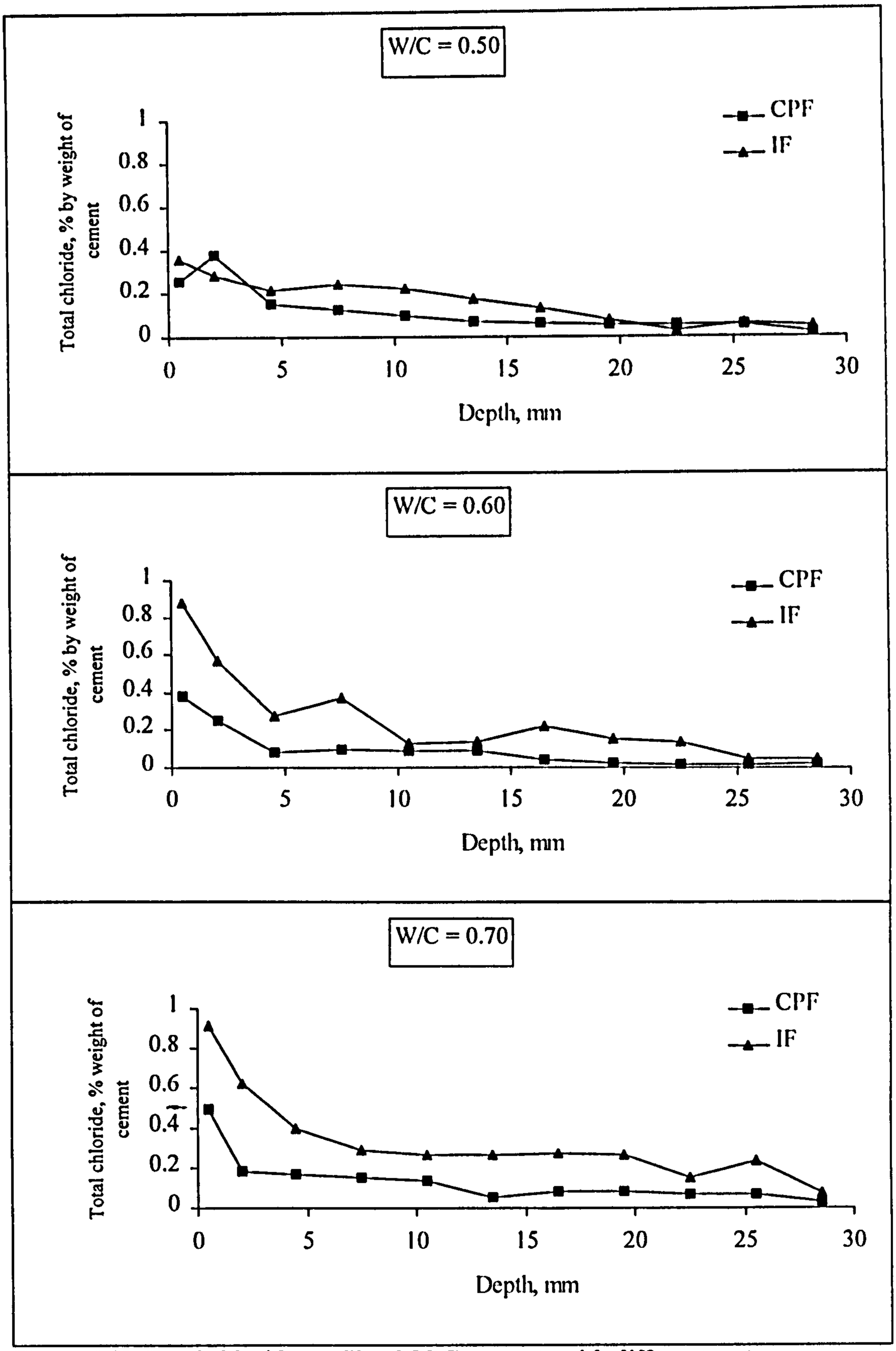

Figure 6.12 Total chloride profile of OPC concrete with different water cement ratios, cast in CPF and IF.

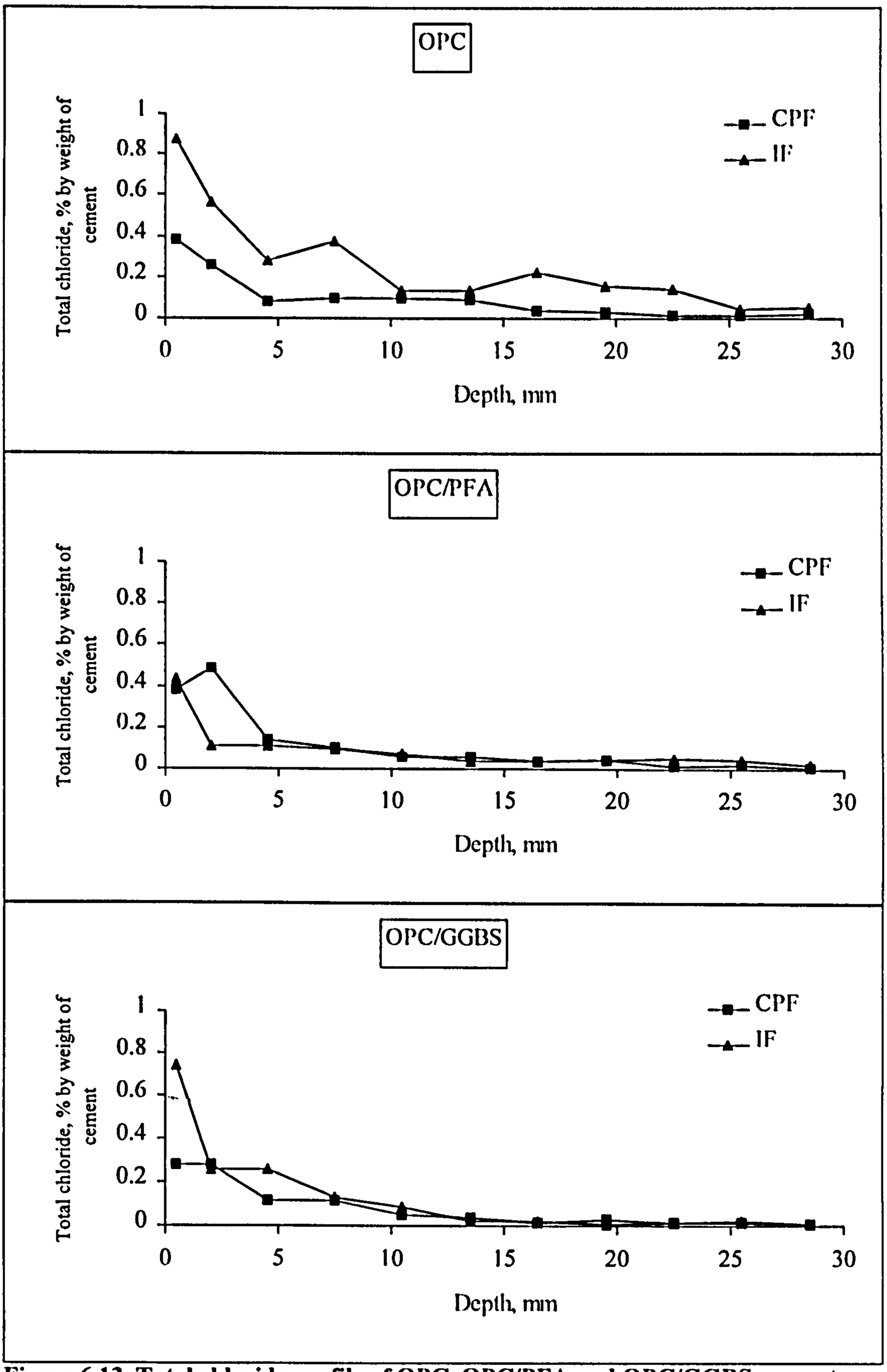

Figure 6.13 Total chloride profile of OPC, OPC/PFA and OPC/GGBS concrete cast in CPF and IF (w/c = 0.60).

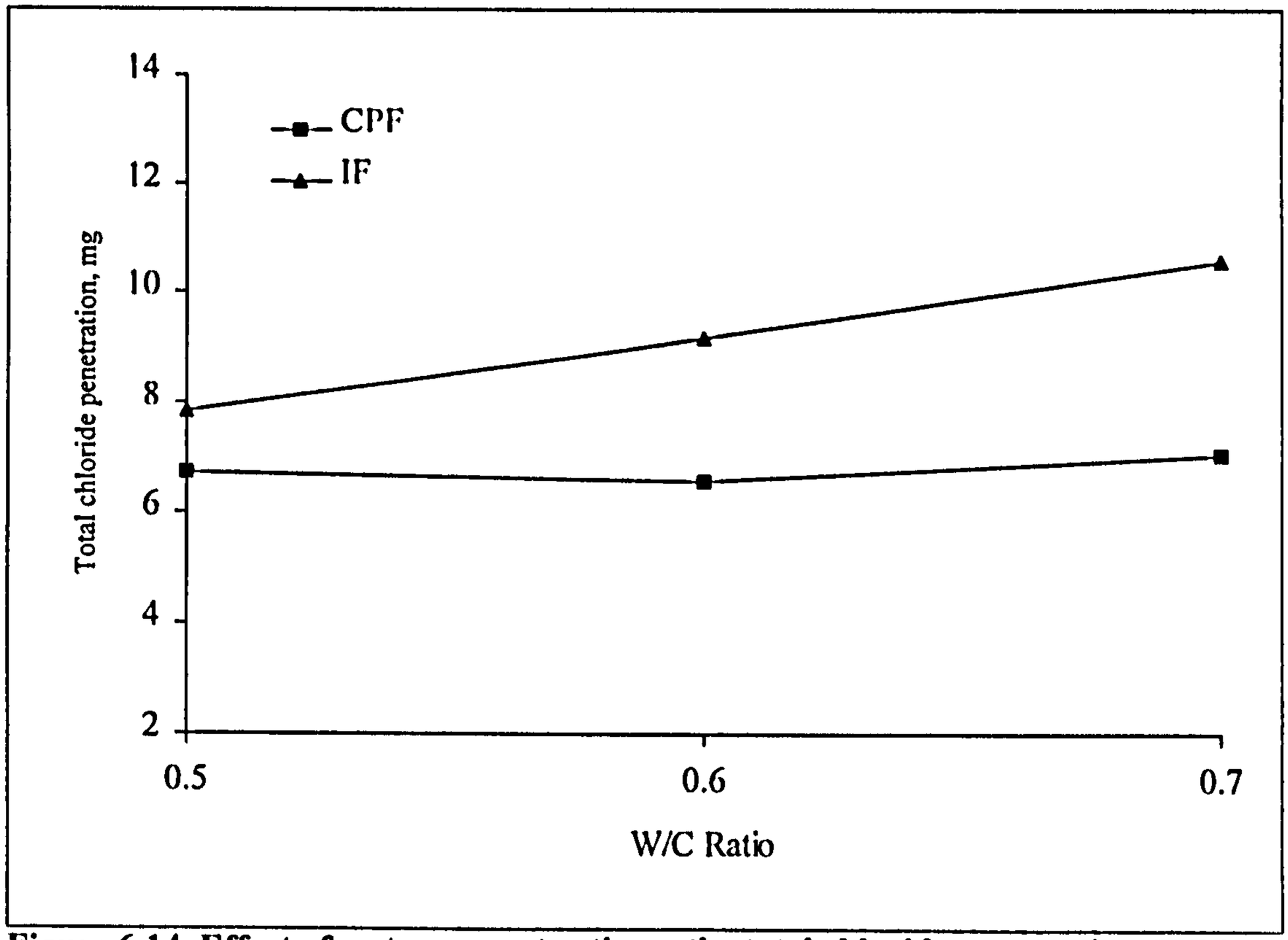

Figure 6.14 Effect of water cement ratio on the total chloride penetration (TCP) of OPC concrete cast in CPF and IF, w/c = 0.60.

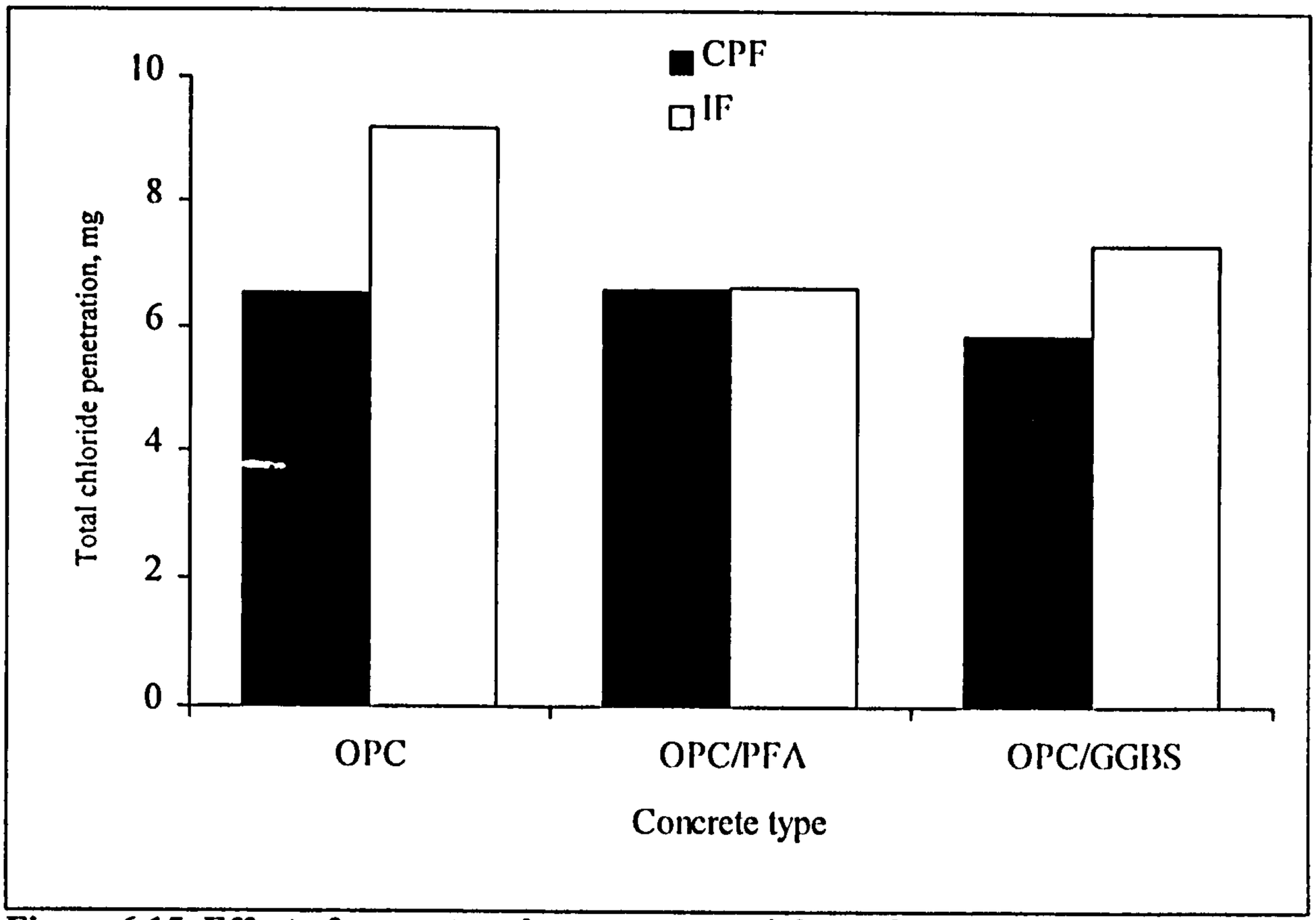

Figure 6.15 Effect of cement replacement materials on the total chloride penetration (TCP) of concrete cast in CPF and IF, w/c = 0.60.

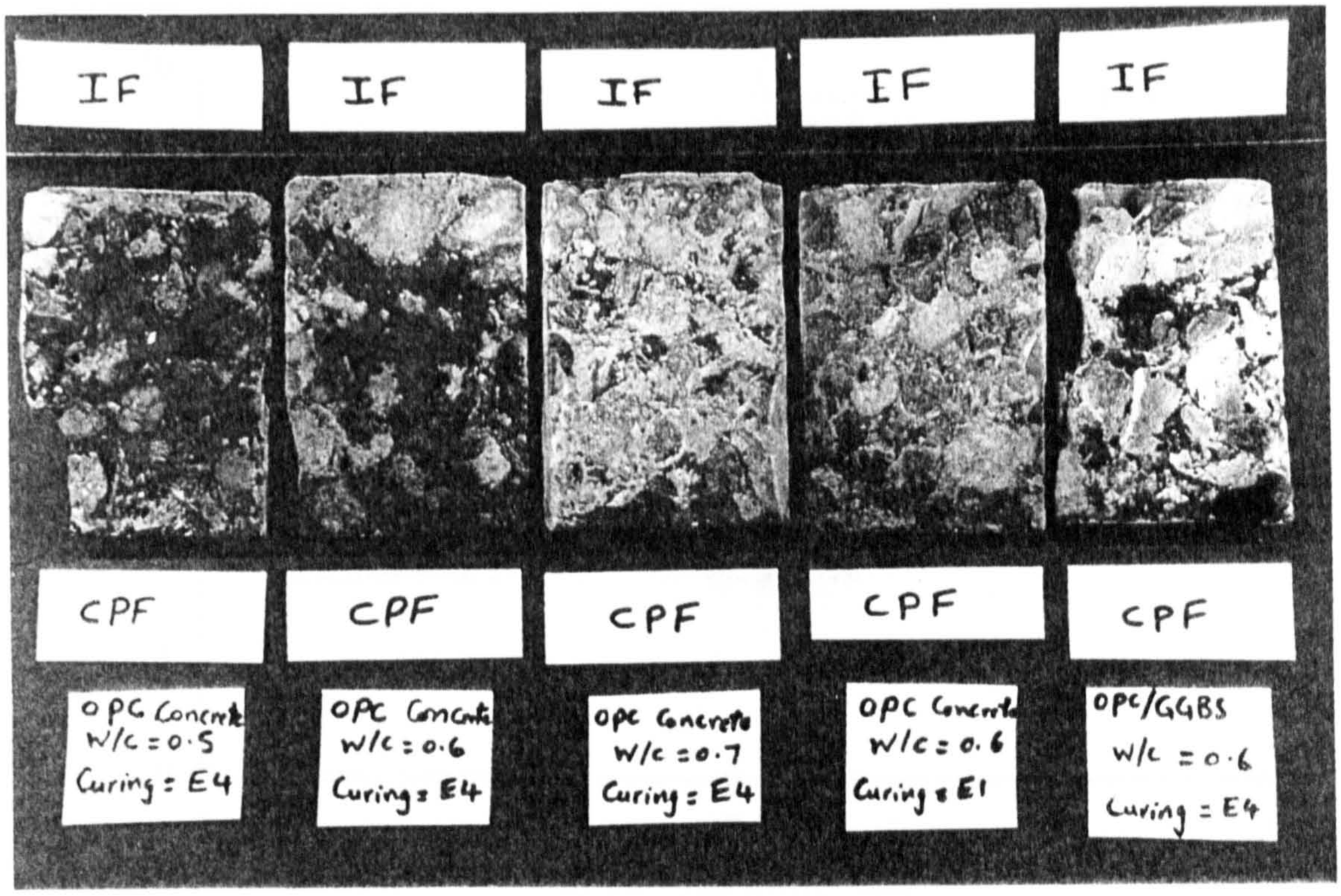

Figure 6.16 Carbonation profile of different concretes cast against CPF and IF.

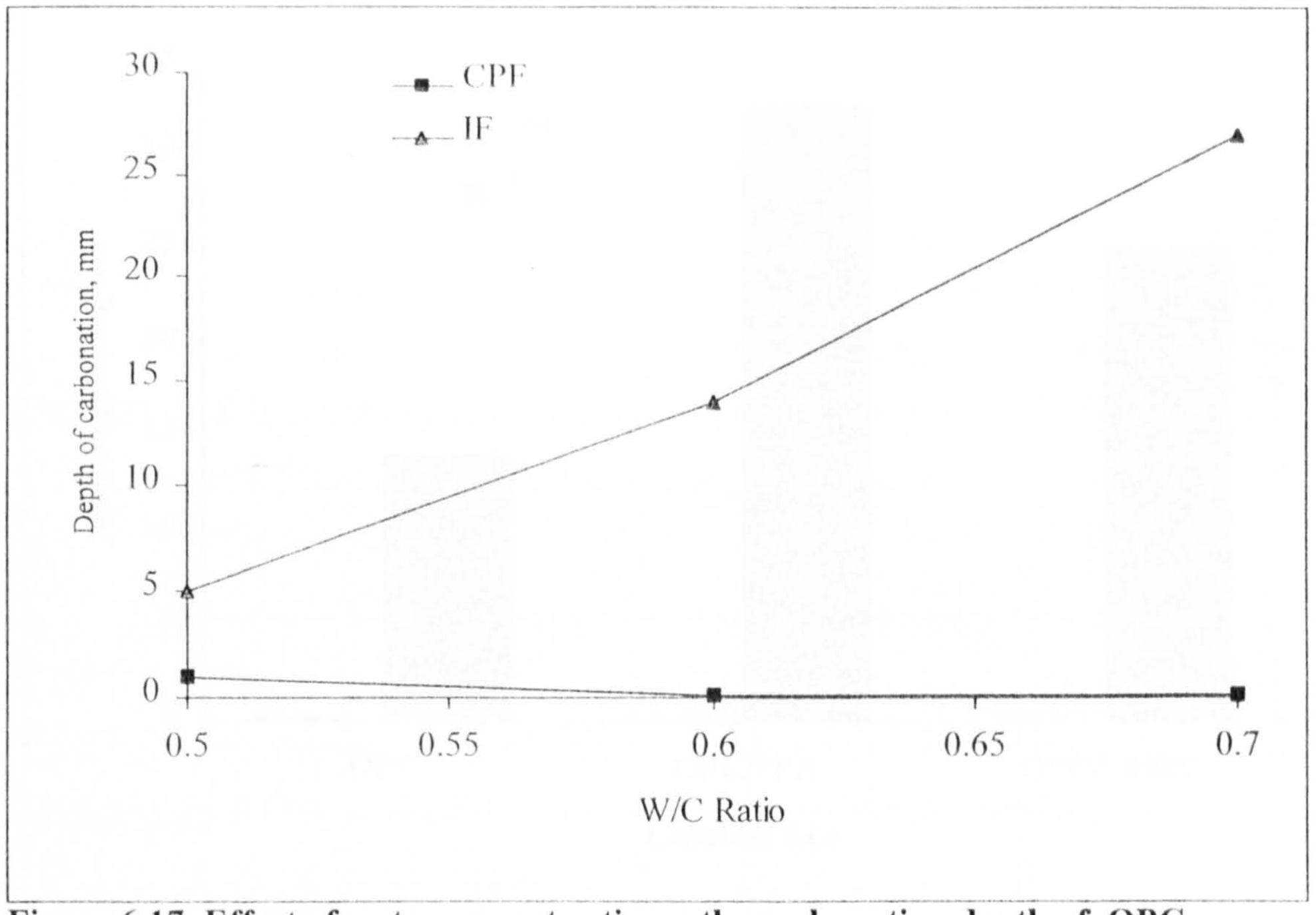

Figure 6.17 Effect of water cement ratio on the carbonation depth of OPC concrete cast in CPF and IF, exposed to 100% CO_2 for 24 days.

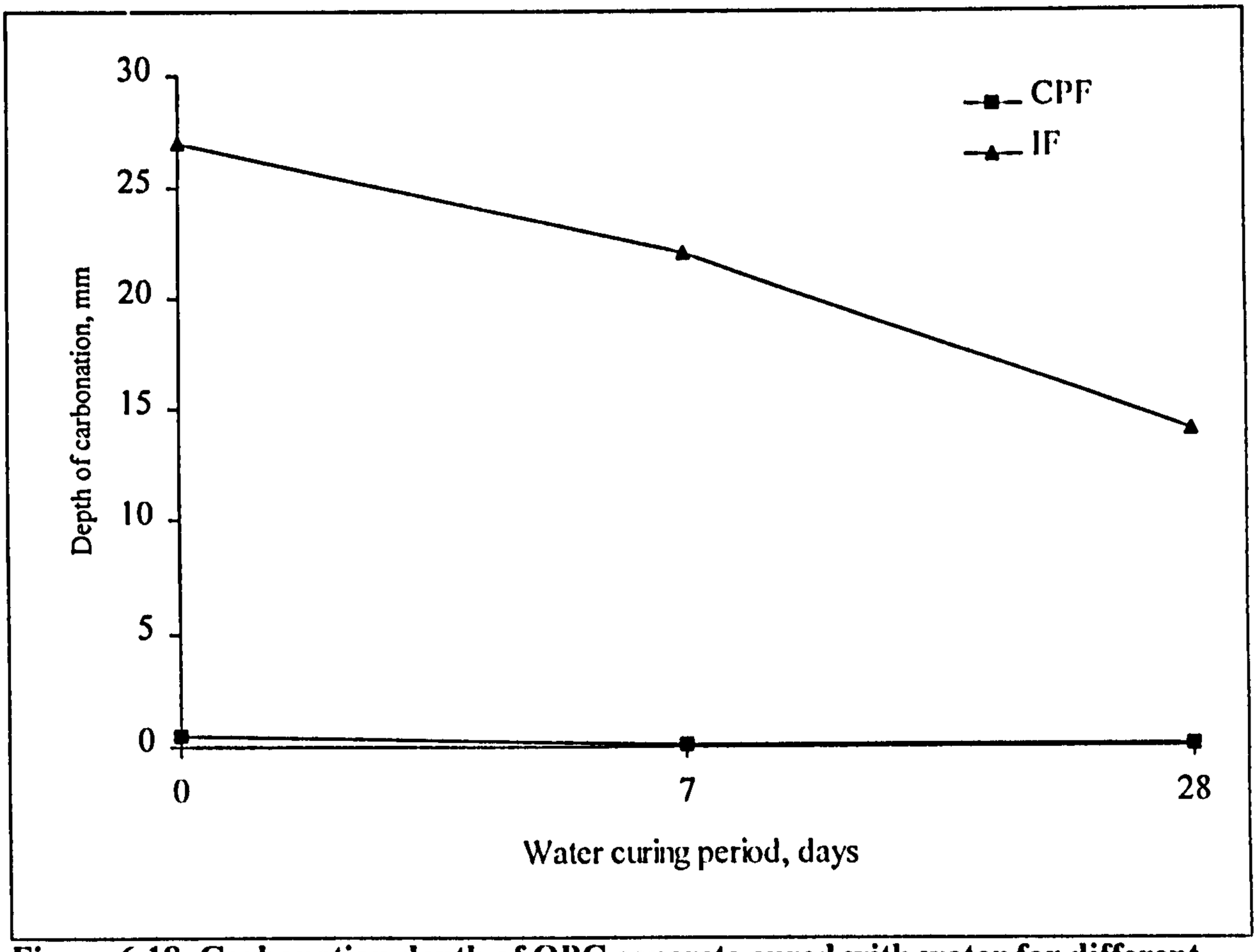

Figure 6.18 Carbonation depth of OPC concrete cured with water for different periods and cast in CPF and IF, exposed to 100% CO_2 for 24 days.

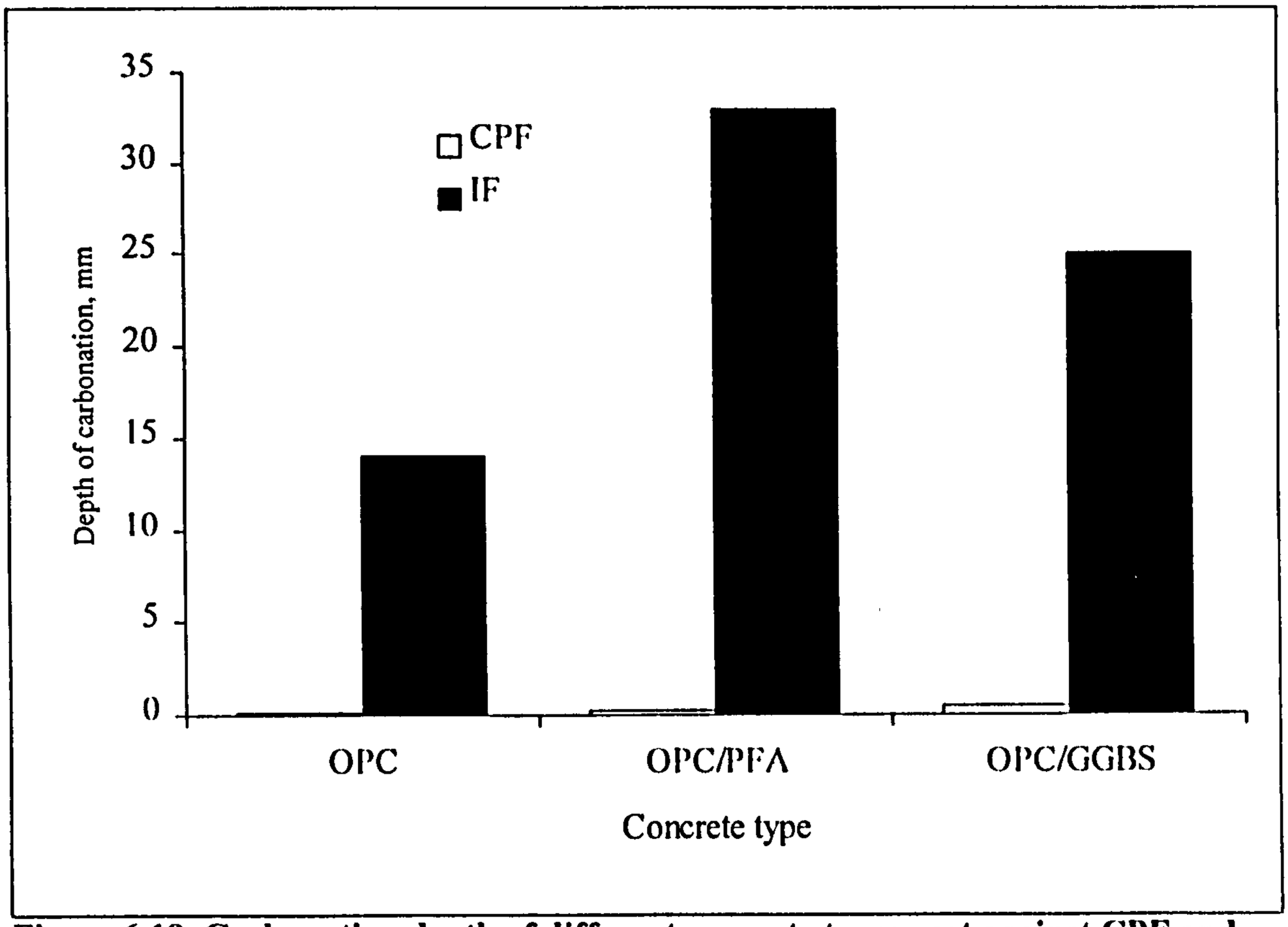

Figure 6.19 Carbonation depth of different concrete types cast against CPF and IF, using w/c = 0.60 and E4 curing.

CHAPTER 7

INFLUENCE OF ELECTRO-CHEMICAL REALKALISATION TREATMENT ON PORE STRUCTURE AND CHEMICAL COMPOSITION OF SURFACE AND TRANSITION ZONES

7.1 INTRODUCTION

One of the main problems associated with the ingress of carbon dioxide into concrete is steel reinforcement corrosion which causes a reduction in the serviceability of the structure concerned. Many techniques have, therefore, been developed for the repair and subsequent protection of the reinforcement (Miller, 1994). Two such techniques are patch repairs and electro-chemical rehabilitation. The patch repair technique is the traditional method advised by consulting engineers for remedying carbonation-induced reinforcement corrosion. In such a case unrepaired concrete remains at risk and it is not uncommon for further patch repairs to be needed close to the original repair area (Al-Kadhimi et al, 1996).

In order to avoid disadvantages of conventional rehabilitation of the patch repair type, various electro-chemical techniques for corrosion protection of reinforcing steel have been developed in the last few years (Al-Kadhimi et al, 1996). One of these methods is electro-chemical realkalisation (ECR) which offers a non destructive means of treating reinforced concrete suffering from carbonation (Mietz and Isecke, 1994a and 1994b). The ECR technique is also preferred for the following structures:

- Concrete facades which cannot or should not be changed.
- Silos, cooling towers.
- Concrete structures where additional weight is not desired or not possible.

Two methods, controlled permeability formwork (CPF) and electro-chemical realkalisation (ECR), were studied in work described in this thesis to provide a solution for preventing or remedying the reinforcement corrosion due to carbonation, which is mainly a function of the surface zone properties (CAZ). CPF sheet was adopted in the work described in Chapter 6 and can be used for new concrete members for providing a

dense microstructural layer at the surface zone. The ECR approach, described in this chapter, can be used for remedying existing structures suffering from such a problem. However, ECR is a relatively new repair method without a clear track record, so the main aims of this chapter are; first to clarify the mechanism of ECR, secondly, to study the factors which affect the ECR treatment and finally to investigate the changes that occur due to such a treatment in microstructure and composition of the surface zone (CAZ) and steel/cement paste transition zone (TZ).

7.2 LITERATURE REVIEW

7.2.1 General

According to the Pourbaix diagram for Fe/H_2O, the passive oxide film on Fe deteriorates at a pH below 9 (Pourbaix, 1966). As the pH of concrete pore water is decreased by carbonation, the passive film on reinforcing steel is undermined and the whole surface of the metal becomes exposed to corrosion. Thus, the corrosion mechanism induced by carbonation can be described as a 'uniform attack', i.e. there is general corrosion over the whole affected surface, anode and cathode reactions are taking place throughout. The corrosion mechanism can be described by the following reactions (Odden and Miller, 1994):

Anodic reaction

$$Fe_{(s)} \rightarrow 2Fe^{2+} + 4e^{-} \qquad \text{.....} \quad (7.1)$$

Cathodic reaction

$$O_{2(g)} + 2H_2O_1 + 4e^{-} \rightarrow 4OH^{-} \qquad \text{.....} \quad (7.2)$$

Net reaction

$$2Fe_{(s)} + O_{2(g)} + 2H_2O_{(1)} \rightarrow 2Fe(OH)_2 \qquad \text{.....} \quad (7.3)$$

The iron hydroxide ($Fe(OH)_2$) will oxidise further to form "rust" which is a mixture of several oxides and hydroxides. One way, to stop carbonation-induced corrosion and avoid costly repair to buildings and structures, is to re-establish the lost passivity.

Passive realkalisation (applying a surface layer of cement mortar or cement-based coatings on a concrete surface) is a widely used method for stopping deterioration of reinforcement in carbonated concrete. These coatings can retard the corrosion of reinforcement as a result of transferring alkalis into carbonated concrete. Such a coating may also affect the corrosion rate by controlling the moisture content of the carbonated concrete surrounding the reinforcement (Bier et al, 1989 and Mattila and Pentti, 1996).

In the ECR technique, the surface of the structure is usually covered with a layer of gelatinous composition containing some alkaline compounds, normally a mixture of sodium carbonate and sodium hydroxide. On the top of this layer a conducting net is placed and the net is connected to the positive terminal of an electric power source. The negative terminal of the power source is connected to the reinforcing bars. The voltage difference is adjusted so that electrolysis starts (Hommond, 1993; Chatterji, 1994 and Mietz, 1994a and 1994b), as shown in Figure 7.1. Most studies (Polder and Hondel, 1992, Mietz and Isecke, 1994a and 1994b, NCT Report, 1994 and Miller, 1994) recommend that the design current should be typically varied between 0.8-2 A / m^2, with an upper limit of 5 A / m^2 to avoid any excessive deterioration of the concrete. They also suggested 3 to 14 days for the ECR treatment. In theory, ECR is based on two processes, cathodic generation of hydroxide ions at the steel which increases the pH of the interior of the concrete, and transport of alkaline material from the electrolyte into the concrete by capillary absorption, diffusion and possibly electro-osmosis. This leads to an increase in pH from the exterior and provides an alkaline buffer which improves the durability of the corrosion protection.

7.2.2 Mechanism of Electro-Chemical Realkalisation of Concrete

Polder and Hondel (1992); Odden (1993 and 1994); Banfill, (1994); and Mietz and Isecke (1994a and 1994b) have suggested that the electro-chemical realkalisation process may involve a combination of mechanisms whose relative importance are not yet fully resolved. The principal effects are outlined below:

7.2.2.1 Electrolysis

Electrolysis proceeds via reactions at the electrodes as follows:

Cathodic reaction

Hydroxide ions (OH^-) are generated around the cathode (reinforcement) due to splitting of water by the passage of electric current, according to the following equation:

$$2H_2O + 2e^- \rightarrow H_2 + 2OH^- \qquad \text{.....} \quad (7.4)$$

In addition, reaction with oxygen diffused into concrete takes place as follows:

$$\frac{1}{2}O_2 + H_2O + 2e^- \rightarrow 2OH^- \qquad \text{.....} \quad (7.5)$$

Anodic reaction

Oxidation occurs according to the following equations:

$$2OH^- \rightarrow \frac{1}{2}O_2 + H_2O + 2e^- \qquad \text{(at high pH)} \qquad \text{.....} \quad (7.6)$$

or

$$H_2O \rightarrow \frac{1}{2}O_2 + 2H^+ + 2e^- \qquad \text{(at lower pH)} \qquad \text{.....} \quad (7.7)$$

As a result of the cathodic reactions, the concrete zone around the reinforcement becomes enriched with OH^- ions so the passive film can be reinstated to halt corrosion.

7.2.2.2 Electro-migration

Concrete is an ionic conductor and current flows as a result of the movement of ions as follows:

- All negatively charged ions such as OH^- and SO_4^{2-} migrate towards the anode.
- All positively charged ions (Na^+, K^+, Ca^{2+}) migrate towards the cathode (reinforcement).

As a result of the electro-migration process, a higher concentration of sodium and potassium ions would be expected to occur around the reinforcement.

7.2.2.3 Electro-osmosis

Concrete pore surface particles in contact with an electrolyte acquire a surface charge because the relative affinity of cations and anions to the surfaces and the solution is different. A charged particle is surrounded by counter-ions to form a diffuse electric double layer whose extent depends on the electrolyte concentration. The net-work of fine capillaries in concrete is linked with particles of colloidal size carrying an electric charge which is balanced by the envelope of counter-ions in the pore solution (Banfill, 1994). Generally, electro-osmosis is a process of moving electrolyte towards the cathode (reinforcement) due to the electric field (Mietz and Isecke, 1994b).

7.2.2.4 Diffusion

This mechanism occurs when concentration gradients exist in the pore solution. In this process, Na^+, CO_3^{2-} diffuse towards the reinforcement (cathode). However, the process of diffusion is slow and is, therefore, not an effective contributor to the realkalisation treatment.

7.2.2.5 Absorption

Absorption is another transport mechanism and occurs when the treated concrete is not fully saturated, so it will absorb the external sodium carbonate solution. The alkaline electrolyte penetrating from the surface into the concrete pores delays the subsequent decrease of the pH-value of the pore solution down to corrosion initiating levels. This is based primarily on the reaction between sodium carbonate and carbon dioxide according to the following equation:

$$Na_2CO_3 + CO_2 + H_2O \rightarrow 2NaHCO_3 \quad \text{.....} \quad (7.8)$$

In the state of equilibrium with a constant carbon dioxide concentration of the atmosphere only a small amount of sodium carbonate will react to form sodium hydrogen carbonate ($NaHCO_3$) and hence further carbonation would lead only to a slight decrease of pH. In this way, the ingress of sodium carbonate should act as a carbon dioxide trap. However, this only works if the concrete remains wet.

Nevertheless, the physical, chemical and electro-chemical mechanisms of this treatment are not yet clarified quantitatively in the current literature.

7.2.3 Factors Affecting Realkalisation Treatment

Bier et al (1987, 1988 and 1989) has shown that the rate of passive realkalisation was dependent on the phase composition and pore structure, when he applied a mortar layer of OPC and OPC/GGBS to the surface of carbonated mortars in order to observe the rate of alkaline penetration into the carbonated zone using pH indicator (phenolphthalein). They found that the rate of realkalisation was higher for samples previously stored in 0.03 % CO_2 (by volume) than for those stored in 2 %CO_2 (by volume). It was also higher for specimens made of OPC cement compared to those made of OPC/GGBS. They attributed this behaviour to the reactions of silica gel in carbonated mortars with Ca^{2+} ions which diffused from the overlaying layer and he also pointed out that realkalisation is not caused by significant changes of the microstructure and composition of the carbonated HCP but rather by diffusion of Ca^{2+} ions in the pore solution from the alkaline mortar overlay to the carbonated concrete. However, the rate of realkalisation depends on the moisture available for the diffusion of ions.

Odden and Miller (1993) studied the effect of electrolyte concentration (0.01-1M sodium carbonate) on the pH of concrete subjected to ECR. The results showed that at all concentrations an alkaline environment in the covercrete of pH $\geq$ 11 was produced, except for the case of 0.01 Na_2CO_3 molar solution. Sergi et al (1996) studied the effectiveness of ECR using different electrolytes, Na_2CO_3, LiOH, $Li(NO)_2$, $Li(BO)_2$ and $Li(NO)_3$, with different concentrations and found that LiOH and Na_2CO_3 were the most effective electrolytes used.

Mietz and Isecke (1994a and 1994b), studying effects of ECR, reported that both the outer realkalisation layer (measured from concrete surface) and the inner realkisation layer (measured from reinforcement surface), measured by phenolphthalein indicator, were increased by increasing water/cement ratio and treatment time. They also found that the electro-chemical polarisation had a minor effect on the realkalisation progress

developing from the concrete surface, suggesting that the electro-osmosis mechanism has an insignificant role on the process of ECR.

Mattila et al (1996) reported that the rate of passive realkalisation due to surface coating depends on the porosity of the concrete and the realkalisation front proceeds at least as rapidly as the carbonation front proceeded into the concrete when it was new (square root model). They also found that the rate of realkalisation is dependent on RH% and the threshold moisture for reasonably rapid realkalisation was about 90% RH. It means that, as far as moisture requirements are considered, realkalisation is able to occur when reinforcement corrosion is also likely to proceed.

However, there is a contradiction in the literature regarding the effect of current density (electro-osmosis) on the processes of ECR. Some authors, such as Polder and Hodel (1992), believes that the role of electro-osmosis in ECR treatments is significant while others (Mietz and Isecke, 1994a and 1994b) reported the reverse. In addition, there is a lack of evidence in the literature regarding other parameters such as period of ECR, electrolyte type and moisture content which can affect the mechanism and rate of electro-chemical realkalisation. So, there is a need for more study to clarify the role of these parameters.

7.2.4 Effect of Realkalisation on Concrete Properties

Bier et al (1989) found that, in a passive realkalised matrix, the broad infra-red absorption bands of silica gel formed during the carbonation processes disappeared and those of C-S-H gel were established in the presence of calcium carbonate. The reformation of the C-S-H phases in the realkalised zone leads to changes in the pore structure as shown in Figure 7.2. They also observed a marked reduction of coarse pores with $10 < r < 100$ nm, and formation of fine pore space with $r < 10$ nm. This suggests that realkalisation produces a much denser concrete. However, this work was done using an overlay of an OPC or an OPC/GGBS mortar layer above the treated concrete. The result may have been different if impressed current was used.

Unless paths are provided for easy escape, the liberated hydrogen (equation 7.4) at the reinforcement during ECR treatments will cause pressure development at this site. This pressure increase by electrolysis may lead to cracking and changes in the pore structure

at the area concerned. It is also possible that this area may be softened due to the high concentration of alkali (Chatterji, 1994).

Al-Kadhimi et al (1996) recently found that ECR modifies the pore size distribution of the cement paste matrix in the vicinity of the cathode by changing it in the direction of smaller pores. They also concluded that the total water absorption, capillary absorption and initial surface absorption all decrease as a result of the ECR treatment, while the compressive, pullout and flexural strength, dynamic modulus of elasticity and ultrasonic pulse velocity all increase.

However, there are insufficient studies dealing with the effect of ECR on the pore solution, microstructure and chemical composition of the cement matrix of the concrete.

7.2.5 Side Effects of Electro-Chemical Realkalisation

The RILEM Draft Recommendation (1994), Miller (1994) and Chatterji (1994) identified the possible draw-backs due to the application of ECR on carbonated reinforced concrete structures, as follows:

(1) Reduction of bond strength between reinforcement and concrete, caused by softening of the concrete immediately around the steel due to the high concentration of alkali.

(2) Hydrogen embrittlement of reinforcement (HE), as a result of the evolved hydrogen shown in equation (7.4) which may be absorbed by high strength steel reinforcements, thereby making them brittle. The longer the electrolysis proceeds the higher will be the chance of this embrittlement of the steel. The NCT Report (1994) does not however show any adverse effect of HE either on prestressing or conventional reinforcing steel.

(3) Cracking of the concrete cover, caused by high pressure built up owing to the evolution of hydrogen.

(4) Alkali-aggregate reaction, the possibility of this being increased due to the high alkalinity around the reinforcement caused by the ECR treatment. This reaction occurs between certain types of aggregate and alkali ions contained in the concrete. It results in the production of an alkali silicate gel and, under certain conditions, can cause expansion and cracking of concrete.

The above-mentioned effects are hypothetical however, and not based on experimental studies.

7.3 EXPERIMENTAL PROCEDURES

7.3.1 Preparation of Steel Cathode

A 35x35x1 mm mild steel plate with a 4 mm diameter steel rod spot welded on the centre of one edge was used as a cathode. The chemical composition of the mild steel plate cathode is shown in Table 7.1. Regular holes of 2 mm diameter and of spacing 2 mm were drilled in the steel plate to allow electrolyte to pass through the cathode during the ECR treatment, owing to possible electro-osmosis effects. An electrical wire was then soldered at the top of the steel rod as shown in Figure 7.3.

Prior to casting of the HCP specimens for ECR, the steel cathode was cleaned by sand blasting followed by wiping with an acetone soaked tissue. The steel rod was coated with a slurry of cement and Styrene-Butadiene Rubber (SBR), where crevice attack might be expected to occur. Shrink tubing was then used to cover the upper part of the steel rod.

7.3.2 Preparation of Specimens

Prismatic specimens (100x50x50 mm) of OPC cement paste cast with 0.70 w/c ratio were used for this study. The mixing technique employed for making these specimens was based on the method devised by Gukild and Carlsen for minimising "bleeding" (Markestad, 1976). This method was previously used by Page and Vennesland (1983) and Hornain et al (1995) and they reported that the method causes substantial reduction in bleeding of high w/c ratio HCP's. 10% of the whole mix was prepared as a slurry of cement (w/c = 3.0) before casting the specimens by ball-milling for 48 hours at 1 rev./sec. The slurry was then manually mixed with additional cement and water to the correct final mix proportions by means of a spatula for 5 minutes.

After mixing, the fresh cement paste was then cast in a specially made ply-wooden mould. The steel cathodes were embedded in the cement paste and kept in the right position by means of plastic handles which were held tight to the mould. The steel cathodes were arranged so that they were perpendicular to and in the centre of the

longest dimension of the specimen. The mould was then vibrated for 1 minute on a vibrating table for compaction. The cement paste was then levelled and the mould was wrapped in a polythene sheet. The HCP prisms were demolded after 48 hours and transferred to the curing room. The specimens were cured in water at 38°C for 7 days as described in Section 2.5.

After curing, the specimens were transferred to a 100% CO_2 /65% RH chamber and were then left for 3 months. Some of the carbonated specimens were split into two halves and were sprayed with phenolphthalein indicator to establish that the specimens were fully carbonated. The details of the experimental set-up and the carbonation test were described in Section 5.3. The specimens were then pre-conditioned in 65% and 100% RH environments by storing in different desiccators containing sodium nitrite solution and de-ionised water, respectively. The pre-conditioning of the specimens was carried out for a period of more than three months until a steady weight was achieved. This was followed by sealing of the specimens with three layers of water proof epoxy resin on all sides apart from the surface chosen for electrolyte exposure and its opposite surface (see Figure 7.4). After sealing, the specimens were stored again in the desiccators at 65% and 100% RH until the beginning of the ECR treatment.

7.3.3 ECR Set-up

The five electrolytes used were, de-ionised water, 1 mol/litre solutions of sodium carbonate (Na_2CO_3), sodium hydroxide (NaOH) and lithium hydroxide (LiOH) and 0.50 mol/litre sodium phosphate (Na_3PO_4) solution, as shown in Table 7.2. All the reagents were AR grade and were made up with de-ionised water. The pH of these electrolyte solutions were measured as described in Section 2.6.10 and the results are given in Table 7.2.

Each specimen was positioned with its exposed surface on two plastic dividers which were in turn placed on an activated titanium mesh (50x50 mm). The mesh and the first 3 mm of the specimen were immersed in 80 ml of the appropriate electrolyte inside a shallow dish. The titanium mesh as the anode and the steel cathode were then connected to a galvanonstat which maintained the current at appropriate levels for the required time of treatment (see Figure 7.4). Care was taken to ensure that the concentration of the electrolyte was constant throughout the treatment by changing the electrolyte solutions

daily. The completed specimens were then stored in PVC chambers at 25 ±2C° throughout the whole test period. The treatment was carried out at variable polarisation currents (0, 1 and 5 A/m^2) and for different periods (0, 7, 14 and 28 days). Four treatment regimes were used throughout this study, as listed in Table 7.3.

7.3.4 Analysis

7.3.4.1 Moisture movement

The moisture movement of the electrolytes owing to the ECR treatment was monitored by measuring the weight change which occurred in the realkalised specimens. The weight change (ΔW) was calculated using the following equation:

$$\Delta W\ (\%) = \frac{(W_i - W_o)}{W_o} \times 100 \quad \text{.....} \quad (7.9)$$

where,

ΔW : weight change, %.

W_o : weight of specimen at the beginning of the treatment (t=0), gm.

W_i : weight of specimen at any time during the treatment, gm.

In this study, the average weight change of five specimens for each treatment regime was calculated.

7.3.4.2 Depth of realkalisation

Immediately after the ECR treatment, the treated specimens chosen for the determination of the realkalisation depth were sliced in half with a single cut at the steel cathode surface in such a way that two equal sections (50x50 mm) were produced. Each section was split in two halves so that two freshly exposed surfaces were produced. These surfaces were quickly sprayed with phenolphthalein and thymolphthalein indicators, respectively. The zones of apparent realkalisation were measured for each indicator from the cathode surface (X) and specimen surface (Y) (see Figure 7.4), using a travelling microscope. Five readings of the realkalisation depths from both surfaces (X and Y) were recorded for each sprayed surface and the average depths were then calculated. The details of techniques and the test procedures are described in Section 2.6.10. and 5.3. In this study, the overall average realkalisation depths, measured from

the steel cathode surface (X) and specimen surface (Y), for five specimens were considered.

7.3.4.3 Pore solution

For each polarisation regime, four treated specimens specified for pore solution analysis were disconnected from their wiring system and were dry-sliced into sections at 10, 20, 35, 45, 55 and 65 mm from the specimen surface with the use of a mechanical hacksaw. The cutting-up arrangement for the treated HCP specimen is shown in Figure 7.5. Corresponding sections from the four specimens were grouped and stored in 100% RH environments for at least 2 months until steady weight was obtained. The specimens were pre-conditioned to produce enough pore solution in the specimen to be expressed by the pore solution device and to obtain valid comparison between the specimens treated with different polarisation currents. The pre-conditioning of the specimens prior to pore solution extraction was previously used by Walker (1994) with reasonable success.

The pore solution was extracted using the pore expression device described in Section 2.6.5. The load was applied at a rate of 0.3 kN/s to a value of 600 kN. The solution was collected in a sterile polythene vial and immediately sealed until ready for analysis. The sodium and carbonate ion concentrations and pH were then thus determined at 0-10, 10-20, 20-35, 35-45, 45-55 and 55-65 mm from the specimen surface as described in Section 2.6.6.

7.3.4.4 Pore structure

After dry-slicing the specimens for pore solution analysis, fragmented samples were taken from the cathode (45-55 mm) and from the specimen surface (0-10 mm) slices. The specimen sampling was done in such a way to ensure that the cathode sample was obtained from the first 3 mm around the cathode, while the surface sample was from the first 6 mm near the surface which was exposed to the electrolyte. The specimens were stored in desiccators containing silica gel until analysis by MIP. The specimen preparation and test procedures were carried out as described in Section 2.6.3.

7.3.4.5 Indentation microhardness

The treated specimens specified for indentation microhardness analysis were sliced into two sections (50x50 mm) at the cathode surface. From the section which was exposed to the electrolyte, a specimen of 10x50x50 mm was sliced from its central region perpendicularly to the cathode surface. The specimen was then prepared for the indentation microhardness test as described in Section 4.3.1. The microhardness measurements were taken at different distances from the cathode surface, ≈0, 0.25, 0.5, 1.0, 5.0 and 10.0 mm and at 3 mm from the specimen surface. The test procedures and technique are described in Section 2.6.7. The average of thirty microhardness measurements for triplicate specimens of the same treatment regime was determined in this study.

7.3.4.6 Cement phases

The cement hydrate phases of the treated HCP were identified in this study with the aid of differential thermal analysis/ thermo-gravimetry (DTA/TG) and X-ray diffraction (XRD) techniques. Fragmented specimens were obtained from the cathode and surface zones in a similar way to those obtained for MIP pore structure analysis. The specimens were then ground to a powder and sieved to size 150 μm. The sieved powder was stored in a desiccator containing silica gel until required. Details of the techniques and the test procedures are described in Section 2.6.4.

7.4 RESULTS AND DISCUSSION

7.4.1 Mechanism of ECR and the Factors Affecting the Treatment

As described in Section 7.2.2, the ECR process is thought to be dependent on a combination of mechanisms which include capillary absorption, diffusion and electro-osmosis. These mechanisms occur mainly near the surface and result in the inward movement of the electrolyte. It was thought necessary, therefore, in this part of the investigation to monitor the % weight change (Δw) during the treatment to provide information about the rate of the electrolyte ingress in the surface zone.

7.4.1.1 Moisture movement

The rates of weight change (%Δw) for HCP specimens pre-conditioned at 65 and 100% RH and treated with 1 mole/litre sodium carbonate (Na_2CO_3) at different current

densities (I = 0, 1 and 5 A/m^2) for 14 days were determined and the results are shown in Figure 7.6. It can be seen from figure 7.6 that the %Δw for all ECR regimes increases with increasing time of the treatment (t) and with the reduction of the pre-conditioning RH of the treated specimens. A significant increase in %Δw was noted when the pre-conditioned RH was reduced from 100% to 65%. The level of increase was of the order of 400% for the specimens treated with the same current density. The significant effect of the pre-conditioning RH on the ECR treatment rate reflects the role of the capillary absorption mechanism on the ECR process.

The effect of the polarisation current on the rate of the moisture movement (%Δw) can also be seen in Figure 7.6. The polarisation intensity had no systematic effect on the rate of the moisture movement of the carbonated cementitious material. For the 65% RH pre-conditioning (Figure 7.6.a), the specimens treated with a 1 A/m^2 current density had a higher %Δw than that recorded in the corresponding specimens treated at 0 A/m^2, whilst the reverse effect was noted for the specimens treated at 5 A/m^2. On the other hand, at the 100% RH pre-conditioning, the %Δw of the specimens treated with 0 and 1 A/m^2 current densities appear to be similar (see Figure 7.6b).

7.4.1.2 Pore solution chemistry

The chemical analyses of the pore solution of the specimens pre-conditioned at 65 and 100% RH and treated with different current densities (I = 0, 1 and 5 A/m^2) are shown in Figures 7.7 to 7.9. It can be seen in Figure 7.7 that the Na^+ concentration is high near the surface for all treated specimens and decreases with increasing distance away from the specimen surface. The high concentration of Na^+ near the surface (first 25 mm) seems to be affected by altering the level of polarisation but in an arbitrary manner and is significantly reduced when the pre-conditioning RH increases from 65% to 100%. The amount of Na^+ reduction due to the increase of the pre-conditioning RH from 65 to 100% reaches approximately 100%. The results also show that there is a limited increase in Na^+ concentration at the cathodic zone (50 mm) for 65% RH specimens, which appears to be affected by the current density, but a less significant increase for the 100% RH specimens.

The effect of current density and the pre-conditioning RH on the concentration of carbonate ion profiles (present in the electrolyte solution, as Na_2CO_3) of the HCP treated with ECR for 14 days is shown in Figure 7.8. A similar effect to that obtained for the Na^+ concentration profiles is observed, when the results in Figures 7.7 and 7.8 are compared. The concentration of carbonate ions (CO_3^{2-}) is at its highest in the first 5 mm from the specimen surface and starts to diminish with depth with only a limited increase at the cathodic zone (50 mm) owing to the passage of current. The carbonate ion concentrations near the surface of the specimens pre-conditioned at 65% RH are greater by about 160% than the corresponding specimens pre-conditioned at 100% RH. The results also indicate that the polarisation current has a minor effect on the concentration of these ions near the surface when compared to the effect of the pre-conditioning RH.

The high concentration of the sodium (Na^+) and carbonate (CO_3^{2-}) ions near the surface zone can be attributed mainly to the role of the capillary absorption and diffusion processes as described earlier and shown in Figure 7.6. The increase in the amount of these ions at the surface zone for the specimens pre-conditioned at 65% RH compared to those specimens pre-conditioned at 100% RH is attributed to the significant role of capillary absorption on the ECR treatment. In contrast, the role of the current polarisation on the concentration of these ions was limited, as a result of the insignificant effect of electro-osmosis on the ECR process. Furthermore, the insignificant levels and low increase of the sodium ions at the cathodic zone may be due to the absence of these ions in the pore solution after carbonation, and to slow electro-migration during the treatment. This observation is in agreement with previous work carried out by Sergi (1986), who found that the sodium ions disappeared almost totally from the pore solution when the hydrated cement pastes were carbonated.

Figure 7.9 illustrates the pH profiles of the treated HCP specimens pre-conditioned at 65% and 100% RH and treated with 0, 1 and 5 A/m^2 current densities for 14 days, using 1 mol/litre sodium carbonate (Na_2CO_3) as an electrolyte. It can be seen from Figure 7.9 that, near the surface, the alkalinity is greater than in the bulk of the specimens and that the pH in the first 10 mm zone ranged from 8.5 to 10.5. These pH values seem to be dependent upon the pre-conditioning RH, where the pH at the first few mm increases with the lowering of the amount of moisture in the pores of the cementitious material.

Once again, the role of the polarisation current on the alkalinity near the surface is not systematic compared to the role of the pre-conditioning RH.

Figure 7.9 also shows a significant increase in the pH at the cathode zone (50 mm) when an impressed current (1 or 5 A/m^2) was used compared to the corresponding specimens treated at 0 A/m^2. The amount of increase in pH rises with increasing amount of electric charge passed and reduces with increasing distance from the cathode surface. It is also apparent from the results shown in Figure 7.9 that the pH around the cathode reaches about 12 when the ECR treatment is carried out with 1 and 5 A/m^2 for 14 days. This value of pH is generally enough to reinstate the passive film of the reinforcement and provides some protection for the reinforcement against further attack by CO_2. For the HCP treated with 1 A/m^2 the pre-conditioning RH seems to have an insignificant effect on the alkalinity at the cathodic zone, as pH results at the cathodic zone of both pre-conditioned specimens were similar. It should be noted that the accuracy of these results may be affected by the size of the slices used for pore solution analysis, as the pH and concentration of the ions are not likely to be uniformly distributed in the slice width.

The effect of current density (I) and the pre-conditioning RH on depths of realkalisation (from specimen and cathode surfaces) was again studied with the use of pH indicators which were successfully used in most of the previous investigations (Mietz and Isecke, 1994a and 1994b; Sergi et al, 1996 and Mattila et al, 1996). The pH indicators were used in this study to provide extra information about the exact realkalisation depths which were difficult to obtain from the pore solution results as a result of using relatively thick slices for the analysis.

The results of realkalisation depths measured from the cathode surface (X) and specimen surface (Y) using phenolphthalein and thymolphthalein indicators for HCP specimens pre-conditioned at 65 and 100% RH and treated with 0, 1 and 5 A/m^2 for 14 days are presented in Table 7.4. It can be seen from these results that the realkalisation depth measured from the specimen surface (Y) is similar for all polarisation levels, whilst, a substantial increase in X with increasing current density was noted. The insignificant effect of the current density on the rate of realkalisation of the surface zone

is in agreement with the findings reported earlier by Mietz and Isecke (1994a and 1994b), confirming that electro-osmosis is plays no significant role in the ECR process.

The results in Table 7.4 also demonstrate the significant role of the pre-conditioning RH on the realkalisation depth which was measured from the specimen surface (Y), where approximately a 100% increase in Y was found when the moisture of the capillary pores was reduced from 100 to 65% RH. This effect was however negligible at the cathodic zone. These findings are in agreement with those of the pore solution results shown in Figure 7.9.

The increase in the alkalinity (pH) of the surface zone is likely to be caused by diffusion and absorption of sodium carbonate (Na_2CO_3) from the electrolyte solution so that higher pH is observed for the specimens which were pre-conditioned at low RH (65%) compared with those pre-conditioned at the higher RH (100%). On the other hand, the substantial increase in the pH at the cathodic zone is mainly attributed to the generation of hydroxide ions (OH^-) around the cathode by the electrolysis processes (as described earlier in Section 7.2.2.1). These ions, consequently, electro-migrate from the negative pole (steel cathode) to the positive pole (titanium mesh) producing a highly alkaline zone around the cathode. The increase in pH around the cathode with increasing current density was an expected phenomenon and is as a result of the reactions shown in Equations 7.4 and 7.5.

The role of the treatment period (T) on the chemical properties of the pore solution (pH, Na^+ and CO_3^{2-} ions) and depths of realkalisation (X and Y) of HCP specimens pre-conditioned at 65% RH and treated with 1 A/m^2 current density is shown in Figure 7.10 and Table 7.4, respectively. The results in Figure 7.10 show that the concentration of Na^+ and CO_3^{2-} ions near the surface increase with increasing T. The concentration of these ions decreases with increasing distance from the surface (Y). It can also be seen from Figure 7.10.c that the pH at both the anode and cathode zones is significantly increased with increasing T, especially for the specimens treated for 14 and 28 days. In addition, the width of the highly alkaline zone around the cathode (X) is also increased with T, whilst the corresponding surface zone (Y) seems to be similar for all treatment periods.

Table 7.5 demonstrates the realkalisation depths (X and Y) for HCP specimens treated with 1 A/m^2 for different periods (T = 7, 14 and 28 days). It shows that both the realkalisation depths (X and Y) increase with increasing T. However, the effect of the treatment period is more pronounced on X than that on Y. The level of increase in the X parameter increased by 140 and 520 % when T was increased from 7 to 14 and 28 days, respectively, whilst the corresponding increase in Y was about 60 and 120%, respectively.

The pH increase around the steel cathode with increasing period of treatment (T) could be attributed to the amount of OH^- ions generated around the cathode as a result of the cathodic reactions (see Section 7.2.2.1). On the other hand, as explained earlier (Figure 7.6), the increase in the realkalisation depth measured from the specimen surface (Y) with increasing T is mainly attributed to the increase in the absorbed and diffused Na_2CO_3, which increases with increasing period of ECR treatment.

The role of the electrolyte type on the realkalisation depth measured from the specimen surface (Y) was also investigated using the pH indicators and the results of this investigation are presented in Table 7.6. The results show that the use of sodium phosphate solution (Na_3PO_4) as an electrolyte resulted in a deeper realkalisation zone (Y) than that produced by the other electrolytes investigated viz. sodium carbonate (Na_2CO_3), sodium hydroxide (NaOH) and lithium hydroxide (LiOH). The depth of realkalisation (Y) for the specimens treated with Na_3PO_4 solution was 300% greater than the corresponding depth produced by the more widely used electrolyte Na_2CO_3. The results reported in Table 7.6 also show that the depth of realkalisation measured from the specimen surface treated with lithium hydroxide solution (LiOH) is greater by 50% than the corresponding specimens produced when sodium carbonate was used, which is in agreement with the findings reported earlier by Sergi et al (1996).

The significant effect of using sodium phosphate as an electrolyte on the processes of ECR treatment has not been understood yet and the role of this substance on any possible enhancement of properties of the cementitious material should be subject to further investigation.

7.4.2 Effect of ECR Treatment on the Microstructure and Cement Hydrate Phases of the Near Surface and Steel/Cement Paste Transition Zones

7.4.2.1 Microstructure

The effect of ECR treatment on the PSD and porosities (total, capillary and gel) of the cement paste matrix at the cathode (transition zone) and near surface zones was studied using the MIP technique. The results are represented in Figures 7.11 to 7.13 and Tables 7.7 to 7.9.

The PSD of the cement paste/cathode transition zones of HCP specimens treated with different current densities (I = 0, 1 and 5 A/m^2) for 14 days are illustrated in Figure 7.11. It can be seen that the PSD of the cement paste/ cathode transition zone (TZ) becomes finer when an electric charge is impressed compared to the corresponding untreated HCP (I = 0 A/m^2). The PSD of the specimens treated with 1 and 5 A/m^2 current density seems to be similar. The threshold pore diameter D_{th} is reduced from 800 to 100 nm as a result of increasing the intensity of polarisation from 0 to 1 or 5 A/m^2.

A similar effect was also obtained when the period of treatment was altered (see Figure 7.12). The results in Figure 7.12 demonstrate the PSD of the TZ of the carbonated OPC specimens treated with 1 A/m^2 current density for 0, 7, 14 and 28 days. The PSD of the TZ becomes more dense as a result of the ECR treatment for 7, 14 and 28 days compared to those corresponding to the untreated specimens (T = 0 days).

The total, capillary (pore diameters $\geq$ 30 nm) and gel (pore diameters $\leq$ 10 nm) porosities of the TZ of HCP treated with regimes I and III (see Table 7.3) are represented in Tables 7.7 and 7.8, respectively. These results were deduced from the PSD's shown in Figures 7.11 and 7.12. It can be seen from these results that the total and capillary porosities of the treated cementitious material at the cathode decrease with increasing I and T. However, the effect of the ECR treatment is more significant on the capillary porosity than the total porosity. The amount of total porosity reduction reaches 15 and 20% when I and T were increased from 0 to 5 A/m^2 and from 0 to 28 days, respectively, whilst the corresponding reductions in capillary porosity are approximately 50 and 35%, respectively. On the other hand, the gel porosity increases with applied

current and with increasing period of ECR treatment. The amount of this increase reaches 50% for the specimens treated with 5 A/m^2 current density for 14 days, compared to that of the untreated specimens.

The effect of the electrolyte type on the PSD and porosities of the near-surface zone is illustrated in Figure 7.13 and Table 7.9, respectively. The electrolytes investigated, sodium carbonate (Na_2CO_3), sodium hydroxide (NaOH), sodium phosphate (Na_3PO_4) and lithium hydroxide (LiOH) solutions were introduced into the carbonated specimens for 14 days, using zero current density. The following observations can be made from these results:

(1) The PSD and D_{th} of HCP treated with sodium carbonate solution (Na_2CO_3) were relatively similar to those of the carbonated specimens treated with water (control specimens).

(2) The use of sodium phosphate solution as an electrolyte resulted in finer PSD and a greater reduction in the D_{th} than that produced by the other electrolytes in the investigation, whilst the reverse was true when sodium hydroxide solution was used.

(3) The total porosities of the specimens treated with sodium carbonate, sodium hydroxide and lithium hydroxide were greater than those of the corresponding specimens treated with water by 10, 25 and 10%, respectively, while the use of sodium phosphate resulted in a significant reduction in the total porosity. The level of this reduction was approximately 25%.

(4) The capillary porosity was significantly reduced when sodium phosphate was used compared to that of the other electrolytes. The amount of this reduction was about 350%, whilst the reverse was true for the specimens treated with sodium hydroxide.

(5) A slight enhancement in the amount of the capillary pores was produced when sodium carbonate or lithium hydroxide solution was used. The levels of enhancement were about 20 and 40%, respectively, compared to the results for the corresponding specimens treated with water.

(6) The gel porosity of HCP at the near surface zone seemed to be similar for the specimens treated with sodium hydroxide, sodium phosphate or lithium

hydroxide solution. However, the gel porosity of this zone was increased when sodium carbonate solution was used.

The effect of the ECR treatment on the microhardness of the cement matrix in the steel cathode/cement paste transition (TZ) and surface zones was studied and the results are shown in Figures 7.14 and 7.15, respectively. The statistical analysis of these results was also carried out using a t-test to study the significance of the differences between the microhardness averages (see Tables 7.10 to 7.12). The microhardness results seem to be highly scattered and unaffected by either the polarisation currents or the period of the treatment. The statistical analyses carried out in Tables 7.10 and 7.11 support this observation, since the difference between the averages of the microhardness results are insignificant.

Figure 7.15 shows the microhardness of the near-surface zone of HCP specimens treated with sodium carbonate, sodium hydroxide, sodium phosphate and lithium hydroxide solution for 14 days, using $I = 0\ A/m^2$. The microhardness results appear to be similar for all the electrolytes used, except for those treated with sodium hydroxide where a slight reduction in the microhardness is shown. The statistical analysis presented in Table 7.12 supports this finding, where it shows insignificant differences between the averages of all but one of the results and a significantly adverse effect when sodium hydroxide was used.

The microhardness results shown in Figures 7.14 and 7.15, generally indicate that the ECR treatment processes have an insignificant effect on the microhardness properties of the treated cementitious matrix, which appears to contradict the earlier findings obtained from the MIP technique. This may be attributed to the insensitivity of the microhardness technique in evaluating such variations in the cement matrix.

7.4.2.2 Cement matrix composition

In order to understand the variations that occur in the pore structure owing to the use of ECR and clarify the role of the ECR treatment, DTA/TG and XRD techniques were adopted in this investigation. This was carried out by analysing the samples taken at the

cathode and near surface zones which were treated under regime I, III and V. The results of these analyses are represented in Figures 7.16 to 7.21 and Tables 7.13 to 7.18.

The DTA thermographs of the steel cathode/cement paste transition zone of HCP specimens treated with 0, 1 and 5 A/m^2 current density for 14 days and 1 A/m^2 for 0, 7, 14 and 28 days are shown in Figures 7.16 and 7.17, respectively. It can be seen that the size of the endo-thermic peak associated with calcite (750-900°C) decreases with the level of ECR, whilst the shallow hump associated with calcium silicate hydrate (110-250°C) starts to grow as a result of the treatment. The size of this hump appears to increase with increasing current density and the period of the ECR treatment. Non-identified exo-thermic (NIP) peaks at 450-600°C were also observed when the specimens were treated. These exo-thermic peaks appear not to be due to calcium hydroxide (C-H), which decomposes at this range of temperatures causing an endo-thermic peak. It was, however, difficult to identify such a phase in the course of this investigation.

These thermographs obtained from the DTA technique are only qualitative. So, a TG technique was adopted in this investigation for two reasons: first, to support the findings obtained from the DTA thermographs and secondly to quantify the components of the untreated and treated HCP which were shown as peaks in the DTA thermographs. The amount of any particular cementitious phase was estimated in terms of the % weight loss at a certain temperature range. The range of temperatures was defined for each cement phase from the DTA thermo-graphs and from the literature (see Appendix 5).

Table 7.13 and 7.14 show the % decomposition of calcium silicate hydrate (C-S-H), non-identified phase (associated at 425-550°C), calcite ($CaCO_3$), evaporable water (EW) and the non evaporable water (NEW) of the cathode/cement paste transition zone of the HCP specimens treated under regime I and III, respectively. It can be seen that the amount of C-S-H and non-identified phase increases with increasing current density and the period of the ECR treatment. The amount of C-S-H increase, due to increasing I from 0 to 5 A/m^2 and t from 0 to 28 days, reaches 40 and 10%, respectively, whilst the corresponding increase in the non-identified phase is 35 and 15%, respectively. On the other hand, the amount of calcite ($CaCO_3$) was reduced when an electric charge was

induced into the carbonated specimens and the amount of these reductions reach 30 and 15% when I and T were increased from 0 to 5 and from 0 to 28 days, respectively. In addition, the results presented in Table 7.13 show a significant increase in %EW and a slight reduction in %NEW as a result of increasing the level of polarisation and the period of the ECR treatment.

The modifications occurring in the chemical composition of the carbonated HCP due to the ECR processes suggest that the induction of an electric charge into the cementitious matrix could lead to decomposition of some substances such as calcium carbonate, the re-formation of others such as C-S-H and the creation of new phases (NIP). This means that the use of the ECR could not only lead to the reinstatement of the passive oxide film around steel reinforcement but also to some degree of reformation of the main hydration products (C-S-H) of the cement paste matrix, which have been consumed during the carbonation processes.

The decomposition of calcite and reformation of C-S-H could be the reasons behind the significant increase in the %EW and the modifications occurring in the pore structure (PSD and porosities) of the treated matrix, which were noted in the MIP and TG results. Similarly, the slight changes observed in the %NEW could be attributed to the difference between the amount of $CaCO_3$ decomposed and the corresponding C-S-H reformation during the ECR treatment.

The effect of the electrolyte type on the chemical composition of carbonated HCP was also studied using DTA and TG techniques and the results are represented in Figure 7.18 and Table 7.15. Figure 7.18 demonstrates the DTA thermographs of HCP exposed to sodium carbonate, sodium phosphate, sodium hydroxides and lithium hydroxide solutions for 14 days. The results show that the size of the peaks associated with calcite (750-900°C) seems to decrease simply by exposing the surface of the HCP to the above electrolytes, compared to those treated with water, especially for those treated with the sodium phosphate solution. This observation is in agreement with the results obtained by the TG technique, where the % decomposition of calcite decreases by 25, 45, 15 and 10% when the HCP specimens were treated with sodium carbonate, sodium phosphate, sodium hydroxide and lithium hydroxide solution, respectively (see Table 7.15). The reverse of this effect was noted for the non-identified phase (NIP). The amount of

increase in the non-identified phase as a result of these electrolytes ranged from 40 to 80%.

The results illustrated in Figure 7.18 also show that the size of the shallow hump associated with C-S-H (110-250°C) seems to be unaffected for all the electrolytes used. However, a slight reduction in the amount of C-S-H was noted for the specimens treated with sodium carbonate and sodium hydroxide solutions. The %EW increases with the use of sodium carbonate, sodium phosphate and sodium hydroxide solution as electrolytes when compared to the corresponding specimens treated with water. Furthermore, it seems that the effect of the electrolyte on %NEW is insignificant, except for the specimens treated with the sodium phosphate solution.

These variations in the amount of calcite, C-S-H and non-identified phase which occurred due to the use of different electrolyte solutions may be caused by the chemical reactions between these electrolytes and the carbonated cement phases (mainly calcium carbonate). These chemical reactions could be accompanied with modifications in the microstructure of the cement paste matrix, discussed earlier (see Figures 7.11 to 7.13 and Tables 7.7 to 7.9).

The possibility of the decomposition of calcium carbonate (calcite) as a result of inducing an electric field and the electrolyte into the cementitious matrix during the ECR treatment was also examined by XRD. An example of identification of an XRD trace is given in Appendix 6. The XRD graphs of the cement pastes (presented around the cathode and near surface zones) treated with regimes I, III and V (see Table 7.3) are shown in Figures 7.19 to 7.21, respectively. These graphs show that the calcite peaks are present for all untreated specimens and the specimens treated with ECR, whilst the corresponding peaks of vaterite disappeared when the specimens were treated with ECR ($I = 1$ or $5\ A/m^2$) and with using sodium phosphate or lithium hydroxide solution as electrolytes. In addition, non-identified peaks (NIP) at 38.5° appeared when the electro-chemical polarisation was applied to the carbonated specimens. The nature of these peaks (38.5°) was difficult to identify from the standard XRD data. However, this non-identified crystal (present at 38.5°) could possibly be associated with the non-identified phase shown by the DTA and TG results.

To clarify the role of ECR processes on the amount of calcite disintegrated during the treatment, the calcite content was estimated from XRD graphs as a function of the total intensity of the first four major peaks. The results based on this estimation for the HCP specimens treated with different regimes (I, III and V) are represented in Table 7.16. It shows that the calcite content was reduced by 20% by either increasing the current density from 0 to 1 or 5 A/m^2 or the period of the treatment from 0 to 14 days. The calcite content was also decreased when sodium phosphate solution was used rather than water. The level of decrease reached approximately 15%. To the contrary, the use of lithium hydroxide or sodium carbonate solution appeared to increase the calcite content by approximately 15%.

These findings are in agreement with those obtained by DTA and TG techniques, which confirmed the phenomenon of disintegration of calcium carbonate (calcite) as a result of inducing an electric field into the cementitious matrix and using sodium phosphate as an electrolyte. The decomposition of calcite and the disappearing of vaterite from the XRD graphs could lead to the formation of a new cement phase which is represented by the peaks shown at 38.5°. However, further investigations of these phenomenen are required.

7.5 CONCLUSIONS

The present work has shown the following findings:

(1) The rate of the electrolyte movement at the carbonated surface zone is significantly influenced by the moisture content of the pores (%RH) but is not directly related to the increasing level of polarisation during the ECR treatment.

(2) Capillary absorption is considered the major controlling mechanism of the ECR process at the near surface zone compared to the other mechanisms such as diffusion and current-induced (electro-osmosis). Hence the rate of penetration of the external electrolyte is considerably less for specimens conditioned at 100% RH than for those conditioned at 65% RH.

(3) Electro-osmosis seems to play no significant role on the realkalisation rate of the surface zone.

(4) Hydrolysis and electro-migration are the main mechanisms controlling the processes of ECR at the cathode zone and are significantly dependent on the level of polarisation and the period of the treatment. In addition, insignificant effects of these mechanisms were found in relation to the internal RH of the cementitious matrix at the cathode.

(5) Significant increases in the concentrations of sodium and carbonate ions and the alkalinity at the surface zone were observed with increasing time periods of the ECR treatment and lowering moisture content within the pores. In contrast, the role of the polarisation current density on the chemistry of the pore solution of this zone was found to be insignificant. On the other hand, at the cathode zone, the increase of the current density and the period of the treatment lead to an enhanced pH and enlarged the high alkalinity zone around the cathode. The effect of these parameters on sodium and carbonate ions was insignificant.

(6) The use of sodium phosphate as an electrolyte resulted in a substantial increase (≈300%) in the realkalisation rate compared to that observed when sodium carbonate was used. Lithium hydroxide also increased the realkalisation rate by about 50%.

(7) The passage of an electric current during the ECR treatment appeared to result in a denser pore structure. Both the total and capillary porosity of the cathode/cement paste transition zone were reduced. The effect was more pronounced for capillary porosity than for total porosity.

(8) The use of sodium phosphate as an electrolyte resulted in a significant densification of the pore structure of the treated materials (in terms of PSD and porosities), whilst the reverse effect was observed when sodium hydroxide was used.

(9) The ECR process lead to notable variations in the chemical compounds of the treated cementitious matrix. Decomposition of some calcite and reformation of the

C-S-H phase were both observed. This variation was more pronounced with increasing grade of polarisation and with the use of sodium phosphate as an electrolyte.

Table 7.1 Chemical composition of mild steel plate (%).

Fe	C	Si	Mn	S	Cr	Mo	Ni	Al	Cu	Sn
99.5	0.04	0.01	0.28	0.03	0.04	0.01	0.03	0.01	0.02	0.01

Table 7.2 Concentration and pH of the electrolytes used.

Electrolyte	Concentration	pH
1- De-ionized water (H_2O)	1 mol/litre	7.0
2- Sodium carbonate (Na_2CO_3)	1 mol/litre	10.8-11.0
3- Sodium hydroxide (NaOH)	1 mol/litre	13.9-14.0
4- Lithium hydroxide (LiOH)	1 mol/litre	13.9-14.0
5- Sodium phosphate (Na_3PO_4)	0.5 mol/ litre	10.4-11.0

Table 7. 3 ECR treatment regimes.

Regime	Pre-conditioning RH, %	Electrolyte type	Current density, A / m^2	Period of treatment, day
I	65	Na_2CO_3	0 1 5	14
II	100	Na_2CO_3	0 1	14
III	65	Na_2CO_3	1	0 7 14 28
V	65	H_2O Na_2CO_3 Na_3PO_4 NaOH LiOH	0	14

Table 7.4 Effect of current density on the realkalised depths (from specimen and cathode surface) pre-conditioned at different RH and treated with ECR for 14 days, using different indicators.

RH, %	Current density, A / m^2	Realkalised depth from specimen surface (Y), mm		Realkalised depth from cathode surface (X), mm	
		Phenolphthalein	Thymolphthalien	Phenolphthalein	Thymolphthalien
65	0	8.10	8.0	0	0.00
	1	8.31	8.3	6	5.20
	5	7.85	7.8	27	16.50
100	0	4.25	4.25	0	0.00
	1	4.15	4.10	6	4.90

Table 7.5 Effect of ECR treatment period on the realkalised depths (from specimen and cathode surface), using current density of $1 A / m^2$.

RH, %	Treatment period, day	Realkalised depth from specimen surface (Y), mm		Realkalised depth from cathode surface (X), mm	
		Phenolphthalein	Thymolphthalien	Phenolphthalein	Thymolphathlien
65	7	5.15	5.15	3.0	2.00
	14	8.31	8.30	6.0	5.20
	28	11.25	11.1	16.0	10.30

Table 7.6 Effect of electrolyte type on the realkalised depth measured from specimen surface (Y) treated with ECR for 14 days (pre-conditioning RH = 65%).

Electrolyte type	Realkalised depth (Y), mm	
	Phenolphthalein	Thymolphthalien
Sodium carbonate	8.10	8.00
Sodium phosphate	33.5	33.5
Sodium hydroxide	11.0	10.95
Lithium hydroxide	12.5	12.50

Table 7.7 Effect of current density on porosity of OPC paste specimen (around cathode) treated with ECR for 14 days.

Current density, A / m^2	Porosity, cc/g		
	Total	Capillary	Gel
0	0.1470	0.0672	0.0063
1	0.1192	0.0322	0.0068
5	0.1252	0.0334	0.0097

Table 7.8 Effect of ECR treatment period on porosity of OPC paste specimen (around cathode), using I = 1 A / m^2.

Treatment period, day	Porosity, cc/g		
	Total	Capillary	Gel
0	0.1407	0.0672	0.0063
7	0.1265	0.0672	0.0077
14	0.1192	0.0322	0.0068
28	0.1153	0.0440	0.0076

Table 7.9 Effect of electrolyte type on porosity of OPC paste specimen (near surface) treated for 14 days, I = 0 A / m^2.

Electrolyte type	Porosity, cc/g		
	Total	Capillary	Gel
De-ionized water	0.1407	0.0672	0.0063
Sodium carbonate	0.1520	0.0552	0.0095
Sodium hydroxide	0.1725	0.0733	0.0069
Sodium phosphate	0.1090	0.0146	0.0056
Lithium hydroxide	0.1515	0.0477	0.0058

Table 7.10 Summary of statistical results carried out at OPC paste specimen (at zero distance from cathode surface) treated with ECR using different current densities for 14 days, using t-test.

Current density, A / m^2	Mean, IIV	Variance	Standard deviation	Variation, %	P(T<=t) two tail	Significance of the difference
0	37.90	138.00	11.74	30.90	0.40	insignificant
1	34.60	150.30	12.25	35.40		
0	37.90	138.00	11.74	30.90	0.71	insignificant
5	39.25	134.83	11.62	29.56		
1	34.60	150.30	12.25	35.40	0.23	insignificant
5	39.30	134.83	11.62	29.56		

Table 7.11 Summary of statistical results carried out at OPC paste specimen (at zero distance from cathode surface) treated with ECR for different treatment periods (I = 1 A / m^2), using t-test.

Treatment period	Mean, IIV	Variance	Standard deviation	Variation, %	P(T<=t) two tail	Significance of the difference
0 day	37.90	138.00	11.74	30.90	0.73	insignificant
7 day	39.06	105.77	10.28	26.34		
0 day	37.90	138.00	11.74	30.90	0.39	insignificant
14 day	34.60	150.25	12.25	35.40		
0 day	37.90	150.30	11.74	30.90	0.33	insignificant
28 day	34.95	35.94	5.94	17.02		

Table 7.12 Summary of statistical results carried out at OPC paste specimen (near surface) treated with different electrolytes for 14 days (I = 0 A / m^2), using t-test.

Electrolyte type	Mean, IIV	Variance	Standard deviation	Variation, %	P(T<=t) two tail	Significance of the difference
H_2O	37.70	67.80	8.23	21.84	0.33	insignificant
Na_2CO_3	34.75	111.60	10.56	30.75		
H_2O	37.70	67.80	8.23	21.84	0.49	insignificant
Na_3PO_4	35.70	97.91	9.89	27.71		
H_2O	37.70	67.80	8.23	21.84	0.03	significant
NaOH	31.60	70.90	8.42	26.60		
H_2O	37.70	67.80	8.23	21.84	0.30	insignificant
LiOH	35.00	61.68	7.85	22.44		

Table 7.13 Effect of current density used at ECR treatment on the chemical compounds of OPC paste (around cathode) treated for 14 days, deduced from DTA/TG technique.

Current density, A / m^2	Decomposition, %				
	C-S-H (110-250°C)	NIP* (450-600° C)	Calcite (750-900° C)	E.W (20-110° C)	NEW (110-950° C)
0	4.70	2.15	17.79	2.16	36.73
1	5.90	2.72	12.18	6.02	32.55
5	6.53	2.87	12.45	6.94	34.20

* Non-Identified Phase

Table 7.14 Effect of ECR treatment period on the chemical compounds of OPC paste (around cathode) using current density of 1 A/m^2, deduced from DTA/TG technique.

Treatment period, day	Decomposition, %				
	C-S-H (110-250 °C)	NIP* (450-600° C)	Calcite (750-900° C)	E.W (20-110 C)	NEW (110-950° C)
0	4.70	2.15	17.79	2.16	36.73
7	4.59	2.17	18.14	2.35	36.74
14	5.90	2.72	12.18	6.02	32.55
28	4.99	2.44	15.53	5.11	35.31

* Non-Identified Phase

Table 7.15 Effect of electrolyte type on the chemical compounds of OPC paste (near surface) treated for 14 days (I = 0 A/m^2), using DTA/TG technique.

Electrolyte type	Decomposition, %				
	C-S-H (110-250° C)	NIP* (450-600° C)	Calcite (750-900°C)	E.W (20-110°C)	NEW (110-950°C)
H_2O	4.70	2.15	17.79	2.16	36.73
Na_2CO_3	3.66	3.55	13.50	2.23	34.94
Na_3PO_4	4.88	3.00	10.03	2.69	30.93
NaOH	3.86	3.41	15.52	2.65	35.30
LiOH	4.34	3.87	16.15	2.53	35.79

* Non-Identified Phase

Table 7.16 Effect of current density, ECR period of treatment and the electrolyte type on the calcite content (in terms of the highest four intensities), deduced from XRD diagrams.

Current density, A / m^2	Calcite content
0	67
1	54
5	54

Period of treatment	Calcite content
0 days	67
14 days	54
28 days	63

Electrolyte type	Calcite content
H_2O	67
Na_2CO_3	79
Na_3PO_4	57
NaOH	76
LiOH	68

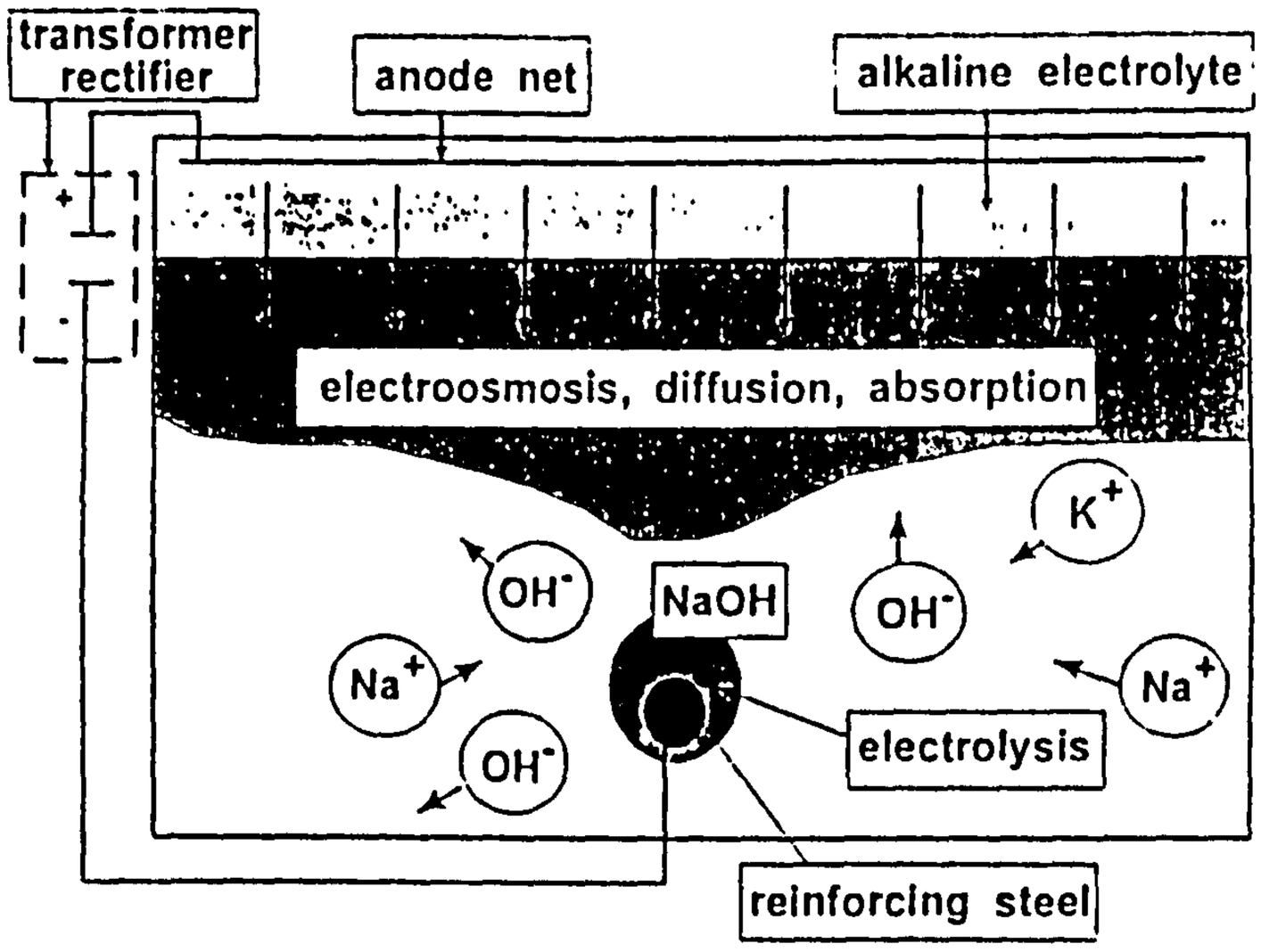

Figure 7.1 Principle of electro-chemical realkalisation (Mietz and Isecke, 1994).

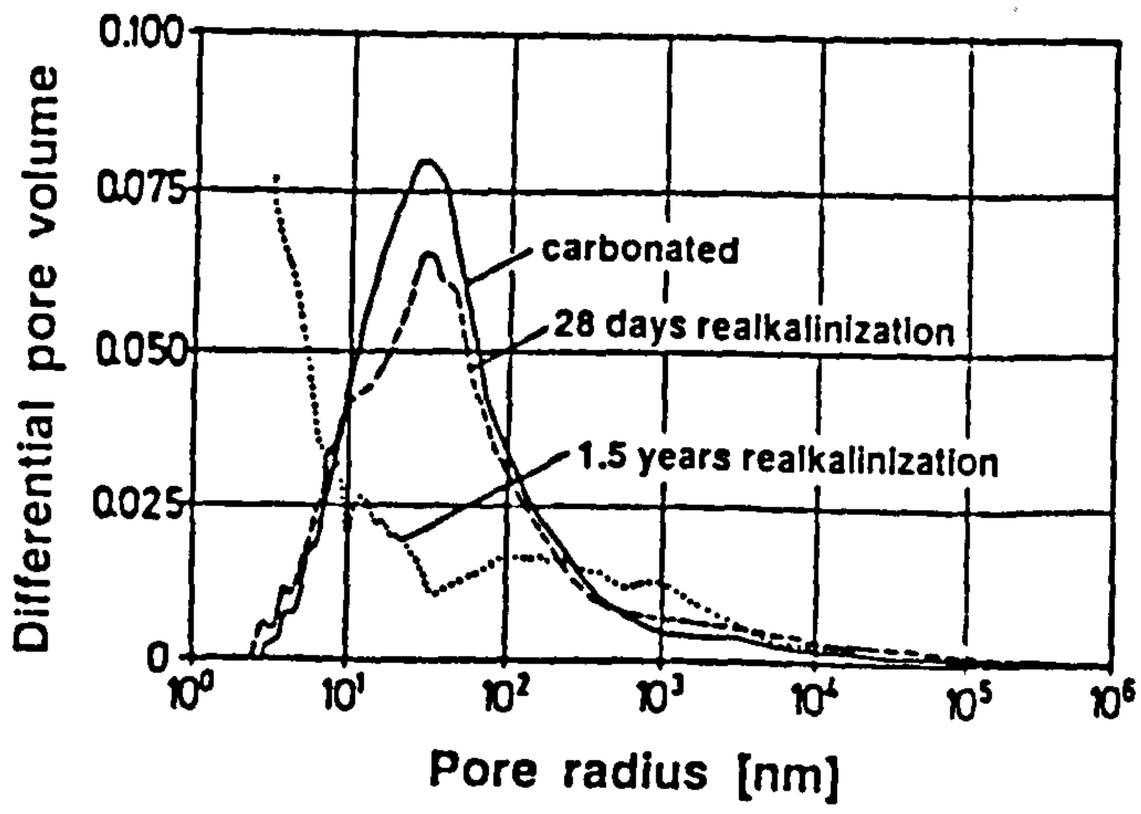

Figure 7.2 PSD of carbonated and realkalised cement paste matrix of GGBS concrete (Bier et al, 1989).

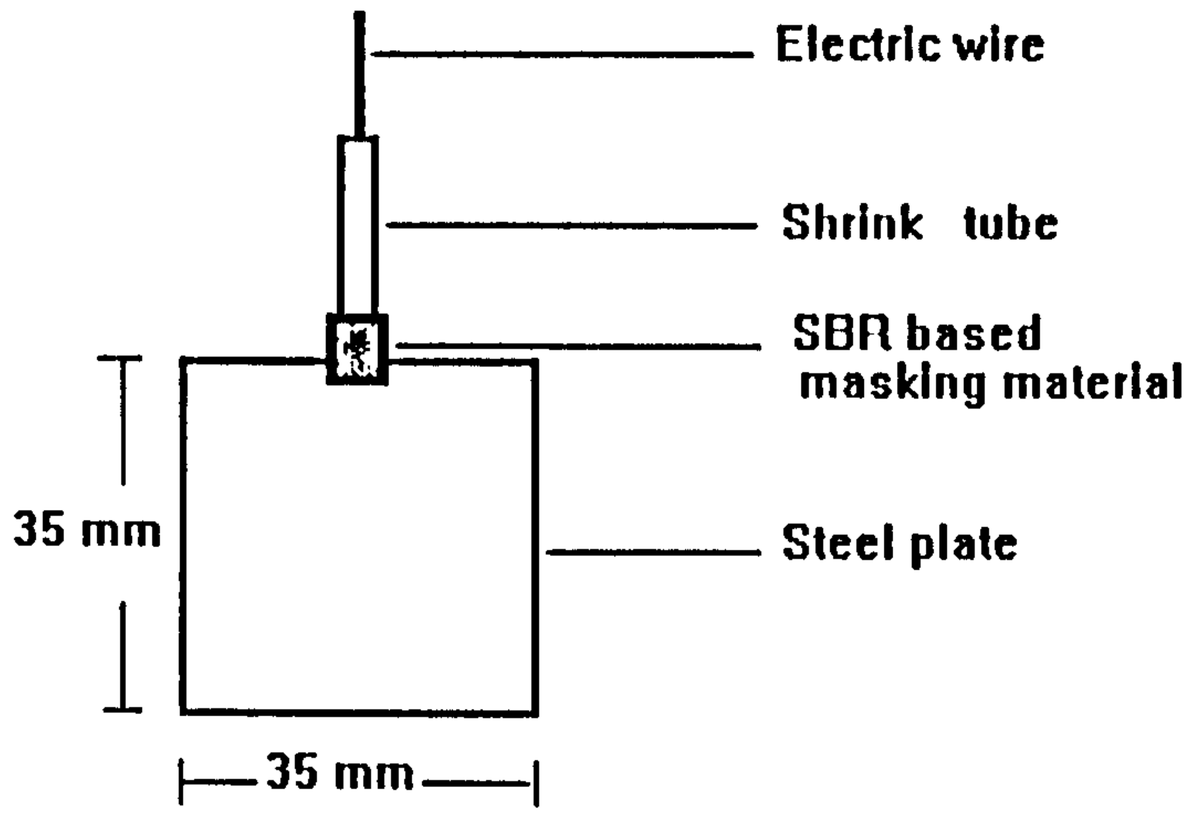

Figure 7.3 Steel cathode.

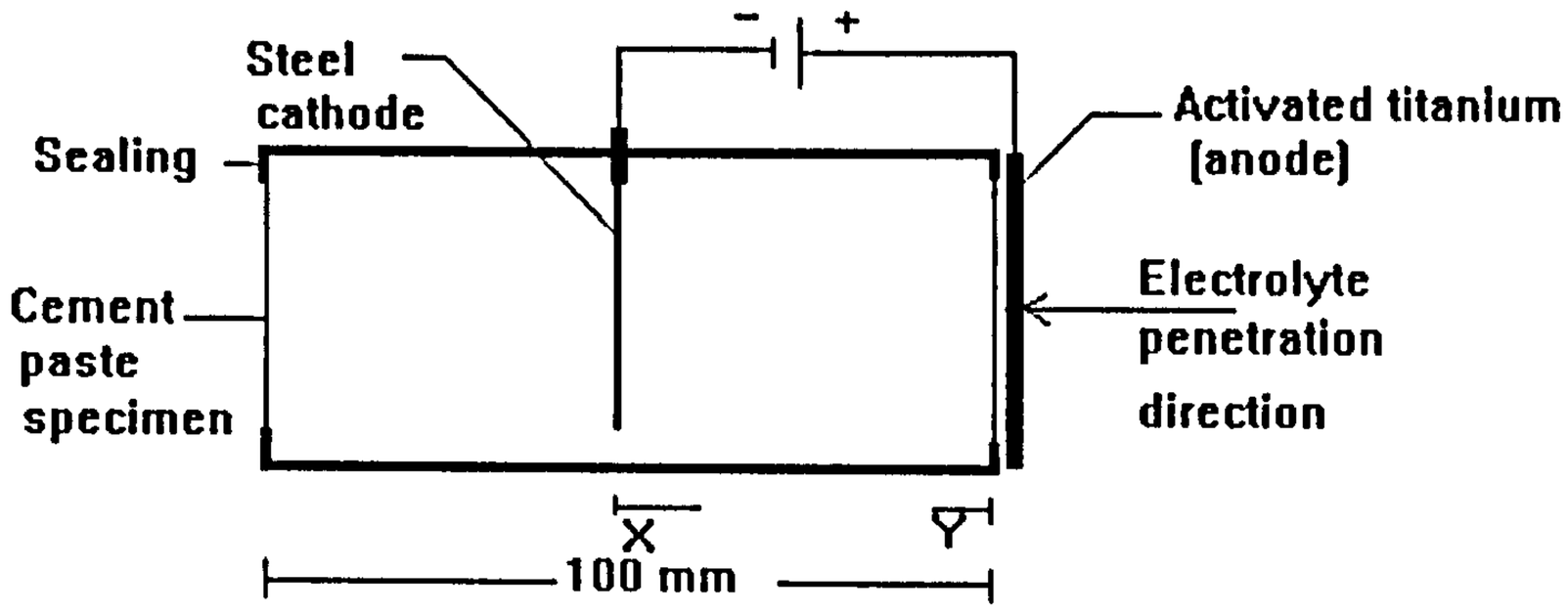

Figure 7.4 Electro-chemical realkalisation experimental arrangement for OPC paste.

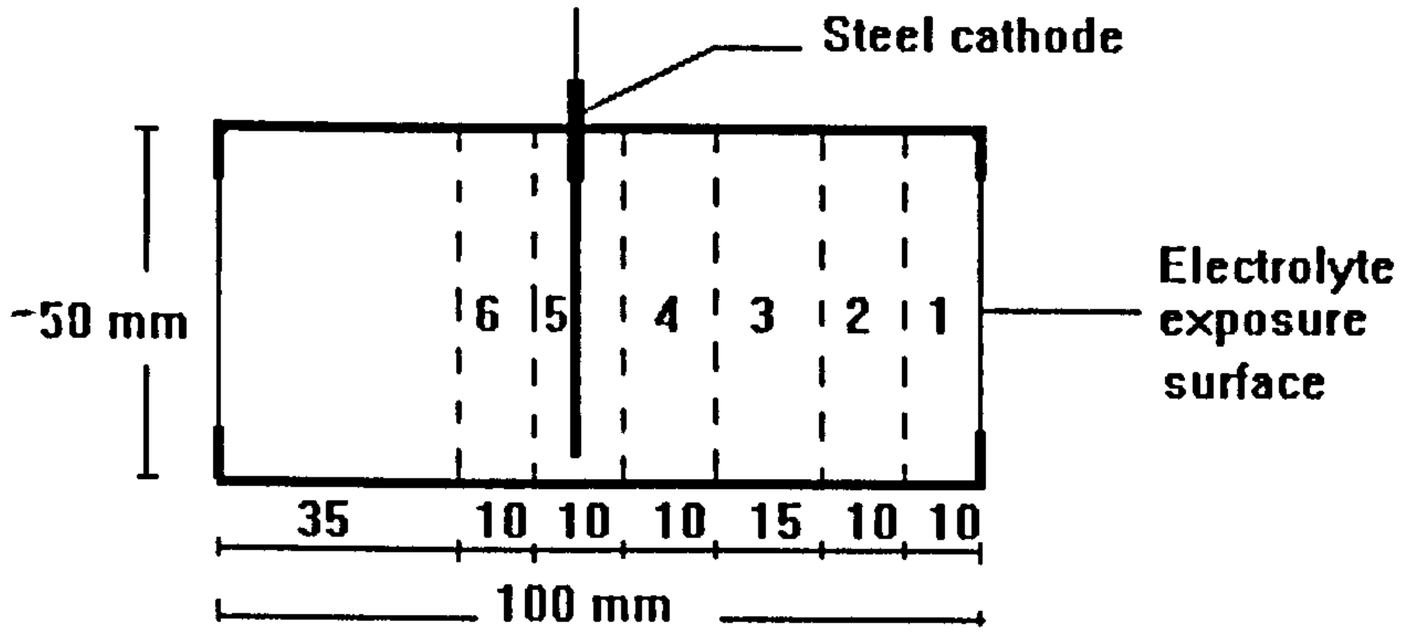

Figure 7.5 Cutting up arrangement.

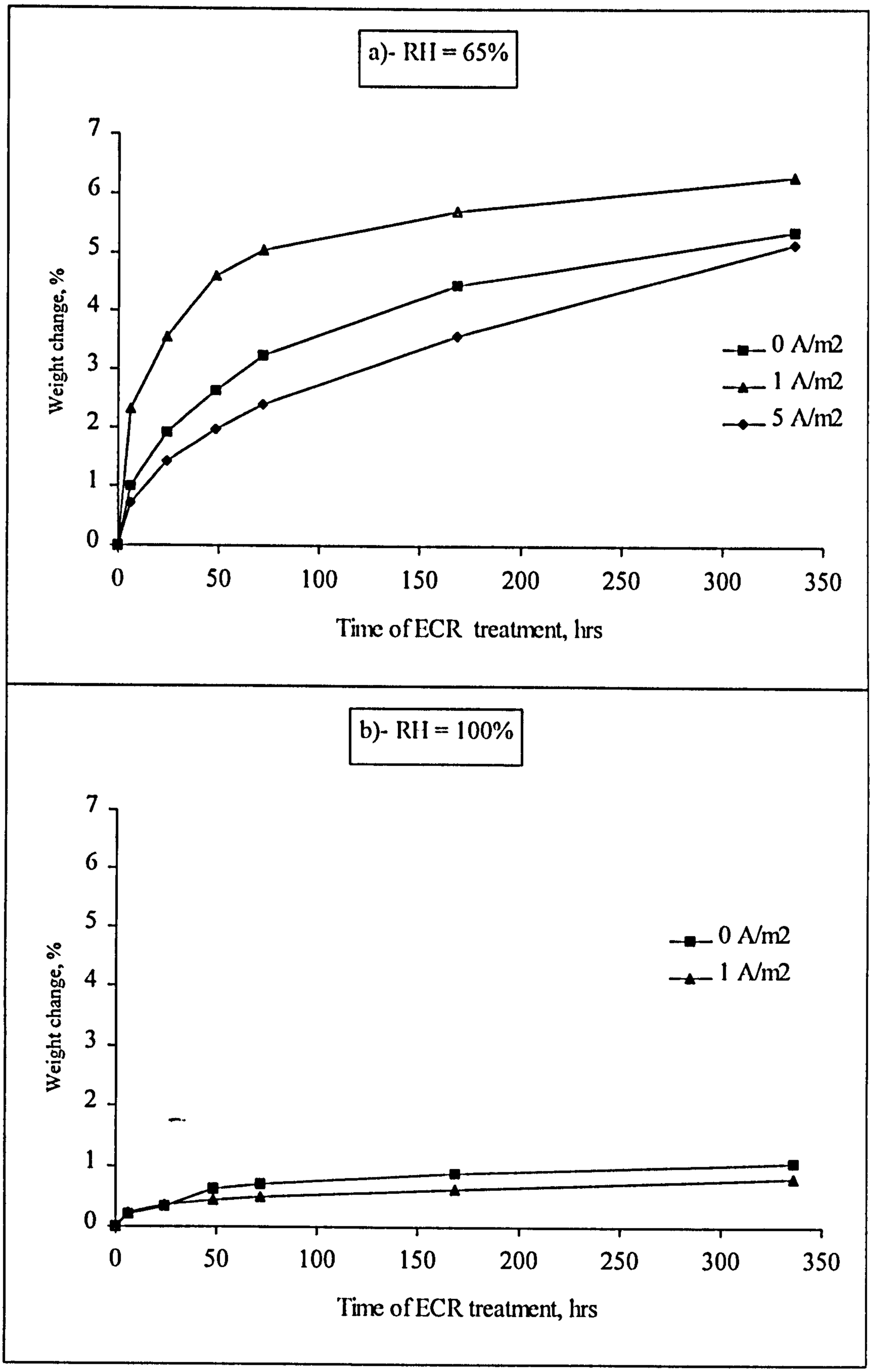

Figure 7.6 Effect of current density on the weight change of OPC specimens pre-conditioned at a) 65% and b) 100% RH environment prior to ECR treatment.

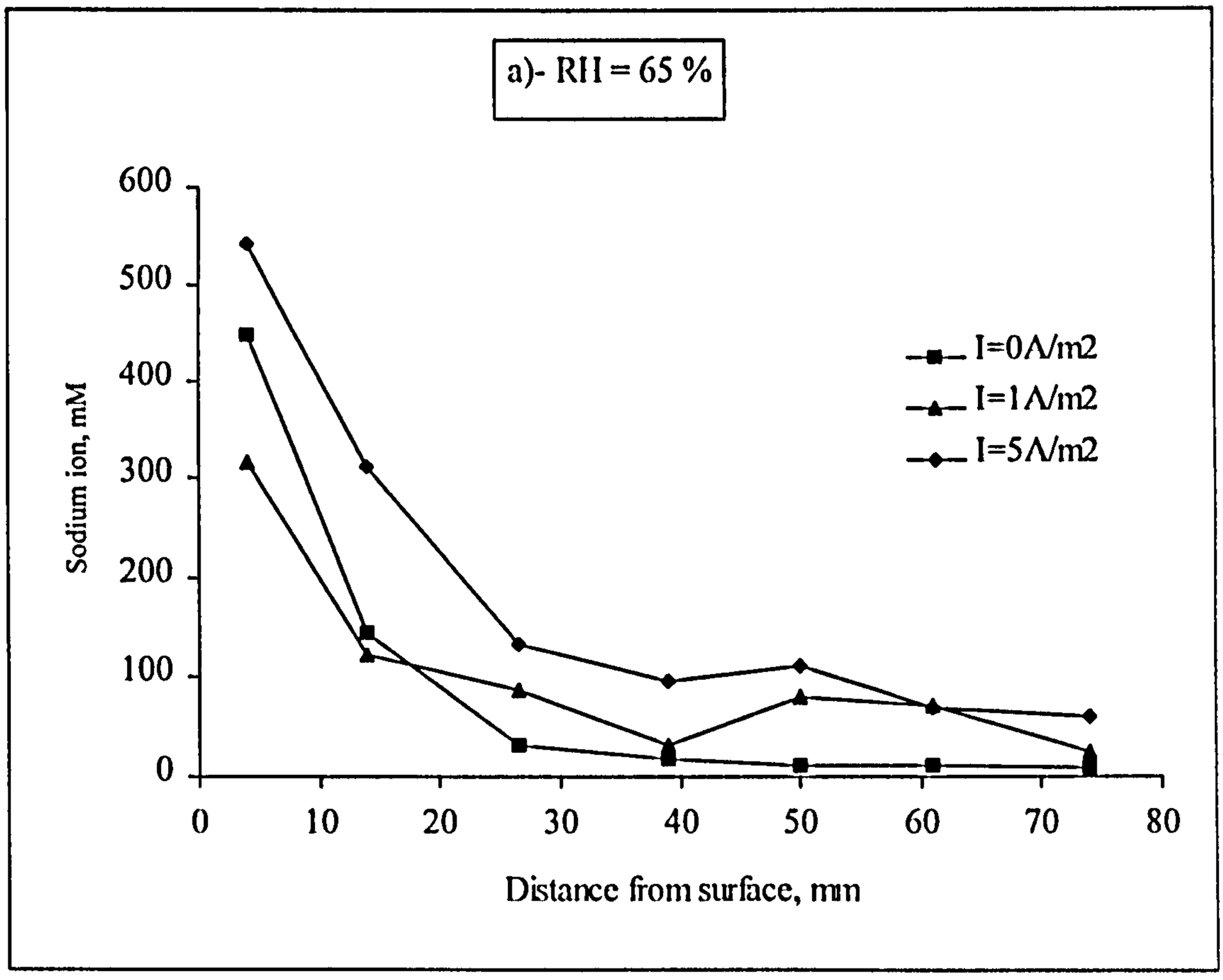

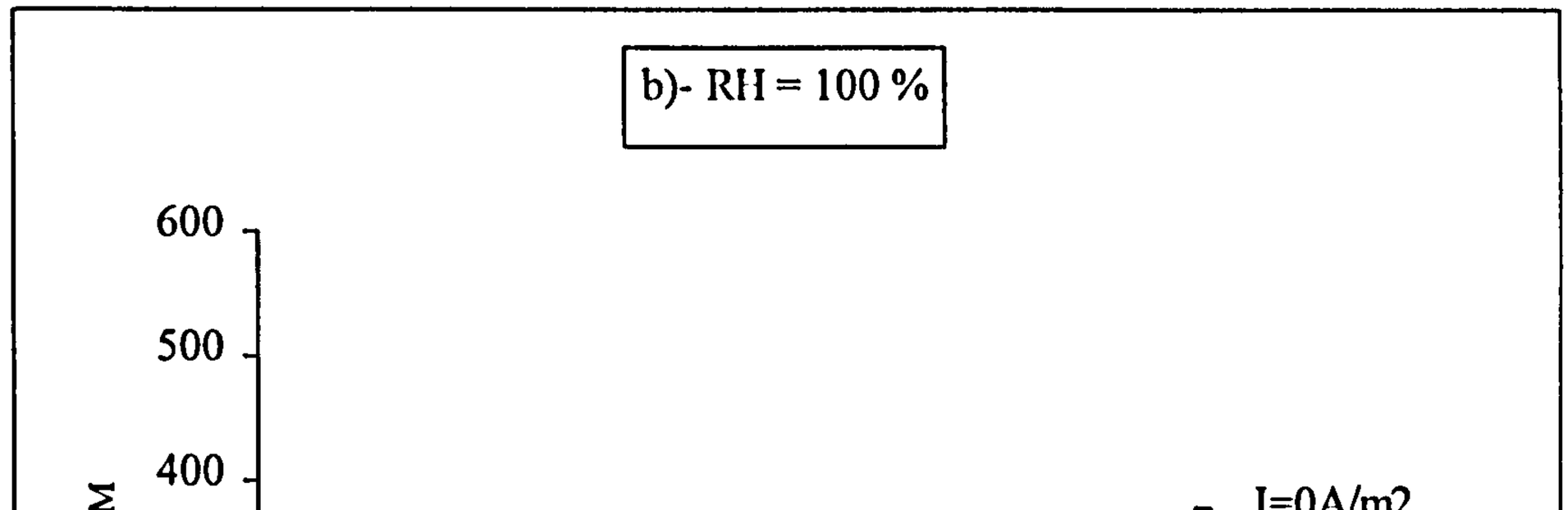

Figure 7.7 Effect of current density on sodium ion concentration profile of OPC specimens pre-conditioned at a) 65% and b) 100% RH environment prior to ECR treatment, T = 14 days.

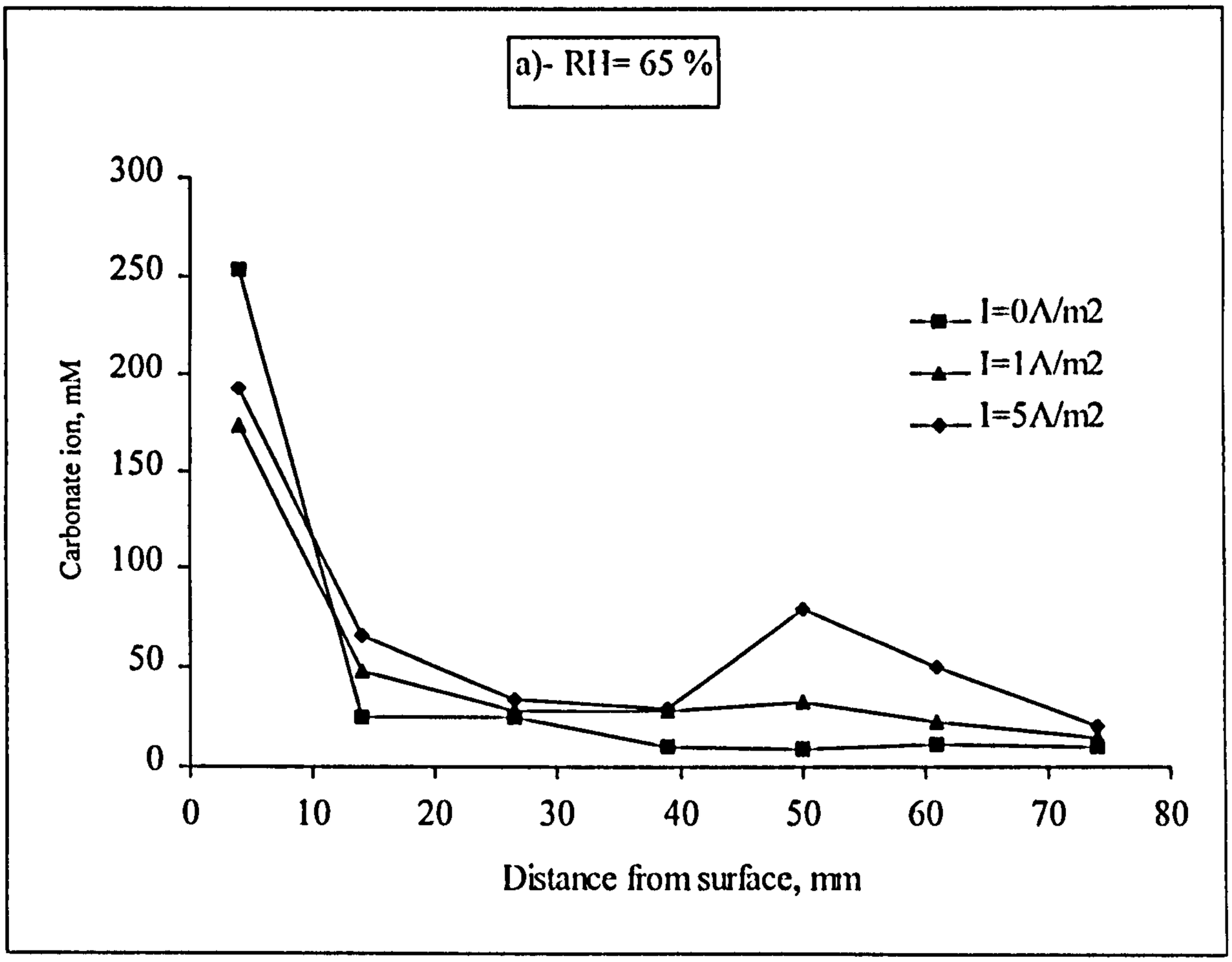

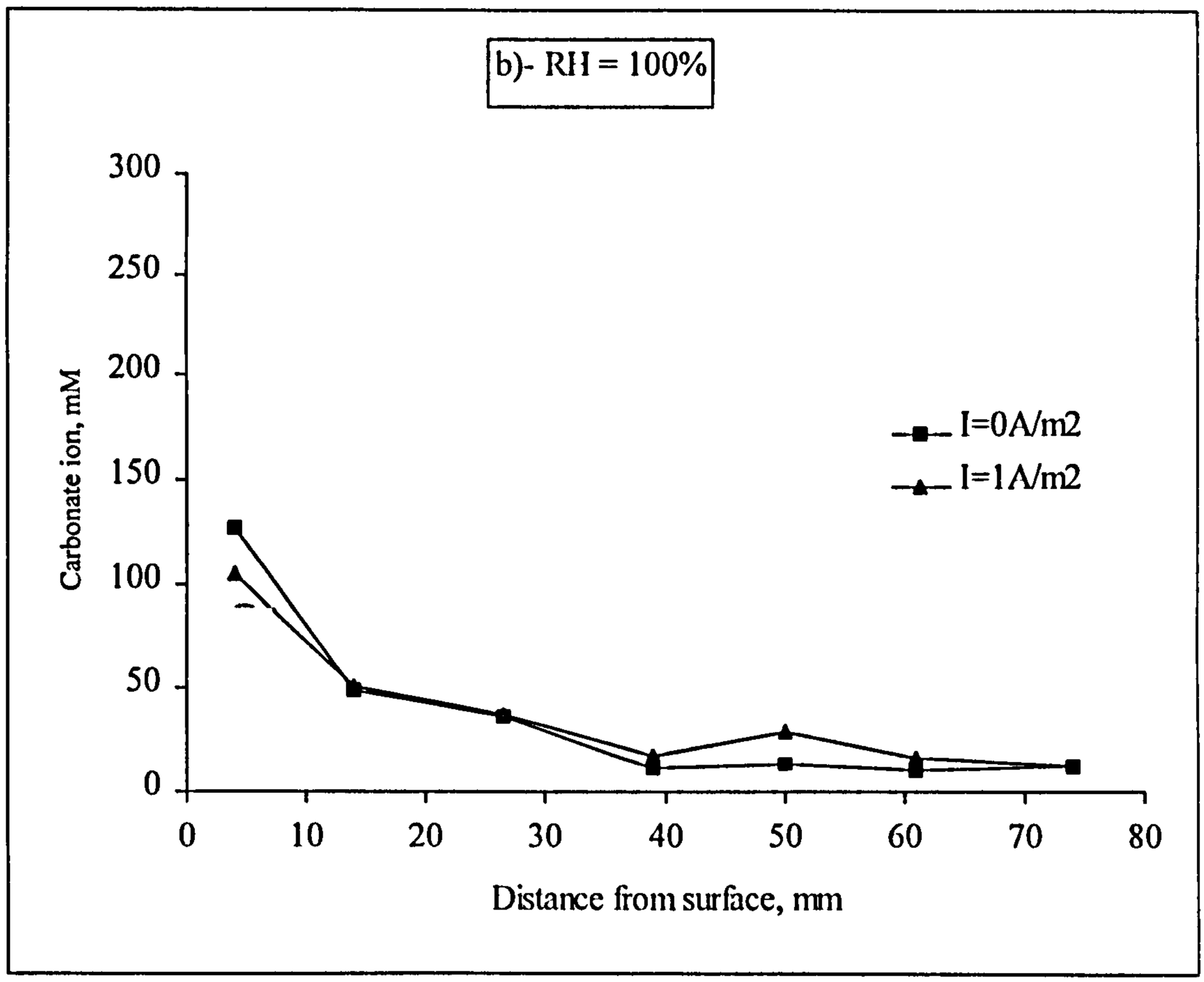

Figure 7.8 Effect of current density on carbonate ion concentration profile of OPC specimens pre-conditioned at a) 65% and b) 100% RH environment prior to ECR treatment, T = 14 days .

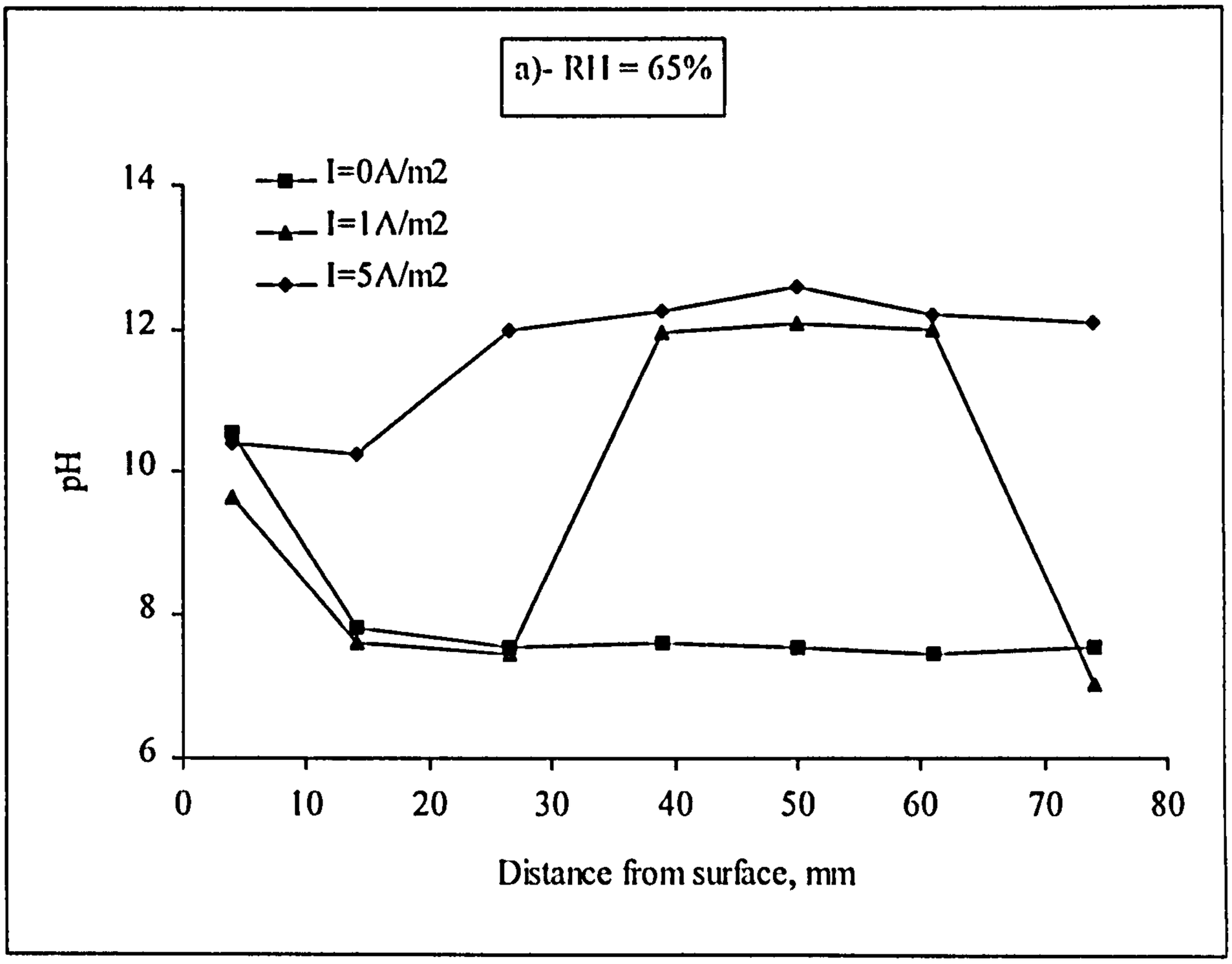

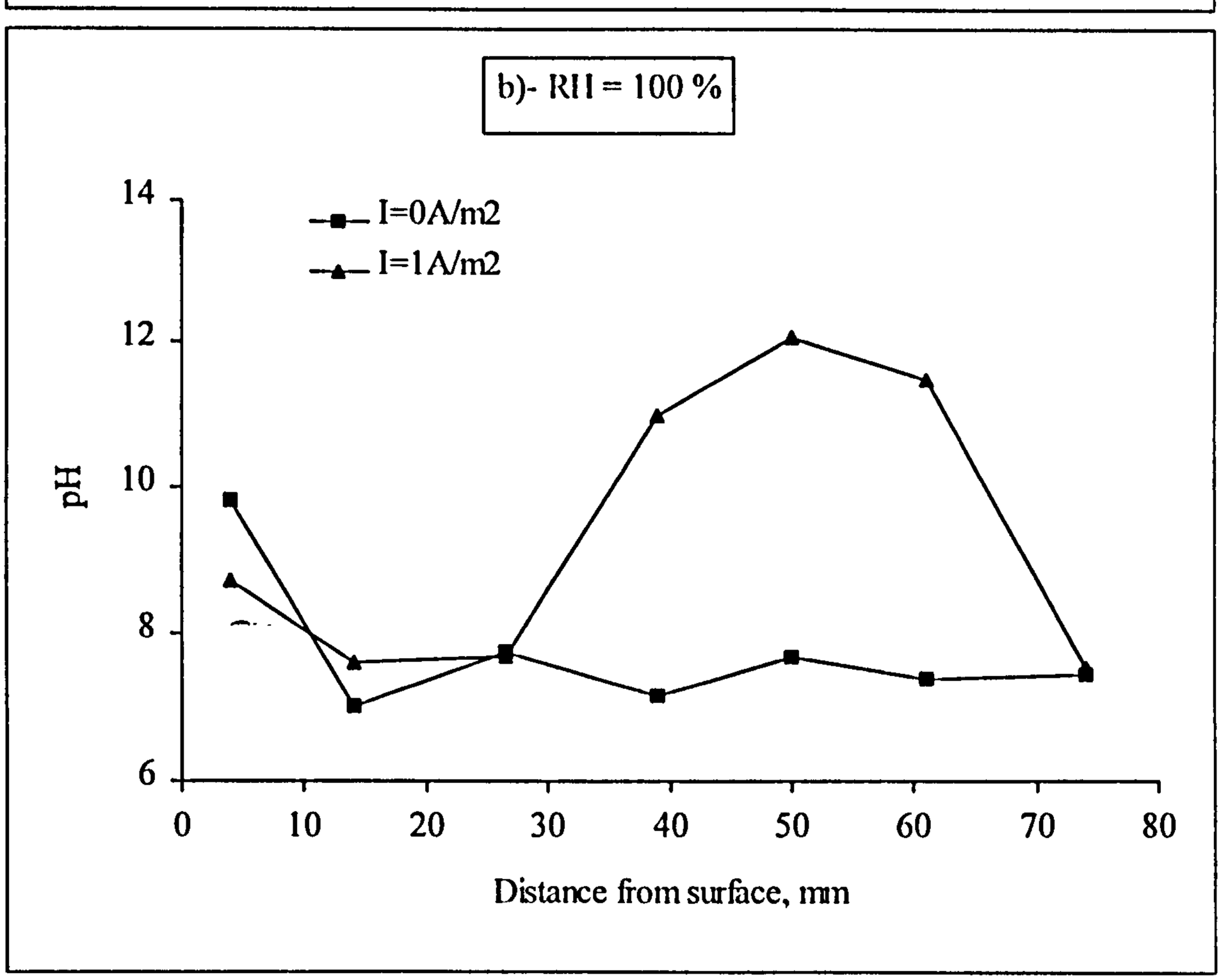

Figure 7.9 Effect of current density on pH profile of OPC specimens pre-conditioned at a) 65% and b) 100% RH environment prior to ECR treatment, T = 14 days.

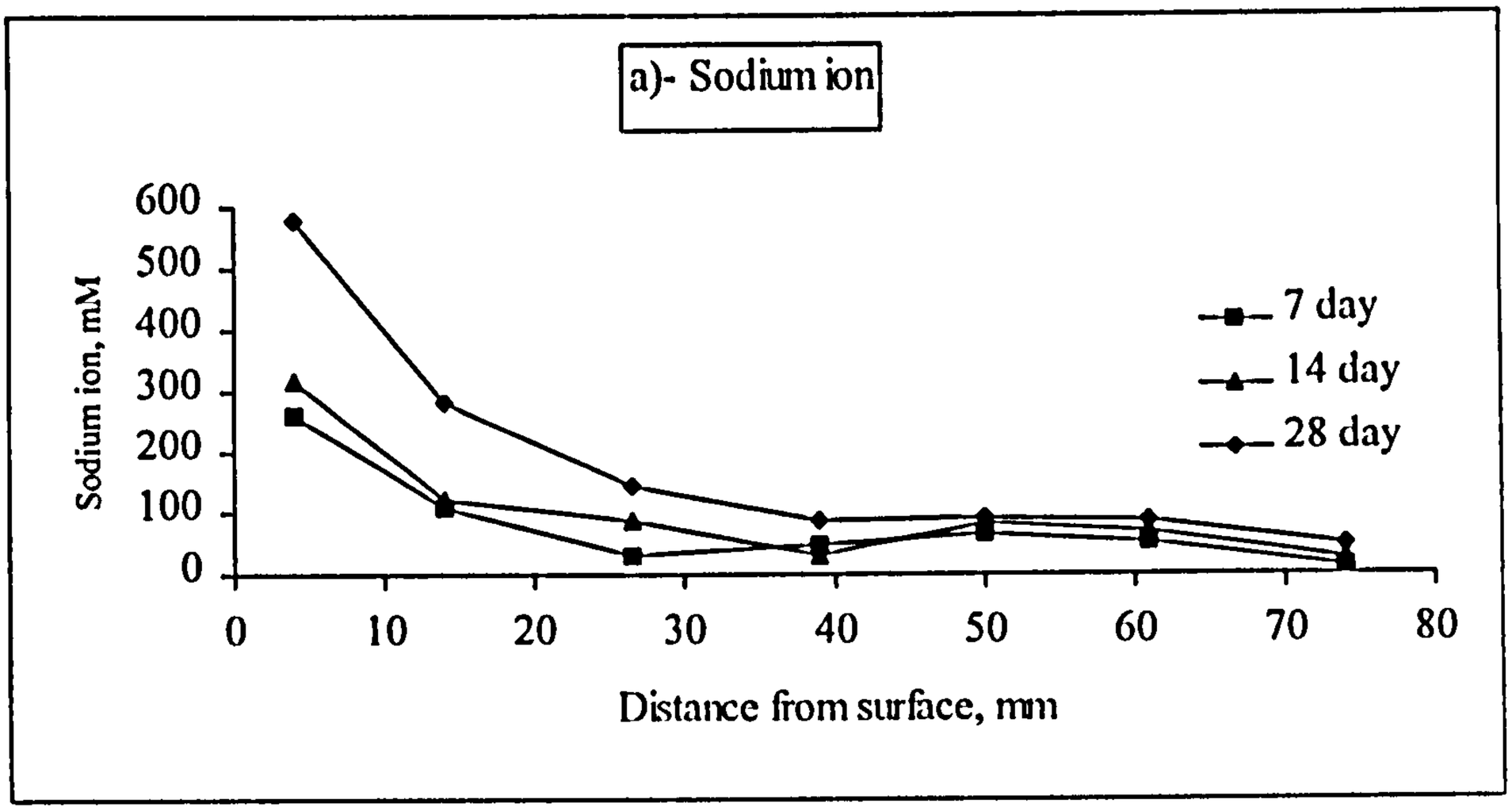

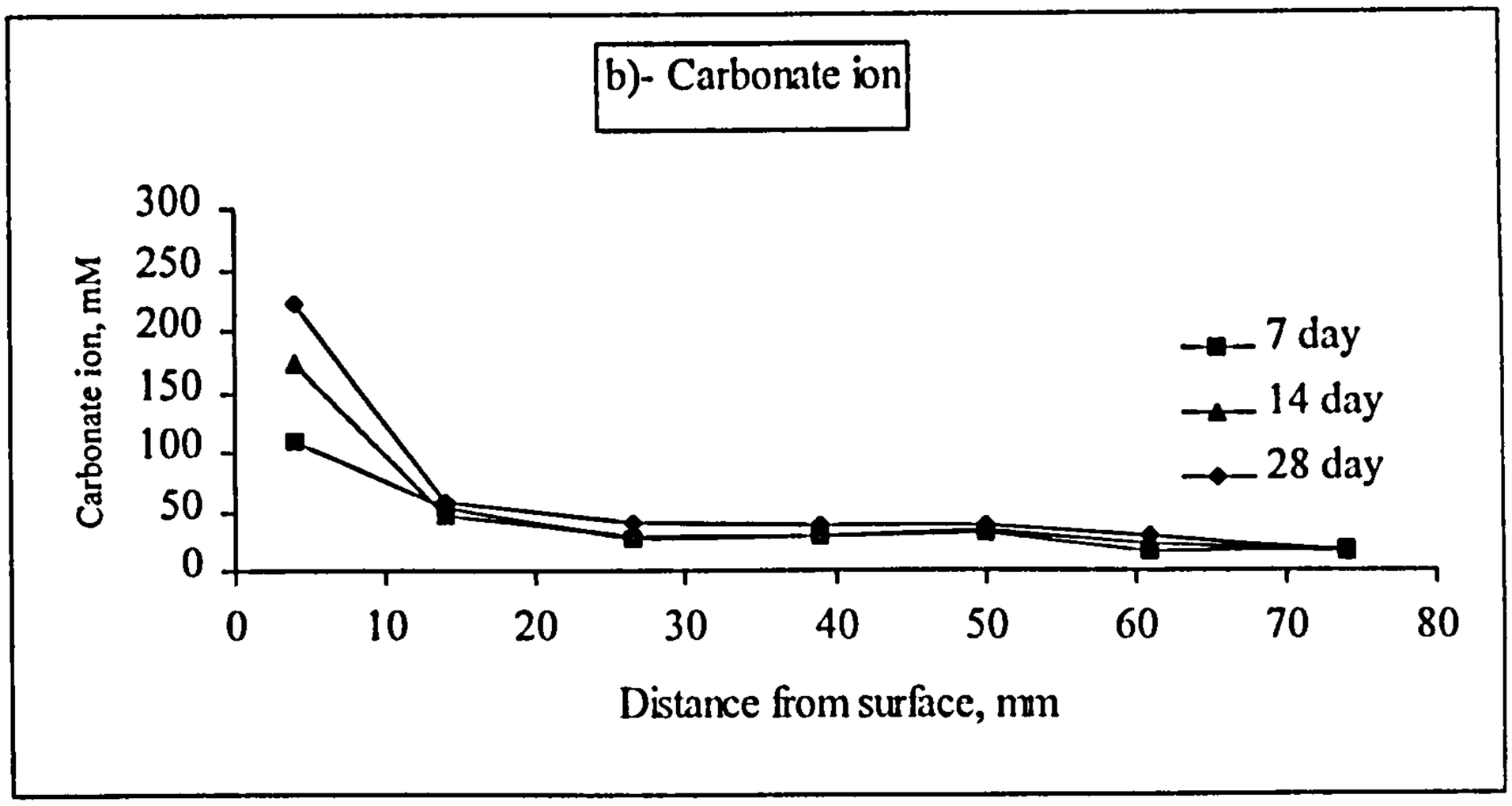

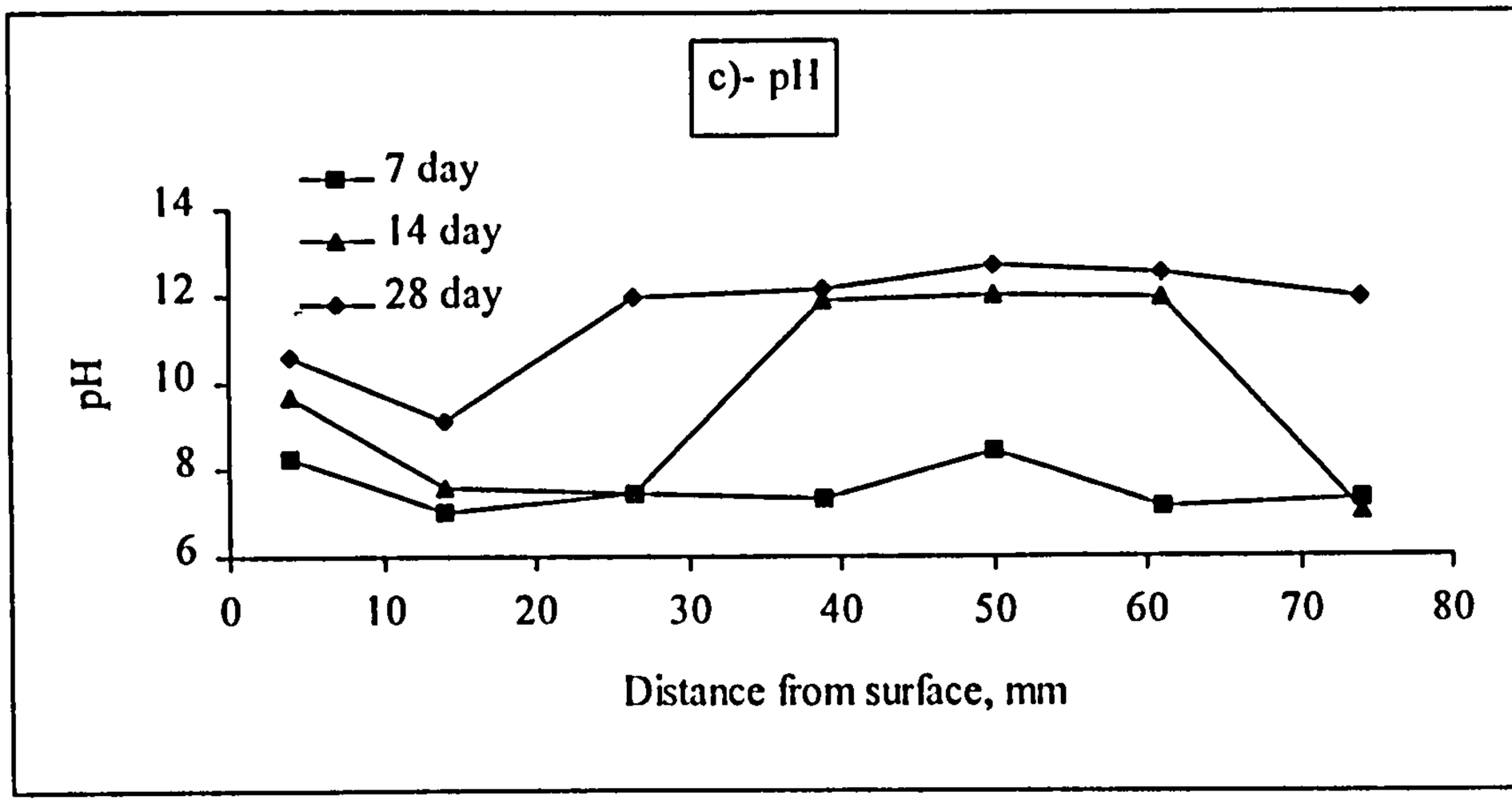

Figure 7.10 Effect of ECR treatment period on a) sodium ion concentration, b) carbonate ion concentration and c) pH profiles of OPC specimens pre-conditioned at 65% RH and treated with 1A/m^2.

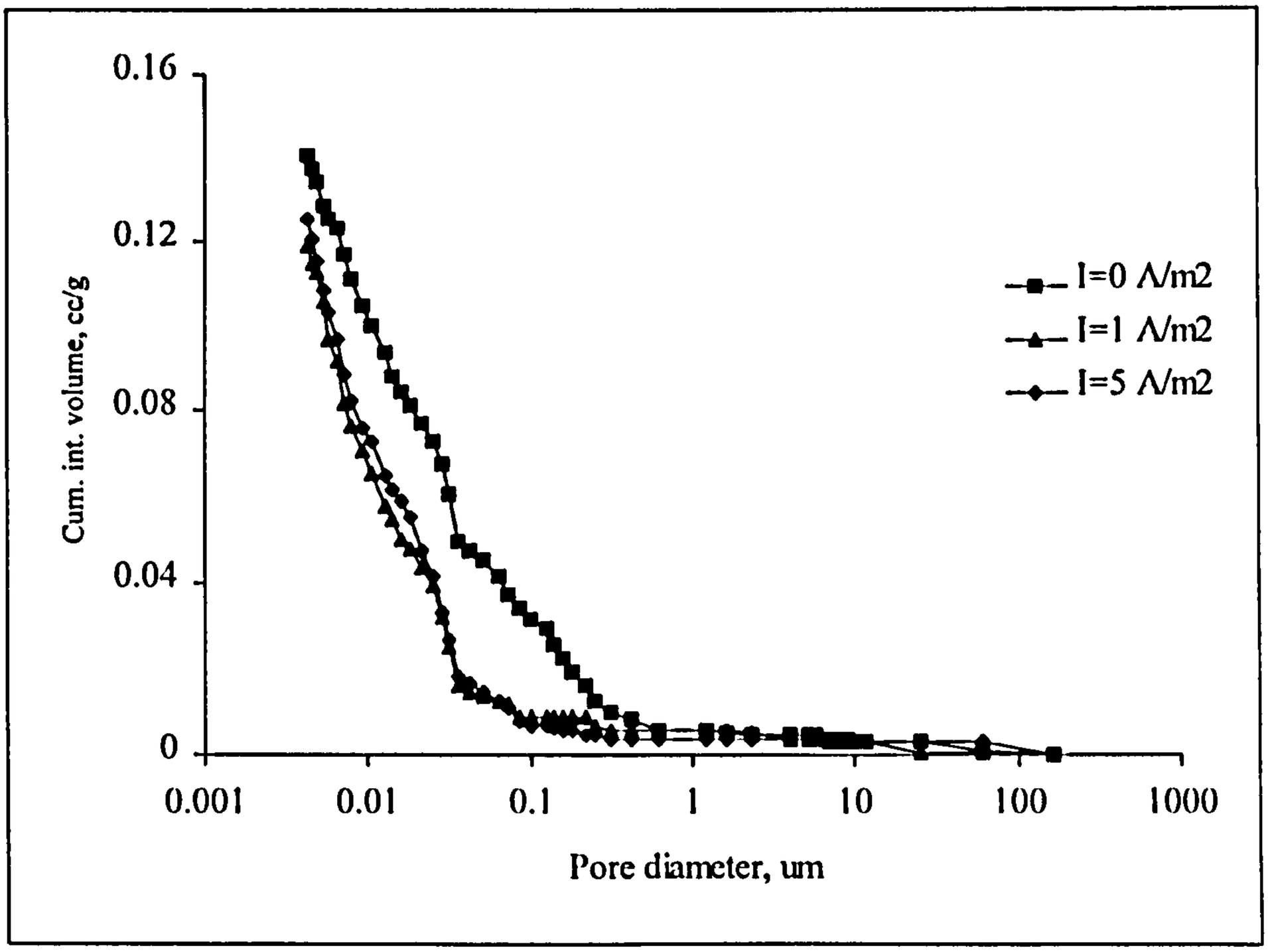

Figure 7.11 Effect of current density on the PSD of cement paste matrix (around cathode) treated for 14 days.

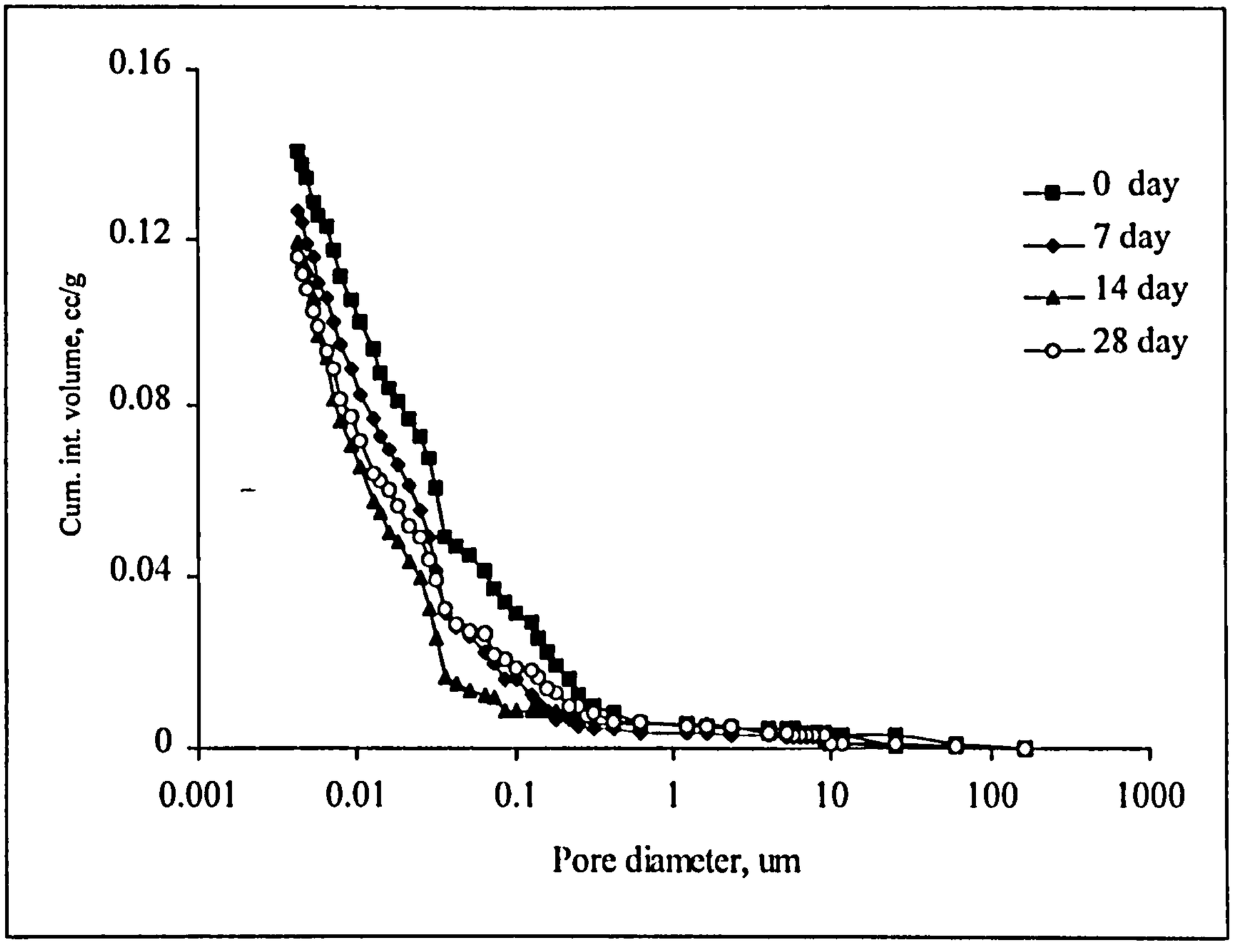

Figure 7.12 Effect of ECR treatment period on the PSD of cement paste matrix (around cathode), using 1 A/m^2.

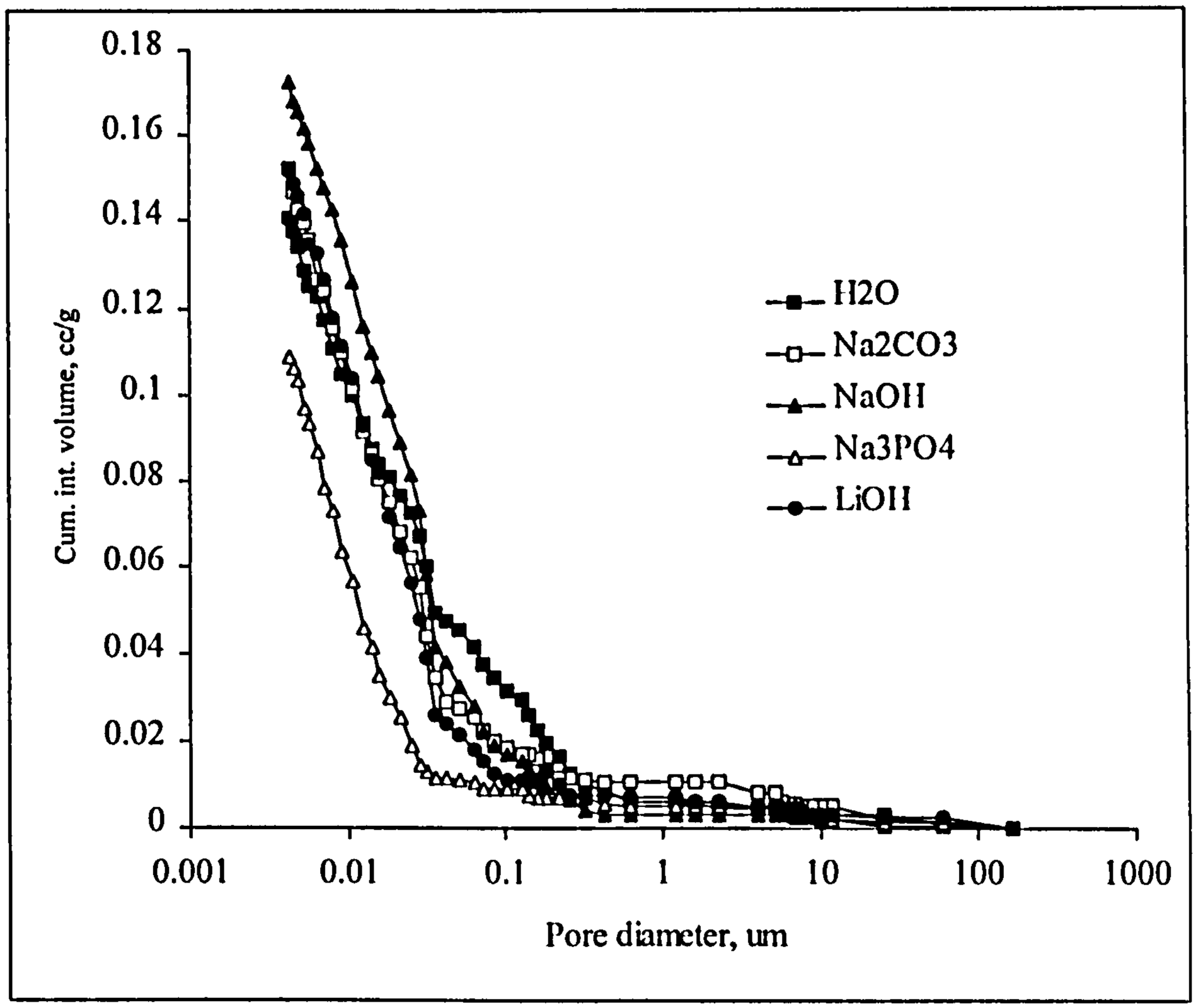

Figure 7.13 PSD of OPC paste (near surface) treated with different electrolytes for 14 days, I = 0 A/m^2.

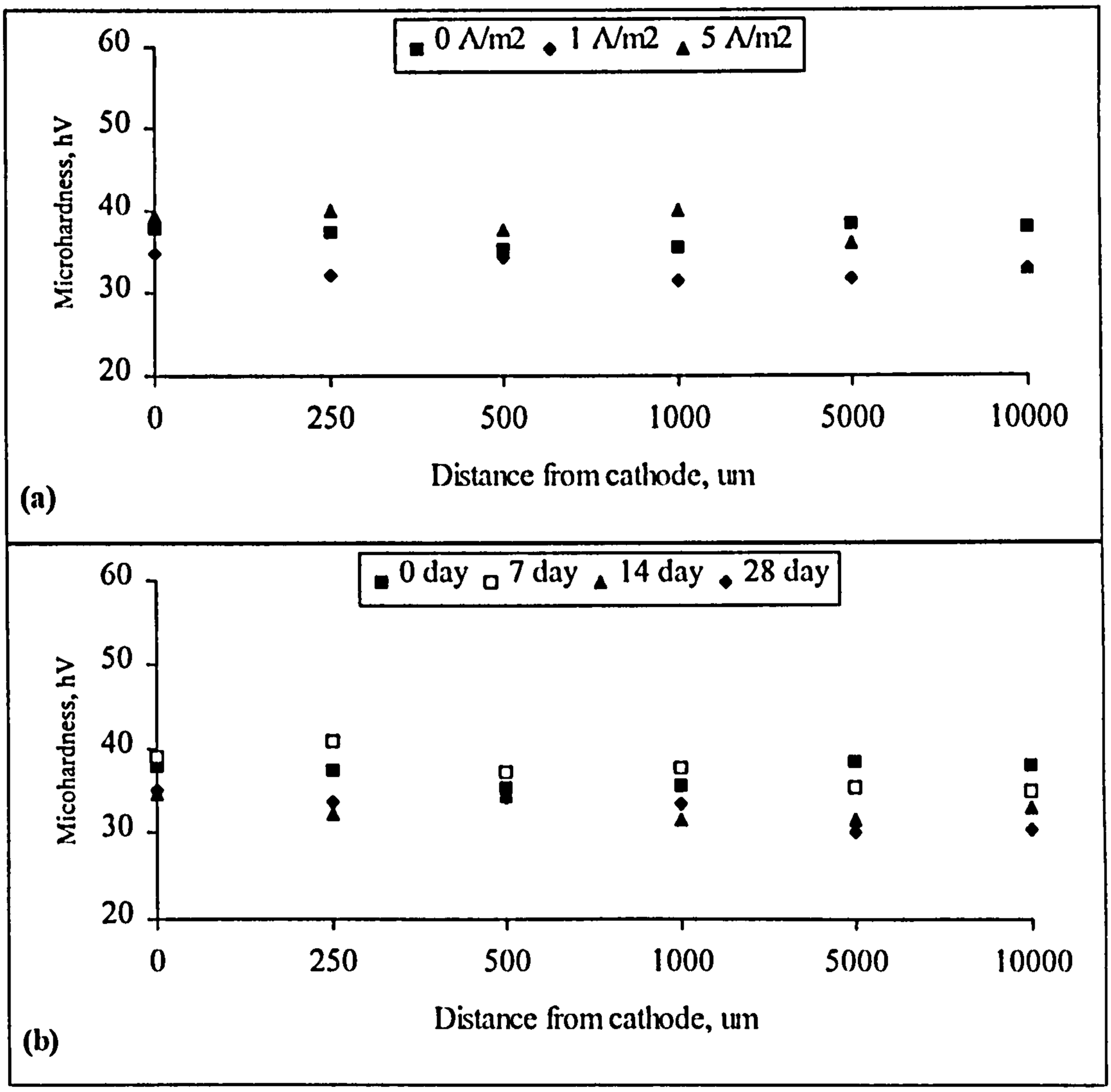

Figure 7.14 Microhardness profiles of OPC paste specimen around cathodic treated with ECR using a) different current densities and for b) different period of treatment.

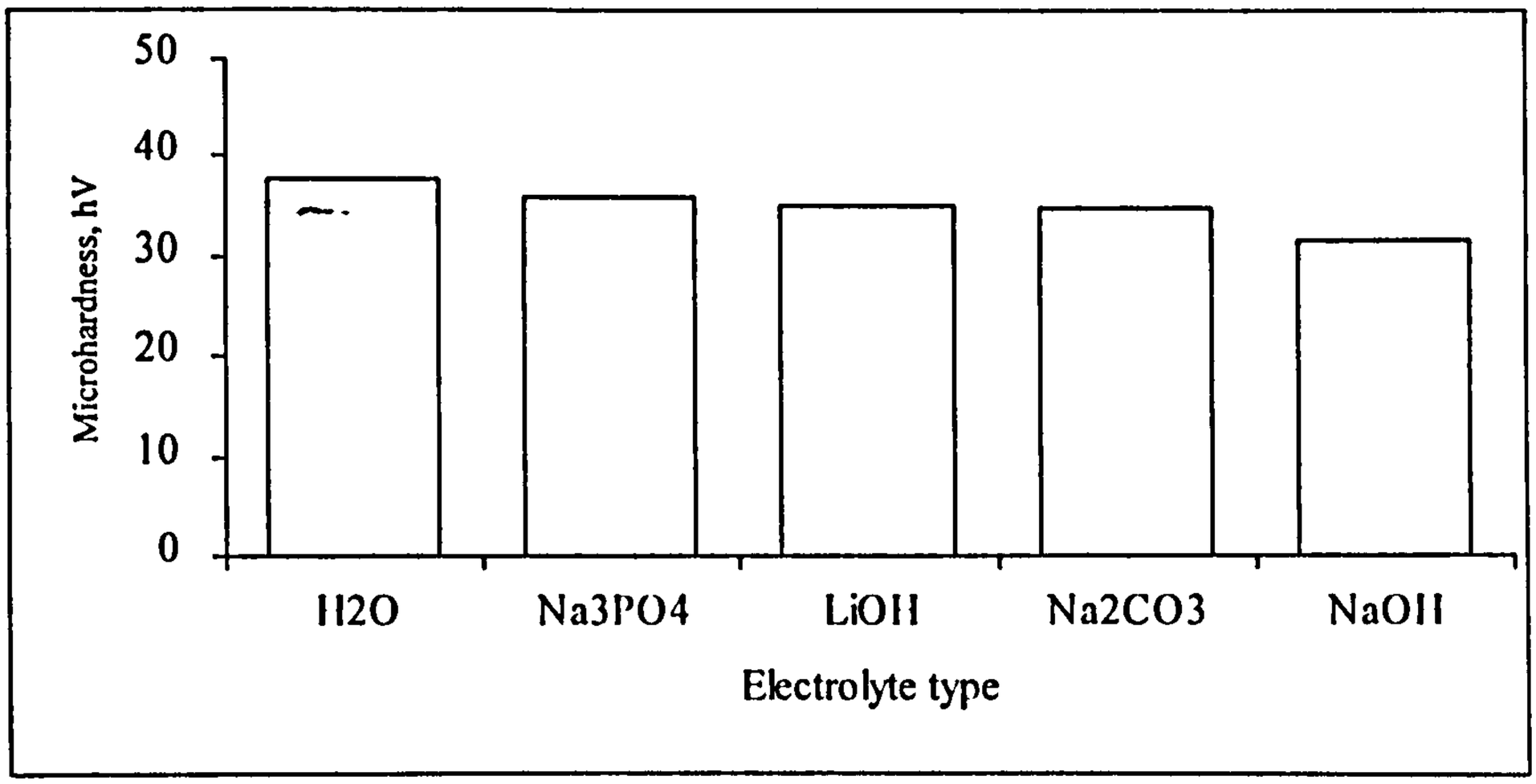

Figure 7.15 Microhardness of OPC cement paste (near surface) treated with different electrolytes, I = 0 A/m^2.

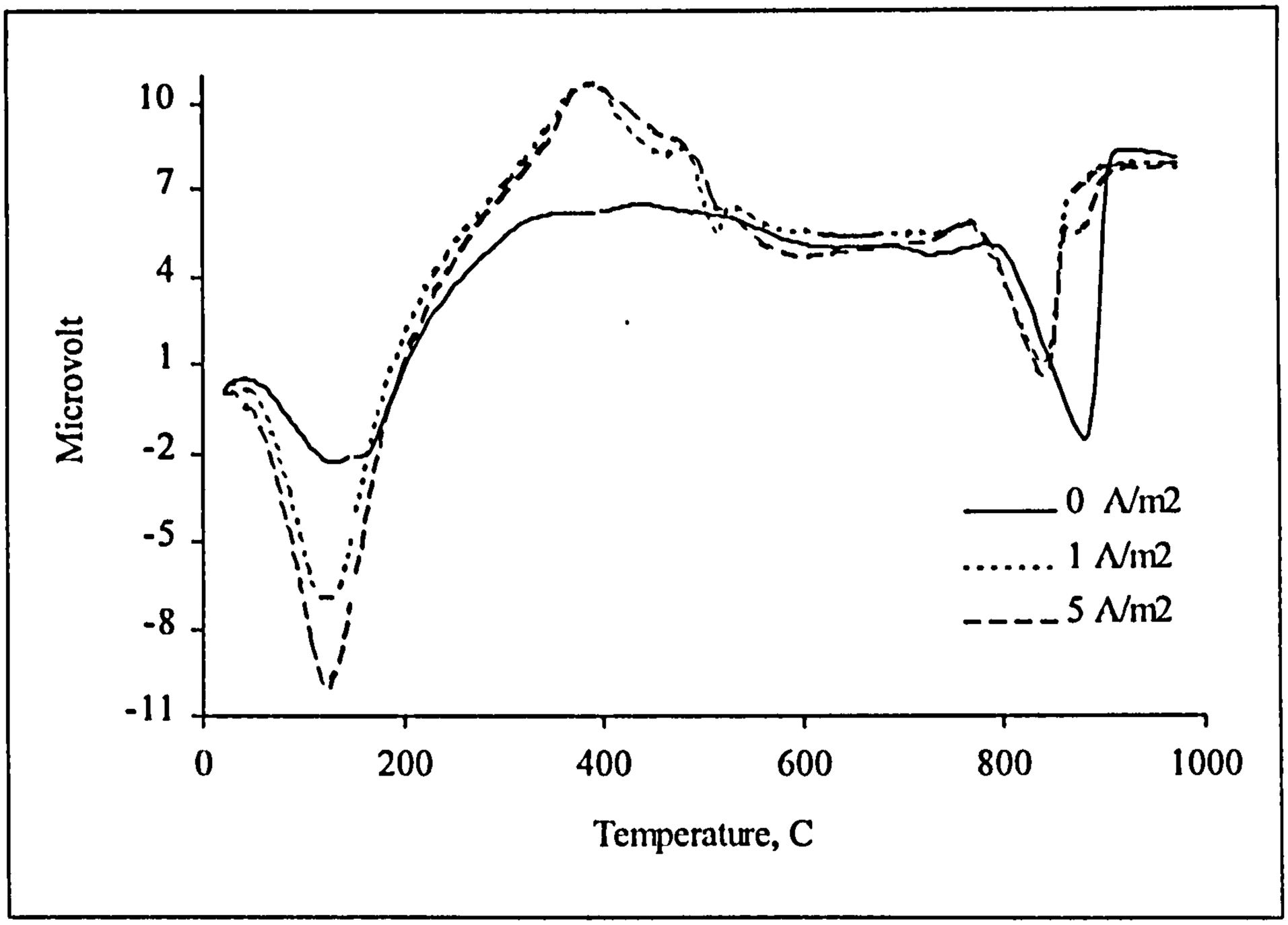

Figure 7.16 DTA thermo-graphs of OPC paste specimen (around cathode) treated with ECR with different current densities for 14 days.

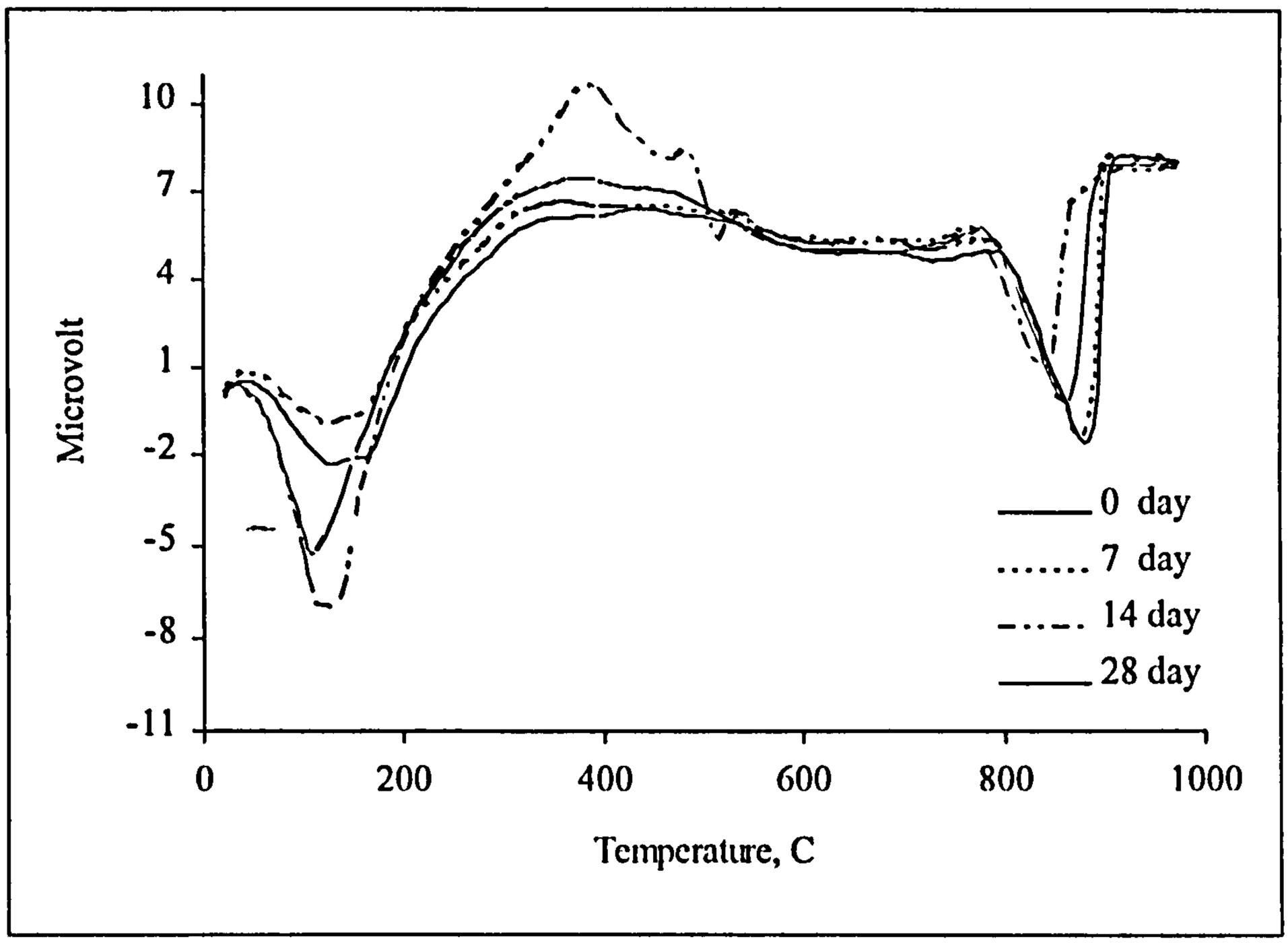

Figure 7.17 DTA thermo-graphs of OPC paste specimen (around cathode) treated with ECR for different treatment periods, I = 1 A/m^2 .

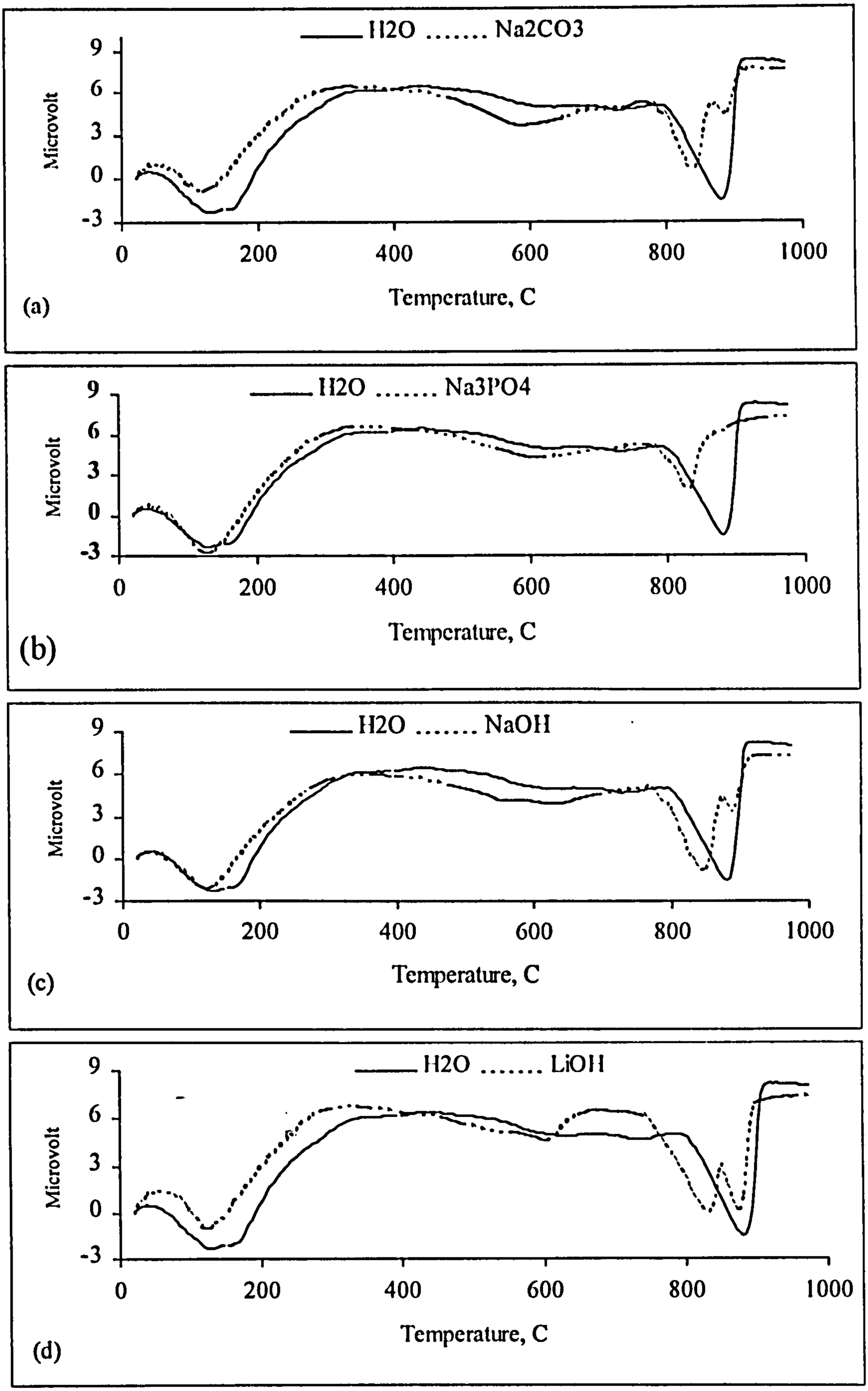

Figure 7.18 DTA thermo-graphs of OPC specimen (near surface) treated with different electrolytes, a) sodium carbonate, b) sodium phosphate, c) sodium hydroxide and d) lithium hydroxide, for 14 days, I = 0 A/m^2 .

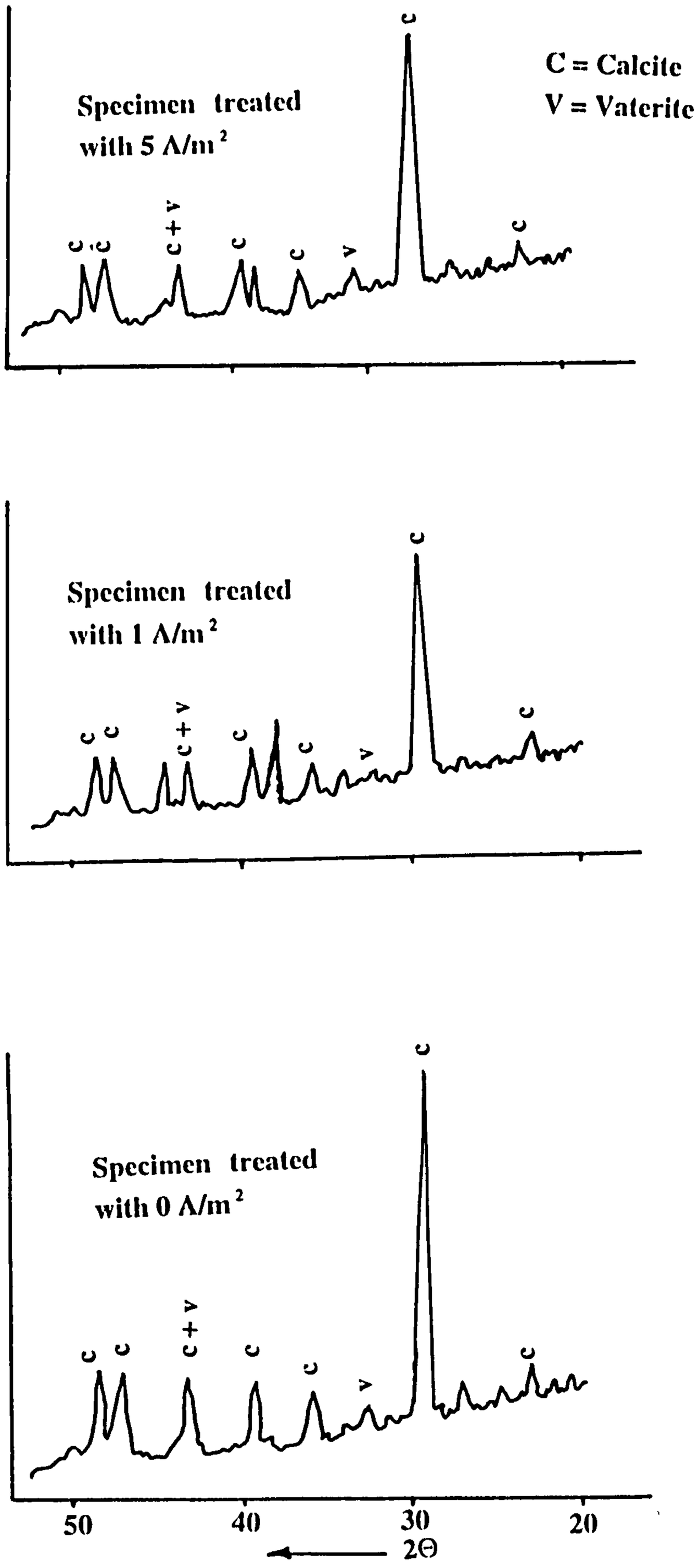

Figure 7.19 XRD traces of OPC paste specimen (around cathode) treated with ECR with different current densities for 14 days.

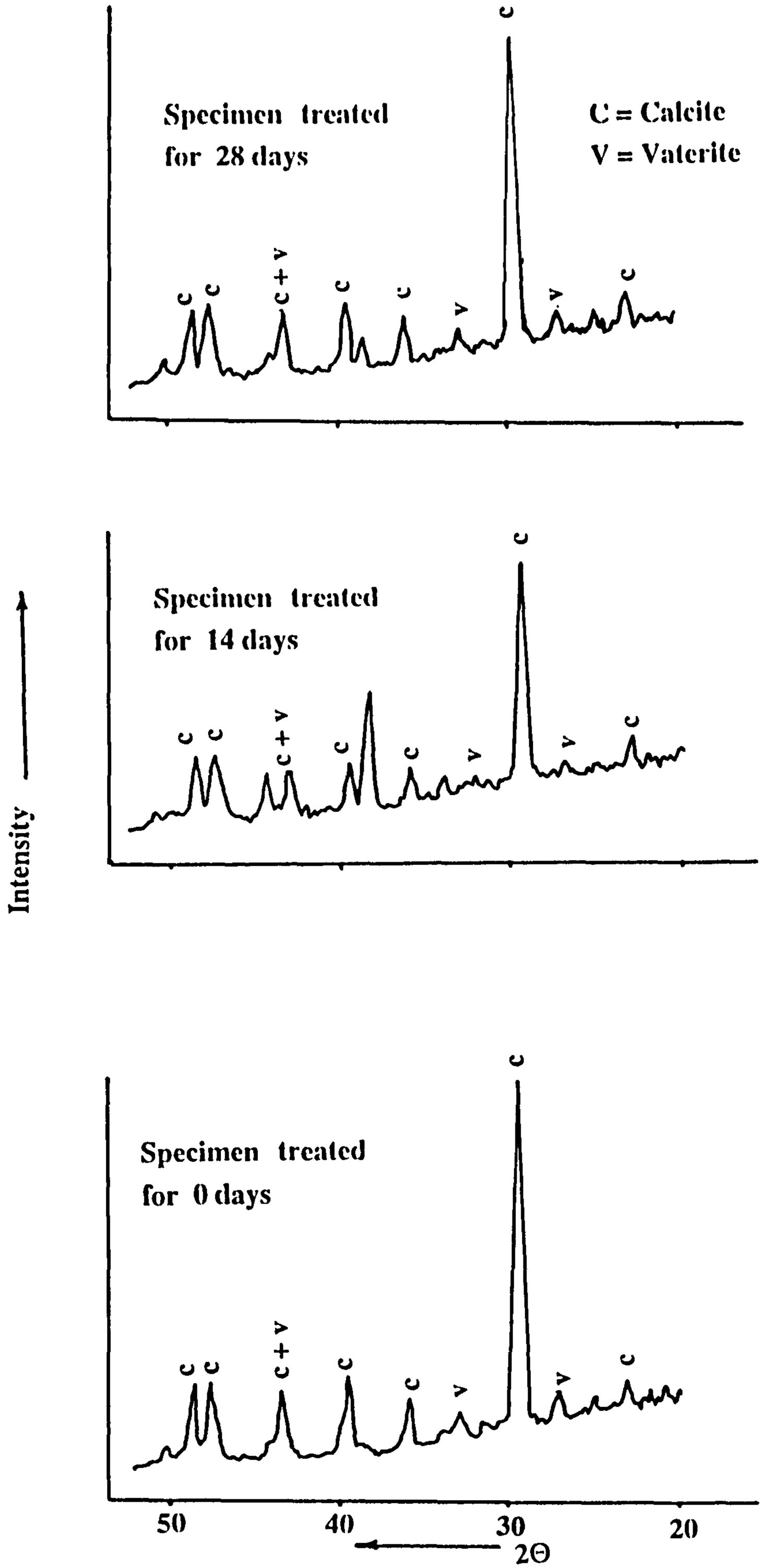

Figure 7.20 XRD traces of OPC paste specimen (around cathode) treated with ECR for different treatment periods, I = 1 A/m ^{2} .

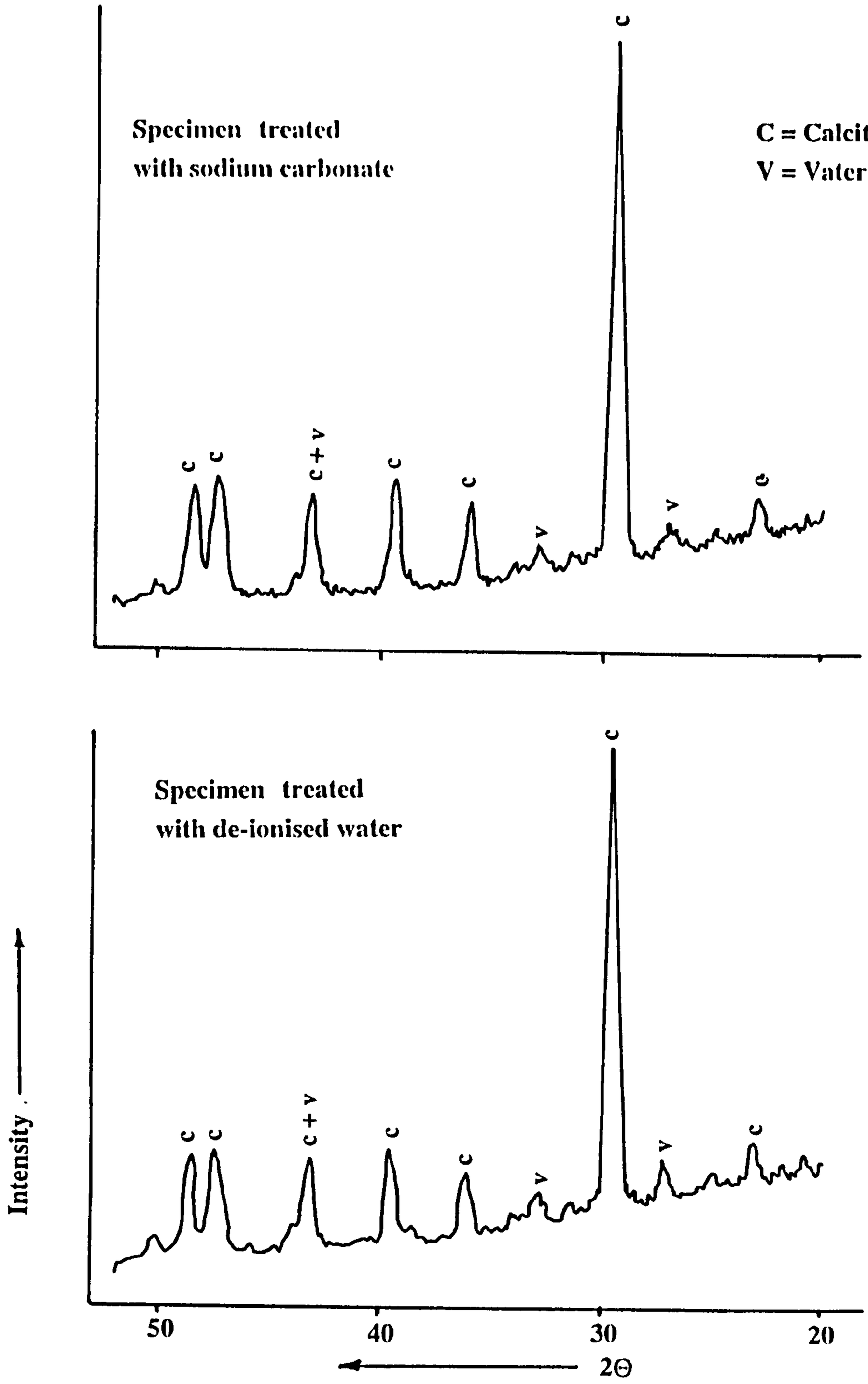

Figure 7.21a XRD trace of OPC specimen (near surface) treated with 1M sodium carbonate solution for 14 days, I = 0 A/m^2 .

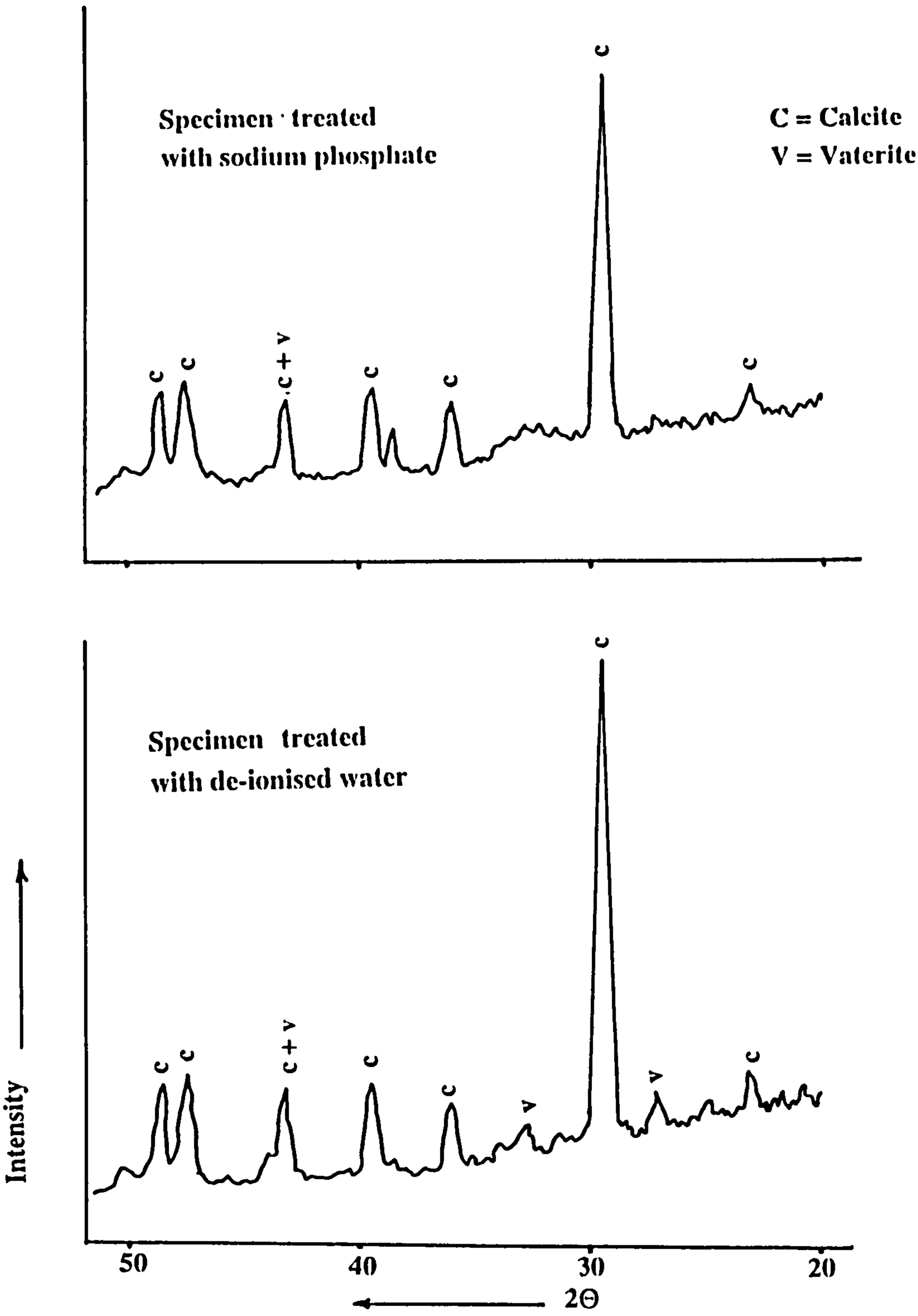

Figure 7.21b XRD trace of OPC specimen (near surface) treated with 0.5 M sodium phosphate solution for 14 days, I = 0 A/m^2 .

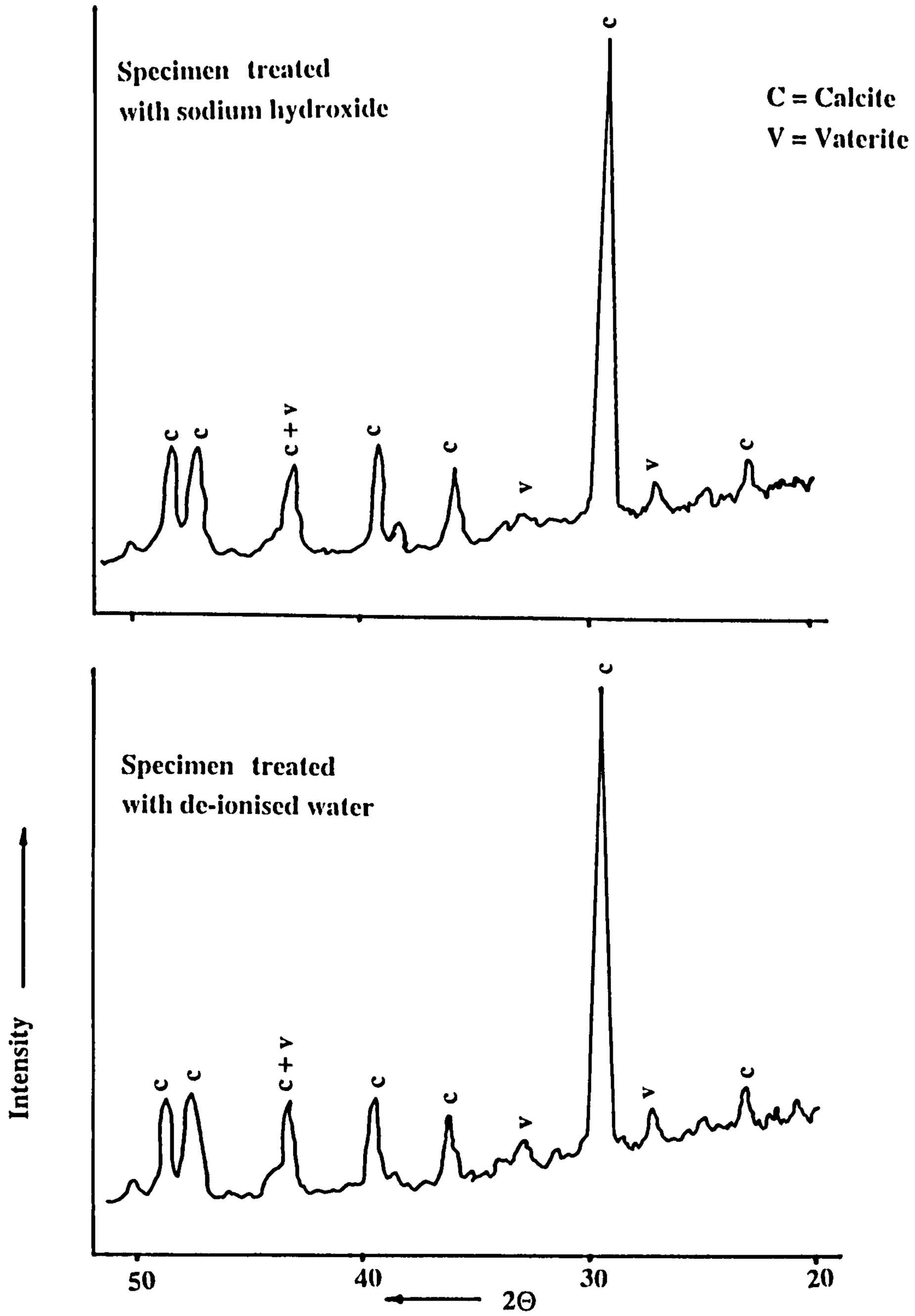

Figure 7.21c XRD trace of OPC specimen (near surface) treated with 1M sodium hydroxide solution for 14 days, I = 0 A/m^2 .

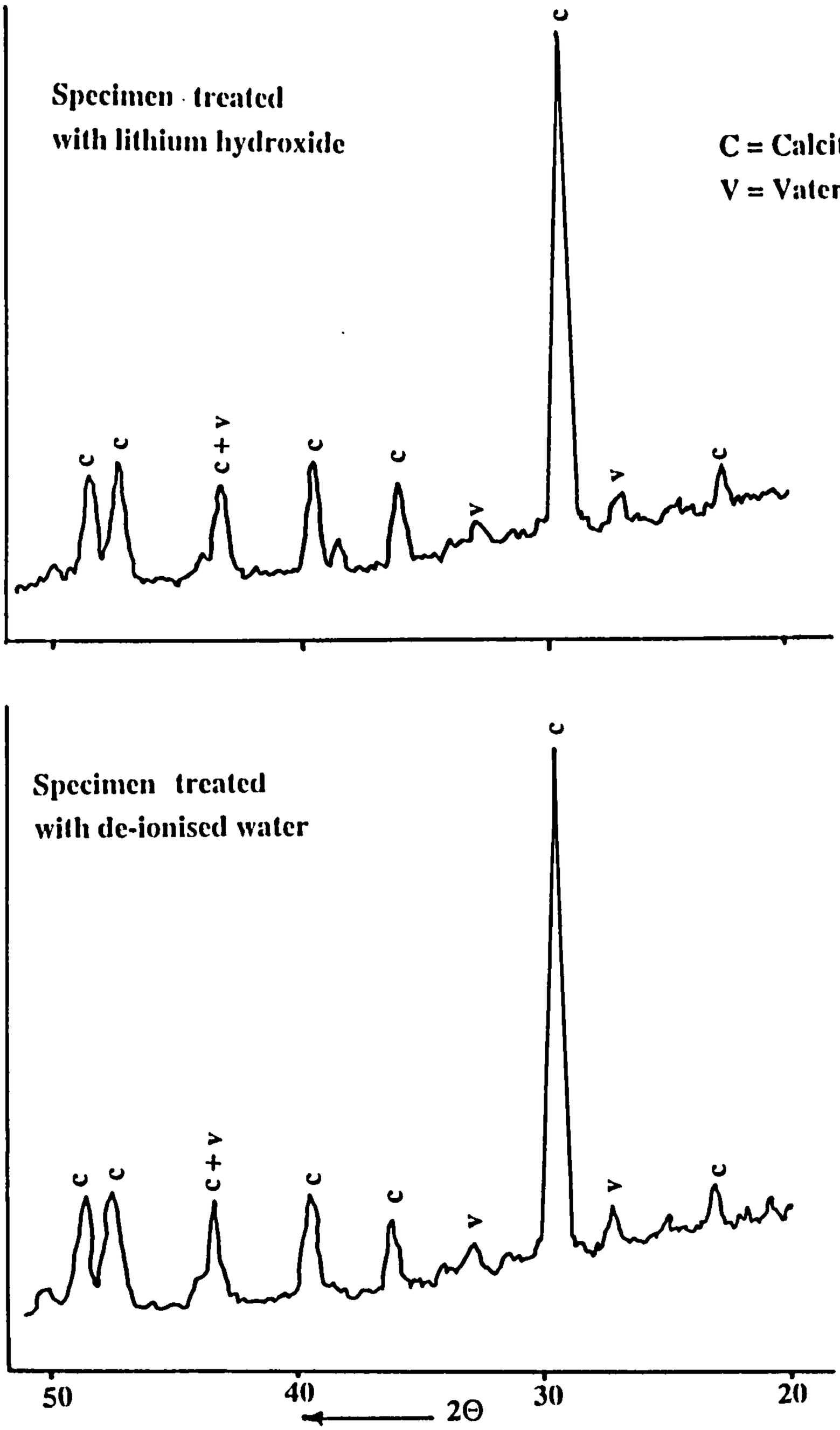

Figure 7.21d XRD trace of OPC specimen (near surface) treated with 1M lithium hydroxide solution for 14 days, I = 0 A/m^2 .

CHAPTER 8

GENERAL CONCLUSIONS AND RECOMMENDATIONS FOR FURTHER WORK

Detailed conclusions drawn from the results of the different experiments undertaken for this investigation have been presented at the end of each chapter. However, it is appropriate at this stage to summarise the major findings in relation to the original aims of the investigation and moreover to identify the areas where further studies are needed.

8.1 GENERAL CONCLUSIONS

1- The thickness of the microstructure gradient of cover concrete is significantly decreased with increasing period of water curing but is relatively unaffected by curing temperature, w/c ratio and the use of cement replacement materials.

2- Important correlations were established between the microstructure and both the mass transport properties (in terms of the effective chloride diffusion coefficient) and the microhardness of the surface zone of cover concrete. The effective chloride diffusion coefficient decreased with decreasing porosity, whilst the microhardness increased with decreasing total and capillary porosity.

3- The scratch hardness technique was developed and shown to be potentially useful for characterising the microstructure and microhardness of cement paste and concrete. It is relatively rapid and produces results compatible with those obtained from conventional techniques (such as thermo-gravimetry, water desorption and indentation microhardness) for determining the thickness of the microstructure gradient of cover concrete.

4- A relationship between the thickness of the microstructure gradient and mass transport properties of cover concrete was established . For a given water/binder ratio, as the thickness of the microstructure gradient increased, the depth of carbonation of OPC paste increased as did the depth of chloride penetration. Surface chloride concentration

was, however, decreased significantly with increasing thickness of the microstructure gradient.

5- It has been demonstrated that the use of CPF refined the PSD, reduced total and capillary porosity and enhanced the microhardness of the OPC covercrete. The use of CPF also improved the microhardness properties of the aggregate/cement paste transition zone in the near surface zone affected by the CPF.

6- The use of CPF resulted in a significant improvement in the transport properties of high w/c ratio concretes. Carbonation was reduced substantially for all types of concrete (OPC, OPC/PFA and OPC/GGBS) and chloride penetration was reduced significantly for OPC concrete.

7- This investigation has demonstrated that capillary absorption is a major controlling mechanism for the electro-chemical realkalisation (ECR) processes at the near surface zone of HCP when compared to other mechanisms such as diffusion and current-induced electro-osmosis. It also confirmed that electro-osmosis plays no significant role in the realkalisation of the carbonated cementitious material.

8- The use of sodium phosphate as an electrolyte in the ECR treatment resulted in a substantial increase (≈300%) in the realkalisation rate compared to that observed when sodium carbonate was used. Lithium hydroxide also increased the realkalisation rate by about 50%.

9- The passage of an electric current during the ECR treatment resulted in the densification of the pore structure, reducing both total and capillary porosity of cathode/cement paste transition zone. This effect was more pronounced for capillary porosity than for total porosity. The ECR process also led to some decomposition of calcite and the reformation of C-S-H gel. These effects were more pronounced with increasing intensity of polarisation and with the use of sodium phosphate as an electrolyte.

8.2 RECOMMENDATIONS FOR FURTHER WORK

It might be possible to carry out further development of the scratch hardness tool to achieve more accurate and precise measurements of microstructural gradients that exist over 10-50 μm distances, such as aggregate/cement paste and reinforcing steel/cement paste transition zones. This could be done by 1) altering the geometrical details of the scratch bit, which should be made more durable in terms of wear resistance, 2) connecting the scratch hardness tool with an image analysis system to ease tracing of the variations of the pore structure along the scratch, and 3) modifying the mechanism of the scratch bit movement such that it would not be displaced by hard particles (i.e. coarse aggregate and reinforcing steel).

The work reported in Chapter 6 showed that the use of CPF led to a remarkable enhancement in the microstructure and mass transport properties of the surface zone. However, these enhancements were insignificant for low w/c ratio concretes (≤0.5). It is therefore suggested to use water reducing or superplastizer admixtures in manufacture of such concretes to overcome this drawback. The use of these admixtures could increase the amount of free water within the concrete mix, leading to an increase in the amount of water to be drained from the CPF sheets and hence reducing the w/c ratio at the surface further. This, consequently, could improve the properties of the cover zone.

As a result of the improvement in the properties of the cover concrete due to the use of CPF, the thickness of cover concrete cast against CPF could be reduced compared to that cast against IF. However, the question arises as to how much extra covercrete can be saved due to the use of CPF. It is suggested that an economic study might be carried out in order to compare the savings during construction, having used IF, with the savings in the long-term due to the use of CPF. The main aim of this suggested study would be to show whether the use of CPF could offer the most cost effective solution for producing durable and high strength concretes.

The preliminary results reported in Chapter 7 show that the use of sodium phosphate as an electrolyte has a significant effect on the processes of ECR. However, this apparently beneficial effect has not been fully understood. Further studies are therefore necessary to investigate the following aspects in order to clarify the underlying phenomena. The following points need to be examined:

(1) the diffusion and absorption of sodium phosphate solutions in carbonated concrete,

(2) the stability of the alkaline environment formed due to the penetration of this electrolyte,

(3) the nature of the reaction products of cement phases formed during ECR process using sodium phosphate.

Further work is needed on the nature and stability of the passive film which is formed around the reinforcement after the ECR treatment. If such information were available, it might ultimately lead to a more comprehensive recommendation concerning the future ECR treatments required for maintaining the reinforcement in a passive state.

There is a need for a long term study on the durability of reinforced concrete against further CO_2 exposure treated with ECR. The durability of the concrete treated with surface coatings after ECR could also be investigated. This could be achieved by monitoring the changes in the microstructure and composition of the treated concrete and the corrosion activity of reinforcement for an extended period.

Adopting ECR to remove the chloride ions present in carbonated concrete could be the subject of further investigation. This could be done by altering the intensity of polarisation and the period of ECR treatment until both a highly alkaline zone is achieved around the reinforcement and the chloride content is reduced to below the threshold value. This might ultimately help to restore reinforced concrete which suffers from the dual action of chlorides and carbonation.

The work that has been done in this thesis and in the literature regarding the ECR treatment has been mainly carried out on OPC paste and concrete, whilst there is a lack of information about the effectiveness of using ECR in treating the carbonated blended concretes, such as OPC/PFA and OPC/GGBS. Thus, more work needs to be carried out in order to clarify the role of ECR treatment on such concretes.

REFERENCES

ACI COMMITTEE 201 (1977). "Guide to durable concrete", ACI journal, pp. 573-609.

ACI COMMITTEE 308-81 (1981). "Standard practice for curing concrete", American Concrete Institute, Detroit, 11 pp.

AITCIN, P., MIAO, B., COOK, W. D. and MITCHELL, D (1994). "Effect of size and curing on cylinder compressive strength of normal and high-strength concretes", ACI Material Journal, Vol. 91, No. 4, pp 349-354.

AHMED, H. E. H. (1990). "Transportion and occurrence of chlorides in PFA concrete", Ph.D. Thesis, University of Dundee, 219 pp.

AL-KADHIMI, T. K. H., BANFILL, P. F. G., MILLARD, S. G. and BUNGEY, J. H. (1996). "An experimental investigation into the effects of electro-chemical realkalisation", 4th Int. SCI Symposium, Corrosion of Reinforcement in Concrete Constructions, Cambridge, edit. by C. L. Page, P. B. Bamforth and J.W. Figg, pp. 501-511.

ARYA, C., BUENFELD, N. R. and NEWMAN, J. B. (1990). "Factors influencing chloride binding in concrete", Cement and Concrete Research, Vol. 20, No 2, pp. 291-300.

ARYA, C. (1994). "Supercover concrete", Concrete, Vol. 24, pp. 30-31.

ARYA, C. and VASSIE, P. R. W. (1996). "Effective cathode to anode ratio and reinforcement corrosion in concrete", 4th Int. SCI Symposium, Corrosion of Reinforcement in Concrete Constructions, Cambridge, edit. by C. L. Page, P. B. Bamforth and J.W. Figg, pp. 33-42.

BABU, K. C. and RAO, K. V. (1993). "Chloride diffusion characteristics of concrete", Concrete 2000, edited by K. Dhir, pp. 1445-1452.

BAMFORTH, P. B. and PRICE, W. F. (1994). "Factors influencing chloride ingress into marine structures", International Conference on Protection of Steel in Concrete, Sheffield University, ed. by R. N. Swamy, pp. 1105-1118.

BANFILL, B. F. G. (1994). "Features of the mechanism of realkalisation and desalination treatments for reinforced concrete", International Conference on Protection of Steel in Concrete, Sheffield University, ed. by R. N. Swamy, 24-28 July, pp. 1489-1498.

BASHEER, P. A. M., SHA'AT, A. A., LONG, A. E. and MONTGOMERY, F. R. (1993). " Influence of controlled permeability formwork on the durability of concrete", Concrete 2000, Dundee, edited by K. Dhir, pp. 737-747.

BARFOOT, J. (1991). "Controlled permeability formwork", Concrete, Vol. 24, pp. 12-14.

BARNES, B. D., DIAMOND, S. and DOLTCH, W. L. (1979). "The contact zone between Portland cement paste and glass "aggregate" surfaces", Cement and Concrete Research, Vol. 8, No. 2, pp. 233-244.

BEAUDOIN, J. J. (1987). "Validity of using methanol for studying the microstructure of cement paste", Materials and Structures, Vol. 20, pp. 27-31.

BEAUDOIN, J. J. and BROWN, P. W. (1992). "The structure of hardened cement paste", 9 th Int. Congress on the Chemistry of cements, N. Delhi, India, ed. By J. J. Brown, Vol. 1, pp. 485-525.

BENTUR, A. and JAEGERMANN, C. (1988). "Effect of curing in hot climate on the development of the properties of the outer skin concrete", Proceeding FIP, 48th International Congress, pp. 45-52.

BENTUR, N. and FOY, C. (1989). "Marine curing of steel fibre composites", Journal of Materials in Civil Engineering, Vol. 1, No. 2, pp. 86-95.

BENTUR, A. (1991). "Microstructure, Interfacial effects and Micromechanics of cementitious composites", Ceramic Translations, Vol./Part 16, pp. 523-549.

BENTUR, A. and JAEGERMANN, C. (1991). "Effect of curing and composition on the properties of the outer skin of concrete", Journal of Material in Civil Engineering, Vol. 3, No. 4, pp. 252-262.

BENTUR, A. and ODLER, I. (1996). "Development and nature of interfacial microstructure", RILEM Report 11, Interfacial Transition zone in Concrete, Edited by J. C. Maso, E&FN Spon, London, pp. 20-44.

BENTZ, D. P. (1994). " Evolution of porosity and calcium hydroxide in laboratory concretes containing silica fume", Cement and Concrete Research, Vol. 24, No. 6, pp. 1044-1050.

BERNS, H., FISHER, A., and KLEFF, J. (1991). "Design and construction of a new scratch tester for elevated temperatures", Wear of Materials ASME, pp. 661-665.

BHANSALI, K. J. and KATTAMIS, T. Z. (1990). "Quality evaluation of coatings by automatic scratch testing", Wear, Vol. 14, pp. 59-71.

BIER, T. A., KROPP, J. and HILSDORF, H. K. (1987). "Carbonation and realkalisation of concrete and hydrated cement paste", 1 st Int. RILEM Congress from Materials Science to Construction, Materials Engineering, Vol. 3, Versailles, France, pp. 927-934.

BIER, T. A., KROPP, J. and HILSDORF, H. K. (1988). "Realkalisation of carbonated concrete surfaces using cementitious materials", Proc. of Conf. Durability of Non-Metallic Inorganic Building, Karlsruke, pp. 125-132.

BIER, T. A., KROPP, J. and HILSDORF, H. K. (1989). "The formation of silica gel during carbonation of cementitious systems containing slag cements", Fly Ash, Silica Fume, Slag and Natural Pozzolans in Concrete, ACI SP-114, Trondheim, Vol. 2, pp. 1413-1428.

BOURDETTE, B., RINGOT, E. and OLLIVER, J. P. (1995). "Modelling of the transition zone porosity", Cement and Concrete Research, Vol. 25, No 4, pp. 741-751.

BROWNE, R. D. (1980). "Mechanism of corrosion of steel in concrete in relation to design, inspection and repair of offshore and coastal structures", ACI SP-65, pp. 169-204.

BRITISH STANDARD 12 (1978). "Ordinary and rapid Portland cement".

BRITISH STANDARD 882 (1983). "Specification for aggregates from natural sources for concrete".

BRITISH STANDARD 1881: PART 125 (1970). "Method of testing concrete".

BYFORS, K. (1986). "Chloride in cement paste", Nordic Concrete Research, No 4, pp. 27-28.

CABRERA, J. G. (1985). "The use of pulverised fuel ash to produce durable concrete", Improvement of Concrete Durability, Thomas Tel. Limited, pp. 29-57.

CABRERA, J. G., GOWRIPALAN, N. and WAINWRIGHT, P. J. (1989). "An assessment of concrete curing efficiency using gas permeability", Magazine of Concrete Research, Vol. 41, No. 149, pp. 193-198.

CAO, Y. and DETWILER, R. J. (1995). "Backscattered electron imaging of cement pastes at elevated temperatures", Cement and Concrete Research, Vol. 25, No 3, pp. 627-638.

CARRIER, R. E. (1983). "concrete curing tests", Concrete International, Vol. 13, pp. 23-26.

CATHER, B. (1994). "Curing: the true story", Magazine of Concrete Research, Vol. 46, No 186, pp. 157-161.

CHALKER, P. R., BALL, S. J. and RICKERBY, D. S. (1991). "A review of the methods used for evaluation of coating substrate adhesion", Material Science and Engineering, pp. 583-592.

CHATTERJI, S. and GUDMUNDSSON, H. (1977). "Characterisation of entrained air bubble system in concrete by means of image analysis microscope", Cement and Concrete Research, Vol. 7, pp. 423-428.

CHATTERJI, S. (1994). "Simultaneous chloride removal and realkalisation of old concrete structures", Cement and Concrete Research, Vol. 24, No. 6, pp. 1051-1054.

DAY, R. L. and SHI, C. (1994). "Effect of initial water curing on the hydration of cements containing natural pozzolan", Cement and Concrete Research, Vol. 24, No. 3, pp. 463-472.

DEPARTMENT OF TRADE AND INDUSTRY (1989). "Controlled permeability formwork in Japan", Conf. on Formwork Practice in Japan, London, pp. 29-32.

DIAMOND, S. (1971). "A critical comparison of mercury porosimetry and capillary condensation pore size distribution of Portland cement pastes", Cement and Concrete Research, Vol. 16, No. 5, pp. 531-545.

DIAMOND, S. (1976). "Cement paste microstructure", Conf. on Hydraulic cement pastes: Their Structure and Properties, Sheffield, Cement and Concrete Association, Slough, pp. 2-30.

DIAMOND, S., ABO-EL-ENEIN, A., HOSAKA, G., GOTO, S. and KONDO, R. (1977). "Pore structure of calcium silicate hydrate in hydrated Tricalcium Silicate", Journal of American. Ceramic Society, Vol. 60(3-4), pp. 110-114.

DIAMOND, S., AKIBA, T. and KONDO, R. (1981). "Through pore size distribution and kinetics of the carbonation reaction of Portland cement mortars", Journal of American Ceramic Society, Vol. 54, No. 9, pp. 423-428.

DHIR, R. K., LEVITT, M. and WANG, J. (1989). "Membrane curing of concrete: water vapour permeability of curing membrane", Magazine of Concrete Research, Vol. 41, No. 149, pp. 221-228.

DHIR, R. K. (1989). "Near-surface characteristics of concrete: prediction of carbonation resistance", Magazine of Concrete Research, Vol. 41, No 148, pp. 137-143.

DHIR, R. K., HEWLETT, P. C., and CHAN, Y. N. (1991). "Near-surface characteristics concrete: abrasion resistance", Materials and Structures, Vol. 24, pp. 122-128.

DHIR, R. K. (1993). "PFA concrete: chloride diffusion rate", Magazine of Concrete Research, Vol. 45, No162, pp. 1-9.

FATTUHI, N. I. (1986). "Curing Compound for fresh or hardened concrete", Building and Environment, Vol. 21, No. 2, pp. 119-125.

FELDMAN, R. F. and SEREDA, P. J. (1970). "A new model for hydrated Portland cement and its practical implications", Journal of American Ceramic Society, Vol. 53 (8-8), pp. 53-59.

FELDMAN, R. F. (1972). "Density and porosity studies of hydrated Portland cement", Cement Technology, Vol. 3, No 1, pp. 5-9 and 11-14.

FELDMAN, R. F. (1984). "Pore structure damage in blended cement pastes caused by mercury intrusion", Journal of American Ceramic Society, Vol. 67, pp. 30-33.

FELDMAN, R. F. and BEAUDOIN, J. J. (1991). " Pre-treatment of hardened cement pastes for mercury intrusion measurements", Cement and Concrete Research, Vol. 21, pp. 297-308.

FORRESTER, J. (1976). "Measurement of Carbonation: In carbonation of concrete", RILEM International Symposium, Cement and Concrete Association, paper 2-1, 6 pp.

FRAAY, A. L. A., BIJEN, J. M. and MAAN, Y. M. (1989). "The reaction of fly ash in concrete: A critical examination", Cement and Concrete Research, Vol. 19, No. 2, pp. 235-246.

HANSSON, C. M., STRUNGE, H., MARKUSSEN, J. B. and FROLUND, J. (1985). "The effect of cement type on the diffusion of chloride", Nordic Concrete Research, No 4, pp. 70-80.

HANSSON, C. M. and SORENSEN, B. (1987). "The influence of cement fineness on chloride diffusion and chloride binding in hardened cement paste", Nordic Concrete Research, No 6, pp. 57-72.

HEDENQVIST, P., OLSSON, M. and JACOBSON, S. (1990). "Failure mode analysis of TiN coated speed steel: In-situ scratch adhesion testing in the scanning electron microscope", Surface and Coatings Technology, Vol. 41, pp. 31-49.

HIGGINS, D. D. (1995). "The effect of some test variables on chloride profiles", RILEM International Workshop on Chloride Penetration into Concrete, France, 9 pp.

HILSDORF, H., KROPP, J. and GUNTER, M. (1984). "Carbonation, pore structure and durability", Proc. RILEM Seminar, Hannover, pp. 182-196.

HOBBS, D. W. (1994). "Carbonation of concrete containing PFA", Magazine of Concrete Research, Vol. 46, No. 166, pp 35-38.

HOMMOND, A. D. (1993). "Electro-chemical techniques for the repair of concrete", Structural Faults and Repairs, Vol. 93, pp. 181-193.

HONG, C. Z. and PARROTT, L. J. (1989). "Air permeability of cover concrete and the effect of curing" BCA Report, 22 pp.

HORNAIN, H., MARCHAND, J., DUHOT, V. and MORANVILLE-REGOURD, M. (1995). "Diffusion of chloride ions in limestone filler blended cement pastes and mortars", Cement and Concrete Research, Vol. 25, No 8, pp. 1667-1678.

HOUST, Y. F. and WITTMANN, F. H. (1994). "Influence of porosity and water content on the diffusivity of CO_2 and O_2 through hydrated cement paste", Cement and Concrete Research, Vol. 24, No. 6, pp. 1165-1176.

IGARASHI, S., BENTUR, A., and MINDESS, S. (1996). "Characterisation of the microstructure and strength by Microhardness testing", Advances in Cement Research, Vol. 8, No 30, pp. 87-92.

JENNINGS, H. M. and PARROTT, L. J. (1986). "Microstructural analysis of hardened alite paste", Journal of Materials Science, Vol. 21, pp. 4048-4052.

JONES, M. R. MCCARTHY, M. J. and DHIR, R. K. (1993). "Chloride reistant concrete", Concrete 2000, Dundee, Edit. by K. Dhir, pp. 1445-1452.

JUNGERMANN, B. (1982). "The chemical process of the carbonation of concrete ", Betonwerk+ Fertigeil-Technik, Vol. 48, No 6, pp. 358-362.

KASAI, Y., SATO, K. and SUGA, K. (1988). "Comparison of cement contents in concrete surface prepared in permeable form and conventional form", CAJ Review, pp. 298-301.

KATTMIS, T. Z., CHANG, F. and LEVY, M. (1990). "Evaluation of adhesion of some mtallic coatings on a depleted U0.75Ti alloy", Surface and Coatings Technology, 43/44, pp. 390-401.

KHOLMYANSKY, M., KOGAN, E. and KOVLER, K. (1994). "On the hardness determination of fine grained concrete", Materials and Structures, Vol. 27, pp. 584-587.

KILLOH, D. C., PARROTT, L. J. and PATEL, R. G. (1989). "Influence of curing at different relative humidities on the hydration and porosity of a Portland/fly ash cement paste", Trondheim Conference, pp. 157-174.

KJELLSEN, K. O. (1996). "Heat curing and post-heat curing regimes of high performance concrete: influence on microstructure and C-S-H composition", Cement and Concrete Research, Vol. 26, pp. 295-307.

KHAN, M. S. and AYERS, M. E. (1995). "Minimum of curing of silica fume concrete", Journal of Materials in Civil Engineering, Vol. 7, No. 2, pp. 134-139.

KOBAYASHI, K., SUZAKI, K. and UNO, Y. (1994). "Carbonation of concrete structures and decomposition of C-S-H", Cement and Concrete Research, Vol. 24, pp. 55-61.

KREIJGER, P. C. (1984). "The skin of concrete composition and properties", Materials and Structures, Vol. 17, No 100, pp. 275-283.

KUMAR, A., ROY, D. M. and HIGGINS, D. D. (1987). "Diffusion through concrete", Concrete, Vol. 21, No 1, pp. 31-32.

LAMBERT, P. (1983). "Corrosion and Passivation of steel in concrete", Ph.D. Thesis, Aston University, England, pp. 31-34.

LAMBERT, P., PAGE, C. L. and SHORT, N. R. (1985). "Pore solution chemistry of hydrated cement tricalcium silicate/ sodium chloride/ water", Cement and Concrete Research, Vol. 15, No 4, pp. 675-680.

LANGE, D. A., JENNINGS, H. M. and SHAH, S. P. (1994). "Image analysis techniques for characterisation of pore structure of cement-based materials", Cement and Concrete Research, Vol. 24, No. 5, pp. 841-853.

LARBI, J. A. (1991). "The cement paste-aggregate interfacial zone in concrete", Ph.D thesis, University of Delft, Netherlands, 127 pp.

LAWERANCE, C. D. (1981). "Durability of concrete: Molecular transport processes and test methods", C&CA, Technical Report 544, 25 pp.

LI, S. and Roy, D. M. (1986). " Investigation of relations between porosity, pore structures, and Cl^- diffusion of fly ash and blended cement pastes", Cement and Concrete Research, Vol. 16, pp. 749-759.

LONG, A., BASHEER, M. and CALLANAN, A. (1992). "Controlled permeability formwork", Construction Repair and Maintenance, 1992, pp. 36-40.

LONGUET, P., BURGLEN, L. and ZELWER, A. (1973). "La phase liquid du ciment hydrate", Materiaux de Construction et Travaux Publics, Vol. 676, pp. 35-41.

LOO, Y. H., CHIN, M. S., TAM, C. T. and ONG, C. G. (1994). "A carbonation prediction model for accelerated carbonation testing of concrete", Magazine of Concrete Research, Vol. 46, No 168, pp. 191-200.

MALAMI, C. and KALOIDAS, V. (1994). "Carbonation and porosity of mortar specimens with pozzolanic and hydraulic cement admixtures", Cement and Concrete Research, Vol. 24, No. 8, pp. 1444-1454.

MALEK, R. I. A. and ROY, D. M. (1988). "The permeability of chloride ions in fly ash cement pastes, mortars and concrete", Mats. Res. Soc. Symp. Proc., Vol. 114, pp. 325-334.

MANGAT, P. S. and MOLLORY, B. T. (1995). "Chloride binding in concrete containing PFA, GGBS or Silica fume under sea water exposure", Magazine of Concrete Research, Vol. 47, No 171, pp. 129-141.

MARKESTAD, S. A. (1976). "The Gukild-Carlsen method for making stabilised pastes of cements", Material and Constructions, Vol. 9, No 50, pp. 115-117.

MASLEHUDDIN, M., PAGE, C. L., RASHEEDUZZAFAR and AL-MANA, A. I. (1996). "Effect of temperature on pre solution chemistry and reinforcement corrosion in contaminated concrete", 4th Int. SCI Symposium, Corrosion of Reinforcement in Concrete Constructions, Cambridge, edit. by C. L. Page, P. B. Bamforth and J.W. Figg, pp. 67-76.

MATTILA, J. S. and PENTTI, M. J. (1996). "Realkalisation of carbonated concrete by cement-based coatings", 4th Int. SCI Symposium, Corrosion of Reinforcement in Concrete Constructions, Cambridge, edit. by C. L. Page, P. B. Bamforth and J.W. Figg, pp. 512-521.

MATTILA, J. S., PENTTI, M. J., and RAISKI, T. A. (1996). "Durability of electrochemically realkalised concrete structures", 4th Int. SCI Symposium, Corrosion of Reinforcement in Concrete Constructions, Cambridge, edit. by C. L. Page, P. B. Bamforth and J.W. Figg, pp. 481-490.

MARSH, B. K. and DAY, R. L. (1985). "Some difficulties in the assessment of pore structure of high performance blended cement pastes", Material Research Symposium Proceedings, Vol. 42, pp. 113-121.

MARSH, B., K., DAY, R. L. and BONNER, D. G. (1985). " Pore structure characteristics affecting the permeability of cement paste containing fly ash", Cement and Concrete Research, Vol. 15, pp. 1027-1038.

McCARTER, W., J. (1993). "Influence of surface finish on sorptivity on concrete", Journal of Materials in Civil Engineering, Vol. 5, No. 1, pp. 130-136.

MEHTA, P. K. and MANMOHAN, C. (1980). "Pore size distribution and permeability of hardenrd cement pastes", 7 th Int. Cong. Chem. Cem., Paris, Vol. III, pp. 1-5.

MEHTA, P. K. and GJØRV, O. E. (1982). "Properties of Por
tland cement concrete containing fly ash and condensed silica fume", Cement and Concrete Research, Vol. 12, No. 5.

MEHTA, P. K. (1986). "Concrete: Structure, Properties, and Materials", Prentice Hall, Inc., pp. 450.

MEYER, A. (1968). "Investigation on the carbonation of concrete", Proc. Chem. Cement, Tokyo, V. 3, pp. 394-401.

MIETZ, J. and ISECKE, B. (1994a). "Investigation on electrochemical realkalisation for carbonated concrete", Corrosion 94, NACE International, Paper No 297, pp. 1-14.

MIETZ, J. and ISECKE, B. (1994b). "Mechanisms of Realkalisation of concrete", International Conference on Protection of Steel in Concrete, International Conference on Protection of Steel in Concrete, Sheffield University, ed. by R. N. Swamy, 24-28 July, 24-28 July, pp. 216-227.

MILLER, J. B. (1994). "Structural aspects of high powered electro-chemical treatment of reinforced concrete", International Conference on Protection of Steel in Concrete, Sheffield University, ed. by R. N. Swamy, 24-28 July, pp. 1499-1514.

MOUKWA, M. and AITCIN, P. C. (1988). "The effect of drying on cement pastes pore structure as determined by mercury porosimetry", Cement and Concrete Research, Vol. 18, pp. 745-752.

NCT REPORT, (1994). "NORSK HYDRO KARM ØY: Realkalisation of alumina silo no. 5", 31 pp.

NEVILLE, A. M. (1981). "Properties of concrete", Longman (London), 779 pp.

NGALA, V. T. (1995). "Pore structure and diffusional properties of hardened cement pastes", Ph.D. Thesis, Aston University, England, UK

NGALA, V. T., PAGE, C. L., PARROTT, L. J. and YU, S. W. (1995). "Diffusion in cementitious materials: II Further investigations of chloride and oxygen diffusion in well-cured OPC and OPC/30% PFA pastes", Cement and Concrete Research, Vol. 25, pp. 819-826.

NGALA, V. T. and PAGE, C. L. (1997). "Effect of carbonation on pore structure and diffusional properties of hydrated cement pastes", Cement and Concrete Research, Vol. 27, No 7, pp. 995-1007.

NIEMINEN, I., ANDERSSON, P. and HOLMBERG, K. (1989). "Friction measurement by using a scratch test method", Wear, Vol. 130, pp. 167-178.

NISHER, P. (1986). "The quality of concrete texture", Betonwork and Fertigteil Technik, Vol. 6, pp. 363-368.

ODDEN, L. and MILLER, J. B. (1993). "Migration of alkalis in electro-chemically realkalised concrete", NACE Conf., Stand F Jord, Norway, pp. 54/1-54/11.

ODDEN, L. (1994). "The repassivating effect of electro-chemical realkalisation and chloride extraction", International Conference on Protection of Steel in Concrete, Sheffield University, ed. by R. N., 24-28 July, pp. 1473-1488.

PAGE, C. L., SHORT, N. R. and EL TARRAS, A. (1981). "Diffusion of chloride ions in hardened cement pastes", Cement and Concrete Research, Vol. 11, pp. 395-406.

PAGE, C. L. and VENNESLAND, Ø. (1983). "Pore solution composition and chloride binding capacity of silica-fume cement pastes", Material and Constructions, Vol. 16, No 19, pp. 19- 25.

PAGE, C. L. (1992). "Nature and properties of concrete in relation to reinforcement corrosion", Civ. Eng. Dept., Aston Univ., Commett Course: Aachen , 10 pp.

PAGE, C. L., YU, S. W. and BERTOLINI, L. (1994). "Some potential side-effect of electrochemical chloride removal from reinforced concrete", UK Corrosion and Eurocorr 94, 31 october -3 November 1994, Bournemouth Centre, U.K., Vol. 3, 228-238.

PAGE, C. L. and NGALA, V. T. (1995). "Steady-state diffusion characteristics of cementitious materials", RILEM International Workshop on Chloride Penetration into Concrete, France, 7 pp.

PARROTT, L. J. (1983). "Thermogravimetric and sorption studies on methanol exchange in alite paste", Cement and Concrete Research, Vol. 13, pp. 18-22.

PARROTT, L. J. (1986). "Modelling the development of microstructure", Proceedings of Engineering Foundation Conference on Cement Manufacture and Use, Hennicker, pp. 43-73.

PARROTT, L. J. (1987). "A review of carbonation in reinforced concrete", British Cement Association Report, C/1-0987.

PARROTT, L. J. (1990a). "Assessing carbonation in concrete structures", Durability of Building Materials and Components, pp. 575-585.

PARROTT, L. J. (1990b). "Carbonation, Corrosion and standardisation", Proc. Conf. on Protection of Concrete, Dundee, ed. by R. K. Dhir, pp. 1009-1023.

PARROTT, L. J. (1991a). "Factors influencing relative humidity in concrete", Magazine of Concrete Research , Vol. 43, No. 154, pp. 45-52.

PARROTT, L. J. (1991b). "Carbonation, moisture and empty pores", Advances in Cement Research, Vol. 4, No 15, pp. 111-118.

PARROTT, L. J. (1992). "Variations of water absorption rate and porosity with depth from an exposed concrete surface: Effect of exposure conditions and cement type", Cement and Concrete Research, Vol. 22, pp. 1077-1088.

PARROTT, L. J. (1993). "Effects of curing and cement type on the performance of cover concrete", Proc. Concrete 2000, Dundee, ed. by R.K Dhir, E&FN Spon, pp. 705-715.

PARROTT, L. J. (1994). "A study of carbonation-induced corrosion", Magazine of Concrete Research, Vol. 46, No. 166, pp. 23-28.

PATEL, R. G., PARROTT, L. J., MARTIN, J. A. and KILLOH, D. C. (1985). "Gradients of microstructure and diffusion properties in cement paste caused by drying", Cement and Concrete Research, Vol. 15, pp. 343-356.

PATEL, R. G., KILLOH, D. C., PARROTT, L. J. and GUTTERIDGE, W. A. (1988). "Influence of curing at different relative humidities upon compound reactions and porosity in Portland cement paste", Materials and Structures, Vol. 21, pp. 192-197.

PIHLAJAVAARA, S. E. (1968). "Some results of the effect of carbonation on the porosity and pore size distribution of cement paste", Materials and Structures, Vol. 6, pp. 521-526.

POLDER, R. B. and HONDEL, H. J. (1992). "Electrochemical realkalisation and chloride removal of chloride removal of concrete-State of the art, Laboratory and field experience", RILEM Int. Conf., Melbourne, pp. 135-147.

POURBAIX, M. (1966). Atlas of Electrochemical Equilibria in Aqueous Solutions, Pegammon, Oxford, pp. 1-20.

POWERS, T. C. and BROWNYARD, T. L. (1948). " Studies of physical properties of hardened Portland cement paste", Bull. 22, Portland Cement Assoc., pp. 276-287.

POWERS, T. C. (1958). "Structural and physical properties of hydrated cement paste", Journal of American Ceramic Society, Vol. 41, No 1, pp. 1-6.

PRATT, P. L. (1988). "Physical methods for the identification of microstructures", Structures and Materials, Vol. 21, pp. 106-117.

PRICE, W. F. and WIDDOWS, S. J. (1991). "The effect of permeable formwork on the surface properties of concrete", Magazine of Concrete Research, Vol. 43, No. 155, pp. 93-104.

PRICE, W. F. and WIDDOWS, S. J. (1992). "Durability of concrete in hot climates: benefits from permeable formwork", 3 rd Int. RILEM Concrete in Hot Climate, pp. 207-220.

PRICE, W. F. (1993). "The improvement of concrete durability using controlled permeability formwork", 5 th Int. Conf. on Structural Faults and Repairs, Vol. 2, pp. 233-2.38.

RAMACHANDRAN, V. S. (1969). "Applications of differential thermal analysis in cement chemistry", 1969.

RAMACHANDRAN, V. S. (1971). "Possible states of chlorides in hydration of tricalcium in the presence of calcium chloride", Materiaux et Constructions, Vol. 4, No 9, pp. 3-12.

RAHMAN, A. A. and GLASSER, F. P. (1989). "Comparative studies of the carbonation of hydrated cements", Advances in Cement Research, Vol. 2, No. 6, pp. 49-54.

RAIVIO, P. and SARVARANTA, L. (1994). "Microstructure of fibre mortar composities under fire impact-effect of polypropylene and polyacrylonitrile fibres", Cement and Concrete Research, Vol. 24, No 5, pp. 896-906.

RASHEEDUZZAFAR, S., HUSSAIN, S. E., and AL-SAADOUN, S. S. (1992). "Effect of tricalcium aluminate content of cement on chloride binding and corrosion of reinforcing steel in concrete", ACI Material, Volume 89, No 1, pp. 3-12.

RILEM DRAFT RECOMMENDATION CPC-18 (1984). "Measurement of hardened concrete carbonation depth", Materiaux et Constructions, Vol. 17, pp. 435-440.

RILEM DRAFT RECOMMENDATION (1994). "Draft recommendation for repair strategies for concrete structures damaged by reinforcement corrosion", Materials and Structures, Vol. 27, pp. 415-436.

ROSTASY, F. S., WEIß, R. and WIEDEMANN, G. (1980). "Changes of pore structure of cement mortars due to temperature", Cement and Concrete Research, Vol. 10, pp. 157-164.

SADEGZADEH, M. (1985). "Abrasion resistance of concrete", Ph.D. Thesis, Aston University, England, UK, 365pp.

SADEGZADEH, M. and KETTLE, R. (1986). "Indirect and non-destructive methods for assessing abrasion resistance of concrete", Magazine of Concrete Research, Vol. 38, No. 137, pp. 183-190.

SADEGZADEH, M., PAGE, C. L. and KETTLE, R. J. (1987). "Surface microstructure and abrasion resistance of concrete", Cement and Concrete Research, Vol. 17, pp. 581-590.

SADEGZADEH, M., PAGE, C. L. and KETTLE, R. J. (1989). "Influence of curing on surface characteristics of concrete", Material Research Society, Vol. 137, pp. 307-312.

SCRIVENER, K. L. and PRATT, P. L. (1987). "The characterisation and quantification of cement paste and concrete microstructures", Material Science to Construction Materials Engineering, Vol. 3, No 1, pp. 61-68.

SCRIVENER, K. L. and PRATT, P. L. (1996). "Characterisation of interfacial microstructure", RILEM Report 11, Interfacial Transition zone in Concrete, Edited by J. C. Maso, E&FN Spon, London, 1996.

SEREDA, S. (1968). "Mechanism of the carbonation shrinkage of lime and hydrated cement", J. Applied Chemistry, Vol. 18, pp. 111-117.

SHI, D. and WINSLOW, D. N. (1985). "Contact angle and damage during mercury intrusion into cement paste", Cement and Concrete, Vol. 15, pp. 645-654.

SCHIESSL, P. (1983). "Corrosion of reinforcement", CEB-RILEM, Int. Workshop of Concrete, Copenhagen, Durability of Concrete, pp. 73-93.

SCHIESSL, P. (1989). "Corrosion of steel in concrete", CEB-RILEM, Int. Workshop of Concrete, 100 pp.

SERGI, G. (1986). "Corrosion of steel in concrete: Cement matrix variables", Ph.D. Thesis, Aston University, England, UK, 395 pp.

SERGI, G., WALKER, R. J. and PAGE, C. L. (1996). "Mechanism and criteria for realkalisation of concrete", 4th Int. SCI Symposium, Corrosion of Reinforcement in Concrete Constructions, Cambridge, edit. by C. L. Page, P. B. Bamforth and J.W. Figg, pp. 491-500.

SHAPIRO, M., WESTERVELT, J., GERDS, D., LARSON, M., and BROWNFIELD, K. R. (1993). "Grass 4.1 programmer's manual", US Army Construction Engineering Research Laboratory.

SIMS, I. (1994). "The assessment of concrete for carbonation", Concrete, Vol. 24, pp. 33-37.

SMOLCZYK, H. G. (1976). "Explorations to the German long-time study on the rate of carbonation", Carbonation of Concrete, RILEM International of Symposium, Cement and Concrete Association, Theme 3 Paper 2.

SPEARS, R. (1983). "The 80 percent solution to inadequate curing problems", Concrete International, Vol. 16, pp. 15-18.

SUGAWARA, T., SAEKI, N., SHOYA, M. and TSUKINAGA, Y. (1993). "Frost resistance of concretes with permeable sheets and surface coating", Durability of Building Materials and Components, Proc. 6 th Int. Conf., Omiya, Japan, pp. 497-505.

SUGIYAMA, J., BREMNER, T. W. and TSUJI, Y. (1996). "Determination of chloride diffusion coefficient and gas permeability of concrete and their relationship", Cement And Concrete Research, Vol. 26, No 5, pp. 781-790.

SURYAVANSHI, A. K. and SWAMY, R. N. (1996). "Stability of Friedel's salt in carbonation concrete structural elements", Cement and Concrete Research, Vol. 26, No 5, pp. 729-741.

SWAMY, R. N. and TANIKAWA, S. (1993). "External surface coating to protect concrete and steel from aggressive environments", Materials and Structures, Vol. 26, No 162, pp. 465-478.

TAN, K. and GJORV, O. E. (1996). "Performance of concrete under different curing conditions", Cement and Concrete Research, Vol. 26, No 3, pp. 355-365.

TAXT, T., FLYNN, P., AND JAIN, A. K. (1985). "Segmentation of document images", IEEE Transaction on Pattern Analysis and Machine Intelligence, Vol. 11, No 12, pp. 1322-1329.

THOMAS, M. D. A. and MATTHEWS, J. D. (1992). "Carbonation of fly ash concrete", Magazine of Concrete Research, Vol. 44, No 160, pp. 217-228.

THOMAS, M. (1995). "Chloride threshold in marine concrete", RILEM International Workshop on Chloride Penetration into Concrete, France, 10 pp.

TRITTHART, J. (1989). "Chloride binding in cement II-The influence of hydroxide concentration in the pore solution of hardened cement paste on chloride binding", Cement and Concrete Research, Vol. 19, No 5, pp. 683-691.

TSUKINAGA, Y. and SHOYA, M. (1993). "Air void character and pull off strength in the surface of concrete using permeable sheets", Durability of Building Materials and Components, Proc. 6 th Int. Conf., Omiya, Japan, pp. 507-515.

TUMIDAJSKI, P. J. and CHAN, G.W. (1996). "Effect of sulphate and carbon dioxide on chloride diffusivity", Cement and Concrete Research, Vol. 26, No 4, pp. 551-556.

TUUTTI, K. (1982). "Corrosion of steel in concrete", Swedish Cement and Concrete Institute, S-100 44-CBI, Forskning Research, Stockholm, 468 pp.

TUUTTI, K. (1983). "Service life of structures with regard to corrosion of embedded steel", CIB 83, pp. 233-243.

VAYSBURD, A. M., SABNIS, G. M. and EMMONS, P. H. (1993). "Concrete carbonation -A fresh look", The Indian Concrete Journal, Vol. 83, pp. 215-221.

VERBECK, G. J. (1958). "Carbonation of hydrated Portland cement", American Society of Testing and Materials, Special Technical Publication, No 205, pp. 21-38.

VERBECK, G. J. and HELMUTH, R. H. (1968). "Structures and physical properties of cement paste", 5 th Int. Symposium of the Chemistry Cement, Tokyo, pp. 1-32.

VERBECK, G. J. (1975). "Mechanisms of corrosion of steel in concrete", ACI Publication, SP 49-3, 21-38.

WAKELY, L. D. and ROY, D. M. (1982). "A method of testing the permeability between grout and rock", Cement and Concrete Research, Vol. 12, pp. 533-534.

WALKER, R. J. (1994). "Aspects of the prevention and repair of chloride induced corrosion of steel in concrete", Ph.D. thesis, Aston University, UK, 245 pp.

WALLBANK, E., J. (1989). "The performance of concrete in bridges: A survey of 200 highway bridges", Department of transport, UK, 96 pp.

WANG, J., DHIR, R. K. and LEVITT, M. (1994). "Membrane curing of concrete: moisture loss", Cement and Concrete Research, Vol. 24, No. 8, pp. 1463-1474.

WEST, G. (1989). "Technical note: Rock abrasiveness testing for tunnelling", Int. J. of Rock. Mech. Min. Sci.& Geemoch. Abstr., Vol. 26, No 2, pp. 151-160.

WILSON, D. J. (1994a). "Controlled permeability formwork (CPF)", Concrete, Vol. 24, pp. 20-22.

WILSON, D. J. (1994b). "A review of the use of controlled permeability formwork (CPF) systems", International Conference on Protection of Steel in Concrete, Sheffield University, ed. by R. N. Swamy, 24-28 July, pp. 1132-1141.

WINSLOW, D. N. and DIAMOND, S. (1970). "A mercury porosimetry study of the evaluation of porosity in Portland cement", Journal of Materials, Vol. 5, No 3, pp. 564-585.

WINSLOW, D. and LIU, D. (1990). "The pore structure of paste in concrete", Cement and Concrete Research, Vol. 20, pp. 227-235.

WINSLOW, D. N., COHEN, M. D., BENTZ, D. P., SNYDER, K. A. and GARBOCZI, E. J. (1994). "Percolation and pore solution in mortars and concrete" Cement and Concrete Research, Vol. 24, No 1, pp. 25-37.

WOOD, J. G. M. (1994). "Quantifying and modelling concrete durability performance", Meeting at Building Research Establishment, November 10 th, pp. 1-5.

YOUNG, J. F. (1988). "A review of the pore structure of cement paste and concrete and its influence on permeability", ACI, SP 108-1, pp. 1-18.

ZIMBELMANN, R. (1978). "The problem of increasing the strength of concrete, Betonwerk + Fertigteil-Technik, Heft 2, pp. 89-96.

ZIMBELMANN, R. (1985). "A contribution to the problem of cement aggregate bond", Cement an Concrete Research, Vol. 15, pp. 801-808.

APPENDICES

APPENDIX 1

DETERMINATION OF NON-EVAPORABLE WATER

1.1 Derivation

Equation 2.1 used for the determination of non evaporable water (NEW) in cement pastes was derived as follows (Lambert, 1983 and Sergi, 1986):

The mass of the cement paste before and after heating to 105 and 950°C may be defined using the following equations.

$$Wo = Wc + We + Wn + Wa \quad \text{..... (1)}$$

$$W105 = Wc + Wn + Wa \quad \text{..... (2)}$$

$$W950 = Wc\frac{(100 - i)}{100} + Wa \quad \text{..... (3)}$$

where,

Wo = original mass of cement (g)

$W105$ = mass of cement at 105°C (g)

$W950$ = mass of cement at 950°C (g)

Wc = mass of unhydrated cement (g)

We = mass of evaporable water (g)

Wn = mass of non-evaporable water (g)

Wa = mass of admixtures (g)

and i = loss-on-ignition (% g/g of unhydrated cement)

From these Equations (1 to 3) expression for non-evaporable water may be developed as follows:

if $Wa = \frac{(Wc)x(a)}{100}$ ..... (4)

where,

a = admixture content(% g/g of unhydrated cement)

From (3),

$$W950 = \frac{Wc(100 - i)}{100} + \frac{(Wc)x(a)}{100} = \frac{Wc(100 - i + a)}{100} \quad \text{..... (5)}$$

$$Wc = \frac{(100)x(W950)}{(100 - i + a)} \qquad \ldots\ldots \quad (6)$$

Non-evaporable water (NEW) = $\frac{Wn}{Wc} x100\%$

From (2),

$$Wn = W105 - Wc - Wa$$

Sub. Wa from (4)

$$Wn = W105 - Wc - \frac{(Wc)x(a)}{100}$$

$$Wn = W105 - Wc\left(1 + \frac{a}{100}\right)$$

Sub. Wc from (6)

$$Wn = W105 - \frac{(100)x(W950)}{(100 - i + a)}(1 + \frac{a}{100})$$

$$Wn = \frac{W105(100 - i + a) - (100 + a)W950}{(100 - i + a)}$$

Divide by Wc from (6) and multiply by 100 to give the non-evaporable water (%)

$$NEW(\%) = \frac{[W105(100 - i + a) - (100 + a)W950][100 - i + a]}{(100 - i + a)x(100)x(W950)}$$

$$NEW(\%) = \frac{W105(100 - i + a) - W950(100 + a)}{W950}$$

1.2 WORKED EXAMPLE

For specimen at 26-30 mm into OPC paste cured with E4, w/c = 0.55, (Figure 3.8)

Mass of specimen at 105°C =3.64980 g = $W105$

Mass of specimen at 950°C =3.09214 g = $W950$

% Loss-on-ignition =0.89731 % = i

% Admixture content =0.0 % = a

$$NEW(\%) = \frac{W105(100 - i + a) - W950(100 + a)}{W'950}$$

$$NEW(\%) = \frac{3.6498(100 - 0.89731 + 0.0) - 3.09214(100 + 0.0)}{3.09214}$$

$$NEW(\%) = 16.9756\%$$

APPENDIX 2

WORKED EXAMPLE OF DETERMINATION OF TOTAL AND CAPILLARY POROSITY

For specimen at 26-30 mm into OPC paste cured with E4, w/c = 0.55, (Figures 3.11 and 3.13)

Weight of specimen in water	=1.8565 g	= W1
Weight of specimen in SSD condition	=3.9358 g	= W2
Weight of specimen pre-conditioned at 90.7% RH	=3.8334 g	= W3
Weight of specimen at 105°C	=2.9335 g	= W4

$$\text{Capillary porosity (\%)} = \frac{W2 - W3}{W2 - W1} x100$$

$$\text{Capillary porosity (\%)} = \frac{3.9358 - 3.8334}{3.9358 - 1.8565} x100$$

$$\text{Capillary porosity (\%)} = 4.9218\ \%$$

$$\text{Total porosity (\%)} = \frac{W2 - W4}{W2 - W1} x100$$

$$\text{Total porosity (\%)} = \frac{3.9358 - 8.8006}{3.9358 - 1.8565} x100$$

$$\text{Total porosity (\%)} = 48.2005\ \%$$

APPENDIX 3

DETERMINATION OF CARBONATE CONCENTRATION IN EXPRESSED PORE SOLUTION

3.1 Derivation

To calculate the content of carbonate ions (CO_3^{2-}) present in the pore solution of HCP treated with ECR using sodium carbonate as an electrolyte, the following derivation may be developed (Walker, 1994).

Using a pH electrode it was seen that, in an acid-base titration, the colour change of

1) Phenolphthalein indicator occurred at pH 8.31
2) Bromocresolgreen indicator occurred at pH 3.95

Using equilibrium equations (Pourbaix, 1966)

$$\frac{(CO_3^{2-})}{(HCO_3^-)} = -10.34 + pH \quad \ldots\ldots \quad (1)$$

$$\frac{(HCO_3^-)}{(H_2CO_3)} = -6.38 + pH \quad \ldots\ldots \quad (2)$$

Let:

Total carbonate $= CO_3^{2-} + HCO_3^- + H_2CO_3 = a$ moles ..... (3)

Addition of acid (H^+) to take pH from 8.31 to 3.95 = b moles ..... (4)

<u>At pH 8.31</u>

$H_2CO_3 \approx 0.0$ ..... (5)

From (1),

$$\frac{CO_3^{2-}}{HCO_3^-} = 10^{-2.03} \approx 0.009 \quad \ldots\ldots \quad (6)$$

Sub. (5) and (6) in (3),

$0.009\,(HCO_3^-) + (HCO_3^-) + 0.0 = a$

$1.009\,(HCO_3^-) = a$

HCO_3^- = 0.991a ..... (7)

Sub. (7) in (6) this gives,

CO_3^{2-} = 0.009a ..... (8)

<u>At pH 3.95</u>

CO_3^{2-} ≈ 0.0 ..... (9)

From (2),

$\frac{HCO_3^-}{H_2CO_3} = 10^{-2.43}$ ≈ 0.004 ..... (10)

Sub. (9) and (10) in (3), this gives,

HCO_3^- = 0.004a ..... (11)

H_2CO_3 = 0.996a ..... (12)

Hence:

Titration from pH 8.31 to pH 3.95 causes:

0.991a moles HCO_3^- + 0.009a moles CO_3^{2-} + b moles H^+

to be converted to

0.996a moles H_2CO_3 + 0.004a HCO_3^-

Therefore,

b = (0.991 - 0.004)a + 2(0.009a)

<u>a = 1.005b</u>

3.2 WORKED EXAMPLE

For the case of U-10 mm slice of HCP treated with ECR for 28 day using 1 A/m^2 current density, it takes

202 mM H^+ to reach the phenolphthalein colour change

and 425 mM H^+ to reach the Bromocresolgreen colour change

b = 425 - 202 = 223 mM

Carbonate content (a) = 1.005b

Carbonate content (a) = 224.115 mM

APPENDIX 4

DETERMINATION OF THE EFFECTIVE CHLORIDE DIFFUSION COEFFICIENT

4.1 CHLORIDE CALIBRATION CURVE

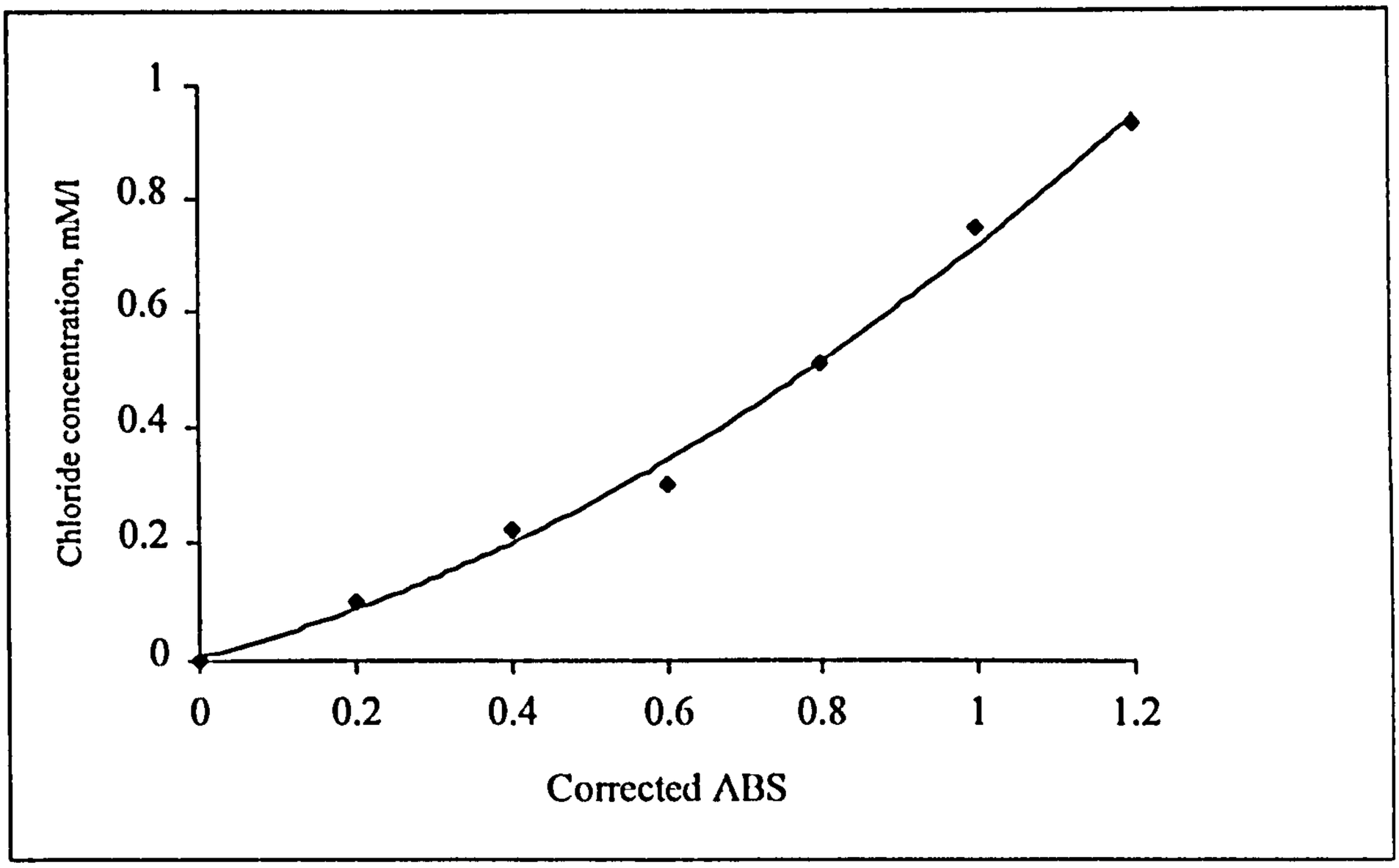

4.2 PROOF OF THE EQUATION USED IN THE DETERMINATION OF EFFECTIVE CHLORIDE DIFFUSION COEFFICIENT

The derivation of equation (2.10) is based on Fick's first law of diffusion and may be developed as follows.

The flux, J, of chloride ion entering compartment 2 is given by;

$$J = \frac{V}{A}.\frac{dC_2}{dt} = \frac{D_{cl}}{l}(C_1 - C_2) \qquad \text{.....} \qquad (1)$$

where,

D_{cl} = effective chloride diffusion coefficient

V = volume of the solution in compartment 2

A = cross-sectional area of diffusion

l = thickness of disc

C_1 = concentration of solution in compartment 1

C_2 = concentration of solution in compartment 2

Rearranging Equation (1) gives,

$$\frac{dC_2}{dt} = \frac{D_{cl}A}{lV}(C_1 - C_2)$$

$$\frac{d(C_1 - C_2)}{(C_1 - C_2)} = -\frac{D_{cl}A}{lV}dt \qquad \text{.....} \qquad (2)$$

Integrating Equation (2) for t>t_o and $C_1 >> C_2$ yields;

$$\left[\log_e(C_1 - C_2)\right]_{c_2=0}^{c_2=c_2} = -\frac{D_{cl}A}{lV}[t]_o$$

$$\log_e\left(\frac{C_1 - C_2}{C_1}\right) = -\frac{D_{cl}A}{lV}(t - t_o)$$

$$\log_e\left(\frac{C_1}{C_1 - C_2}\right) = \log_e\left(1 + \frac{C_2}{C_1 - C_2}\right)$$

$$= \frac{D_{cl}A}{lV}(t - t_o)$$

Expand the logarithm;

$$\frac{C_2}{C_1 - C_2} \approx \frac{D_{cl}A}{lV}(t - t_o)$$

$$C_2 \approx \frac{D_{cl}AC_1}{Vl}(t - t_o)$$

Thus the effective chloride ion diffusion coefficient, D_{cl}, can be calculated from the slope, S, of the plot of C_2 against t as follows:

$$D_{cl} \approx \frac{Vl}{AC_1}S$$

4.3 WORKED EXAMPLE

For disc at 26-30 mm into OPC paste cured with E4, w/c = 0.55, (Figure 3.15)

Volume of solution in compartment 2	= 84.8 ml	$= V$
Thickness of disc	= 0.331 cm	$= l$
Cross sectional area of diffusion	= 9.1616 cm^2	$= A$
Concentration of solution in Compartment 2	= 1.0×10^{-3} moles/cm^3	$= C_2$
Slope of plot of C_2 against t	= 8.428×10^{-13} moles/cm^3 .s	$= S$

From $$D_{cl} \approx \frac{Vl}{AC_1}S$$

$$D_{cl} = \frac{84.8x0.331}{9.1616x1.0x10^{-3}} x 8.428x10^{-13}$$

$$D_{cl} = 25.8x10^{-9} cm^2 / s$$

4.4 SUMMARY OF THE EFFECTIVE CHLORIDE DIFFUSION COEFFICIENT RESULTS

The effective chloride diffusion coefficient (D_d x 10^-9 cm^2/s) results for OPC paste specimens subjected to different curing regimes (Figure 3.15)

Curing regime	Depth below surface, mm							
	2-6	6-10	10-14	14-18	18-22	22-26	26-30	30-34
E4	33.7	26.6	63.6	30.7	30.3	29.6	26.0	40.3
	58.5	78.0	19.5	17.2	41.3	26.2	29.6	15.5
	63.5	26.4	32.1	20.6	25.0	22.2	20.5	24.1
	48.5	33.3	38.9	27.9	10.9	20.5	26.6	26.5
Average	51.0	41.0	38.5	24.1	26.9	24.6	25.7	26.6
E7	34.8	50.5	60.1	40.2	24.0	42.9	35.5	29.9
	44.2	25.2	32.4	44.5	31.1	38.2	30.2	28.5
	22.1	36.5	31.5	20.2	37.2	36.5	38.4	42.3
	38.9	39.0	40.4	37.1	51.7	34.0	35.7	60.1
Average	35.0	37.8	41.1	35.3	36.0	37.9	35.0	40.2
E8	75.0	70.7	36.8	52.2	38.7	45.9	19.9	45.0
	100.5	70.0	64.4	54.1	60.5	47.2	80.2	46.2
	88.2	68.8	56.7	50.2	59.5	40.5	47.5	50.2
	28.7	70.1	62.9	25.5	61.7	42.2	30.8	42.6
Average	73.1	69.9	55.2	45.4	55.1	44.0	44.6	46.0

APPENDIX 5

A WORKED EXAMPLE OF DETERMINATION OF CHEMICAL COMPOSITION OF CEMENT PASTE

For carbonated OPC paste cured with E4 (Table 5.2)

Summary of TG data

Temperature, C	20	110	250	450	600	700	750	900	950
% weight of spec.	100	95.30	90.07	87.40	84.16	79.92	74.50	65.41	65.12

Knowing that (Ramachandran, 1969 and Rahman, 1989);

- C-S-H decomposes at range of 110-250° C.
- C-H decomposes at range of 450-600° C.
- Ca_xCO_y (all phases) decompose at range of 700-900° C.
- Calcite (Ca_xCO_y) decompose at range of 750-900° C.
- All evaporable water (EW) releases when the temperature reaches 110° C.
- All non-evaporable water (NEW), bound water, releases when the temperature reaches 950° C.

Therefore, the following calculations based on the above criterias may be carried out as follows;

Let;

The effect of loss-on-ignition and the other phases which might decompose at these ranges of temperature are negligible.

% Weight loss due to decomposition of C-S-H

= % weight of spec. at 110°C - % weight of spec. at 250°C

= 95.30 - 90.07 = 5.23 %

% Weight loss due to decomposition of C-H

= % weight of spec. at 450°C - % weight of spec. at 600°C

= 87.40 - 84.16 = 3.24 %

% Weight loss due to decomposition of all phases of calcium carbonate (Ca_2CO_1)

= % weight of spec. at 700°C - % weight of spec. at 900°C

= 79.92 - 65.41 = 14.51%

% Weight loss due to decomposition of calcite (Ca_2CO_1)

= % weight of spec. at 750°C - % weight of spec. at 900°C

= 74.50 - 65.41 = 9.09 %

% Weight loss due to evaporable water (EW)

= % weight of spec. at 20°C - % weight of spec. at 110°C

= 100 - 95.30 = 4.7 %

% Weight loss due to evaporable water (NEW), bound water

= % weight of spec. at 110°C - % weight of spec. at 950°C

= 95.30 - 65.12 = 30.18 %

APPENDIX 6

EXAMPLE OF IDENTIFICATION OF XRD TRACE

For OPC specimen, at steel cathode/cement paste interface zone, treated with ECR at I = 1 A/m^2 for 14 days (Figure 7.20), the following values for 2θ, d-spacing (based on CuKα = 1.542 A°) and relative intensity I were determined:

2θ	d-spacing d (A°)	Intensity (I)	Standard data	
			Calcite	Vaterite
25.0	3.559	2		3.58 (vvs)
27.0	3.3	2		3.3 (vvs)
29.5	3.025	26	3.04 (vvs)	
35.0	2.562	2	2.50 (m)	
38.5*	2.336	15	NIP*	
39.5	2.279	6	2.29 (s)	
43.0	2.102	5	2.10 (s)	
44.0	2.056	2		2.06 (vvs)
47.5	1.913	7	1.91 (ms)	
48.5	1.875	6	1.875 (ms)	
50.0	1.823	2		1.83 (vvs)

* Non-identified Peak

The calculation of d-spacing shown in the above table was carried out using Bragg's equation (n λ=2 d sinθ), assuming the order of reflection (n) =1 and the wave length of the X-ray beam (λ) =1.542.

The values of d and I were compared to standard data as shown in the table, to identify calcite and vaterite phases. In this case, calcite was easily to be identified, whilst vaterite was difficult to identify as a result of absence some major peaks. Non-identified peak was also appeared in this trace at 38.5°.

Key to table: scale of decreasing relative intensities:

vvs, vs, s, ms, m, mw, w, vw, vvw